N70 72021

DESIGN CRITERIA FOR SPACECRAFT PROPULSION SYSTEMS

VOLUME III-A

DETAILED PROPULSION SCALING
AND DESIGN DATA

REPORT 1069 FR-1

LIBRARY COPY

FEB 20 1968

MANNED SPACECRAFT CENTER
HOUSTON, TEXAS

AEROJET GENERAL

SPACE DIVISION

JAN 1970
RECEIVED
NASA STI FACILITY
INPUT BRANCH

DESIGN CRITERIA FOR SPACECRAFT PROPULSION SYSTEMS

Final Report

Contract NAS 7-519

VOLUME IIIA - APPENDICES B, C AND D

SG Report 1069FR-1

October, 1967

DESIGN CRITERIA FOR SPACECRAFT PROPULSION SYSTEMS

Prepared for

National Aeronautics and Space Administration
Office of Advanced Research and Technology
NASA Headquarters, Washington, D.C.

Prepared by

C.N. Jennings

SPACE-GENERAL PLANT
9200 E. Flair Drive
ElMonte, California

ACKNOWLEDGMENT

NASA

This program has been sponsored by Messrs. F. Compitello and R. Ziem of NASA-OART and was under the technical direction of Mr. J. Kelley of the Jet Propulsion Laboratory.

INDUSTRY

Propulsion organizations which have completed subcontracted efforts and have contributed propulsion scaling and design data include:

Thiokol Chemical	- Messrs. G. Andrews, D. Reed, and S. Racik
Lockheed Propulsion	- Messrs. N. Cohen and D. Taylor
United Tech. Center	- Messrs. T. Meyers, J. Spano, and L. Fischer
Rocket Research	- Mr. R. Sampson
Thiokol RMD	- Messrs. M. Levoy and P. O'Dea
TRW Systems	- Messrs. E. Rutkowski and R. Miller
Aerojet-General	- Messrs. T. Browne, N. Vaniman, R. Muir, P. Raabe, J. Goddard, R. Harris and W. Sprow

FOREWORD

This final report is submitted in compliance with the requirements of NASA Contract NAS 7-519, Article II, Paragraph D.

ABSTRACT

Design criteria relating the cost, reliability, weight, and performance of spacecraft propulsion systems to total program or mission cost-effectiveness have been defined in terms of influence-coefficients. These influence-coefficients can be used to maintain a balance of the utilization of cost, weight, or reliability resources between systems, and to establish criteria for detailed system or component tradeoff analyses. Total program modeling and use of the resulting design criteria will allow consistent, definable and traceable decisions which can be reviewed by program managers or contracting agencies. Prediction techniques, which have been established by the propulsion industry (under subcontracts) to determine propulsion costs, reliability, weight and performance, are summarized in Volume II of this report and are presented in detail in the Appendices of Volumes III, IV and V. These propulsion data and scaling techniques can be used by the Government and Industry to establish characteristics of propulsion systems for future applications. As an indirect benefit, the propulsion industry has recognized the need for the type of data requested under this program -- and are continuing in-house studies to update the propulsion design and costing guides.

Volume I - Summary and Conclusions

Volume II - Presentation of Design Criteria and Summary of Capabilities and Costs of Space Propulsion Systems

The Appendices included in Volumes III, IV and V present design and scaling characteristics of solid, hybrid, fluid-control, and liquid propellant propulsion systems.

Appendix A* - Solid Rocket Propulsion
Aerojet-General Corporation

Appendix B - Solid Rocket Propulsion
Thiokol Chemical Corporation

Appendix C - RSVP (Restartable Variable Pulse) Propulsion
Lockheed Propulsion Company

Appendix D - Hybrid and Solid Propulsion
United Technology Center

Appendix E* - Monopropellant Liquid Propulsion Systems
Rocket Research Corporation

Appendix F* - Liquid Rocket Propulsion
Rocketdyne, Div. of NAR

(This was a complimentary study completed by Rocketdyne, and not a part of Contract NAS 7-519)

Appendix G - Bipropellant Liquid Propulsion
Reaction Motors Division of Thiokol Chemical Corp.

Appendix H - Liquid Rocket Propulsion
TRW Systems Group

Appendix I - ARES (Advanced Rocket Engine Storable) Space Engine
Aerojet-General Corporation

Appendix J - Bipropellant Liquid Space Engine
Aerojet-General Corporation

Volume III-A - Detailed Propulsion Scaling and Design Data, Appendices B, C, D

III-B - Detailed Propulsion Scaling and Design Data, Appendices G, H, I

Volume IV - Classified Data from Appendices A-I

* Volume V - Restricted (Proprietary) Data from Appendices A-I (Includes Complete Appendices A, E, and F)

1.0 PROPULSION STUDY OBJECTIVES

Unmanned space missions planned for the next fifteen to twenty years include a wide range of propulsion design requirements. Thrust level varies from tenths of pounds for ACS applications to about 20,000 pounds for larger spacecraft main thrusters; storability requirements vary from a few days, to several years for the advanced planetary missions; and propulsion requirements of the various mission maneuvers vary from multiple restart/highly throttlable or pulsed operation to single high impulse maneuvers. A goal of this program was to obtain cost, reliability, and performance data for as wide a range in propulsion system operating requirements and for as many design options as possible within the schedule and funding scope of the contract.

Propulsion systems and subsystems were investigated by propulsion companies which have direct design, development, and production experience with those systems; wherever possible, parallel tasks were conducted to improve confidence in the resulting design and scaling data. Subcontractors* included:

Rocket Research	- Monopropellant Liquids
TRW Systems	- Monopropellant and Bipropellant Liquids
Thiokol RMD	- Bipropellant Liquids
Thiokol Chemical	- Solid Propellants
Aerojet SRP	- Solid Propellants
United Technology Center	- Solid and Hybrid Propellants
Lockheed Propulsion	- Fluid Control Motors
Aerojet LRP	- High P_c Bipropellant Liquids

* Rocketdyne Div. of NAA conducted a parallel study on a non-contractual basis. Results of these studies were submitted directly to JPL, and are included as an attachment to Volume V.

A total of approximately 4400 manhours was committed to these subcontracted investigations; effort on some of the subcontracts far exceeded the funded level.

2.0 PROPULSION STUDY TASKS

Specific tasks of the subcontracted investigations were divided into five primary areas;

1) Performance
2) Weight
3) Reliability
4) Costs
5) Sterilization Influences on Design

For each task, the objective was to provide, based on a "reference" propulsion system or type of propulsion system, the following information:

1. Measured or actual data for the reference* system.
2. Predicted values for the reference system, using the prediction techniques in (3) below.
3. Prediction techniques for scaling the reference system to new sizes or operating conditions.
4. Limitations of the prediction techniques.
5. Expected accuracy of the predicted (scaled) characteristics.

In addition, examples of the use of the prediction techniques was requested, such that misinterpretation would be minimized.

A tabular format was suggested for a summary presentation of the subcontracted tasks (typical tables provided to the subcontractors are presented in Figures 1 through 5).

---

* For example, the LEMDE bipropellant engine was a reference for the TRW bipropellant task; spherical solid space motors for Thiokol Chemical; "Common" C-1 engine for Reaction Motors; etc.

TABLE 2 - PERFORMANCE

Parameter	Measured Value (for "base" system)	Predicted Value (for "base" system)	Prediction Methods (Equations, Tables, Graphs, etc.) For New Systems	Limitations of Prediction Method (Thrust range, P_c range, throttle range, etc.)	Expected Accuracy of Predicted Performance
Steady State Isp / Pulse mode Isp if applicable					
Minimum Impulse Bit					
Reproducibility of Impulse Bit					
Total Impulse Cutoff Accuracy					
Throttled Performance					
Thrust Vector Alignment					
Thrust Centerline Offset					

Figure 1

SUGGESTED SUMMARY PRESENTATION FORMAT FOR SUBCONTRACT TASKS

TABLE 4 - COMPONENT FAILURE MODES AND EFFECTS

Component or Subsystem: _____

Failure Modes		Failure Mode "A"	"B"	"C"	Etc.
Failure Cause					
Probability of Failure Occurring (or failure rates if applicable)	During Launch	Reference data source, general confidence, and Maximum Value Minimum Value Expected Value			
	During Coast				
	At Startup				
	During Operation				
	At Shutdown				
Detection		o Possibilities for detection by pressure sensors or other equip.			
Remedial Action		o Remedial action after detection (shut down, use redundant system, explosion, etc.).			
Effects on Propulsion		o Effects of failure on propulsion performance.			
Failure Mode Elimination		o Methods for eliminating or reducing probability of failure mode (alternate design, redundancy, more conservative design incr d testing, higher test stress levels, etc.).			
Failure Rate Reduction		o Indicate estimated reduction in failure probabilities and			

Figure 2

SUGGESTED SUMMARY PRESENTATION FORMAT FOR SUBCONTRACT TASKS

TABLE 5 - SUBSYSTEM & COMPONENT FAILURE RATES AND DEVELOPMENT FACTORS

Subsystem or Component	Predicted "Inherent" Failure Rate	Expected Operating Failure Rates After "N" Test Seconds					
		Component Development (where applicable)			System Development		
		"X" Seconds	"Y" Seconds	"Z" Seconds	"X" Seconds	"Y" Seconds	"Z" Seconds
Component A							
Component B			Reference data sources and general confidence in data including where possible: Maximum Failure rate Expected Failure rate Minimum Failure rate				
Etc.							
System							

SYSTEM FLIGHT FAILURE RATES

(For the Base or Reference Propulsion System described in Table I)

Historical Flight Failure Rates (If Available)	Number of Equivalent Full Duration Tests

Figure 3

SUGGESTED SUMMARY PRESENTATION FORMAT FOR SUBCONTRACT TASKS

TABLE 6 - SYSTEM DEVELOPMENT COSTS

Typical Subcategories			Actual Costs for "Base" System	Prediction Methods (Equation, Tables, Graphs, etc.) For New Systems	Limitations of Prediction Techniques	Expected Accuracy of Predicted Development Costs
Engineering						
Manufacturing						
Hardware	Comp. A Comp. B Comp. C Etc.		Total testing seconds and No. of equivalent components and engine systems will be shown as a factor in prediction method (to be used in conjunction with reliability development data)			
Pre-Qual. Testing	Components	A B C Etc				
	System					
Quality Assurance Tests			Qual. tests			
Program Manage-ment	Project Engineering Configur. Management PERT and Program Mgt. Submittal of Program Data					

Figure 4

SUGGESTED SUMMARY PRESENTATION FORMAT FOR SUBCONTRACT TASKS

TABLE 8 - SUMMARY OF STERILIZATION OR PLANETARY QUARANTINE DESIGN CONSIDERATIONS

Sub-System	Information Required	STERILIZED SYSTEM								"PLANETARY QUARANTINE"
		Influences on Operating Conditions	Influences on Performance Characteristics	Influences on Material Selection	Influences on Weight	Influences on Development Time	Influences on Development Cost	Influences on Production Cost	Influences on Failure Modes and Expected Reliability	Same as for Sterilized System
"A"	Qualitative Discussion									
	Quantitative Estimates of Influences									
	Most Critical Problem Areas Needing Technology Improvement or Quantitative Study									
"B"										
System										

i.e., (for example only)
1.5 x(Non Sterile System)
1.3 minimum } Discuss primary considerations
1.7 maximum } which would dictate the upper/lower limits

Figure 5
SUGGESTED SUMMARY PRESENTATION FORMAT FOR SUBCONTRACT TASKS

3.0 CONTENTS OF THIS VOLUME

This volume contains the non-proprietary results of the subcontracted solid, RSVP, and hybrid propulsion system investigations.

APPENDIX A

Aerojet-General's Study of Solid Rocket Propulsion Systems for Space Applications. This study is included in its entirety in Volume V. Due to a preponderance of restricted data, it is felt that the non-restricted contents alone would not be of sufficient utility for separate presentation.

APPENDIX B

Thiokol Chemical Corporation's Study of Spherical Solid Rocket Propulsion Systems for Space Applications. Restricted cost data are presented in Volume V.

APPENDIX C

Lockheed Propulsion Company's Study of RSVP Rocket Propulsion Systems for Space Applications. Restricted performance, development, and cost data are presented in Volumes IV and V.

APPENDIX D

United Technology Center's Study of Hybrid and Solid Rocket Propulsion Systems for Space Applications. Restricted cost data are presented in Volume V.

SOLID ROCKET PROPULSION

AEROJET-GENERAL CORPORATION

The Aerojet Solid Propulsion Study has tentatively been included in Volume V. Due to a preponderance of proprietary data, it is felt that the non-restricted contents alone would not be of sufficient utility for separate presentation.

-- APPENDIX A --

SOLID ROCKET PROPULSION

THIOKOL CHEMICAL CORPORATION

E191-67
October 9, 1967

THIOKOL CHEMICAL CORPORATION
ELKTON DIVISION
ELKTON, MARYLAND

FINAL REPORT

PERFORMANCE, WEIGHT AND RELIABILITY STUDY OF SPACE PROPULSION SYSTEMS

PRIME CONTRACT NO. NAS 7-519
SPACE-GENERAL PURCHASE ORDER NO. 1069-P-77816

H. G. Jones
General Manager

12

I. INTRODUCTION

The objectives of this study were:

1. To derive empirical relationships for the prediction of performance and weights for spherical solid propellant rocket motors based on demonstrated performance and weight data;

2. to incorporate these empirical relationships into an available computer program, "Mission Fuel Prerequisite," the purpose being to provide a means of rapidly determining performance and component weights over a wide size and performance range, using a minimal number of design parameters;

3. to evaluate the impulse reproducibility characteristics of spherical rocket motors and relate demonstrated total impulse to specified total impulse for the Surveyor Main Retro (TE-364-1) motor;

4. to describe the design and process controls used to minimize thrust misalignment and offset on the Surveyor Main Retro motor;

5. to qualitatively assess the effect of sterilization and planetary quarantine on motor design/performance parameters; and

6. to cite the quantity of full duration development and qualification tests for the Titan Vernier (TE-M-345) and Surveyor Main Retro, and the reliability estimate at the end of qualification.

During the study, primary emphasis was placed on the modification of the computer program and the compilation of pertinent historical performance and weight data (items 1 and 2). A complete description of program requirements, options, and input and output formats is presented in Section IV and Appendix B.

SUMMARY

Performance and weight statistics of qualified spherical solid propellant rocket motors are analyzed to obtain empirical relationships between design criteria and motor configuration. These equations are used to develop a computer program for the prediction of spherical motor performance and weight based on case, propellant, and mission parameters.

Total impulse reproducibility and thrust misalignment of the Surveyor Main Retro are examined, and thrust vector angular dispersion data obtained during qualification are discussed. Demonstrated reliability figures are presented for the Surveyor Main Retro and the Titan Vernier Motors and methods for determining the level of reliability are examined.

A qualitative discussion of the impact of the sterilization requirement on motor design and performance is presented. Design problems which have been resolved and those in need of further clarification are delineated.

A trade-off study is performed on a typical spherical motor with various combinations of chamber pressure, expansion ratio, and propellant at total impulse levels from 50,000 lbf-sec to 800,000 lbf-sec.

14

TABLE OF CONTENTS

		PAGE
Summary		ii
I.	Introduction	1
II.	Motor Performance Prediction	2
	A. Propellant Weight	2
	B. Case Diameter	10
	C. Burn Time	11
	D. Throat Area	11
III.	Motor Weight Prediction	14
	A. Case Weight	14
	B. Nozzle Weight	17
	C. Insulation Weight	17
	D. Igniter Weight	21
	E. Liner Weight	21
	F. Hardware Weight	25
	G. Attachment Weight	25
IV.	Spherical Performance and Weight Prediction Program	28
	A. Description of Computer Program	28
	B. Parametric Study	31
V.	Total Impulse Reproducibility	32
	A. Impulse Efficiency	32
	B. Theoretical Performance	34
	C. Throat Area Effects	35
	D Demonstrated Impulse Reproducibility	40
VI.	Demonstrated Reliability	44
	A. Reliability Summary for the Surveyor Main Retrograde Motor	44
	B. Reliability Summary for the TE-M-345 (Titan II Vernier)	56
VII.	Thrust Misalignment	57

TABLE OF CONTENTS (Cont'd)

	PAGE
VIII. Effect of Sterilization and Planetary Quarantine on Motor Design and Performance	59
A. Effect of Sterilization on the Propellant-Liner System	59
B. Effects of Differential Expansion	60
C. Thermal Degradation	60
D. Time to Reach Sterilization Temperatures	60
E. Volumetric Loading Density and Web Fraction Constraints	69
IX. Glossary	72

APPENDIXES

A. Spherical Performance and Weight Reduction Program

B. Parametric Study

C. Surveyor Main Retrograde Motor Nozzle Alignment Procedure

LIST OF FIGURES

		PAGE
1.	Typical Spherical Solid Propellant Rocket Motor	3
2.	Case Geometric Parameters	10
3.	Correlation of Spherical Case Diameter Data	13
4.	Correlation of Spherical Case Weight Data ($2 \frac{L}{D} - 1 = 1$)	18
5.	Nozzle Exit Cone Length	19
6.	Correlation of Nozzle Weights	20
7.	Correlation of Insulation Weights	22
8.	Correlation of Igniter Weights	23
9.	Correlation of Liner Weights	24
10.	Correlation of Hardware Weights	26
11.	Correlation of Attachment Weights	27
12.	Theoretical Vacuum Specific Impulse (TP-H-3062)	36
13.	Theoretical Vacuum Thrust Coefficient	37
14.	Typical Throat Area — Time History	39
15.	Thrust and Thrust Misalignment Versus Time	58
16.	Time to Reach Sterilization Temperature Spherical Motor Designs	62
17.	TE-M-385 Temperature Gradient Study — Thermocouple Locations	63
18.	TE-M-385 Temperature Gradient Study — Temperature Distribution	64
19.	TE-M-385 Temperature Gradient Study — Maximum Temperature Gradient	65
20.	Case-Bonded Spherical Circular Perforate Motor Assembly	66
21.	Thermal Model Case-Bonded Spherical Circular Perforate Motor Design	67
22.	Nodal Locations and Notation	68
23.	Temperature Versus Time for Heating by Forced Convection	70
24.	Nodal Temperatures After 40 Hours	71

LIST OF TABLES

		PAGE
I.	Rocket Motor Summary — Motor Performance Characteristics	4
II.	Rocket Motor Summary — Motor/Propellant Characteristics	5
III.	Rocket Motor Summary — Case Configuration-Materials	6
IV.	Rocket Motor Summary — Case Configuration-Geometry	7
V.	Rocket Motor Summary — Nozzle Configuration-Geometry	8
VI.	Rocket Motor Summary — Nozzle Configuration-Materials	9
VIIA.	Rocket Motor Summary — Motor Component Weights	15
VIIB.	Rocket Motor Summary — Motor Component Weights	16
VIII.	Spherical Performance and Weight Prediction Program (E40310) Requirements and Options	29
IX.	Propellant Ballistic Properties	30
X.	Surveyor Main Retro Total Impulse Reproducibility	41
XI.	Specific Impulse Reproducibility	42
XII.	Specific Impulse Efficiency Summary	43
XIII.	Subsystem and Component Test Summary	45
XIV.	Reliability of Surveyor Main Retrograde Motor (TE-M-364-1)	55
XV.	Reliability of Titan II Vernier (TE-M-345)	56

18

II. MOTOR PERFORMANCE PREDICTION

The family of spherical solid propellant rocket motors developed by the Thiokol Chemical Corporation for space and upper-stage application typically uses pyrogen ignition systems with redundant cartridge-type initiators, case-bonded grains of composite propellant, metallic cases, and elastomeric insulation. A single nozzle of convergent-divergent design is usually partially submerged in the combustion chamber. These design features are illustrated in Figure 1.

Tables I and II summarize basic performance and Tables III through VI summarize configuration characteristics of currently available Thiokol spherical motors. The significant design differences between these motors can be summarized as follows:

1) Length and diameter
2) Propellant formulation (specific impulse and density)
3) Propellant burn rate
4) Propellant volumetric loading density
5) Case material (strength-to-density ratio)
6) Case design safety factor
7) Nozzle expansion ratio and expansion contour
8) Nozzle structural design sophistication
9) Total impulse reproducibility tolerance
10) Thrust alignment and offset tolerance
11) Vehicle attachment design complexity and weight

There also have been vast differences in the amount of qualification testing and in the quality assurance program requirements.

The equations used for the prediction of spherical motor performance are described below. They are derived from well-known fundamental ballistic and geometric relations and have been verified many times by actual test firings.

A. PROPELLANT WEIGHT

The propellant weight required to achieve a given total impulse can be determined from the equation:

$$W_p = \frac{I_{tot}}{I_{sp}} \tag{1}$$

On the other hand, if the total impulse requirement is unknown, but instead the gravity-free velocity increment is given, the propellant weight required can be determined from the total stage weight and the propellant specific impulse:

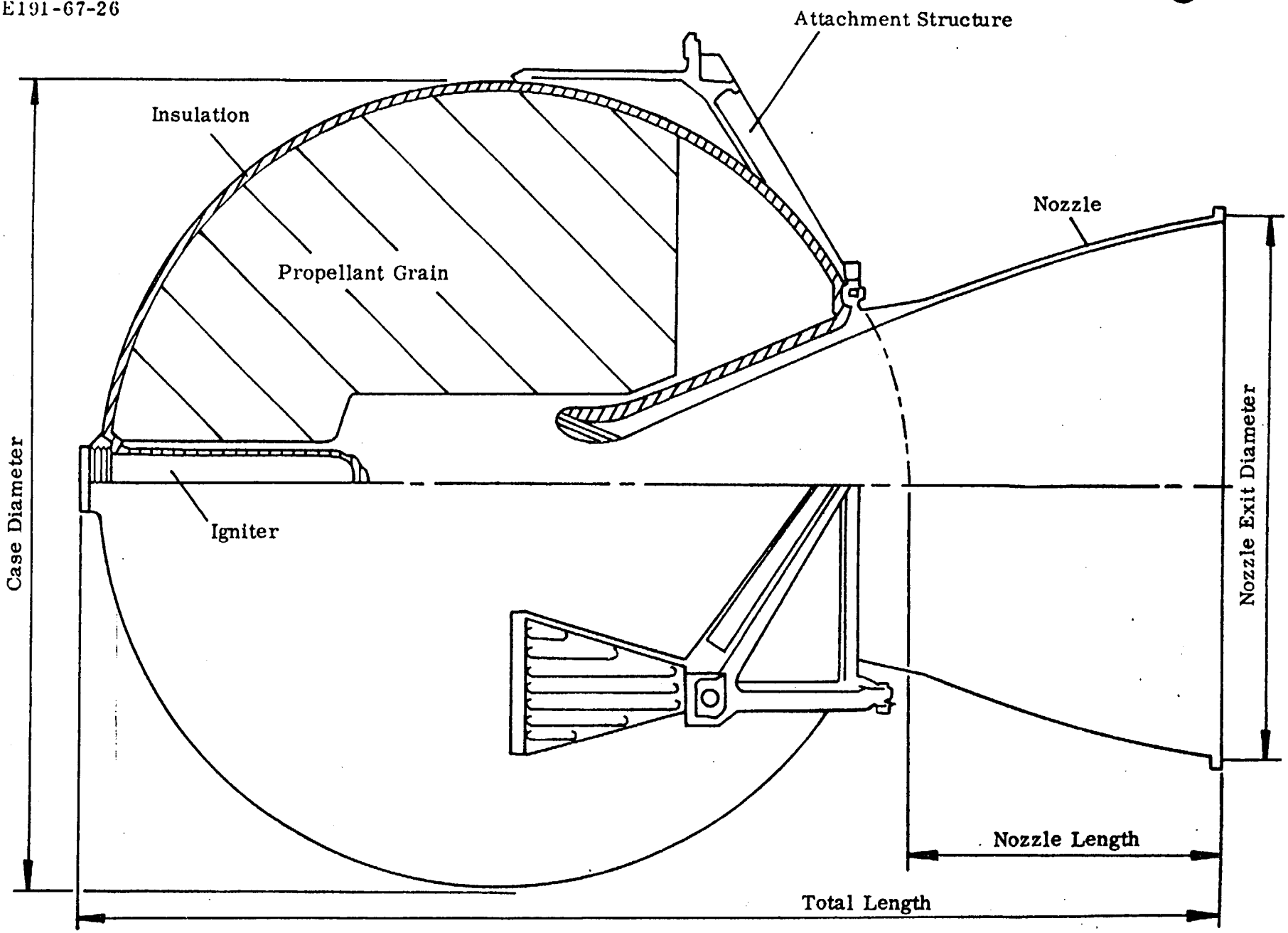

FIGURE 1. TYPICAL SPHERICAL SOLID PROPELLANT ROCKET MOTOR

TABLE I

ROCKET MOTOR SUMMARY

Motor Performance Characteristics

Motor	Case Diameter, in.	Total Impulse, lbf-sec	Average Thrust, lbf	Average Pressure, psi	Maximum Pressure, psi
TE-M-184-3	25.06	129,800	7600	490	585
TE-M-186-2	40.1	443,000	16800	595	727
TE-M-345	13.52	18,200	838	565	607
TE-M-345-11	13.52	17,652	841	565	607
TE-M-360	37.0	414,000	8700	460	590
TE-M-364	37.0	347,130	8376	481	570
TE-M-364-1	37.0	357,000	8930	511	561
TE-M-364-2	37.0	402,000	9248	539	600
TE-M-364-3	37.0	415,440	8945	598	613
TE-M-375	13.52	17,300	776	524	565
TE-M-385	12.8	14,000	2150	790	865
TE-M-427	13.52	17,875	1066	540	620
TE-M-442	26.0	140,000	6420	720	785
TE-M-444	13.52	21,200	1370	855	965
TE-M-456	15.0	24,500	2500	470	575
TE-M-458	13.5	18,780	841	500	560
TE-M-479	17.4	44,500	2290	800	840

TABLE II

ROCKET MOTOR SUMMARY

Motor/Propellant Characteristics

Motor	Propellant	Density, lbs/in.^{3}	Web Fraction, %	Volumetric Loading Density, %	Internal Configurati
TE-M-184-3	TP-H-3034	0.063	36	93.0	9 Pt. Star
186-2	TP-H-3034	0.063	36	94.0	9 Pt. Star
345	TP-G-3129	0.0621	60	82.0	8 Pt. Star
345-11	TP-G-3129	0.0621	60	82.0	8 Pt. Star
360	TP-H-3062	0.0626	60	88.0	8 Pt. Star
364	TP-H-3062	0.0626	56	73.5	7 Pt. Star
364-1	TP-H-3062	0.0626	56	76.0	7 P[illegible] [illegible]tar
364-2	TP-H-3062	0.0626	60	85.5	8 P[illegible] [illegible]ar
364-3	TP-H-3062	0.0626	60	95.8	8 Pt. Star
375	TP-G-3129	0.0621	60	77.5	8 Pt. Star
385	TP-L-3014A	0.0632	60	83.5	8 Pt. Star
427	TP-H-3109	0.0604	60	85.0	8 Pt. Star
442	TP-H-3114	0.0626	61	91.8	8 Pt. Star
444	TP-H-3062	0.0626	62	91.2	8 Pt. Star
456	TP-L-3098	0.0628	50	89.9	7 Pt. Star
458	TP-G-3129	0.0621	62.4	86.0	8 Pt. Star
479	TP-H-3062	0.0626	60	90.0	8 Pt. Star

ROCKET MOTOR SUMMARY

Case Configuration - Materials

Motor	Case Material	Material Thickness, in.	Material Strength, psi	Material Density, lbs/in.^{3}
TE-M-184-3	4130	0.030	180,000	0.283
186-2	4130	0.030	180,000	0.283
345	17-7 PH Cond. TH-1050 Stain. Steel	0.036	150,000	0.276
345-11	17-7 PH Cond. TH-1050 Stain. Steel	0.036	150,000	0.276
360	Ladish D6AC	0.039	200,000	0.283
364	Ladish D6AC	0.039	200,000	0.283
364-1	Ladish D6AC	0.039	200,000	0.283
364-2	Ladish D6AC	0.039	200,000	0.283
364-3	Ladish D6AC	0.039	200,000	0.283
375	SST 17-7 PH	0.036	150,000	0.276
385	6 Al-4V Titanium	0.04	155,000	0.160
427	SST 17-7 PH	0.036	150,000	0.276
442	Ladish D6AC	0.038 (+0.006)	200,000	0.283
444	Stainless 17-7 PH	0.036	150,000	0.276
456	6 Al-4V Titanium	0.018	144,000	0.160
458	6 Al-4V Titanium	0.036	144,000	0.160
479	6 Al-4V Titanium	0.038	155,000	0.160

TABLE IV

ROCKET MOTOR SUMMARY
Case Configuration — Geometry

Motor	Nozzle Length, in.	Case Diameter, in.	Case Safety Factor
TE-M-184-3	17.03	25.1	1.4
TE-M-186-2	21.7	40.1	1.5
TE-M-345	7.9	13.5	1.9
TE-M-345-11	6.8	13.5	2.0
TE-M-360	–	37.0	–
TE-M-364	31.1	37.0	1.6
TE-M-364-1	31.1	37.0	1.6
TE-M-364-2	31.1	37.0	–
TE-M-364-3	31.1	37.0	–
TE-M-375	8.0	13.5	2.0
TE-M-385	10.9	12.7	–
TE-M-427	12.4	13.5	–
TE-M-442	14.3	26.0	1.5
TE-M-444	11.9	13.5	1.4
TE-M-456	9.2	15.0	–
TE-M-458	10.4	13.5	–
TE-M-479	13.8	17.4	–

TABLE V

ROCKET MOTOR SUMMARY

Nozzle Configuration — Geometry

Motor	Throat Area, in.^{2}	Expansion Ratio	Degree of Submergence, %	Exit Half Angle, °	Initial Turning Angle, °
TE-M-184-3	8.788	13.8	0.0	16.0	16.0
TE-M-186-2	19.05	12.8	0.0	18.0	18.0
TE-M-345	0.845	30.0	28.5	17.0	17.0
TE-M-345-11	0.801	22.8	38.1	17.0	17.0
TE-M-360	8.5	46.0	-	15.0	15.0
TE-M-364	8.978	53.0	39.8	14.5	25.0
TE-M-364-1	8.5	53.0	39.8	14.5	25.0
TE-M-364-2	8.5	53.2	39.8	14.5	25.0
TE-M-364-3	8.53	53.0	39.8	14.5	25.0
TE-M-375	0.802	60.0	19.1	17.0	32.0
TE-M-385	1.86	23.0	20.6	16.0	16.0
TE-M-427	1.048	48.2	12.5	15.0	15.0
TE-M-442	6.55	18.7	31.6	20.0	20.0
TE-M-444	0.90	56.0	17.2	17.0	17.0
TE-M-456	6.11	9.0	24.5	18.35	18.35
TE-M-458	0.945	43.3	25.7	17.0	17.0
TE-M-479	1.67	53.2	22.8	15.0	25.0

TABLE VI

ROCKET MOTOR SUMMARY

Nozzle Configuration — Materials

Motor	Material Body	Material Throat Insert
TE-M-184-3	Fiberite MX-2625	ATJ Graphite
TE-M-186-2	Fiberite MX-2625	ATJ Graphite
TE-M-345	Vitreous Silica Phenolic	ATJ Graphite
TE-M-345-11	Vitreous Silica Phenolic	ATJ Graphite
TE-M-360	Bulk Carbon Fiber-Phenolic	Graphite
TE-M-364	Bulk Carbon Fiber-Phenolic	Graph-I-Tite G-90
TE-M-364-1	Bulk Carbon Fiber-Phenolic	Graph-I-Tite G-90
TE-M-364-2	Bulk Carbon Fiber-Phenolic	Graphite
TE-M-364-3	Bulk Carbon Fiber-Phenolic	Graphite
TE-M-375	Vitreous Silica Phenolic	ADHG Graphite
TE-M-385	Carbon Fabric	CGW Graphite
TE-M-427	Carbon Fabric	Graph-I-Tite G-90
TE-M-442	Vitreous Silica Phenolic	Graph-I-Tite G-90
TE-M-444	Vitreous Silica Phenolic	ATJ Graphite
TE-M-456	ZK60Z-T5 Magnesium - Asbestos Phenolic	ATJ Graphite
TE-M-458	Vitreous Silica Phenolic	Graph-I-Tite G-90
TE-M-479	Vitreous Silica Phenolic	Graph-I-Tite G-90

$$W_p = W_s \left[1 - \exp\left(-\frac{\Delta V}{gI_{sp}}\right)\right] \tag{2}$$

B. CASE DIAMETER

Once the propellant weight is known, the volume of the case that will be required to contain it at a given volumetric loading density can be calculated. Volumetric loading density (VLD) is the percentage of the total available case volume that is occupied by the propellant. That is,

$$\text{Total Required Volume} = \frac{W_p}{\rho_p\,(VLD)} \tag{3}$$

By assuming that the case is either spherical or an extended sphere as shown in Figure 2,

E191-67-28

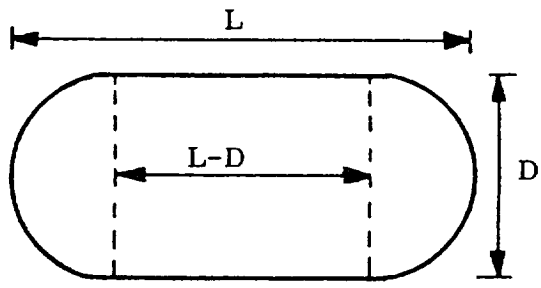

FIGURE 2. CASE GEOMETRIC PARAMETERS

the volume can be determined as a function of the diameter and length-to-diameter ratio. Thus,

$$V = \frac{4}{3}\pi r^3 + \pi r^2 (L-D)$$

or

$$V = \frac{\pi}{12} D^3 \left(3\frac{L}{D} - 1\right) \tag{4}$$

Since the required volume is known from (3) above, the case diameter can be found in terms of known quantities. That is, setting the right side of equations (3) and (4) equal to each other one obtains the relation

$$D = \sqrt[3]{\frac{12W_p}{\pi \rho_p \, (VLD) \, (3 \, \frac{L}{D} - 1)}} \tag{5}$$

Figure 3 illustrates the excellent correlation that exists between theoretical and actual diameters for spherical motors ($\frac{L}{D} = 1$) produced to date.

C. BURN TIME

The burn time of a solid-propellant rocket motor is only dependent on propellant web thickness and chamber pressure. Since the burn rate-chamber pressure relation is

$$r_b = a \, (P_c)^n \tag{6}$$

and the web thickness is equal to the web fraction times the case radius, burn time is defined by:

$$t_b = \frac{W_f \, D \, (P_c)^{-n}}{2a} \tag{7}$$

D. THROAT AREA

The throat area is found from the average thrust equation

$$\overline{F} = \frac{I_{tot}}{t_b} = P_c \, A_t \, C_f \, C_D \, \lambda \tag{8}$$

For nozzles used on spherical rocket motors, the product $C_D \, \lambda$ is approximately equal to 0.96. Since P_c, I_{tot}, and t_b are known, and C_f can be calculated by iteration from the relation

$$C_f = \sqrt{\frac{2\gamma}{\gamma - 1} \left(\frac{2}{\gamma + 1}\right)^{\frac{\gamma + 1}{\gamma - 1}} \left[1 - \left(\frac{P_e}{P_c}\right)^{\frac{\gamma - 1}{\gamma}}\right]}, \tag{9}$$

by rearrangement of equation (8) the throat area can be found from the equation

$$A_t = \frac{I_{tot}}{0.96\,(t_b\,P_c\,C_f)} \tag{10}$$

Since the exit area is the product of the throat area and expansion ratio, the throat and exit diameters are easily found.

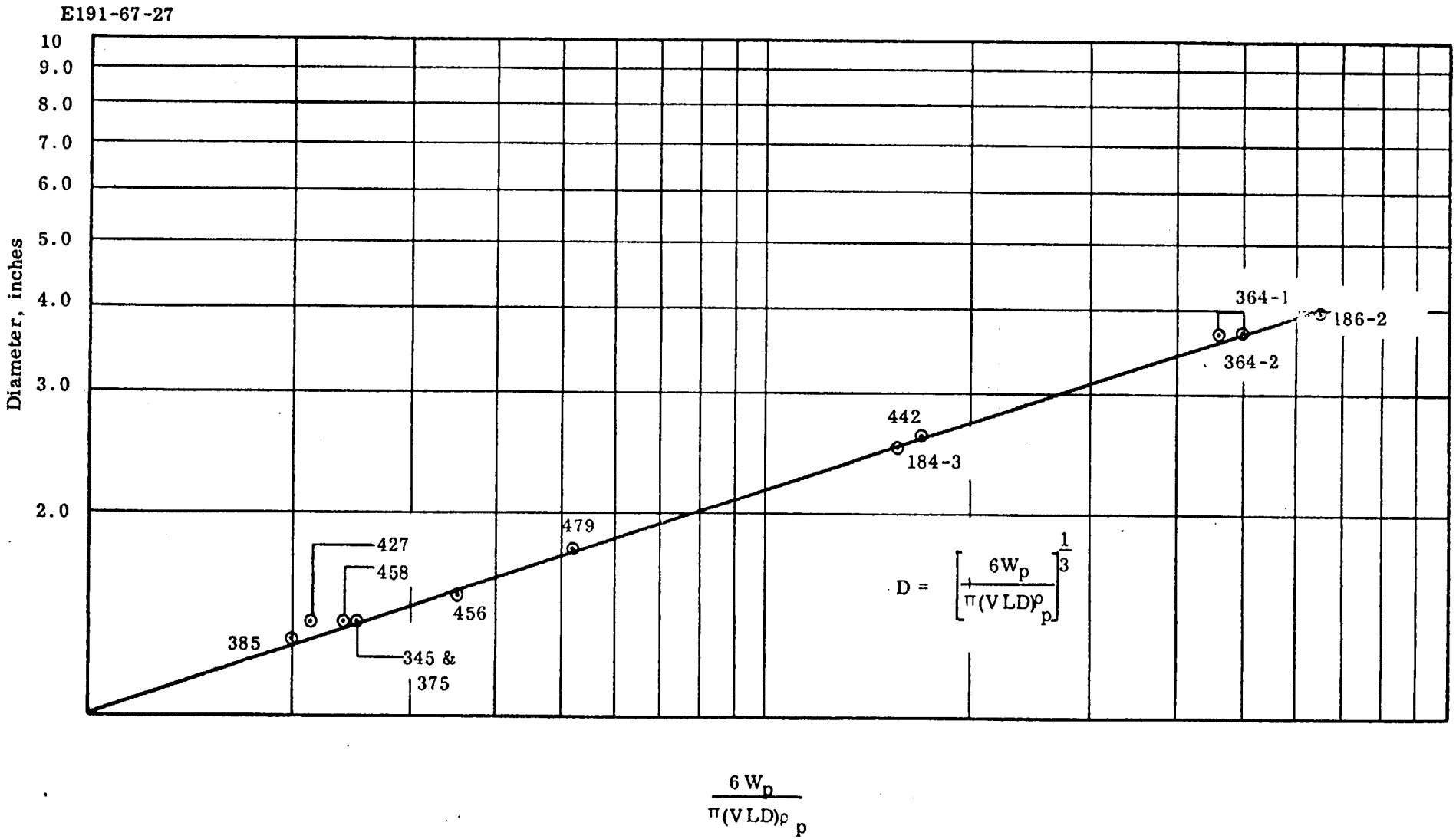

FIGURE 3. CORRELATION OF SPHERICAL CASE DIAMETER DATA

III. MOTOR WEIGHT PREDICTION

The empirical relations derived in this section represent the best curve fit to available motor weight data. For motors which are designed for special applications, such as spin stabilization or for use in high acceleration environments, one must use slightly altered equations to predict the proper weights. A tabulation of spherical motor component weight data is presented in Tables VIIA and VIIB.

A. CASE WEIGHT

The weight of a rocket motor case is dependent on the quantity and density of the case material. For a sphere, the stress in the wall can be calculated from the equation:

$$\sigma = \frac{P_{max} D}{\tau} \tag{11}$$

where P_{max} is the maximum chamber pressure, D is the diameter of the sphere, and τ is the wall thickness. If the case material yield strength is substituted for σ in equation 6, the minimum case wall thickness can be found. This thickness must be increased by a safety factor (S.F.) to get the final case thickness

$$\tau = \frac{P_{max} D (S.F.)}{\sigma} \tag{12}$$

Since the volume of case material required for a spherical case is the product of the case thickness and the surface area, where

$$\text{Spherical Surface Area} = \pi D^2, \tag{13}$$

the case weight is obtained from the product of the material volume and density,

$$W_c = \frac{\pi P_{max} D^3 \rho_c (S.F.)}{\sigma} \tag{14}$$

The extended spherical case has a cylindrical section inserted between the hemispherical end caps. The cylindrical section must be approximately twice as thick as the end sections to maintain the same strength at all points. To calculate the weight of an extended case, the weight of a spherical case of the same diameter must be increased by a factor equal to the ratio of the extended case mass to the spherical case mass. The extended case weight is proportional to the surface area of the spherical ends plus twice the surface area of the cylindrical section. Thus, since cylindrical surface area is equal to $\pi D (L-D)$, and the correction factor for extended cases is $(2 \frac{L}{D} - 1)$,

TABLE VIIA

ROCKET MOTOR SUMMARY

Motor Component Weights

Motor	Case Weight, lbs	Nozzle Weight, lbs	Propellant Weight, lbs	Attachment Weight, lbs
TE-M-184-3	16.43	10.11	477.56	0
TE-M-186-2	95.48	33.77	1995.0	0
TE-M-345	6.22	2.34	66.5	0
TE-M-345-11	6.22	1.98	66.49	0
TE-M-364	55.23	48.00	1191.0	—
TE-M-364-1	56.26	48.8	1197.0	14.4
TE-M-364-2	55.2	49.4	1388.0	19.3
TE-M-364-3	69.4*	41.7	1440.0	7.5*
TE-M-364-5	54.6	48.8	1300.0	14.3
TE-M-364-8	45.6	41.7	1425.0	10.6
TE-M-375	6.82	2.64	63.0	0
TE-M-385	4.2	4.72	55.4	2.0
TE-M-442	39.6*	22.2	517.0	11.8*
TE-M-444	6.85	3.32	73.48	2.06
TE-M-458	4.79	2.92	68.3	1.5
TE-M-479	8.80*	6.75	153.5	1.43*

*Includes Marmon mounting flange and back up.

TABLE VIIB

ROCKET MOTOR SUMMARY

Motor Component Weights

Motor	Igniter Weight, lbs	Insulation Weight, lbs	Liner Weight, lbs	Hardware Weight, lbs
TE-M-184-3	1.42	3.24	1.33	4.83
TE-M-186-2	1.875	20.0	3.37	10.3
TE-M-345	0.87	1.82	0.45	3.181
TE-M-345-11	1.56	1.82	0.45	0.68
TE-M-364	5.8	11.5	2.27	1.5
TE-M-364-1	7.7	10.75	1.99	1.68
TE-M-364-2	2.7	15.7	0.79	1.52
TE-M-364-3	3.7	15.5	0.68	1.62
TE-M-364-5	2.7	12.0	0.91	2.2
TE-M-364-8	2.6	12.4	1.0	1.68
TE-M-375	0.87	1.43	0.2	1.04
TE-M-385	0.82	1.39	0.35	0.28
TE-M-442	2.35	8.67	0.6	0.5*
TE-M-444	0.82	1.4	0.2	0.2
TE-M-458	0.76	1.59	0.17	0.2
TE-M-479	0.82	3.55	0.29	0.27

*Does not include 0.26 lb bracket.

$$W_c = \pi D^3 P_{max} (S.F.) \frac{\rho_c}{\sigma} (2 \frac{L}{D} - 1) \quad (15)$$

for all cases.

This expression must be modified by an emperical constant $(\frac{1}{\pi})$ to account for the weight loss due to a section being extracted for the nozzle attachment port. This constant, when incorporated into equation 15,yields the final equation (16) as derived from historical data (See Figure 4):

$$W_c = D^3 P_{max} (S.F.) \frac{\rho_c}{\sigma} (2 \frac{L}{D} - 1). \quad (16)$$

B. NOZZLE WEIGHT

The nozzle weight of a spherical rocket motor is dependent on the throat area and expansion ratio, and on the degree of submergence of the nozzle. The greater the submergence, the more insulation that is required to keep the nozzle load bearing structure cool. The degree of submergence (S) of the nozzle (see Figure 5) is the ratio of the internal length to the total length of the nozzle. Figure 6 demonstrates the correlation between nozzle weight and the nozzle weight parameter. The prediction equation is:

$$W_n = 0.431 \left(\frac{A_e A_t}{1-S}\right)^{0.512} \quad (17)$$

The product $A_e A_t$ is a measure of the average size of the nozzle and the term 1-S gives an estimate of what percentage of the nozzle does not require the heavy insulation necessary to withstand the high temperatures of the motor cavity.

The two points that lie furthest from the curve are the TE-M-442, which is heavier in almost all aspects than other motors of the same size, and the TE-M-184-3, which was designed to be a very light-weight motor.

C. INSULATION WEIGHT

Since the temperature of the internal combustion gases is essentially constant, and since insulation erodes at a constant rate, the minimum thickness of insulation required to maintain the case wall below a given temperature is a function of the burn time. The most critical area to be protected is the surface of the case not protected by the propellant mass. This area is proportional to the square of the diameter. The weight of insulation is dependent only on the volume of insulation that is used, and the parameter $D^2 t_b$ is related to the volume of insulation by the insulation erosion rate and the protected surface area.

E191-67-29

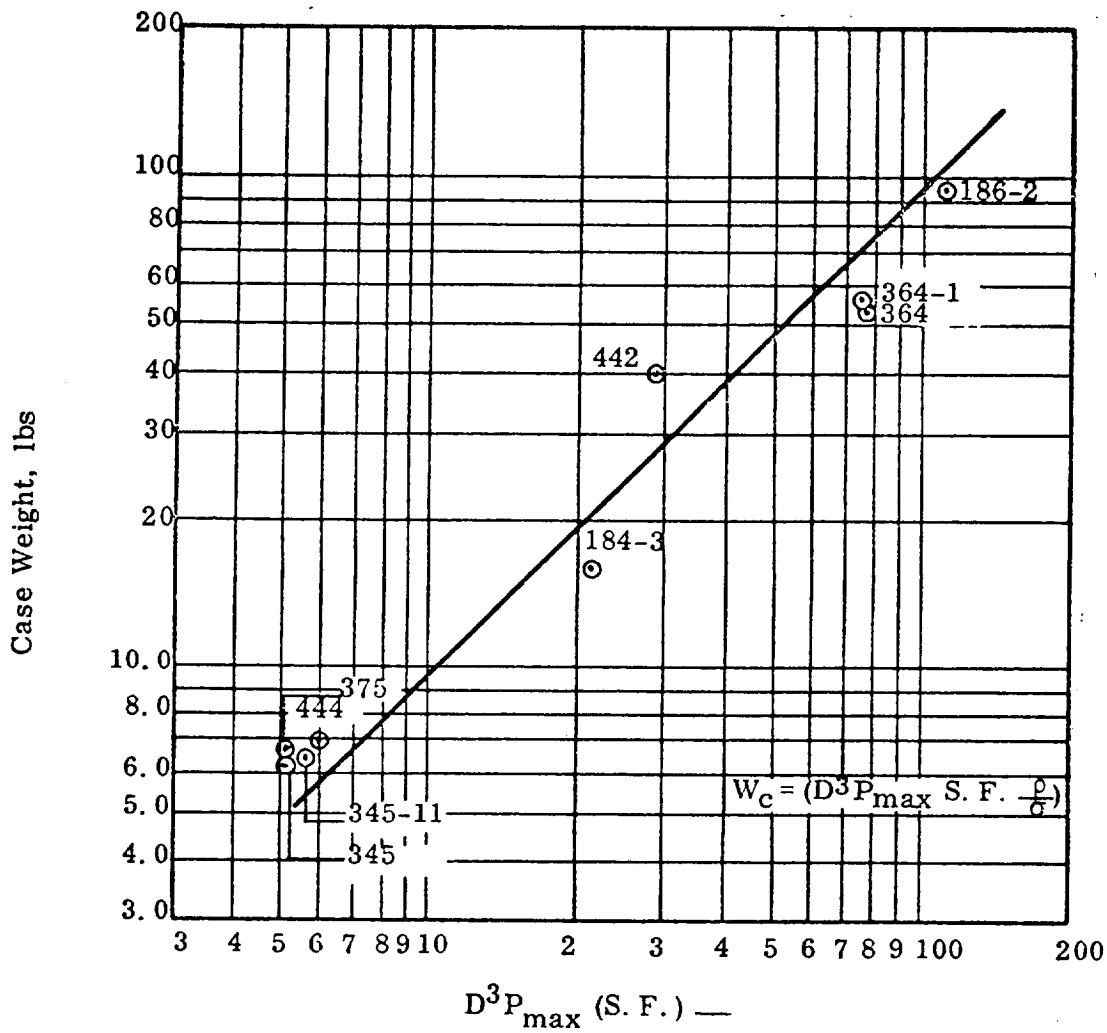

FIGURE 4. CORRELATION OF SPHERICAL CASE WEIGHTS ($2\frac{L}{D} - 1 = 1$)

35

Known Quantities

Nozzle Submergence = S
Exit Diameter = D_e
Throat Diameter = D_t
Nozzle Exit Cone Half Angle = 20°
Case Diameter = D

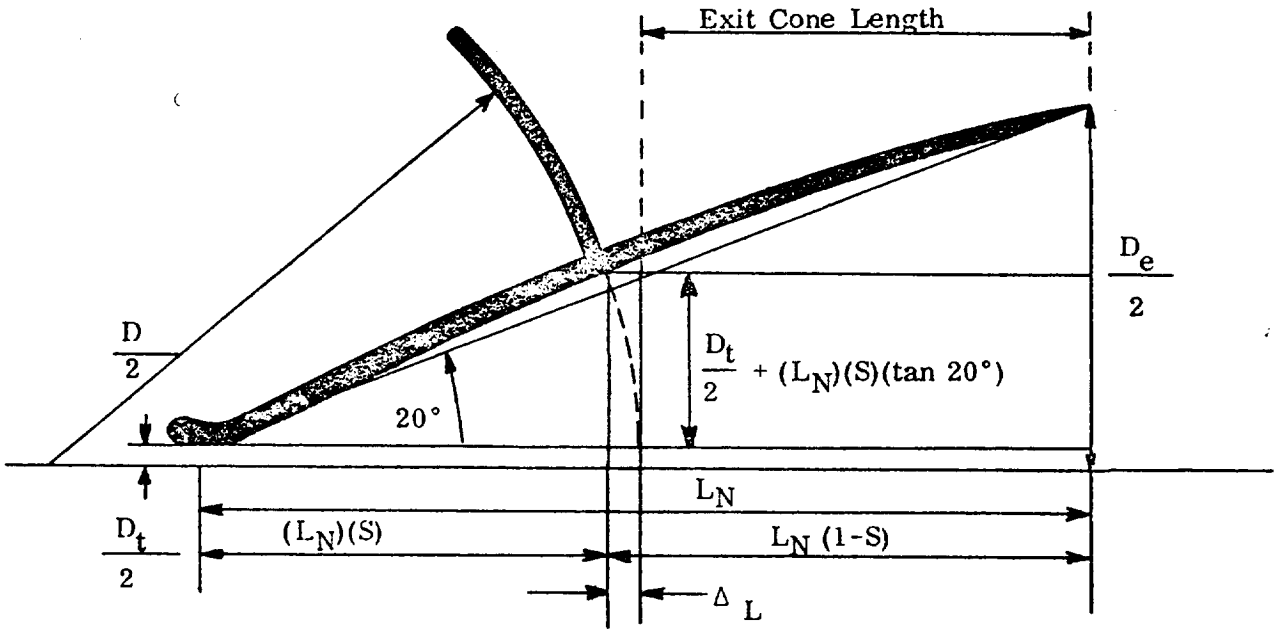

$$L_N = \frac{D_e - D_t}{2 \tan 20°}$$

$$\Delta L = \frac{D}{2} - \sqrt{\frac{D^2}{4} - \left[\frac{D_t}{2} + (L_N)(S)(\tan 20°)\right]^2}$$

Exit Cone Length = $L_N(1-S) - \Delta L$

FIGURE 5. NOZZLE EXIT CONE LENGTH

E191-67-31

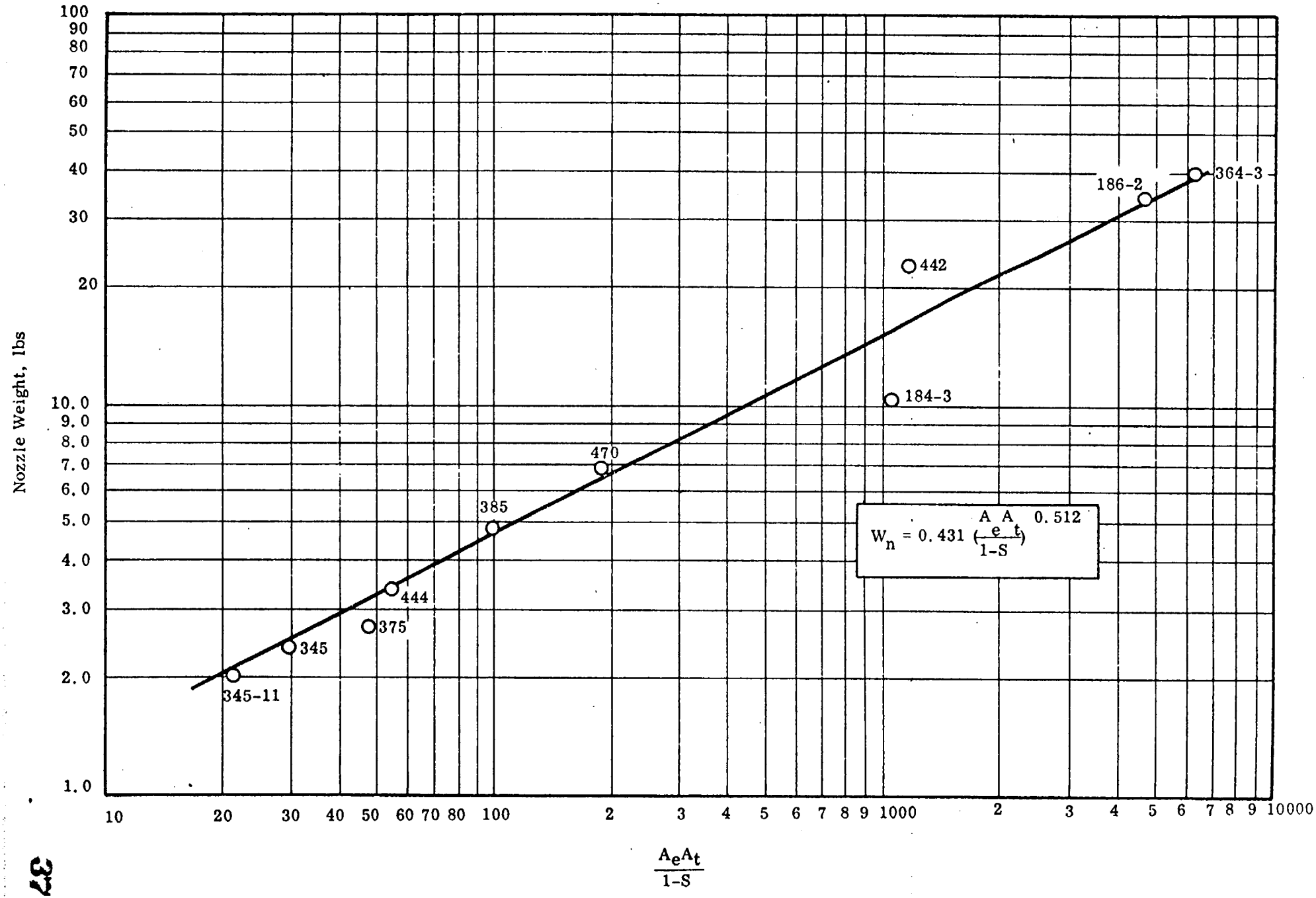

FIGURE 6. CORRELATION OF NOZZLE WEIGHTS

37

The actual insulation weights shown in Figure 7 fall close to the line

$$W_{ins} = 0.00345 \, (D^2 t_b)^{0.673} \left(\frac{L}{D}\right) \tag{18}$$

The two motors that deviate from this line the most are the TE-M-186-2 and the TE-M-442. The TE-M-186-2 was an experimental 40-inch diameter motor built for NASA to establish the feasibility of large spherical motors. Because of its experimental nature, the TE-M-186-2 was overinsulated to ensure that it would not fail. The TE-M-442 is a spin-qualified motor which was insulated up to the maximum permitted by the design requirements and which included a small insulation plug at the head end of the motor to prevent burn through by the vortex which forms in the internal cavity a spinning motor. For this reason, it deviates significantly from other motors with respect to insulation weight. With the exception of these two data points, Figure 7 shows a high degree of correlation between equation (18) and the actual insulation weights. It should be noted that the insulation weight as predicted by equation 18 is adjusted by a surface area correction factor for extended cases.

D. IGNITER WEIGHT

The igniter is a small rocket motor or pyrotechnic device which helps to pressurize the chamber as well as start the burning of the main charge. For this reason, the igniter mass flow rate and, thus, igniter weight must increase as the motor throat area increases. Variations in igniter weight for a given throat area depend on how short an ignition time is desired. Igniter weight is plotted against motor throat area in Figure 8. The equation derived from this plot is

$$W_{ig} = 0.92 \, A_t^{0.5} \tag{19}$$

The TE-M-364 shows a large deviation from the predicted igniter weight. This is due to the fact that the TE-M-364 was the first Surveyor motor to be fired and the igniter was oversized by a large margin. The TE-M-184-3 was one of the first spherical motors to be built by Thiokol; the requirements were for a minimum weight system. This dictated the use of a light igniter with less attention paid to the ignition delay time.

E. LINER WEIGHT

The liner weight is proportional to the surface area of the motor case, which is, in turn, related to the square of the case diameter. The equation of the straight line in Figure 9 is:

$$W_l = 0.00175 \, D^2 \tag{20}$$

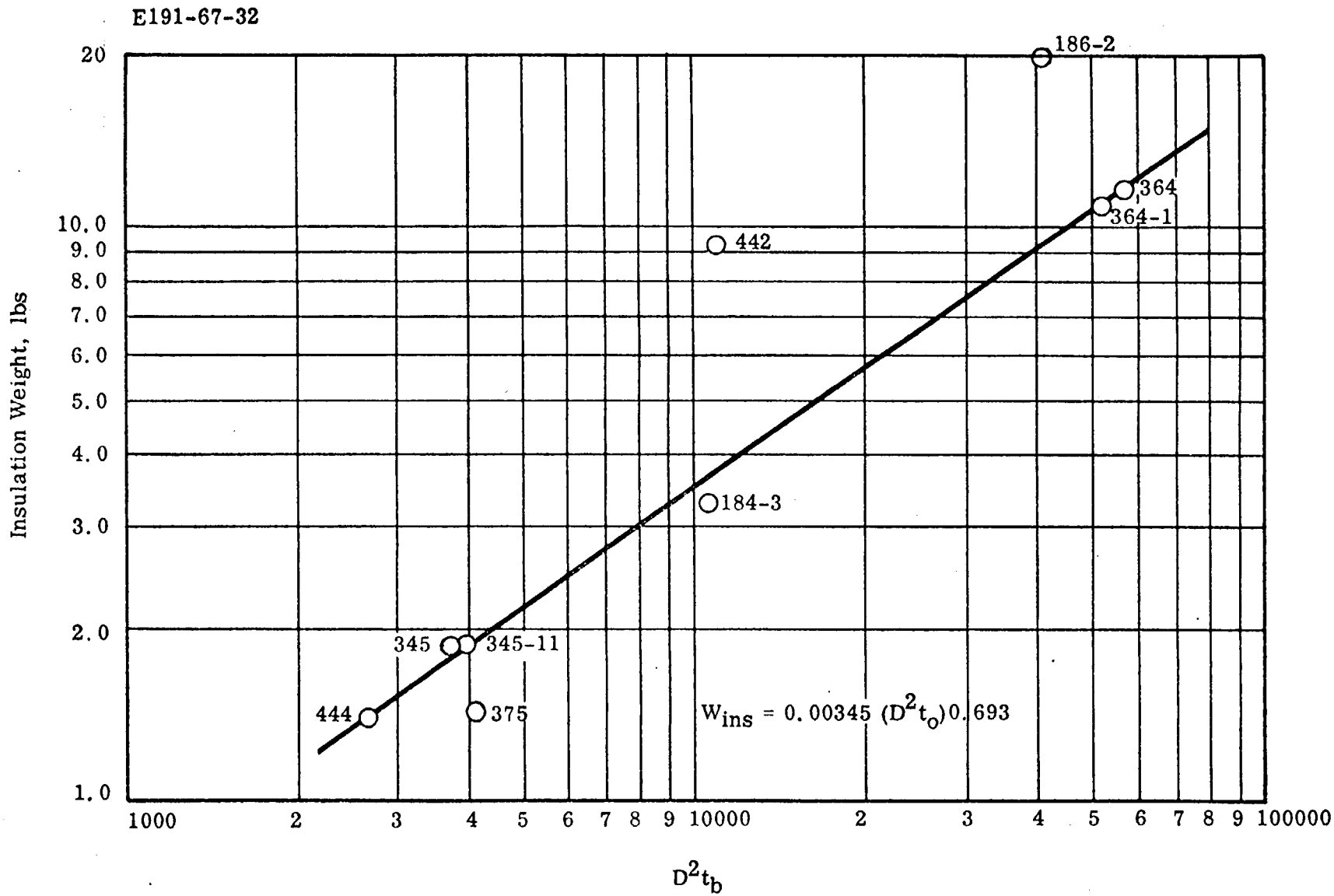

FIGURE 7. CORRELATION OF INSULATION WEIGHTS

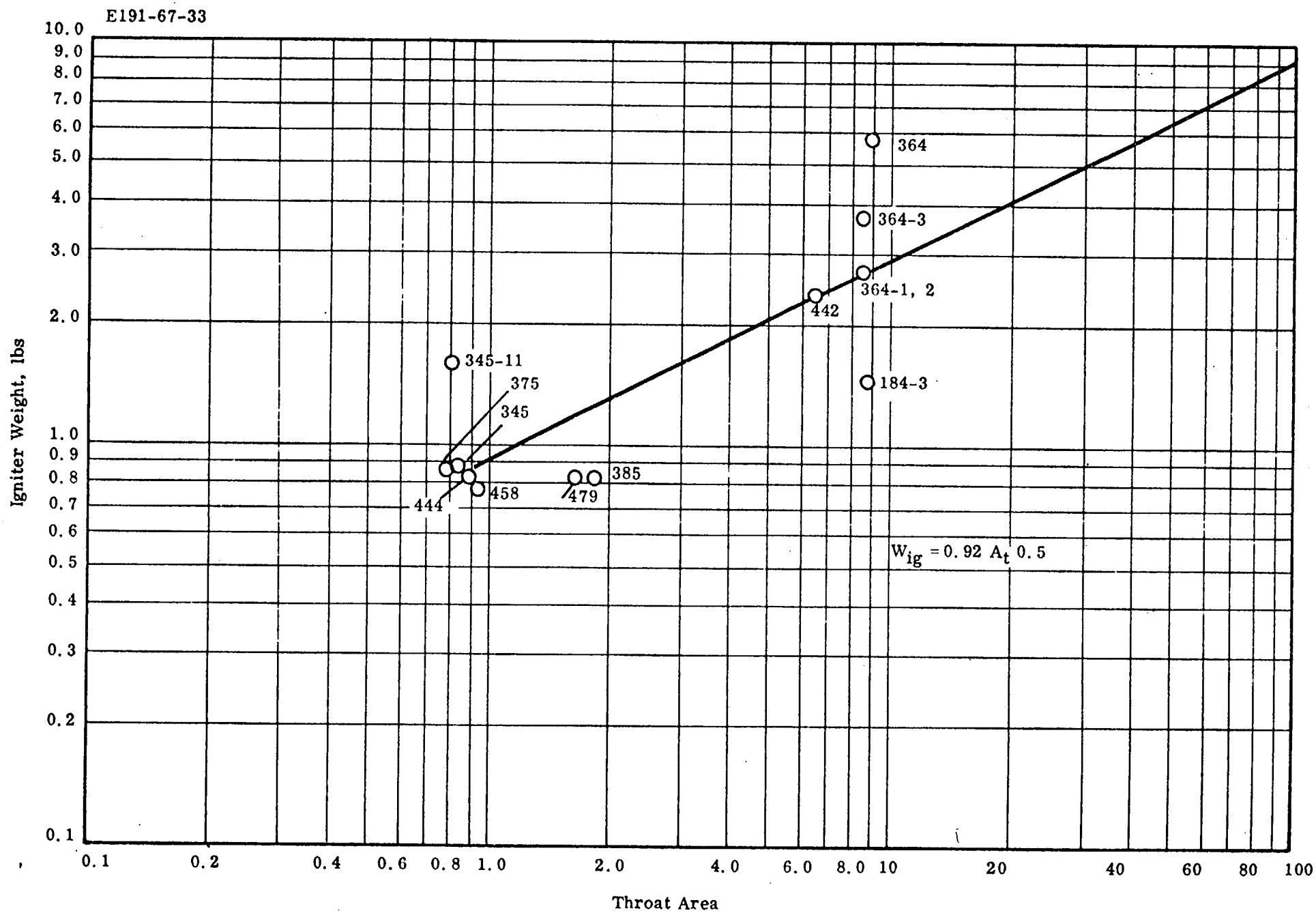

FIGURE 8. CORREL ON OF IGNITER WEIGHTS

E191-67-34

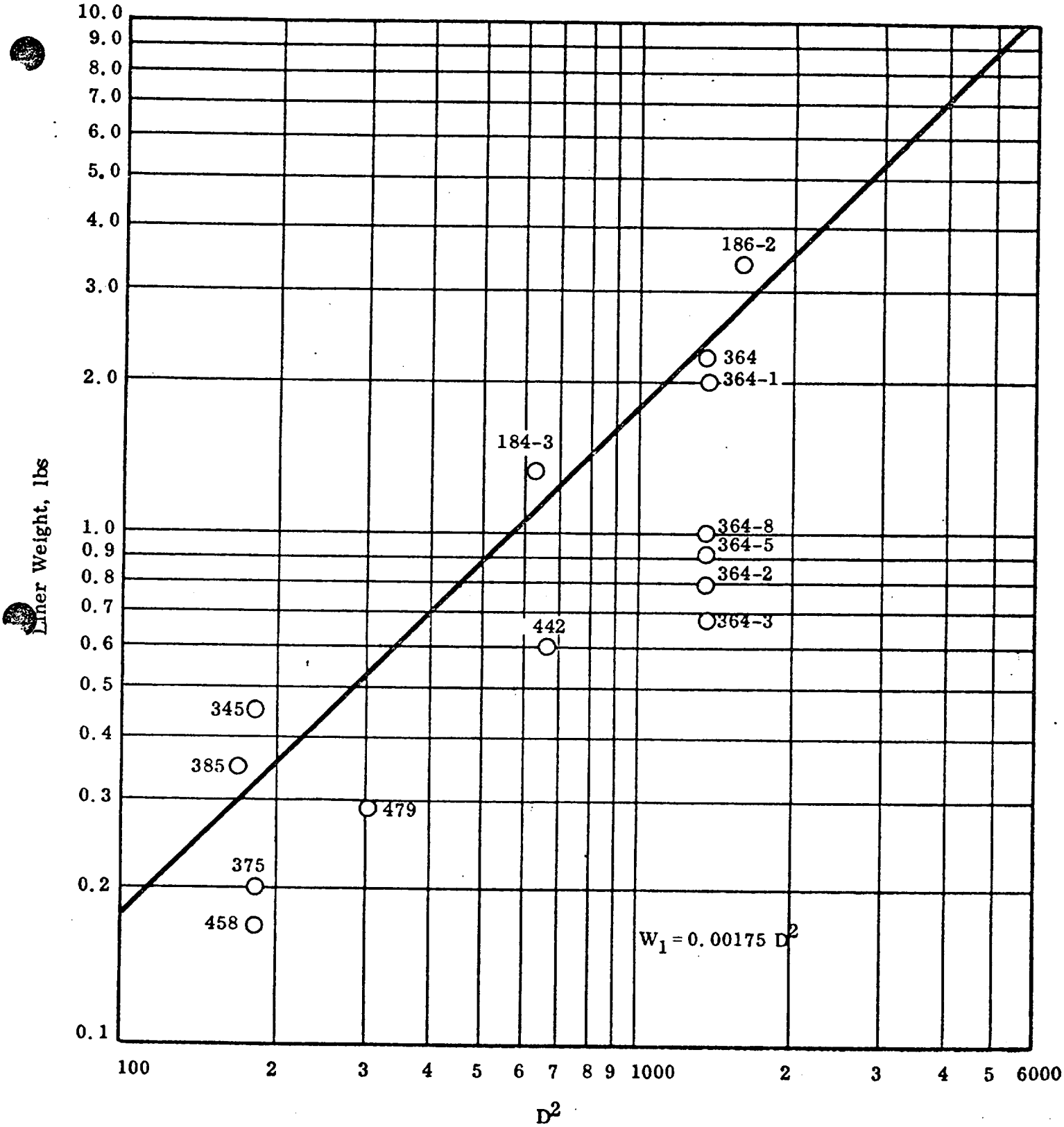

FIGURE 9. CORRELATION OF LINER WEIGHTS

and predicts the maximum expected liner weight. The liner weight is quite small in comparison with the propellant weight (much less than 1%) and because of this, the prediction accuracy can be relaxed somewhat.

F. HARDWARE WEIGHT

Hardware consists of the various nuts and bolts, clips, pins, and other objects that cannot be classified under some other category. Hardware weights appear to be only mildly related to diameter but are more closely related to this parameter than to any other. The equation used to predict hardware weight is (see Figure 10):

$$W_h = \frac{D^3}{15742} \tag{21}$$

G. ATTACHMENT WEIGHT

The weight of the attachment structure is more a function of the particular motor in question than it is of the diameter. If the weight of the mounting bracket is made up of braces and thrust plates, the attachment structure weight will be higher than if it consists simply of a Marmon flange, with the support structure weight credited to the spacecraft. Of course, the attachment weight will increase with the diameter of the motor and this increase is reflected in the attachment weight prediction equation:

$$W_{att} = 0.01\ D^2 \tag{22}$$

which was obtained from the correlation shown in Figure 11.

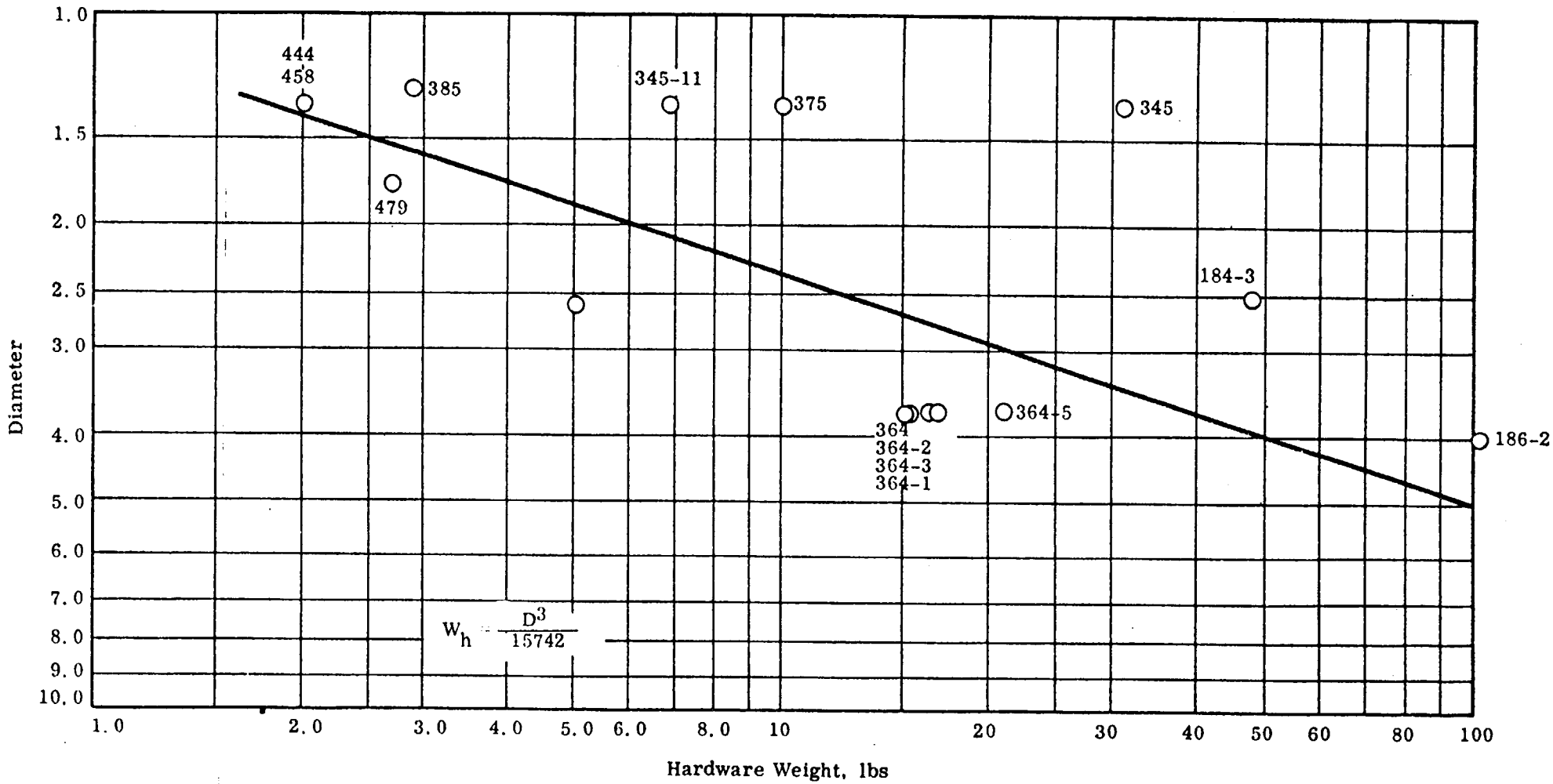

FIGURE 10. CORRELATION OF HARDWARE WEIGHTS

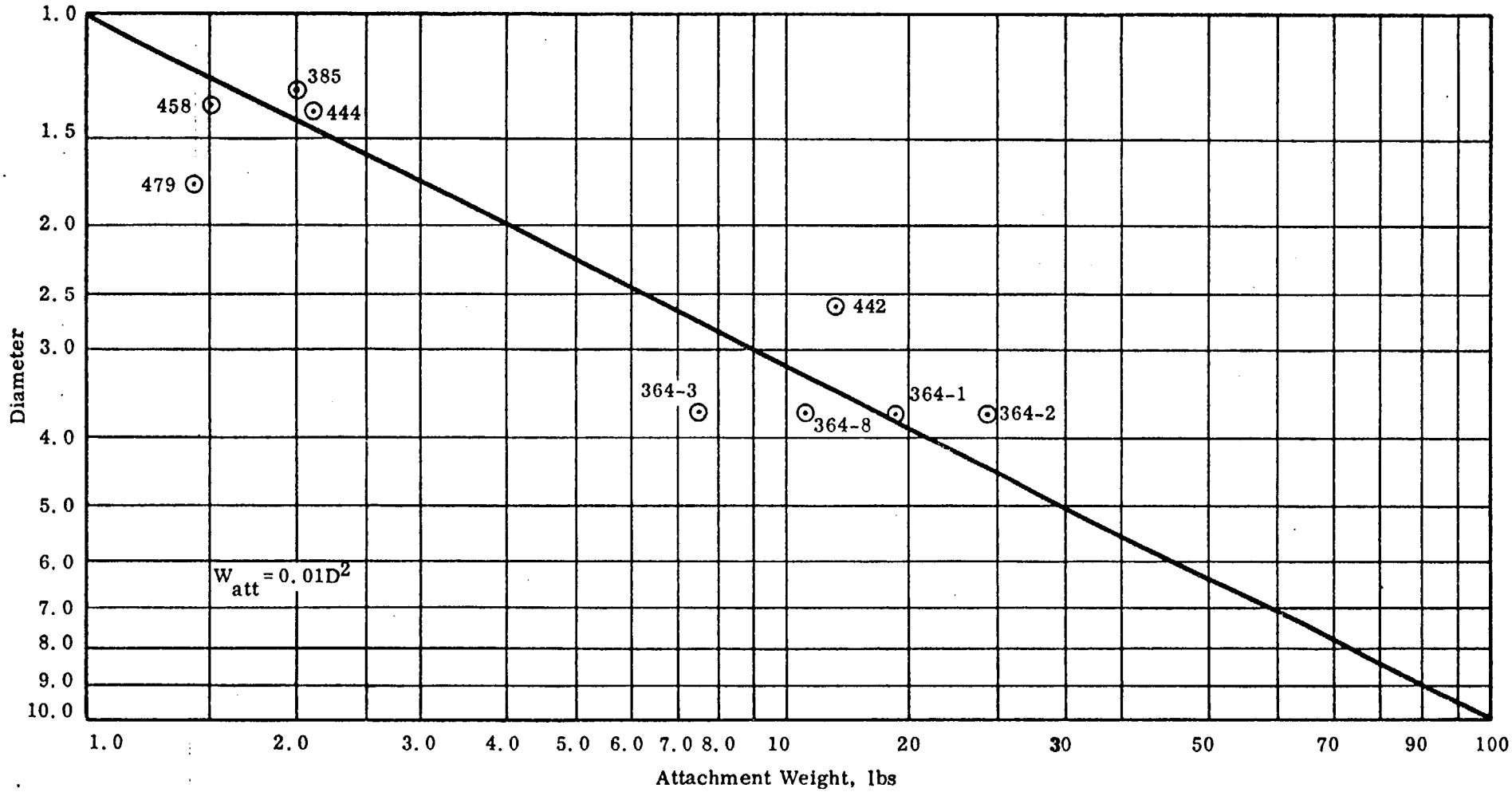

FIGURE 11. CORRELATION OF ATTACHMENT WEIGHTS

IV. SPHERICAL PERFORMANCE AND WEIGHT PREDICTION PROGRAM

A. DESCRIPTION OF COMPUTER PROGRAM

The relations developed in Sections II and III were programmed in the FORTRAN IV language for an IBM 7040-32K digital computer. The computer program, "Spherical Performance and Weight Prediction" (E-40310), is designed to produce data for making tradeoff studies between various parameters affecting the performance, weight, and dimensional envelope of spherical and extended spherical rocket motors.

Appendix A contains an input format, a schematic of an assembled data deck, a sample data set, a program listing, and the sample output corresponding to the sample data set.

Computer program input restrictions and options are summarized in Table VIII.

The design parameters that are most easily varied are chamber pressure, expansion ratio, and total impulse or velocity increment.

The velocity increment required for a specified total stage weight may be input to the program. If this is done, the program calculates the gravity losses accumulated over the burn time and increases the size of the motor to compensate for these losses. If the motor is designed to a total impulse requirement, the propellant weight and volumetric loading density are known and, thus, case dimensions can be found immediately without iterating on the gravity loss.

If an extended version of an existing spherical design is desired, the diameter of the case that is to be extended must be input as DCMAX. If the quantity of propellant required to produce the desired ΔV or total impulse at the specified volumetric loading density requires that the case be larger in diameter than DCMAX, the diameter is held constant at DCMAX, and the length is increased to accommodate the additional propellant. The case length-to-diameter ratio that is specified on the input card will be satisfied until the diameter reaches DCMAX. If additional propellant volume is then required, the case length is increased accordingly.

All propellant-related variables are input on one card so that a number of different propellant cards may be maintained and substituted easily. If the burn rate at a reference pressure and the burn rate exponent are known, they may be input as BRC, BRRP, and BRE, respectively. This causes the program to use these variables to compute burn time. If the values of BRC, BRRP, and BRE are not input to the program, the properties of a Surveyor-type propellant are used (see Table IX).

TABLE VIII

SPHERICAL PERFORMANCE AND WEIGHT PREDICTION PROGRAM (E-40310)
REQUIREMENTS AND OPTIONS

REQUIRED INPUTS	SYMBOL	ALLOWED VALUES
Specified Burn Time, sec.	C5	No Restrictions
Total Stage Weight, lbm	WS	Must be greater than expected motor weight
Number of Chamber Pressures	NP	1 through 8
Number of Expansion Ratios	NFX	1 through 8
Number of ΔV or I_{tot} Levels	NDELUR	1 through 8
Partial Print-Out Key	NPR	0 = Full, 1 = Partial Print-out
Additional Data Key	NC	0 = Last data set, 1 = more data follows
ΔV or Total Impulse Switch	IXX	0 = Total impulse input, 1 = ΔV input
Case Length-to-Diameter Ratio	CLD	Must be equal to or greater than 1.0
Volumetric Loading Density	VLD	Must be between 0.0 and 1.0
Case Safety Factor	SF	Must be greater than 1.0
Case Material Strength-to-Weight Ratio, in.	CSTWR	No Restrictions
Web Fraction	WF	Must be between 0.0 and 1.0
Nozzle Submergence	SUB	Must be between 0.0 and 1.0
Propellant Reference Specific Impulse, lbf-sec/lbm	REFISP	I_{sp} for P_c = 1000 psia P_e = 14.7 psia P_a = 14.7 psia
I_{sp} Efficiency	EFF	0.0 through 1.0
Propellant Specific Heat Ratio	GAM	May not = 1.0
Propellant Burn Rate Coefficient	BRC	No Restrictions
Propellant Burn Rate Exponent	BRE	No Restrictions
Propellant Burn Rate Reference Pressure, psia	BRRP	Must satisfy burn-rate equation of the form $r_b = BRC\ (P_c/BRRP)^{BRE}$
Propellant Density	DENP	Density either in gm/cc or lbm/cu in.
Chamber Pressure Valves, psia	PC	No Restrictions
Expansion Ratios	EX	No Restrictions
Identification Cards	CARD 1 CARD 2	No Restrictions - 142 characters of alphanumeric information
Gravity Term Coefficient	C1	Must be between 0.0 and 1.0
Local Gravitational Acceleration, ft/sec^2	GS	No Restrictions - may be 0.0 for gravity free environment
Propellant Identification	PROP1D (1) PROP1D (2)	No Restrictions - 10 characters of alphanumeric information
Maximum Case Diameter, in.	DCMAX	Must be 0.0 for unrestricted case diameter

OPTIONS

If the burn-rate coefficient, burn-rate exponent, and burn-rate reference pressure are all input as 0.0, the program will assume that the propellant to be used is Surveyor-type propellant and will use the Surveyor burn-rate equations.

If the burn time is not specified, it will be calculated by the program from the burn-rate equation that is used.

If an extended version of an existing spherical design is desired, the diameter of the case that is to be extended must be input as DCMAX.

TABLE IX

PROPELLANT BALLISTIC PROPERTIES

	Density (lbm/in.^{3})	Specific Impulse* (lbf-sec/lbm)	Gamma	Burn Rate (in./sec)
PB-AP-AL (TP-H-3062)	0.0626	245	1.16	$0.31\,(P_c/1000)^{0.29}$
PB-AP-BE (TP-H-1092)	0.0604	251	1.12	$0.326\,(P_c/1000)^{0.35}$
PB-HAP-AL	0.0631	256	1.149	$0.79\,(P_c/1000)^{0.58}$
PB-HAP-BE	0.0607	265	1.078	$0.52\,(P_c/1000)^{0.53}$

*Sea Level, P_c = 1000 psia, optimum expansion.

B. PARAMETRIC STUDY

The results of the parametric study are presented in Appendix B. The trade-off data were obtained for a base system having the following characteristics:

Configuration: Spherical
Volumetric Loading Density: 95%
Web Fraction: 60%
Nozzle Submergence: 40%

Parameters that were varied included:

Case Material: Titanium ($\frac{\sigma}{\rho_c} = 1.1 \times 10^6$)

Steel ($\frac{\sigma}{\rho_c} = 0.707 \times 10^6$)

Case Safety Factor: 1.1, 1.25, 1.4
Chamber Pressure: 300 to 1500 psia
Expansion Ratio: 10 to 80
Total Impulse: 50,000 to 800,000 lbf-sec
Propellants: PB-AP-AL (TP-H-3062)
PB-AP-BE (TP-H-1092)
PB-HAP-AL (no designation)
PB-HAP-BE (no designation)

The properties of the propellants examined in this trade-off study are specified in Table IX.

Combustion efficiency data on TP-H-3062 indicate that an expansion ratio of 53:1 results in a nozzle efficiency of 97%. Since this is the only point for which sufficiently reliable altitude data are available, a nozzle efficiency of 97% was assumed for all expansion ratios and all propellants.

While this certainly introduces some error (by the ratio of the calculated to the actual thrust coefficient), no better estimate of nozzle efficiency for these propellants is available at this time.

V. TOTAL IMPULSE REPRODUCIBILITY

Historically, total impulse reproducibility has been achieved by imposing critical controls over those variables which affect total impulse. Although it can be shown mathematically that Thiokol has successfully implemented these controls, this is difficult to demonstrate because of random measurement errors in production control and test instrumentation.

In general, the variables contributing to deviations in delivered total impulse can be categorized as being either systematic or random. Systematic variables arise primarily due to operational mission requirements, whereas random variables are the result of manufacturing tolerances and differences in material lots. The major systematic variable is motor firing temperature. For spherical motors, the operational temperature range is typically +20°F to 100°F. This variation in propellant grain temperature results in: (1) a change in propellant base burn rate and thus a corresponding change in motor operating pressure, (2) a change in specific impulse due to changes in initial grain temperature and operating pressure, and (3) a change in amount of inerts (liner and insulation) consumed during motor operation.

Another systematic variable arises from changes in propellant specific impulse due to propellant aging. This variable has been shown to be very small through various propellant aging programs.

The major random variables which effect impulse reproducibility are due to: (1) variations in propellant weight and nozzle geometry due to manufacturing tolerances, (2) batch-to-batch variation in propellant characteristics, and (3) variation in nozzle throat erosion due to lot-to-lot differences of throat material properties and the non-uniform characteristics of the throat erosion process.

A. IMPULSE EFFICIENCY

Rocket motor inefficiencies arise in two areas, in the combustion chamber and in the nozzle.

Combustion inefficiencies and flow inefficiencies are the two most significant losses taking place within the combustion chamber. Combustion inefficiencies result when exhaust gases are expelled from the chamber before fuel and oxidizer have completely reacted. Although the exact mechanism of combustion inefficiency is not fully understood, it has been determined that propellant composition, particle size, particle shape, and chamber dwell time are factors which are influential.[1] A second source of

[1] Friedman, R. and Macek, A., "Ignition and Combustion of Aluminum Particles in Hot Ambient Gases," Western States Section, Combustion Institute Paper No. 61-21, September 1961.

chamber inefficiency results from total pressure losses which are associated with severe flow conditions in the propellant cavity. Motor length-to-diameter ratio and propellant port area-to-nozzle throat area ratio are factors which govern these flow losses.

Solid-propellant rocket motors that use metal fuel additives discharge small metal oxide particles during the combustion process. Because of their mass and size, the response of these small particles to large velocity and temperature changes which occur in the nozzle is limited. That is, a finite time interval is required before they transfer heat and accelerate to the same velocity as the surrounding gases. As a result, all of the kinetic and thermal energy of the exhaust gases which is theoretically available is not obtained. The two primary factors governing velocity and thermal lags are particle size and nozzle configuration. The condition gets more adverse with increased particle size. Changes in nozzle configuration which reduce the rate of acceleration of gases reduce velocity and thermal lags.

High-expansion-ratio nozzles may result in the freezing of liquid aluminum oxide particles in the expansion section. Consequently, a divergence in particle-gas temperatures begins, since the freezing particles hold a constant temperature while the gas temperature continues to drop. This adds to the thermal energy which becomes unavailable.[2]

As hot, dissociated combustion products pass through the nozzle, the chemical equilibrium shifts, resulting in the formation of substances having lower heats of formation. The reaction rates gradually decrease because of the reduction in temperature and pressure taking place in the nozzle expansion section. They decrease until they become small with respect to nozzle dwell time. At this time the flow becomes essentially frozen and, as a result, the reaction energy of the dissociated species is lost. Nozzle configuration and nozzle size are important influencing parameters because of their effect on changes in velocity, temperature, and recombination in the nozzle. Chamber pressure influences chemical recombination losses in two ways: As pressure increases, the extent of dissociation in the chamber decreases, thus decreasing the total amount of enthalpy that may be lost. An increase in chamber pressure also increases the gas density at all points in the nozzle and thereby increases all of the chemical reaction rates.[3]

---

[2] "Propellant Optimization Study," by John A. Peterson and Loren Slayer, Thiokol Chemical Corporation, Wasatch Division, TW-245-10-64, October 1964.

[3] "High-Performance Nozzles for Solid-Propellant Rocket Motors," Research and Advanced Technology Department, United Technology Center, Sunnyvale, California, No. C25-5C86, February 25, 1965.

Nozzle performance is further degraded by the action of the boundary layer along the nozzle wall. Momentum and heat energy are transferred from the exhaust gases to the wall. This boundary layer also acts to change the effective size and expansion ratio of the nozzle because of its finite thickness. Small nozzles are more severely affected because a higher percentage of the flow stream is influenced by the boundary layer. Boundary layer losses are inversely related to nozzle half angle and chamber pressure.

The literature contains a number of very thorough theoretical analyses of rocket nozzle inefficiencies. These analyses relate efficiency to the basic independent variables previously discussed. From an academic viewpoint, they are excellent. However, the results are somewhat undermined by the fact that there are still some fundamental areas which are not completely understood, or they are based on parameters which are not readily measurable. Some of these unknowns are: aluminum oxide particle size, particle channeling characteristics, particle drag coefficients, chemical equilibrium constants, and radiation losses.[4] Because of these uncertain areas, a more direct approach at predicting motor efficiency was selected.

For the purpose of this analysis, the definition of impulse efficiency was changed. Previously, this Division has defined a specific impulse efficiency as the ratio of actual to theoretical specific impulse at standard reference conditions (P_c = 1000 psia, P_a = 14.7 psia, nozzle exit pressure = 14.7 psia, zero divergence losses). This can lead to erroneous conclusions, however, because of the variation in motor efficiency with respect to chamber pressure and nozzle configuration. This is especially true when the propulsion system operates at a pressure and expansion ratio far removed from the reference. It is more meaningful to compare values at the motor expansion ratio and motor chamber pressure. Therefore, specific impulse efficiency, as used herein, is defined as the ratio of actual to theoretical specific impulse at motor operating conditions in a vacuum. Divergence losses are included.

B. THEORETICAL PERFORMANCE

The theoretical performance of the various systems studied was determined by using an IBM computer program entitled: "Chemical Equilibrium Composition, Theoretical Rocket Performance and Chapman-Jouquet Detonations." The analysis is based upon the conservation of mass, Dalton's law of partial pressures, adiabatic combustion, and isentropic expansion. An option exists in the program for assuming either shifting equilibrium or frozen flow in the nozzle expansion section.

---

[4]Zeleznik, Frank J. and Sanford Gordon, "A General IBM 704 or 7090 Computer Program for Computation of Chemical Equilibrium Compositions, Rocket Performance, and Chapman-Jouquet Delonations," NASA TN D-1454, 1962.

There is some disagreement within the industry as to whether theoretical specific impulse should be defined while assuming shifting equilibrium or frozen flow in the nozzle expansion section. The chemical equilibrium in a rocket nozzle will shift as long as the rate of change of concentrations of the species required to maintain equilibrium can be met by the rate of change allowed by the chemical kinetics of the system. When this criteria can no longer be met, an apparent frozen equilibrium will result. The position at which this takes place is a function not only of the propellant itself, but of the geometry of the rocket nozzle. With large rocket motors, the position of the equilibrium freezing will be at a higher area ratio than the small rocket. Since the chemical knietics of the reactions taking place in the nozzle are not well defined, this effort uses shifting equilibrium to the exit plane of the nozzle and defines impulse efficiency in terms of this quantity.

The thermochemical data used in these calculations were obtained from standard JANAF compilations. Heats of formation, entropy, enthalpy, and specific heat as functions of temperature were used. The heats of formation for compounds which do not appear in the JANAF tables were obtained from the Propellant Department, Development Laboratories.

The theoretical vacuum specific impulse for TP-H-3062 is illustrated in Figure 12 as a function of chamber pressure. It should be noted that over the normal operating pressure range of spherical motors (500 - 800 psia) the theoretical performance of TP-H-3062 varies by less than 0.1%.

The theoretical vacuum thrust coefficient is presented in Figure 13 as a function of expansion ratio.

C. THROAT AREA EFFECTS

Variations in nozzle throat dimensions due to manufacturing tolerances and/or non-uniform throat erosion contribute to the measured impulse variability. Variability in performance due to manufacturing tolerances can be accounted for by utilizing accurate measuring techniques. It is more important to know what the actual nozzle geometry is rather than what the design calls for. The nozzle throat area erosion time history must be considered in order to accurately evaluate motor performance.

Throat area variations on performance effect changes in: (1) motor operating pressure with associated change in propellant performance, and (2) effective expansion ratio which results in a change in nozzle performance.

The theoretical sensitivity of motor performance can be evaluated utilizing the theoretical performance of TP-H-3062 presented in Figure 12 and the theoretical vacuum thrust coefficient given in Figure 13.

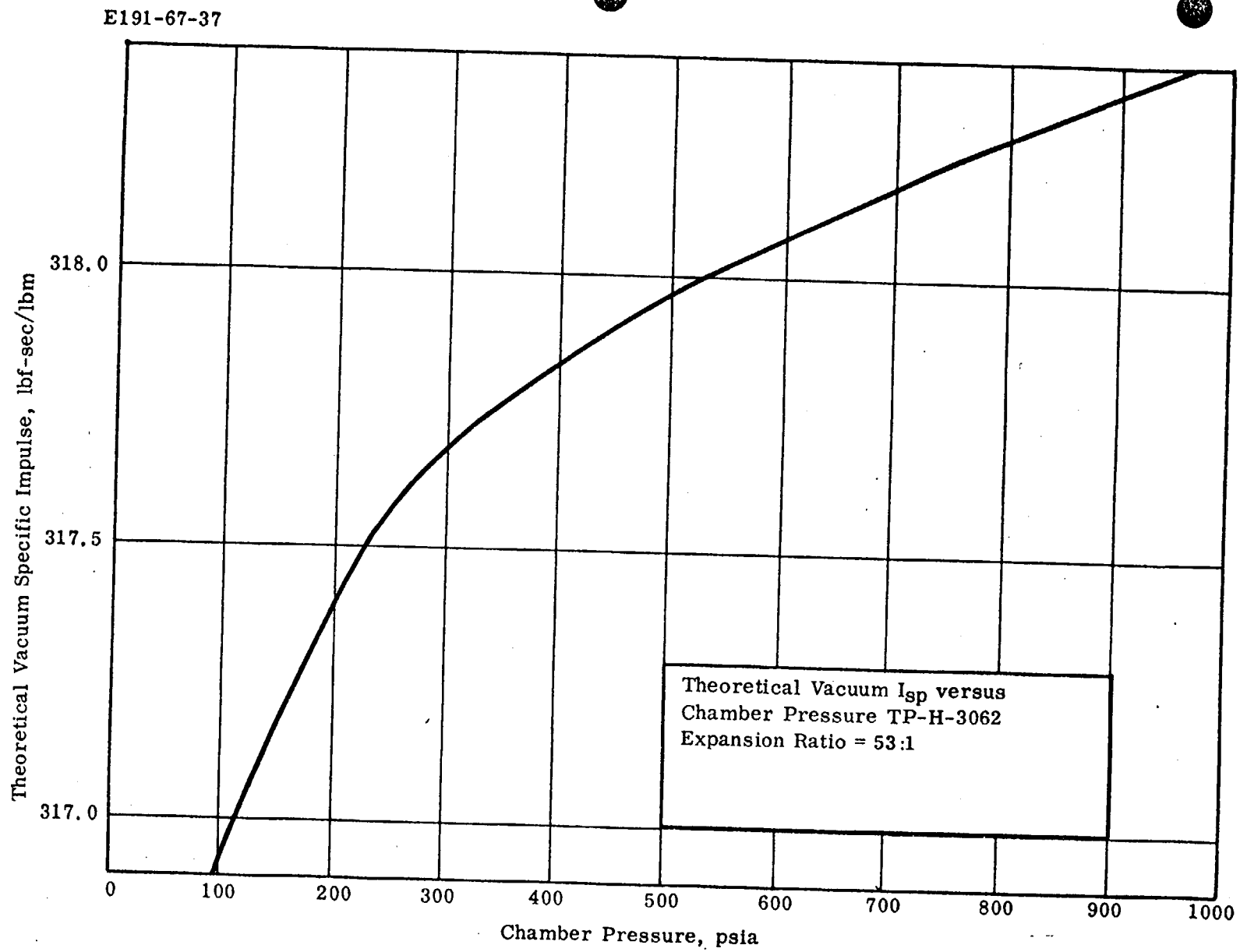

FIGURE 12. THEORETICAL VACUUM SPECIFIC IMPULSE (TP-H-3062)

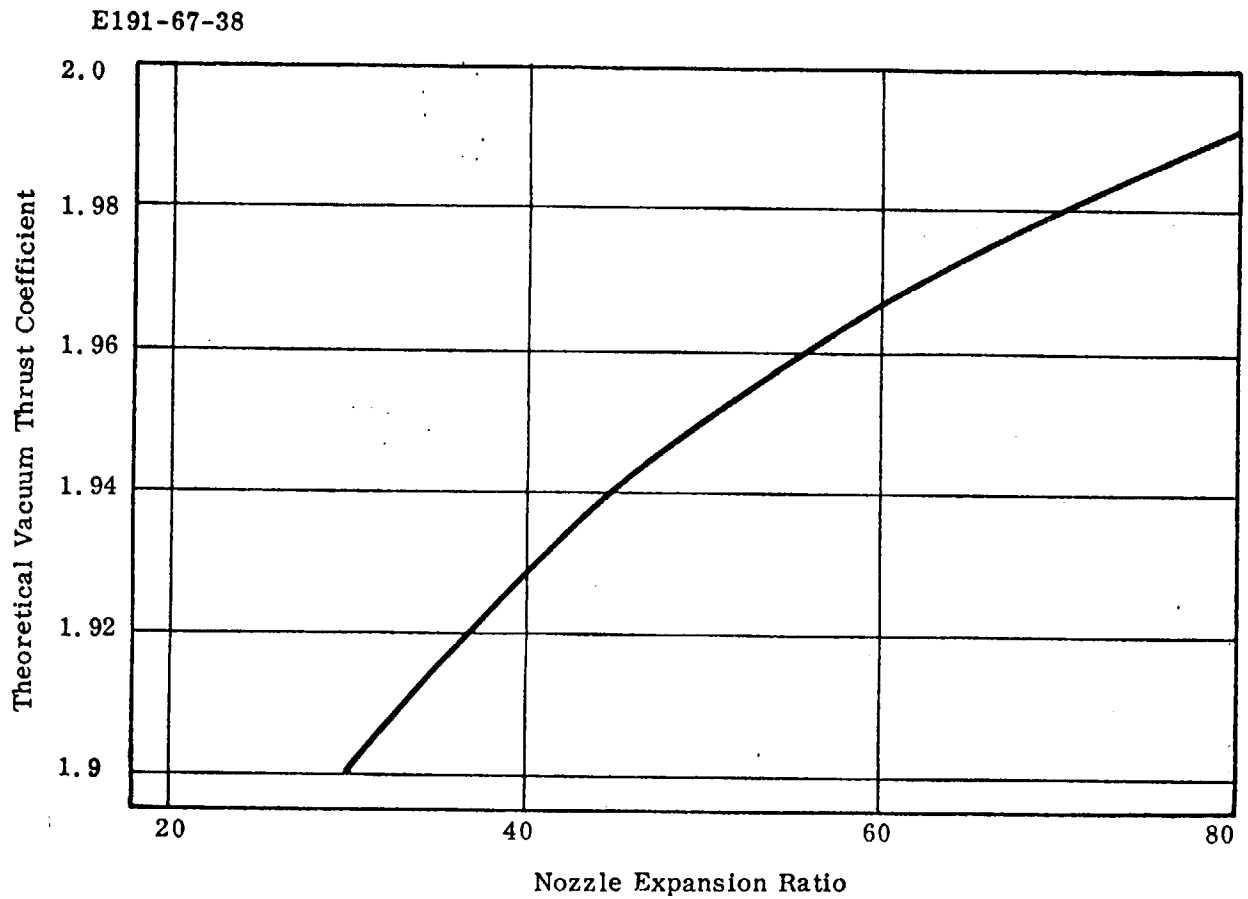

FIGURE 13. THEORETICAL VACUUM THRUST COEFFICIENT

For example, a 10.0% increase in throat area will result in a 14.1% decrease in chamber pressure for a burn-rate exponent of 0.29. This decrease in pressure will result in a 0.028% decrease (refer to Figure 12) in theoretical specific impulse at an operating pressure of 600 psia. Neglecting changes in exit area, a 0.433% decrease (refer to Figure 13) in vacuum thrust coefficient will be experienced for the same 10% increase in throat area. Thus, the total change in theoretical vacuum specific impulse will be -0.461% for a 10% increase in throat area.

Experimental results show that nozzle erosion rates are nearly constant after the nozzle insert begins to erode. The criterion for the onset of nozzle erosion seems to be the surface temperature of the insert. At this temperature, the insert material begins to degrade and ablation and surface erosion of the insert is initiated. The erosion takes place at a constant rate which depends on the material and the conditions in the throat. A range of from 0.005 to 0.010 inch/second is considered normal. Figure 14 illustrates a typical throat area time history. This throat area history was determined by a backfit from pressure and thrust data for a TE-M-479.

This motor was one of two TE-M-479 motor firings at AEDC for which data were available on throat deposition/erosion history. The initial throat area decrease shown in the plot is thought to be aluminum slag condensing on the cold nozzle surface. Slag deposits evidently formed instantly along the throat contour and persisted to 3 to 4 seconds after igntion. During this period, no throat regression occurred and some thermal insulation of the nozzle was experienced. From the character of the deposit thickness history, it is believed that significant amounts of aluminum metal were deposited during the first half second of the test (30 mils maximum thickness).

Initially, the burning particle residence times relative to the nozzle surfaces upstream of the throat section are less than 0.1 millisecond. Aluminum particles require longer times to ignite and, therefore, early deposition of unignited and partially burned aluminum particles is very likely. Deposition of this material would constitute a performance loss early in the test. The deposits formed on the inner and outer surfaces of the nozzle would prevent excessive corrosion by the incompletely burned exhaust.

Examination of six TE-M-479 motor test results indicates that the total measured erosion rate over the burn time varies to 165% of the lowest measured value (0°F soak — 75 rpm). The average erosion rate decreases with increasing spin rate and increases with increasing grain soak temperature. It is doubtful that the graphite erosion rates are actually the variable. It is far more likley that variation of the amount and endurance of the deposits causes the apparent variation in total erosion.

The most reasonable radial erosion rate was found to be 6 ± 1 mils per second during the period when erosion actually occurred.

E191-67-39

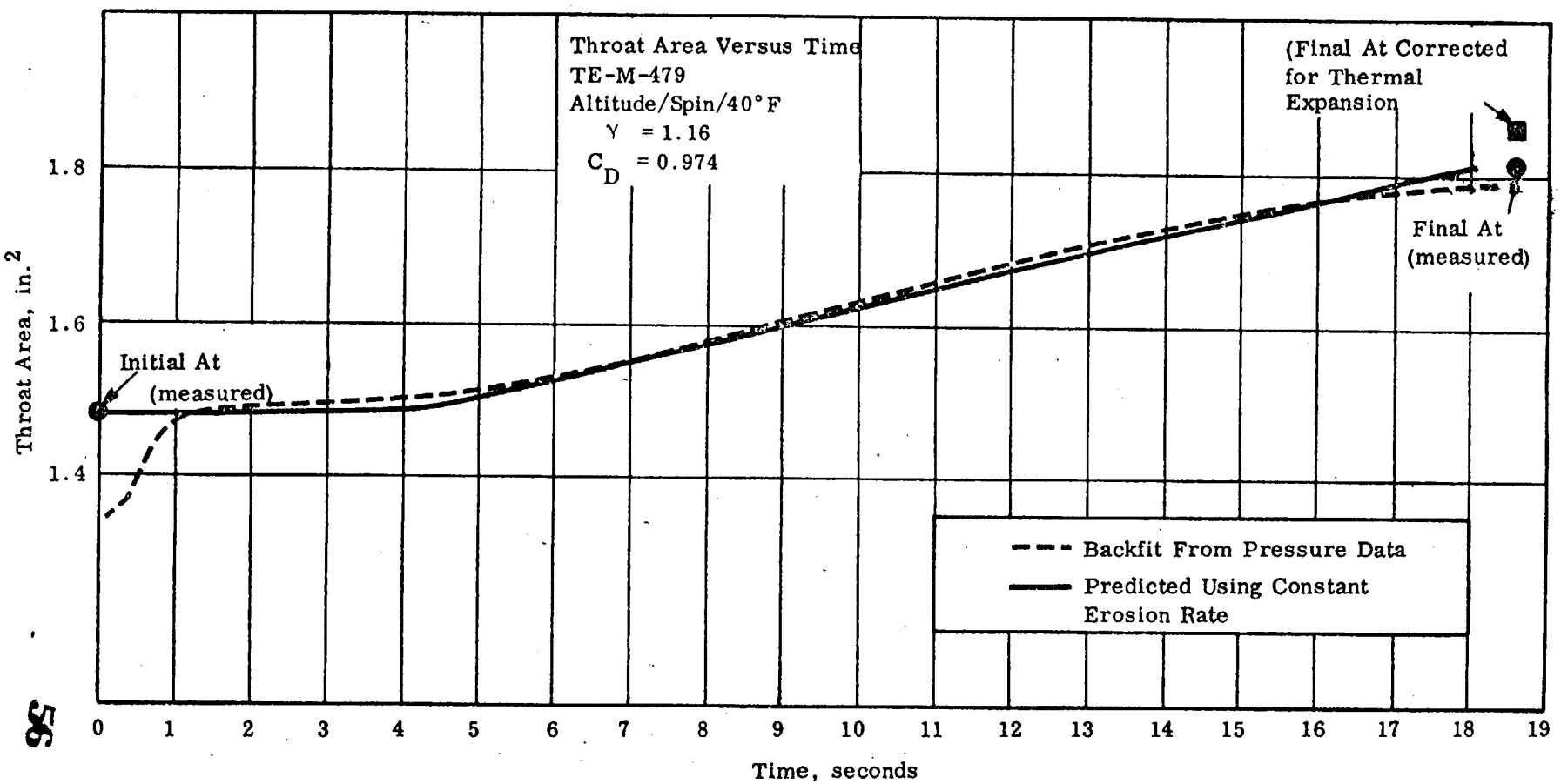

FIGURE 14. TYPICAL THROAT AREA - TIME HISTORY

D. DEMONSTRATED IMPULSE REPRODUCIBILITY

Unfortunately, one characteristic of spherical motors is the small number of motors that have been made of a particular design, and the correspondingly small number of test firings for which accurate impulse data are available. It is this lack of data that prevents a more meaningful analysis of the interrelationships between the variables which determine impulse reproducibility.

Thiokol-Elkton has qualified the Surveyor Main Retro Motor to stringent impulse reproducibility requirements (± 1 percent, 3 sigma, at a specific temperature). Since the motor is maintained at a constant test temperature, this means that the motor should demonstrate ± 1 percent variation in impulse with zero systematic variations.

During the qualification test firings, Thiokol demonstrated an impulse reproducibility of ± 0.6 percent (3 sigma).

Seven motors were cast to a design specification of 347,000 lbf-sec with an allowed tolerance of ± 1%. These motors were then test fired. The results of these tests are shown in Table X. The average total impulse of the test motors differed from the specified total impulse by less than 0.02%. Another batch of six motors was then cast, the propellant weight determined, and the proper amount of propellant removed to provide the correct total propellant weight for a total impulse level of 356,700 lbf-sec. These motors were then test fired at AEDC. The average total impulse differed from the specified 356,700 lbf-sec by less than 0.18% and the three standard deviation dispersion for total impulse was only 0.242%.

Since the actual propellant weight in any particular motor can be measured very accurately, the major random errors associated with propellant weight can be eliminated by considering specific impulse. Accurate impulse data exist for six spherical motor designs. These designs have been static fired under simulated vacuum conditions at AEDC. The results of these tests are tabulated in Table XI. Standard deviations of the data presented ranged from a low of 0.070% for the TE-M-458 to a high of 0.234% for the TE-M-345.

A summary of these results is also tabulated in Table XII. Also given in this table is the specific impulse efficiency. Demonstrated specific impulse efficiencies range from 0.923 for the TE-M-345 to 0.979 for the TE-M-385.

TABLE X

SURVEYOR MAIN RETRO TOTAL IMPULSE REPRODUCIBILITY

Motor Serial No.	Total Impulse, lbf-sec	
A21-10	347,661 AEDC	
A21-11	347,523 AEDC	Specification Requirements 347,000 ± 1%
A21-12	345,808 AEDC	
A21-13	346,740 AEDC	

Avg I_{tot} = 346,933

σ = 852.6

3σ = 2557.8

$$\frac{3\sigma}{\text{Avg } I_{tot}} = 0.737\%$$

A21-17	355,871 AEDC	
A21-18	355,793 AEDC	Specification Requirements 356,700 ± 1%
A21-23	356,255 AEDC	
A21-24	356,382 AEDC	

Avg I_{tot} = 356,075

σ = 287.4

3σ = 862.2

$$\frac{3\sigma}{\text{Avg } I_{tot}} = 0.242\%$$

TABLE XI

SPECIFIC IMPULSE REPRODUCIBILITY

Motor	Total Impulse, lbf-sec	Measured Specific Impulse, lbf-sec/lb	Average Expansion Ratio	Thrust Coefficient, vac.	Specific Impulse @ 53:1 Expansion Ratio, vac lbf-sec/lbm
TE-M-345	18103	267.439	27.33	1.89040	276.72
TE-M-345	18210	268.504	27.21	1.8899	277.89
TE-M-345	18223	267.827	26.93	1.8887	277.37
TE-M-345	18167	267.515	27.13	1.88957	276.92
TE-M-345	18002	267.012	27.32	1.8903	276.30
TE-M-345	17850	266.975	27.37	1.8906	276.21
TE-M-345	17725	266.942	27.78	1.8922	275.95
TE-M-345	17786	267.338	27.75	1.8921	276.37
TE-M-345	17840	267.386	27.59	1.8914	276.52
TE-M-345	17698	266.737	27.71	1.8919	275.78
				Ave I_{sp} =	276.603
				σ =	0.647 = 0.234%
TE-M-385	14205	257.0	22.45	1.8671	269.23
TE-M-385	14189	256.0	22.43	1.8670	268.20
TE-M-385	14187	256.0	22.43	1.8670	268.20
TE-M-385	14238	257.0	22.44	1.8670	269.25
				Ave I_{sp} =	268.72
				σ =	0.601 = 0.224%
TE-M-364-1					
A21-10	347661	290.08	51.607	1.95176	290.71
A21-11	347523	290.1	51.717	1.95196	290.70
A21-12	345808	288.5	51.788	1.95209	289.08
A21-13	346740	289.74	51.581	1.95171	290.37
A21-17	355871	289.6	51.704	1.95194	290.20
A21-18	355793	289.4	51.309	1.95122	290.11
A21-23	356255	289.9	51.677	1.95189	290.51
A21-24	356382	289.3	51.530	1.95162	290.81
A22-2	375000	289.1	51.566	1.95169	289.74
A22-3	362017	289.5	51.509	1.95158	290.15
A22-4	361272	288.9	51.643	1.95182	289.52
				Ave I_{sp} =	290.173
				σ	0.542 = 0.187%
TE-M-364-3	419955	291.8	52.47	1.95502	291.94
TE-M-364-3	419172	291.4	52.39	1.95498	291.55
TE-M-364-3	419483	291.2	51.79	1.95389	291.52
TE-M-364-3	418282	290.6	52.39	1.95498	290.75
TE-M-364-3	419218	290.8	52.33	1.95487	290.97
TE-M-364-3	419581	291.4	51.95	1.95419	291.67
				Ave I_{sp} =	291.40
				σ =	0.449 = 0.154%
TE-M-458	18833	275.78	42.77	1.93586	278.65
TE-M-458	18853	276.03	42.69	1.93570	278.93
				Ave I_{sp} =	278.79
				σ	0.196 0.07%
TE-M-479	44562	290.5	54.60	1.95874	290.10
TE-M-479	44379	289.8	54.72	1.95895	289.30
				Ave I_{sp}	289.70
				σ	0.566 0.195%

TABLE XII

SPECIFIC IMPULSE EFFICIENCY SUMMARY

Motor	Sample Size	Motor Diameter, in.	Propellant Designation	Specific Impulse (corrected to 53:1), lbf-sec/lbm	Standard Deviation, lbf-sec/lbm	Theoretical Specific Impulse*, lbf-sec/lbm	Specific Impulse Efficiency
TE-M-345	10	13.5	TP-G-3129	276.60	0.647	299.69	0.9230
TE-M-364-1	11	37.0	TP-H-3062	290.17	0.542	313.31	0.926
TE-M-364-3	6	37.0	TP-H-3062	291.40	0.449	313.31	0.930
TE-M-385	4	12.8	TP-L-3014A	268.72	0.601	274.37	0.979
TE-M-458	2	13.5	TP-G-3129	278.79	0.196	299.69	0.930
TE-M-479	2	17.4	TP-H-3062	289.70	0.566	313.31	0.925

*Corrected for nozzle divergence.

VI. DEMONSTRATED RELIABILITY

The proven reliability of a solid-propellant rocket motor is determined from the number of successes and failures of a particular configuration of the motor. In general, if a failure occurs, an engineering change solves the problem and the new configuration then begins again to prove its reliability. This means that a production motor has probably had no static test failures that could not be attributed to known abnormalities in the motor. For a given number of successful tests without a failure at a particular level of confidence, the reliability may be found from

$$\log(\text{reliability}) = \frac{\log(1\text{-confidence level})}{\text{number of tests}}$$

If a failure occurs in one component, and a change is made to that component to ensure that the failure mode is eliminated, then a smaller number of tests is required to establish that the component is performing satisfactorily.

A. RELIABILITY SUMMARY FOR THE SURVEYOR MAIN RETROGRADE MOTOR

Surveyor development and qualification firings illustrate how reliability data were obtained on components prior to final qualification of the motor.

Each subsystem was evaluated based on the criteria laid down for that particular subsystem. Table XIII lists the subsystems that make up the complete motor and the requirements for each to qualify as a success in a test firing.

There were 35 development firings in the Surveyor program and 10 qualification firings. Of these, 15 development tests were excluded for evaluation of reliability. Eight were excluded prior to firing the motor, and seven were excluded after the fact.

Since completion of the motor qualification firings, there have been three additional quality assurance firings and three successful flight firings (see Table XIII).

The success record of each subsystem is kept separate from that of the complete motor so that each part can be qualified individually. This also allows the complete motor to achieve a larger number of successes than would be the case if a motor were excluded each time an individual component was excluded. For example, at the end of the qualification program there were 33 Surveyor firings that were classified as successes, even though 11 of those tests had components that were excluded either before or after the firing. At the 50% level of confidence, 33 successes resulted in a reliability of 0.9792, while 22 successes resulted in a reliability of only 0.9690. A reliability summary for the Surveyor Main Retro Motor is presented in Table XIV.

RESULTS CODE
PE - Pretest Exclusion
E - Posttest Exclusion
S - Success
F - Failure

TABLE XIII

SUBSYSTEM AND COMPONENT TEST SUMMARY

Test No.	Motor Serial No.	Date Tested	Firing Temp.	Burn Time	Engine Assy.	Subsys. "A" and Comp.			Subsys. "B" and Comp.			Subsys. "C" and Comp.			Subsys. "D" and Comp.			Remarks
						A	A1	A2	B	B1	B2	C	C1	C2	D	D1	D2	
1 (Dev)	1	8/25/61	70°F	47.15	PE	S	S	S	E	E	E	PE	PE	PE	PE	E (S)*	PE	Heavy wt. Eng. TE-359 with TP-H-3053, propellant and asbestos-phenolic insulation. Sea level nozzle.
2 (Dev)	HW-2	10/16/61	25°F	45.12	PE	S	S	S	E	E	E	PE	PE	S	PE	E (S)*	PE	Heavy wt. Eng. TE-359 with TP-H-3053B propellant and asbestos-phenolic insulation. Fwd-end grain cracks and stress relief boot separation repaired with TAL303; truncated nozzle. Abnormal pressure time trace.
3 (Dev)	HW-3	12/6/61	69°F	45.31	PE	S	S	S	E	E	E	PE	PE	S	E	E	E	Heavy wt. Eng. TE-359 with TP-H-3053B propellant and asbestos-filled buna-N insulation. Cured 64 hrs at 135°F; reduced to 100°F for 48 hrs. Grain cracking in transition section. Pyrolytic graphite insert peeled away, causing pressure and thrust to fall off after 28 sec. of normal engine operation.
4 (Dev)	R1	1/12/62	27°F	45.40	PE	PE	PE	PE	PE	PE	PE	PE	PE	PE	PE	PE	PE	Engine rejected grain cracks. Pretest exclusion from Reliability Engineering.

*([illegible] inal evaluation)

Table XIII (Cont'd)

SUBSYSTEM AND COMPONENT TEST SUMMARY

Test No.	Motor Serial No.	Date Tested	Firing Temp.	Burn Time	Engine Assy.	Subsys. "A" and Comp.			Subsys. "B" and Comp.			Subsys. "C" and Comp.			Subsys. "D" and Comp.			Remarks
						A	A1	A2	B	B1	B2	C	C1	C2	D	D1	D2	
5(Dev)	4	1/22/62	-	-	PE	E	E	E	E	E	E	PE	PE	PE	E	E	E	Heavy wt. Eng. TE-359, HLM-85 insert, thermally sterilized. Pretest exclusion from Reliability Engineering. Catastrophic failure.
6(Dev)	1A	2/15/62	56° F	41.65	S	S	S	S	S	S	S	S	S	S	PE	E (S)*	PE	Heavy Wt. Eng. and Aft Closure TE-359 with TP-H-3062 propellant, asbestos filled buna-N and TL-H-301 Liner. Truncated sea level nozzle with HLM-85 insert.
7(Dev)	5	3/2/62	56° F	43.67	S	S	S	S	S	S	S	S	S	S	E	E (S)*	E	Heavy wt. Eng. and Aft Closure TE-359 with TP-H-3062 propellant asbestos filled buna-N and TL-H-301 liner. Altitude nozzle with HLM-85 insert. Fired at simulated altitude. Reduced mass flow PYROGEN. Nozzle excluded Dec. 1962 (Redesign)
8(Dev)	6	3/27/62	23° F	44.224	S	S	S	S	S	S	S	S	S	S	PE	E (S)*	PE	Flt. wt. eng. and aft closure, attachment fitting components TE-360 with TP-H-3062 propellant, asbestos filled buna-N and TL-H-301 liner, Sea level nozzle with HLM-85 insert. Temp. cycle between 20° and 110° F. Nozzle excluded Dec. 1962 (Redesign)

* ( ) original evaluation

Table XIII (Cont'd)

SUBSYSTEM AND COMPONENT TEST SUMMARY

Test No.	Motor Serial No.	Date Tested	Firing Temp.	Burn Time	Engine Assy.	Subsys. "A" and Comp. A	A1	A2	Subsys. "B" and Comp. B	B1	B2	Subsys. "C" and Comp. C	C1	C2	Subsys. "D" and Comp. D	D1	D2	Remarks
9(Dev)	A25-12	6/20/62	56° F	43.162	S	S	S	S	S	S	S	S	S	S	E (S)*	E (S)*	E (S)*	Heavy wt. Eng. and aft closure, TE-359 with TP-H-3062 propellant, asbestos filled buna-N and TL-H-301 liner. Altitude nozzle with HLM-85 insert. Nozzle excluded Dec. 1962 (Redesign)
10(Dev)	A21-1	6/22/62	28° F	41.02	S	E	S	S	S	S	S	S	S	S	PE	E (S)*	PE	First "Y" configuration TE-364 with TP-H-3062 propellant, V-44 insulation and TLH-301 liner. Flight wt. closure and sea level nozzle with HLM-85 insert. Temp. cycling 110° and 20° F. Ignition time interval of 0.313 seconds is above spec. limit of 0.300 sec. max. Nozzle excluded Dec. 1963 (Redesign)
11(Dev)	A25-9	6/19/62	50° F	44.5	PE	S	S	S	E	E (F)*	S	S	S	S	E	E	E	AEDC firing of heavy wt. engine and aft closure TE-359, with TP-H-3062 propellant, V-44 insulation and TLH-301 liner. Alt. nozzle with HLM-85 insert. Specific impulse too low. Ignition time of 0.148 secs. acceptable. Propellant excluded Oct. 1962 (Nozzle redesign)

* ( ) original evaluation

Table XIII (Cont'd)

SUBSYSTEM AND COMPONENT TEST SUMMARY

Test No.	Motor Serial No.	Date Tested	Firing Temp.	Burn Time	Engine Assy.	Subsys. "A" and Comp.			Subsys. "B" and Comp.			Subsys. "C" and Comp.			Subsys. "D" and Comp.			Remarks
						A	A1	A2	B	B1	B2	C	C1	C2	D	D1	D2	
12(Dev)	A25-10	6/20/62	50° F	45.0	PE	S	S	S	E	E (F)*	S	S	S	S	E	E	E	AEDC firing of heavy wt. engine and aft closure TE-359 with TP-H-3062 propellant, V-44 insulation and TLH-301 liner. Alt. nozzle with HLM-85 insert Specific impulse below required level. Acceptable ignition time of 0.168 secs. Pressure tube failure (test equipment) See Failure Report S-19. Propellant excluded Oct. 1962 (Nozzle redesign)
13(Dev)	A21-2	7/14/62	74° F	39.66	S	S	S	S	S	S	S	S	S	S	PE	E (S)*	PE	TE-364 engine with TPH-3062 propellant, V-44 insulation and TLH-301 liner. Flight wt. closure and sea level nozzle with TS-325 insert. Ignition time of 0.243 sec. acceptable. Nozzle excluded Dec. 1962 (redesign)
14(Dev)	A21-3	10/4/62	57.5	39.89	S	S	S	S	S	S	S	S	S	S	E (S)*	E (S)*	E (S)*	AEDC firing of TE-364 engine with TP-H-3062 propellant V-44 insulation and TL-H-301 liner. Alt. nozzle with TS-325 insert. Acceptable ignition time of 0.208 sec. Nozzle excluded Dec. 1962 (Redesign)

* ( ) original evaluation

Table XIII (Cont'd)

SUBSYSTEM AND COMPONENT TEST SUMMARY

Test No.	Motor Serial No.	Date Tested	Firing Temp.	Burn Time	Engine Assy.	Subsys. "A" and Comp. A	A1	A2	Subsys. "B" and Comp. B	B1	B2	Subsys. "C" and Comp. C	C1	C2	Subsys. "D" and Comp. D	D1	D2	Remarks
15(Dev)	A25-7	10/5/62	58.0	49.38	E (F)*	S	S	S	S	S	S	S	S	S	E (F)*	E (F)*	E	AEDC firing of TE-360 engine with TP-H-3062 propellant, V-44 insulation and TL-H-301 liner. Alt. nozzle with TS-325 insert. Failure caused by loss of insert at 5.5 sec. Nozzle excluded Dec. 1962 (Redesign)
16(Dev)	A25-11	1/18/63	50.0	-	PE	S	S	S	E	E	E	E	E	E	PE	PE	PE	TE-360 engine with TP-H-3062 propellant, V-44 insulation and TL-H-301 liner. Interim weight nozzle assembly. Loss of nozzle caused failure.
17(Dev)	A21-4	2/22/63	70° F	NA	E (F)*	S	S	S	E	E	E	E	E	E	E (F)	E (F)*	E	TE-364-1 engine with TP-H-3062 propellant, V-44 insulation and TL-H-301 liner. Sea level test with full flow conditions in truncated nozzle assembly. E145355 Loss of nozzle insert at 4.4 sec caused failure. Nozzle excluded March 1963 (Redesign)
18(Dev)	A25-8	3/22/63	52° F	43.28	S	S	S	S	S	S	S	S	S	S	E (S)	E (S)*	S	Modified TE-360 engine with TP-H-3062 propellant V-44 insulation and TL-H-301 liner. Sea level test with full flow conditions in truncated nozzle assembly E15223-02. Acceptable ignition tome of .086 sec. Nozzle insert excluded May 63 (Redesign)

') original evaluation

Table XIII (Cont'd)

SUBSYSTEM AND COMPONENT TEST SUMMARY

Test No.	Motor Serial No.	Date Tested	Firing Temp.	Burn Time	Engine Assy.	Subsys. "A" and Comp. A	A1	A2	Subsys. "B" and Comp. B	B1	B2	Subsys. "C" and Comp. C	C1	C2	Subsys. "D" and Comp. D	D1	D2	Remarks
19(Dev)	A21-5	3/27/63	59° F	38.65	S	S	S	S	S	S	S	S	S	S	E (S)	E (S)*	S	TE-364-1 engine with TP-H-3062 propellant, V-44 insulation and TL-H-301 liner. Flight weight altitude nozzle with AHDG insert. Nozzle insert excluded May 1963 (Redesign)
20(Dev)	A21-9	4/12/63	50° F	NA	E (F)*	S	S	S	E	E	E	S	S	S	E (F)	E (F)*	S	AEDC firing of TE-364-1 engine with TP-H-3062 propellant, V-44 insulation and TL-H-301 liner. Flight weight altitude nozzle with AHDG insert. Loss of nozzle insert at 8.77 sec caused failure. Nozzle insert excluded May 1963 (Redesign)
21(Dev)	A21-6	5/8/63	50° F	-	E (F)*	S	S	S	S	S	S	S	S	S	E (F)*	E (F)*	S	TE-364-1 engine with TP-H-3062 propellant, V-44 insulation & TL-H-301 liner. Flight weight nozzle with TS-325 insert. Failure caused by cracked nozzle insert.
22(Dev)	A25-14N	7/25/63	90° F	41.79	E	S	S	S	S	S	S	S	S	S	E	E	E	Nozzle evaluation program - heavy wt. engine. Nozzle insert failure (S-29) Nozzle excluded (Redesign)
23(Dev)	A25-13N	7/31/63	86° F	NA	E	S	S	S	E	E	E	PE	PE	S	E	E	E	Nozzle evaluation program - heavy wt. engine. Nozzle failure (S-30) Nozzle excluded (Redesign).

* ( ) original evaluation

Table [illegible] (Cont'd)

SUBSYSTEM AND COMPONENT TEST SUMMARY

Test No.	Motor Serial No.	Date Tested	Firing Temp.	Burn Time	Engine Assy.	Subsys. "A" and Comp.			Subsys. "B" and Comp.			Subsys. "C" and Comp.			Subsys. "D" and Comp.			Remarks
						A	A1	A2	B	B1	B2	C	C1	C2	D	D1	D2	
24(Dev)	A25-15N	9/24/63	63° F	41.89	E	S	S	S	S	S	S	S	S	S	E	E	E	Nozzle evaluation program - heavy wt. engine. Insert cracked (S-31) Nozzle excluded (Redesign).
25(Dev)	A25-16N	10/4/63	60° F	42.34	S	E	E	E	S	S	S	S	S	S	S	S	S	Nozzle evaluation program - heavy wt. engine. Perturbations noted in PYROGEN data (S-32). Engine performance not affected. Nozzle performed successfully.
26(Dev)	A25-17N	11/22/63	—	—	S	S	S	S	S	S	S	S	S	S	S	S	S	Nozzle evaluation program - heavy wt. engine. Nozzle performed successfully.
27(Dev)	A25-19N	12/4/63	46° F	41.325	S	S	S	S	S	S	S	S	S	S	S	S	S	Nozzle evaluation program - heavy wt. engine. Structural and ballistic performance satisfactory.
28(Dev)	A25-18N	12/12/63	43° F	40.72	S	S	S	S	S	S	S	S	S	S	S	S	S	Nozzle evaluation program - heavy wt. engine - structural and ballistic performance satisfactory.
29(Dev)	A21-10	12/18/63	—	—	S	S	S	S	S	S	S	S	S	S	S	S	S	AEDC firing of TE-364-1 engine. Flight wt. nozzle structural and ballistic performance satisfactory.
30(Dev)	A21-13	12/19/63	50° F	38.547	S	S	S	S	S	S	S	S	S	S	S	S	S	AEDC firing of TE-364-1 engine. Flight wt. nozzle. Structural and ballistic performance satisfactory.
31(Dev)	A21-7	1/25/64	—	—	S	S	S	S	S	S	S	S	S	S	S	S	S	TE-364-1 Flight wt. engine and nozzle. Engine was subjected to vibration, temp cycling and pkg. drop tests.

Table XIII (Cont'd)

SUBSYSTEM AND COMPONENT TEST SUMMARY

Test No	Motor Serial No.	Date Tested	Firing Temp.	Burn Time	Engine Assy.	Subsys. "A" and Comp.			Subsys. "B" and Comp.			Subsys. "C" and Comp.			Subsys. "D" and Comp.			Remarks
						A	A1	A2	B	B1	B2	C	C1	C2	D	D1	D2	
32(Dev)	A21-14	2/20/64			S	S	S	S	S	S	S	S	S	S	S	S	S	TE-264-1 Flight wt. engine and nozzle (E15537-02). Engine was subjected to acceleration test. Structural and ballistic performance satisfactory.
33(Dev)	A21/8	2/27/64			S	S	S	S	S	S	S	S	S	S	S	S	S	TE-364-1 light wt. engine with flight wt. nozzle (E15537-02). Structural and ballistic performance satisfactory.
34(Dev)	A21-11	7/6/64	48	36.861	S	S	S	S	S	S	S	S	S	S	S	S	S	Flight Configuration
35(Dev)	A21-12	7/15/64	49	36.960	S	S	S	S	S	S	S	S	S	S	S	S	S	Flight Configuration
36(Qual)	A21-17	8/17/64	52	37.571	S	S	S	S	S	S	S	S	S	S	S	S	S	Flight Configuration
37(Qual)	A21-18	8/26/64	53	37.828	S	S	S	S	S	S	S	S	S	S	S	S	S	Flight Configuration
38(Qual)	A21-23	9/1/64	54	37.711	S	S	S	S	S	S	S	S	S	S	S	S	S	Flight Configuration
39(Qual)	A21-24	9/9/64	53	37.491	S	S	S	S	S	S	S	S	S	S	S	S	S	Flight Configuration
40(Qual)	A21-19	2/5/65	Grad.	38.014	S	S	S	S	S	S	S	S	S	S	S	S	S	Flight Configuration
41(Qual)	A21-22	2/11/65	Grad.	38.418	S	S	S	S	S	S	S	S	S	S	S	S	S	Flight Configuration
42 (Special)	A22-1	3/11/65	Grad.	39.602	S	S	S	S	S	S	S	S	S	S	S	S	S	Flight Configuration
43 (Special)	A22-3	5/13/65	Grad.	40.790	S	S	S	S	S	S	S	S	S	S	S	S	S	Flight Configuration
44 (Special)	A22-2	5/18/65	Grad.	40.345	S	S	S	S	S	S	S	S	S	S	S	S	S	Flight Configuration

Table XIII (Cont'd)

SUBSYSTEM AND COMPONENT TEST SUMMARY

Test No	Motor Serial No.	Date Tested	Firing Temp.	Burn Time	Engine Assy.	Subsys. "A" and Comp.			Subsys. "B" and Comp.			Subsys. "C" and Comp.			Subsys. "D" and Comp.			Remarks
						A	A1	A2	B	B1	B2	C	C1	C2	D	D1	D2	
45 (Special)	A22-4	5/20/65	Grad.	41.812	S	S	S	S	S	S	S	S	S	S	S	S	S	Flight Configuration
46	A21-25	10/16/65	Grad.	40.035	S	S	S	S	S	S	S	S	S	S	S	S	S	Ballistic Performance Satisfactory, two squib Ignition characteristics satisfactory
49	A22-6	12/16/66	Grad.	43.260	S	S	S	S	S	S	S	S	S	S	S	S	S	Ballistic Performance Satisfactory, two squib Ignition characteristics satisfactory
50	A22-10	4/14/67	Grad.	44.692	S	S	S	S	S	S	S	S	S	S	S	S	S	Ballistic Performance Satisfactory, two squib Ignition characteristics satisfactory

TABLE XIII (Cont'd)

DEVELOPMENT AND QUALITY ASSURANCE TEST SUMMARY OF SURVEYOR MAIN RETROGRADE

LEGEND

The symbols and success/failure criteria for the columns of Table XIII are as follows:

Engine Assembly - Used for the calculation of the achieved engine reliability. Combined evaluation of A, B, C, and D

A Ignition System - combined evaluation of A1 and A2

A1 Initiator (squibs and boron pellets) - Initiate pyrogen propellant burning within specified time.

A2 Pyrogen - Upon receipt of the specified ignition current, the pyrogen should ignite the engine propellant within the specified ignition delay time.

B Fuel System - combined evaluation of B1 and B2

B1 Performance - If the ignition system performs as specified, the engine should ignite within the specified ignition delay time and the engine's performance parameters (total impulse, average and maximum pressure, action time, average, maximum and minimum thrust) should be within the specified limits.

B2 Grain - Cracks, voids, or liner separation shall not have caused any of the performance parameters to exceed the specified limits.

C Pressure Vessel - combined evaluation of C1 and C2.

C1 Structure (case and aft closure) - If not subjected to loads or temperatures in excess of the specified values, the pressure vessel shall sustain the maximum pressure specified.

C2 Insulation - If not subjected to loads in excess of the specified values, the pressure vessel shall not be subjected to temperatures in excess of the specified values which could cause a pressure vessel failure.

D Nozzle System - combined evaluation of D1 and D2

D1 Insert - Upon receipt of forces within the specified limits, the insert shall not have a structural failure and its performance shall not cause thrust and total impulse to be outside the specified limits.

D2 Exit Cone - Upon receipt of forces within the specified limits, the exit cone shall not have a structural failure and its performance shall not cause thrust and total impulse to be outside the specified limits.

The Surveyor Firing Summary (Table XIII) is based on the evaluation of test data, failure reports, and failure analyses with regard to the pretest definitions, resulting in appropriate decisions regarding equipment success or failure during the test. Pretest definition of valid reliability tests is accomplished through the Test Plan's Reliability Declaration of Intent. 71

TABLE XIV

RELIABILITY OF SURVEYOR MAIN RETROGRADE MOTOR (TE-M-364-1)

Development Program Firings			20
Qualification Firings			10
Quality Assurance Firings			3
Flight Firings			3*
	TOTAL		36
	Successes	36	
	Failures	0	
Reliability			0.981
Confidence Level			50%

*Two firings have been excluded due to a lack of confirming performance data.

B. RELIABILITY SUMMARY FOR THE TE-M-345 (TITAN II VERNIER)

For the qualification of the Titan II Vernier motor, 21 motors were fired for their full duration, and another 39 motors were terminated prior to burnout to qualify the termination capability and impulse reproducibility characteristics of the motor. Since the completion of the qualification firings, there have been 20 Titan II test flights reported, each carrying two successful motors. In addition, 16 motors have been fired in the quality assurance program. During the program, there were no failures (see Table XV).

TABLE XV

RELIABILITY OF TITAN II VERNIER (TE-M-345)

Qualification Program			
Full Duration Firings			21
Thrust-Terminated Firings			39
Flight Firings			40
Quality Assurance Firings (Full Duration)			16
TOTAL FIRINGS			116
Successes	116		
Failures	0		
Reliability		0.9940	
Confidence Level		50%	

VII. THRUST MISALIGNMENT

To obtain the required nozzle axis alignment on the Surveyor Main Retro Motor, the nozzle is mated to the empty case and rotated until the best alignment position is reached. This position is marked on the case and the nozzle so that it can be repeated after the case is loaded. The procedure which is detailed in Appendix C is used to align the nozzle after the case is loaded. This procedure has consistently produced motors which exhibited average thrust misalignment angles of less than 0.025 degree.

Figure 15 is a plot of thrust versus time and thrust vector misalignment versus time for a Surveyor Main Retro motor firing. Of the four motors that were instrumented to obtain thrust misalignment data during the qualification phase of the Surveyor program, this particular motor exhibited the largest thrust misalignment that was measured. For a complete discussion of the results of these tests the reader is referred to "Quality Assurance Testing of Surveyor Main Retro Engine at AEDC," Hughes Aircraft Company, Space Systems Division, SSD 5118R, February 1965. Due to the length of this report it is not being reproduced here. All motors exhibited approximately 0.30 degree of misalignment at ignition and dropped back to a significantly lower level for the duration of the high-thrust period. The thrust-vector angular excursion specification was met and as a result of these tests the thrust-vector displacement limits were relaxed.

As the thrust and chamber pressure tail off at the end of the burn time, a larger deviation appears in the thrust misalignment data. The spike that occurs at 42 seconds in Figure 15 may be due to non-uniform flow separation in the nozzle or to the diffuser shock wave propagating back up the diffuser. In a true space environment, the above conditions would not be encountered, and the thrust misalignment would follow the uniform pattern that it exhibits during the high-thrust period.

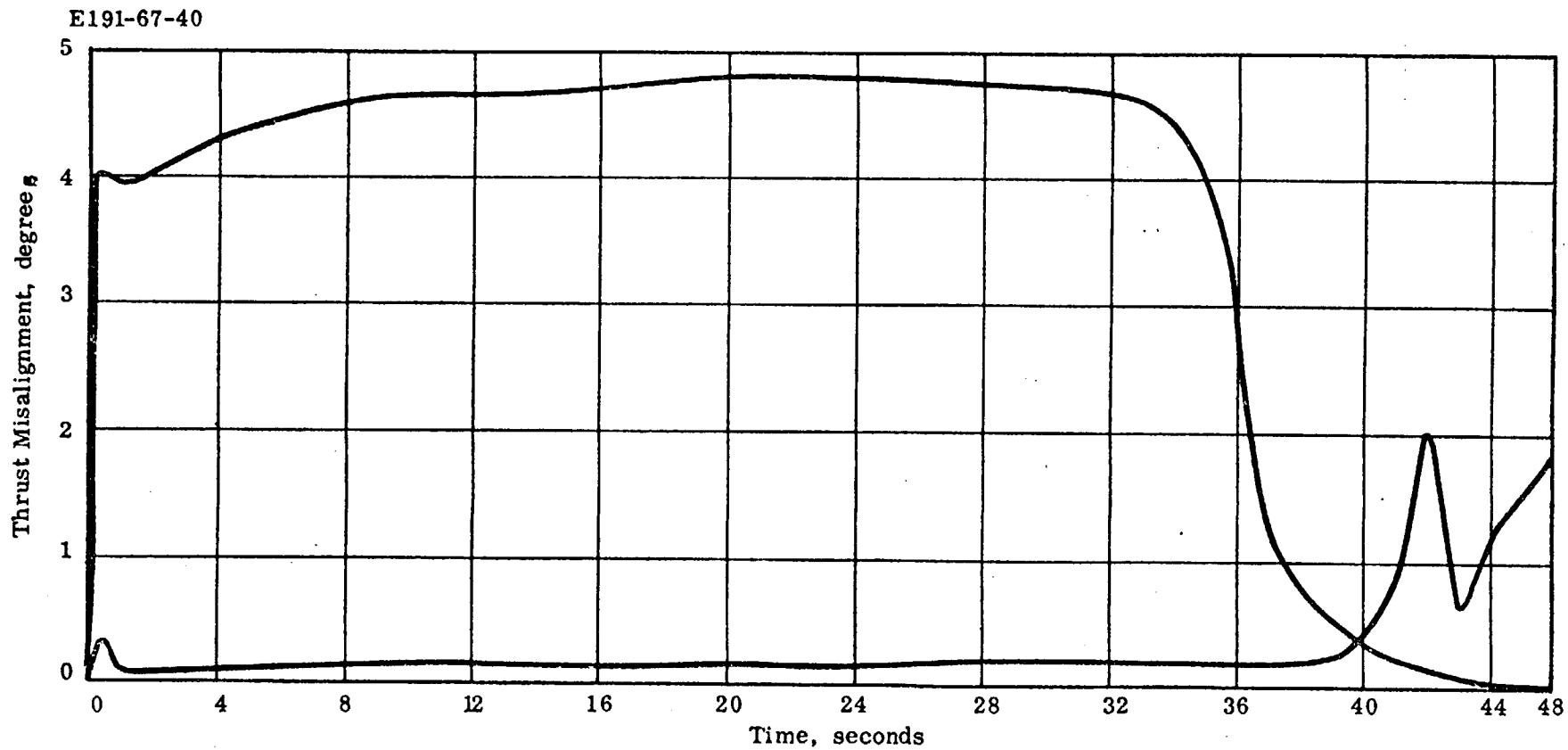

FIGURE 15. THRUST AND THRUST MISALIGNMENT VERSUS TIME

VIII. EFFECT OF STERILIZATION AND PLANETARY QUARANTINE ON MOTOR DESIGN AND PERFORMANCE

The NASA mission requirement that specifies sterilization for all spacecraft that will enter the atmosphere of, or impact upon, any planet, has given rise to numerous spacecraft design problems that heretofore have not been encountered. The following guidelines have been established: the probability of any single probe contaminating a planet with viable earth microorganisms must be less than 1 in 10,000; or alternatively, a 50-year planetary quarantine must be observed. This specification in its broadest interpretation has resulted in the requirement for onboard propulsion systems to withstand the terminal dry-heat-sterilization cycle, because other sterilization techniques have not yet been proven adequate for quarantine requirements.

The design problems resulting from sterilization itself can be surmounted at the present time. However, when these are coupled with the reliability requirements of qualification, the difficulties increase by an order of magnitude. That is, whether the defined time-temperature history of sterilization is 295°F (145°C) for 36 hours or 275°F (135°C) for 53 hours, a flight acceptance specification that necessitates demonstration of capability for six sterilization cycles presents problems that heretofore have not been encountered. With regard to this, it is clear that there exists a definite need for clarification of the sterilization requirements as peculiar to the propulsion area. Further resolution and definition of performance penalties, system scale-up, and time and number of cycles to accomplish motor sterilization and ensure reliability, must await this decision. In the meantime, the need for motor firings to demonstrate the technical feasibility of presently defined design solutions and to clarify certain potential problem areas (such as thermal initiation of the propellant charge due to self-heat from internal chemical decomposition) cannot be too strongly emphasized.

A. EFFECT OF STERILIZATION ON THE PROPELLANT-LINER SYSTEM

During sterilization, two types of chemical reactions involving the propellant binder can be expected:

a. Oxidative crosslinking of polymer chains, and

b. polymer chain scission.

Crosslinking results in increased modulus, decreased elongation, and hardening or embrittlement of the propellant. Chain scission causes loss of tensile strength and propellant softening. Both depend on the presence of oxygen, and typically occur simultaneously. The overall effect on the propellant binder, of course, is determined by whichever reaction is dominant. This, in turn, is influenced by several variables including environmental temperature, the presence or absence of moisture, temperature, and polymer type.

Considerable research and development effort is still required in this area. It would seem at this time that only a thermo-chemically stable binder would be suitable for all mission applications. That is, if a stable system is not available, the use of a binder exhibiting a dominant crosslinking reaction would be desirable (to avoid gross deformation of the grain). It is highly unlikely that this could be accomplished without incurring a severe reliability penalty. In any case, it would be necessary to assess the impact of propellant hardening resulting from extensive heating and sterilization thermal gradients. The magnitude of the resulting damage is not readily assessable at this time; however, the effect on motor design will be most pronounced on exposed surface. It is not expected, based upon information currently available on aged motors, that ignition of a sterilized spherical motor will present a problem. However, it is also quite evident that this local loss of propellant strain capacity must be carefully examined regarding changes in level of resistance to surface fracture.

B. EFFECTS OF DIFFERENTIAL EXPANSION

It has been previously reported[5] that the magnitude of this problem can be significantly reduced, if not completely eliminated, through judicious selection of materials and the use of proper clearances.

C. THERMAL DEGRADATION

A third problem is the thermal decomposition of motor materials, which results in the production of decomposition products. If these products are gases or vapors, then they will generate an internal stress field that can lead to mechanical failure. This problem is not considered serious for inert components because of the wide choice of available materials; however, with a solid propellant that thermally degrades, one is not so fortunate, since compositional changes are limited, and usually such changes will violate other constraints. Thus, in selecting a propellant formulation that can withstand repeated heat cycling, one must perform laboratory or scale tests of the propellant to assure that thermal degradation will not cause motor failure within the required number of heat cycles. Another topic that should be considered in selecting a propellant is the exothermic thermal decomposition of solid propellants (commonly called bulk cook-off), which can lead to deflagration of the propellant grain.

D. TIME TO REACH STERILIZATION TEMPERATURES

The time required to reach sterilization temperatures is a significant motor design consideration. Since propellant is a relatively good thermal insulator, fairly long heating times are to be expected.

---

[5] Andrews, W. G. and Kirschner, T. J., "Heat Sterilizable Solid Propellant Motor Designs for Interplanetary Missions," AIAA Journal of Spacecraft and Rockets, Volume 4, No. 5, May 1967.

Figure 16 illustrates the time required to reach a sterilization temperature of 295°F as a function of spherical case diameter. It can be seen that a 30-inch spherical motor of the Surveyor type would require approximately 55 hours to reach a stabilized temperature of 295°F.

The Gemini Retro Motor (TE-M-385), which has a 12.8-inch spherical motor case, was temperature cycled in a temperature gradient study conducted at Thiokol-Elkton. A continuous strip chart recorder was used to monitor thermocouples which were located at various points in the propellant grain (see Figure 17). Plots of temperature and temperature versus time were made (see Figures 18 and 19). The temperature gradient shown in Figure 19 was obtained by plotting the extreme temperature difference as a function of time where the extreme temperature difference was defined to be the arithmetic difference between the readout of thermocouples No. 1 and No. 4 at any instant.

The Thiokol 100-pound sterilizable motor is a case-bonded, circular-perforate design having a nominal spherical diameter of 16 inches. This motor evolved during a study of heat sterilizable motor design problems which Thiokol conducted for JPL in 1966. The design is shown in Figure 20.

An analysis was made to determine the time required to heat the grain from 70°F to the sterilization temperature of 295 ± 2°F. The results for determining the heating time of the motor were calculated by using a two-dimensional axisymmetrical transient heat transfer analysis. This was performed using Thiokol Program No. 40702, "Arbitrary Node Thermal Computer Program." This program can consider as many as 12 different materials. Material properties can be varied with respect to time and location, and the program can also simulate air gaps by using zero capacity nodes and contact resistances between adjacent nodes.

The thermal model for this design is shown in Figure 21, a two-dimensional nodal array that closely approximates the longitudinal grain section. Figure 22 shows the locations and numbers of nodes. For this analysis, the case material was neglected. This simplifying assumption has little effect on the results of the calculations since the thermal diffusivity of the case material is high compared to that of the propellant and case insulation. Heat flow is allowed to take place through the external spherical surface only. The internal portion of the grain and the end of the grain were assumed to be adiabatic surfaces. This makes the analysis somewhat conservative since, in actuality, case heating of the motor on all surfaces (especially the nozzle structure) would reduce the time required to heat to 295 ± 2°F.

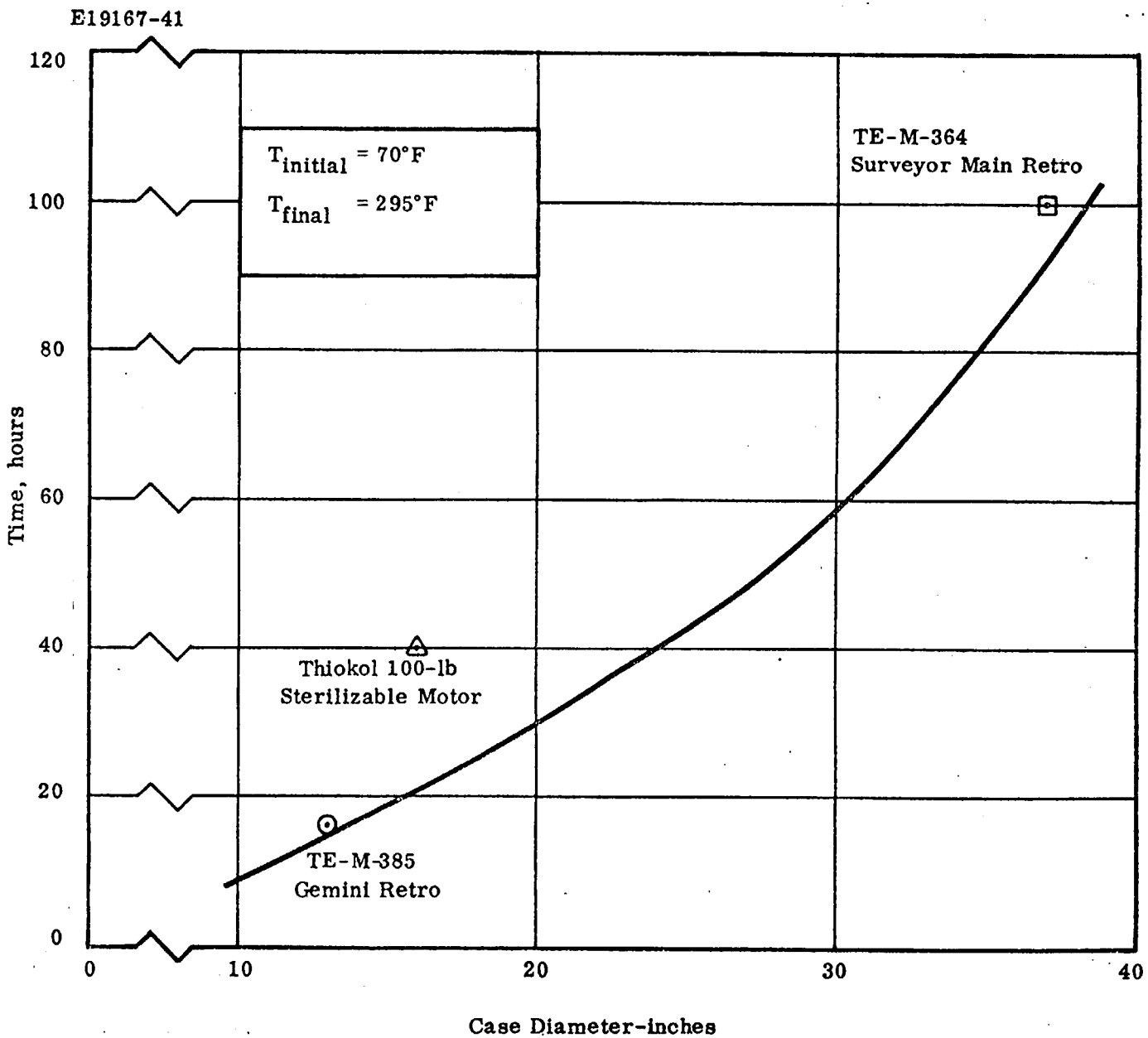

FIGURE 16. TIME TO REACH STERILIZATION TEMPERATURE
SPHERICAL MOTOR DESIGNS

THERMOCOUPLE LOCATIONS

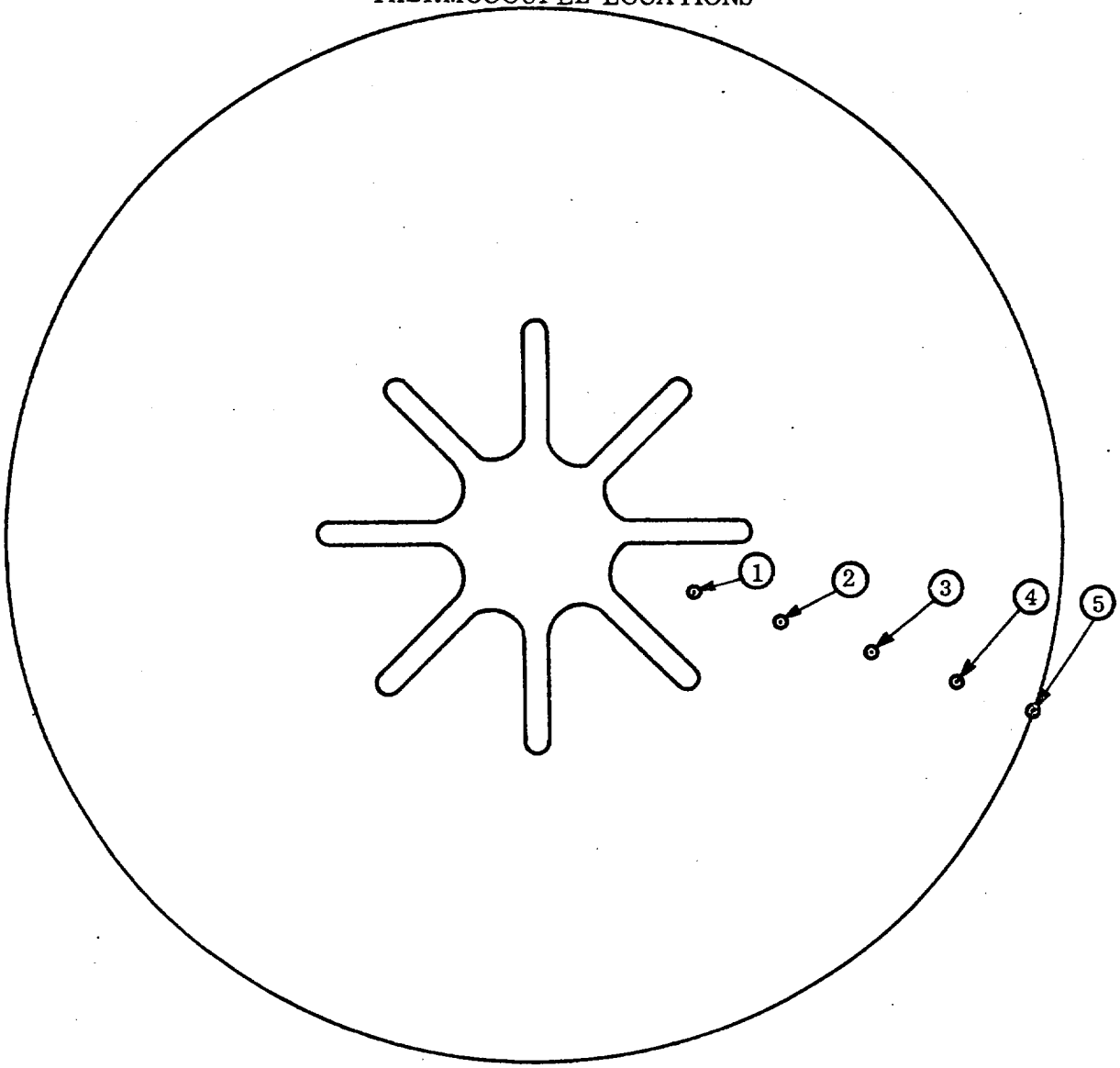

FIGURE 17. TE-M-385 TEMPERATURE GRADIENT STUDY

Locations:

1. All thermocouples imbedded in grain (1 through 4) are located 3/4" above girth weld.
2. No. 1 - 4-1/2" from case wall
   No. 2 - 3-9/16 from case wall
   No. 3 - 2-5/8" from case wall
   No. 4 - 1-3/4" from case wall
   No. 5 Located on case wall
   No. 6 Temperature of box on vacuum conditioned unit and reconditioned unit
   No. 6 Temperature of grain surface on sea level conditioned unit

E191-67-43

TE-M-385

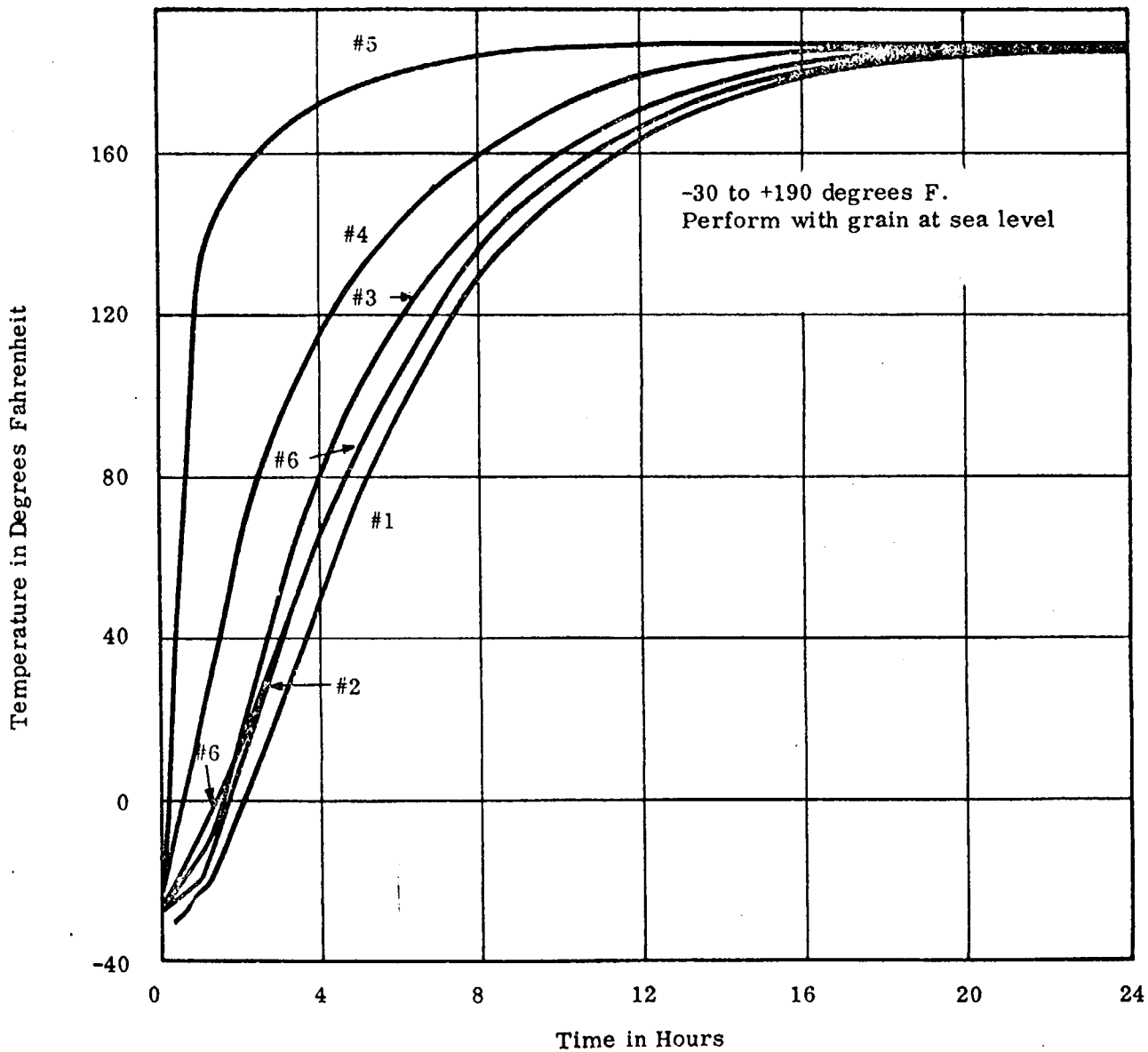

FIGURE 18. TEMPERATURE GRADIENT STUDY, TEMPERATURE DISTRIBUTION

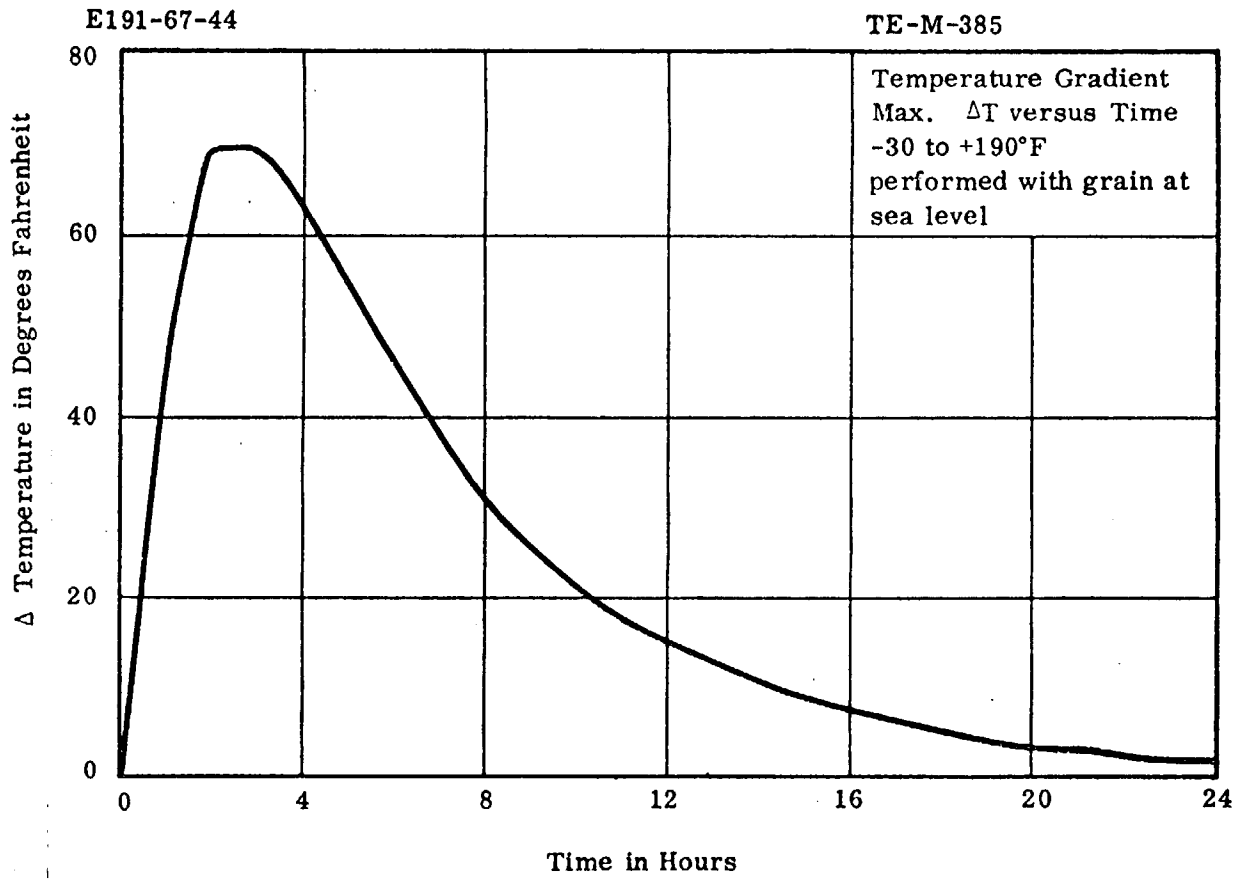

FIGURE 19. TE-M-385 TEMPERATURE GRADIENT STUDY — MAXIMUM TEMPERATURE GRADIENT

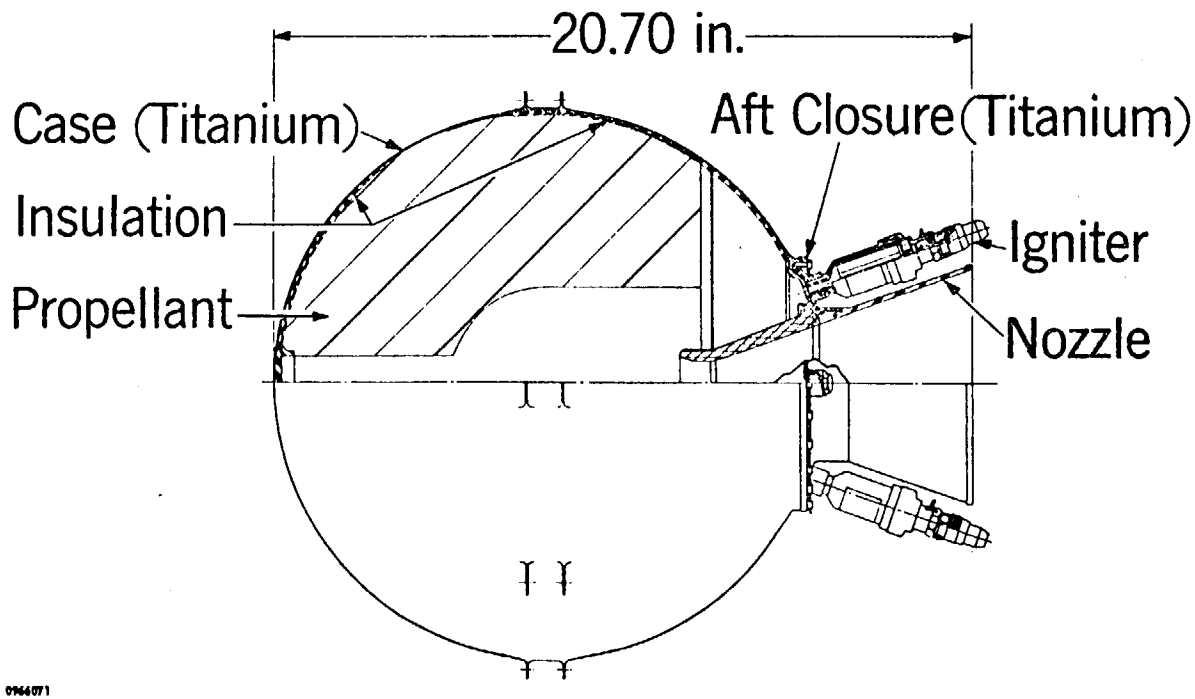

FIGURE 20. CASE-BONDED SPHERICAL CIRCULAR PERFORATE MOTOR ASSEMBLY

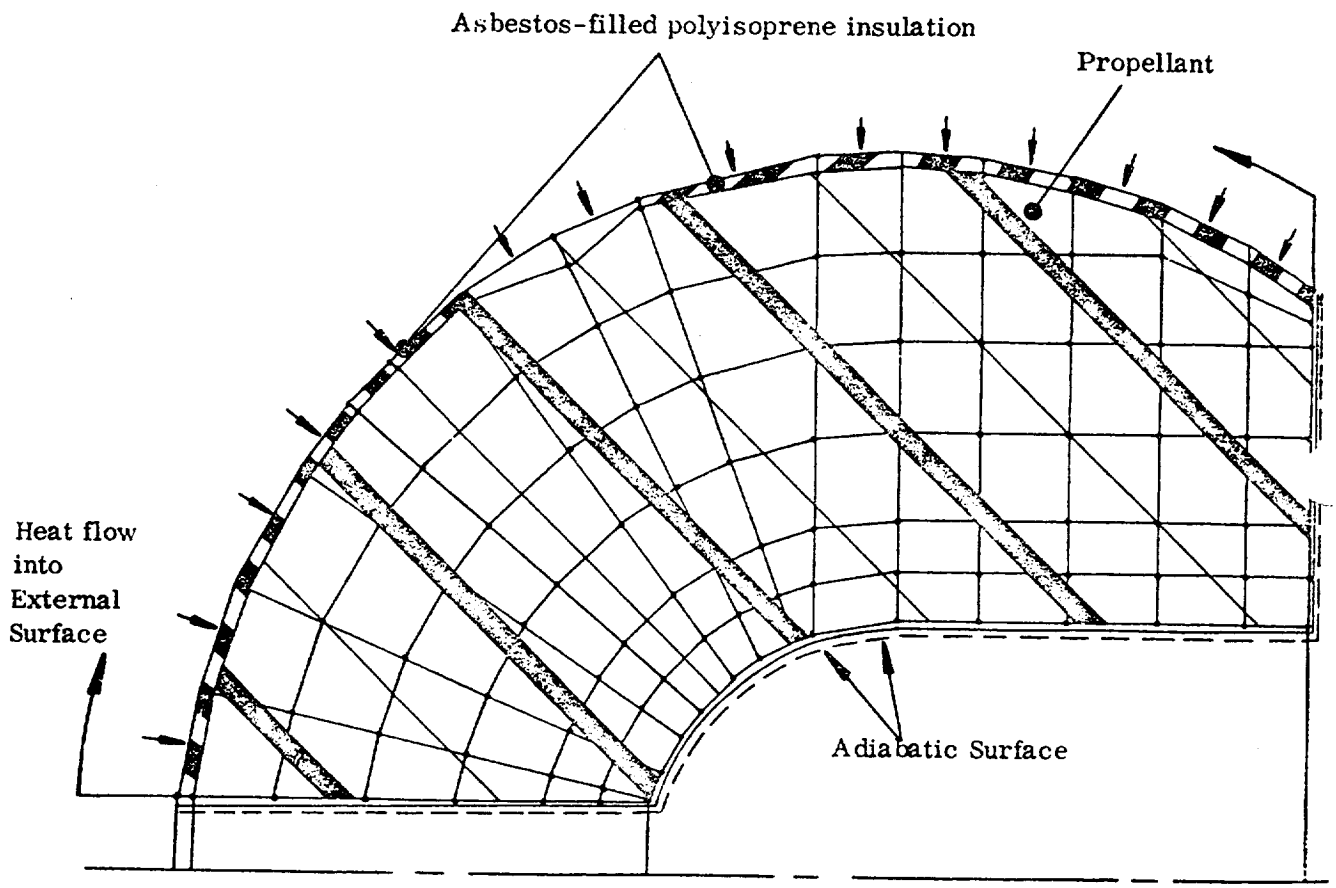

FIGURE 21. THERMAL MODEL CASE-BONDED SPHERICAL CIRCULAR PERFORATE MOTOR DESIGN

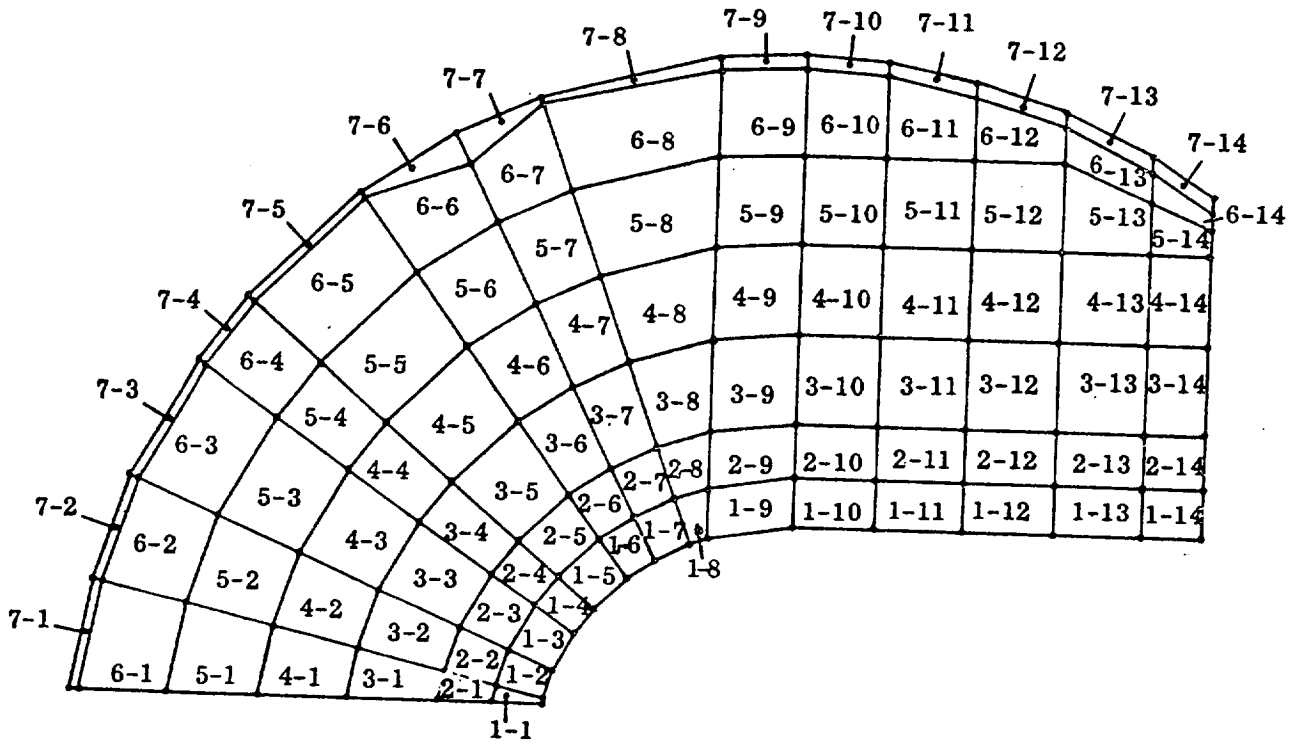

FIGURE 22. NODAL LOCATIONS AND NOTATION

The properties of the propellant and insulation used are as follows:

Material	Density	Specific Heat	Thermal Conductivity
Asbestos-filled polyisoprene insulation	0.043 lb/in.^{3}	0.392 btu/lb/°F	2.638×10^{-6} btu/in. sec °F
TP-H-3105 Propellant	0.0595 lb/in.^{3}	0.272 btu/lb/°F	3.528×10^{-6} btu/in. sec °F

The external film coefficient was based on forced convection on the outside of the motor case. A heat transfer coefficient of 2.0×10^{-6} btu/°F-sec-in.^{2} at 50°F increasing to 2.199×10^{-6} btu/°F-sec-in.^{2} at 305°F was used. The driving temperature for this analysis was 305°F.

Figure 23 presents the temperature-time history of various nodes through the grain and Figure 24 shows the temperature distribution throughout the grain at the end of 40 hours.

The time that it would take a TE-M-364 to reach a sterilization temperature of 295°F was estimated from the results of a study conducted by Thiokol for Hughes Aircraft Company in 1962.[6]

E. VOLUMETRIC LOADING DENSITY AND WEB FRACTION CONSTRAINTS

For a chemically unstable propellant binder system, the combined effects of sterilization and reduced propellant strain capacity do impose maximum VLD and web fraction design limitations. If one excludes potential adhesive propellant/liner bond problems, data available at this time on candidate binders following six 53-hour cycles at 275°F (135°C) would strongly indicate that volumetric loading densities comparable to those of the TE-M-364 could be achieved. However, the desire for extended low temperature operational capability could seriously affect this conclusion. A definitive judgment must be withheld until the candidate propellant's structural response (following sterilization) is determined over the temperature range of interest.

[6] "An Investigation into Methods of Sterilizing the Surveyor Main Retro Engine and their Effects on Engine Components," Thiokol Chemical Corporation, Elkton Division, Elkton, Maryland, Summary Report 23-63, August 3, 1962.

E191-67-01

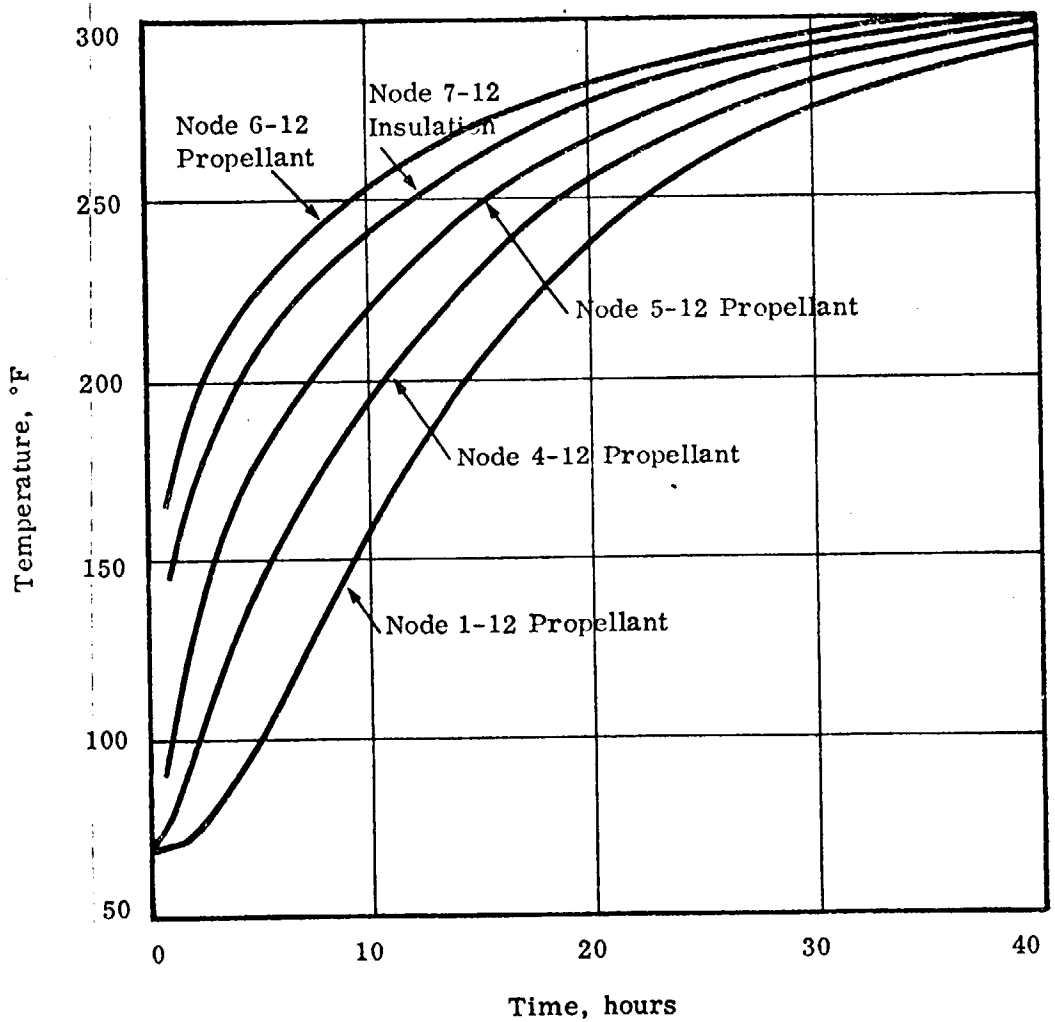

FIGURE 23. TEMPERATURE VERSUS TIME FOR HEATING BY FORCED CONVECTION

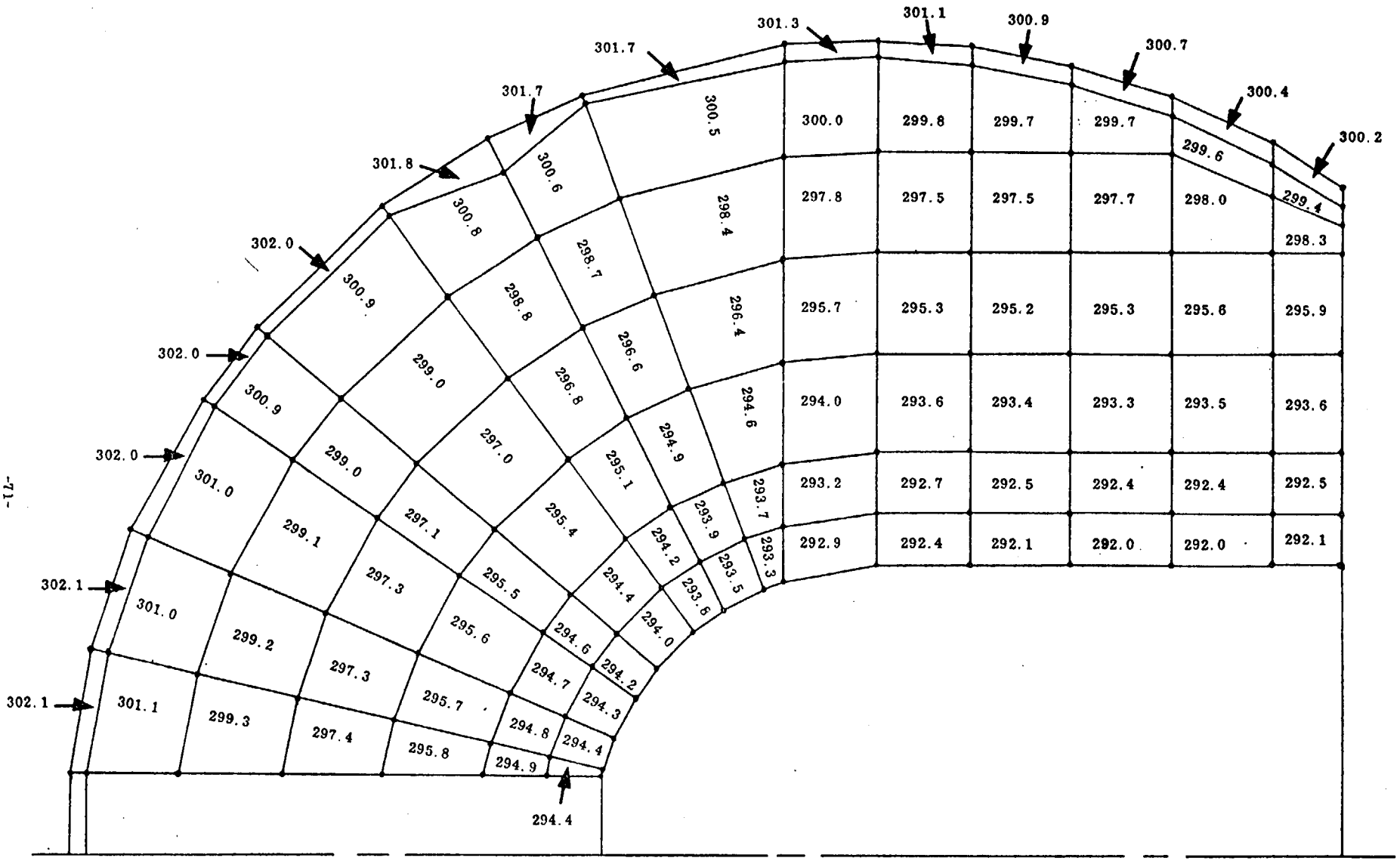

FIGURE 24. NODAL TEMPERATURES AFTER 40 HOURS

IX. GLOSSARY

A_e	—	Exit area, in.^{2}
A_t	—	Throat area, in.^{2}
a	—	Reference burn rate, in./sec
C_f	—	Thrust coefficient
C_D	—	Discharge coefficient
D	—	Diameter, in.
D_e	—	Exit diameter, in.
D_t	—	Throat diameter, in.
F	—	Thrust, lb_f
g	—	Local gravitational acceleration, ft/sec^2
I_{tot}	—	Total impulse, lb_f-sec
I_{sp}	—	Specific impulse, lb_f-sec/lb_m
L	—	Length, in.
n	—	Burn rate exponent
P_c	—	Chamber pressure, psia
P_{max}	—	Maximum pressure, psia
r_b	—	Burn rate, in./sec
S	—	Nozzle submergence, %
S.F.	—	Safety factor
t_b	—	Burn time, sec
VLD	—	Volumetric loading density

W_{att}	—	Attachment weight, lbs
W_c	—	Case weight, lbs
W_f	—	Web fraction
W_h	—	Hardware weight, lbs
W_{ig}	—	Igniter weight, lbs
W_{ins}	—	Insulation weight, lbs
W_l	—	Liner weight, lbs
W_n	—	Nozzle weight, lbs
W_p	—	Propellant weight, lbs
W_s	—	Stage weight, lbs
π	—	3.1415926
γ	—	Specific heat ratio of gases
λ	—	Nozzle divergence factor
ΔV	—	Velocity increment, ft/sec
τ	—	Case thickness, in.
ρ_c	—	Case density, lbs/in.^{3}
ρ_p	—	Propellant density, lbs/in.^{3}
σ	—	Case yield strength, psi Standard deviation

APPENDIX A

SPHERICAL PERFORMANCE AND WEIGHT PREDICTION PROGRAM

A. INPUT FORMAT
B. SCHEMATIC OF AN ASSEMBLED DATA DECK
C. SAMPLE DATA SET
D. PROGRAM FORTRAN IV LISTING
E. SAMPLE OUTPUT

SHEET 1 of 3 SPHERICAL PERFORMANCE AND WEIGHT - E40310

WORD	1
COLUMNS	2 - 72
FORMAT	14A5, A1
CARD #1	IDENTIFICATION CARD #1
SYMBOL	Card 1

WORD	1
COLUMNS	2 - 72
FORMAT	14A5, A1
CARD #2	IDENTIFICATION CARD #2
SYMBOL	CARD 2

WORD	1	2	3	4	5	6	7	8	9	10
COLUMNS	1-10	11-20	21-30	31-40	41-45	46-50	51-55	56-60	61-65	66-70
FORMAT	F10.0	F10.0	F10.0	F10.0	I5	I5	I5	I5	I5	I5
CARD #3	SPECIFIED BURN TIME SEC	TOTAL STAGE WT. INCLUDING R/M LBM	GRAVITY TERM COEFFI-CIENT	LOCAL GRAV. ACC. FT/SEC^2	NO. OF CHAMBER PRESSURES CONSIDERED NP<8	NO. OF EXPANSION RATIOS CONSIDERED NEX≤8	NO. OF ΔV OR TOTAL IMPULSE LEVEL NDELVR≤8	000-FULL PRINTOUT 001-PRINT INITIAL SHEET & SUMMARY	000-LAST SET OF DATA 001-MORE DATA FOLLOWS	000-TOTAL IMPULSE IS INPUT 001-ΔV IS INPUT
SYMBOL	C5	WS	C1	GS	N	NEX	NDELVR	NPR	NC	IXX

WORD	1	2	3	4	5	6	7
COLUMNS	1-10	11-20	21-30	31-40	41-50	51-60	61-70
FORMAT	F10.0	F10.0	F10.0	F10.0	F10.0	F10.0	F10.0
CARD #4	CASE LENGTH TO DIAMETER RATIO	VOLUMETRIC LOADING DENSITY	CASE SAFETY FACTOR	CASE MATERIAL STRENGTH TO WEIGHT RATIO IN.	WEB FRACTION	NOZZLE SUBMERGENCE	MAXIMUM CASE DIAMETER
SYMBOL	CLD	VLD	SF	CSTWR	WF	SUB	DCMAX

WORD	1	2	3	4	5	6	7	8	9
COLUMNS	1-5	6-10	11-20	21-30	31-40	41-50	51-60	61-70	71-80
FORMAT	2A5		F10.0	F10.0	F10.0	F10.0	F10.0	F10.0	F10.0
CARD #5	PROPELLANT IDENTIFICATION		PROPELLANT REFERENCE SPECIFIC IMPULSE LBF-SEC/LBM	ISP EFFICIENCY	PROPELLANT SPECIFIC HEAT RATIO	PROPELLANT BURN RATE COEFFICIENT	PROPELLANT BURN RATE EXPONENT	PROPELLANT BURN RATE REFERENCE PRESSURE PSI	PROPELLANT DENSITY GM/CC OR LBM/IN3
SYMBOL	PROPID(1)	PROPID(2)	REFISP	EFF	GAM	BRC	BRE	BRRP	DENP

WORD	1	2	3	4	5	6	7	8
COLUMNS	1-10	11-20	21-30	31-40	41-50	51-60	61-70	71-80
FORMAT	F10.0	F10.0	F10.0	F10.0	F10.0	F10.0	F10.0	F10.0
CARD #6	CHAMBER PRESSURE VALUES PSIA							
SYMBOL	PC(1)							

WORD	1	2	3	4	5	6	7	8
COLUMNS	1-10	11-20	21-30	31-40	41-50	51-60	61-70	71-80
FORMAT	F10.0	F10.0	F10.0	F10.0	F10.0	F10.0	F10.0	F10.0
CARD #7	EXPANSION RATIOS							
SYMBOL	EX(1)							

WORD	1	2	3	4	5	6	7	8
COLUMNS	1-10	11-20	21-30	31-40	41-50	51-60	61-70	71-80
FORMAT	F10.0	F10.0	F10.0	F10.0	F10.0	F10.0	F10.0	F10.0
CARD #8	VELOCITY INCREMENT REQUIRED (FT/SEC) OR TOTAL IMPULSE REQUIRED (LBF-SEC)							
SYMBOL	DELVR(1) OR DIT(1)							

WORD	
COLUMNS	
FORMAT	
CARD	
SYMBOL	

B. SCHEMATIC OF AN ASSEMBLED DATA DECK

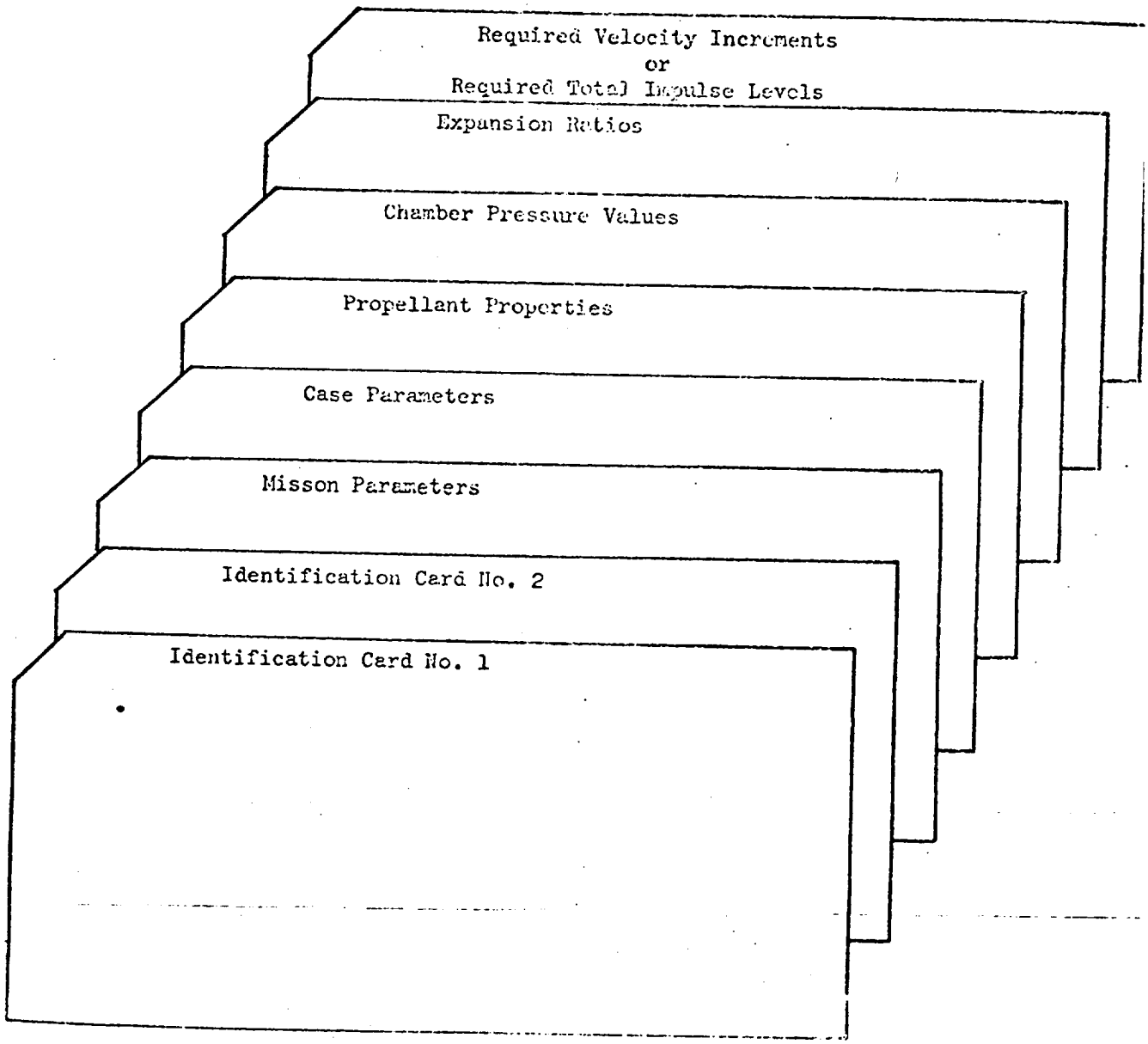

C. SAMPLE DATA SET

```
200000.

0
10.0      30.0      53.0      80.0

0
500.0     400.0     500.0     600.0     700.0     800.0     900.0     1000.0

0
TP-H-3062 245.      .97       1.16      .31       .29       1000.     .0625

1.0       .85       1.4       1100000.  .6        .40

0.0       2100.0    0.0       0.0       8    4    1    000  000  000

200000 LBF-SEC TOTAL IMPULSE MOTOR USING PB-AP-AL PROPELLANT

SAMPLE DATA SET TO DESIGN A
```

D. PROGRAM FORTRAN IV LIST G

```
40310  SPHERICAL PERFORMANCE                    FORTRAN SOURCE LIST                    09/12/67      PAGE  1
       ISN       SOURCE STATEMENT

         0 $IBFTC MAIN    REF
           C       SPHERICAL PERFORMANCE AND WEIGHT PROGRAM E-40310
         1         COMMON / ZTAPES / NTAPES(10)
         2         EQUIVALENCE (NTAPES(2),N2), (NTAPES(3),N3),  (NTAPES(4), 11)
         3         DIMENSION  CARD1(15), CARD2(15), EX(12), PISPT(12),
                  1                PC(12), W11(12,12), NITER(12,12), W12(12,12),
                  1            DIT(12,12),DC(12,12), CL(12,12), W2(12,12), TB(12,12),
                  1            CIGSTB(12,12), DE(12,12), TLN(12,12), W3(12,12),
                  1            W4(12,12), W5(12,12), DELW5(12,12), W6(12,12),
                  1            PWFA(12,12), W7(12,12), WPLWS(12,12), DELVA(12,12)
         4         DIMENSION  PRCPID (100),    DELVR (12)
         5         DIMENSION   RIT(12)
         6         CALL TAPES
         7         LP = 1
        10         REWIND 11
        11         IFILE = 0
        12      99 READ (N2,999) CARD1, CARD2
        13     999 FORMAT (1X14A5,A1/1X14A5,A1)
        14         READ (N2, 1000)GS, WS, C1, GS, NP, NEX, NDELVR, NPR, NC, IXX
        23    1000 FORMAT (4F10.0, 6(3XI2))
        24         READ(N2, 1001) CLD1,VLD, SF, CSTWR, WF, SUB,DCMAX
        25    1001 FORMAT (7F10.0)
        26         READ(N2, 1002) PROPID(LP),PRCPID(LP+1), REFISP, EFF, GAM, BRC,BRE,
                  1BKRP, CENP
        27    1002 FORMAT (2A5, 7F10.0)
        30         READ(N2, 1003) (PC(K), K=1,NP)
        35         READ(N2, 1003) (EX(K), K=1,NEX)
        42    1003 FORMAT(8F10.0)
        43         IF (IXX) 1005,1004,1005
        44    1004 READ(N2,1003) (RIT(K),K=1,NDELVR)
        51         GO TO 1006
        52    1005 READ(N2,1003) ( DELVR(K),K=1,NDELVR)
        57    1006 CONTINUE
           C       CONSTANTS
        60         G = 32.17
        61         IDEL = 0
        62       1 IDEL = IDEL + 1
           C
        63         IF (DCMAX .EQ. 0.0)      DCMAX = 999999.
        66         ZTB = 0.0
        67         ZPWFA = 0.0
        70         ZCIGS = 0.0
        71         ZWPLWS= 0.0
        72         ZW7   = 0.0
        73         ZDC   = 0.0
        74         ZDE   = 0.0
        75         ZLIT  = 0.0
        76         ZPISPT = 0.0
        77         ZEFF = 0.0
       100         YTB   = 1.0E15
       101         YPWFA = 1.0E15
       102         YCIGS = 1.0E15
       103         YWPLWS= 1.0E15
       104         YW7   = 1.0E15
       105         YDC   = 1.0E15
```

```
ISN        SOURCE STATEMENT

106        YLE   = 1.0E15
107        YDIT  = 1.0E15
110        YPISPT = 1.0E15
111        YEFF = 1.0E15
112        KSTAR = 0
113        PEPCD = 0.02
114        W11(1,1) = 0.001
115        GM1G = (GAM - 1.0)/GAM
116        X2GGM = 2.0/GM1G
117        CAPGA2 = GAM*(2.0/(GAM+1.0))**((GAM+1.0)/(GAM-1.0))
120        GG = CAPGA2/X2GGM
121        CAPG = SQRT(CAPGA2 * X2GGM)
122        CFOPTR = CAPG*SQRT(1.0 -(0.0147)**GM1G)
123        DO 104  K=1, NEX
     C
     C     COMPUTE CF - METHOD OF ITERATION ON PE/PC
     C
124    101 PEPC = ((1.0/EX(K))**GAM)*(GG/(1.0-PEPCD**GM1G))**(GAM*.5)
125        IF (ABS(1.0 - PEPC/PEPCD)-.0001) 103,103,102
126    102 PEPCD=PEPC
127        GO TO 101
130    103 CFOPT = CAPG*SQRT(1.0 - PEPC**GM1G)
131        CFX = CFOPT + (PEPC*EX(K))
132        PISPT(K) = REFISP * CFX / CFOPTR
133    104 CONTINUE
135    130 IF (DENP - 1.0) 132, 133, 133
136    132 DENP1 = DENP
137        DENP2 = DENP / 0.03613
140        GO TO 130
141    133 DENP2 = DENP
142        DENP1 = DENP * 0.03613
143    130 TBC =  C5
144        DO 700  K = 1, NEX
145        DO 500  J = 1, NP
146        CLD =CLD1
147        NITER (J,K) = 0
150        IF (IXX) 111,112, 111
151    111 VARA = (DELVR(IDEL) + C1 * GS * TBC)/(PISPT(K) * EFF     * G)
152        W12(J,K) = WS * (1.0 - 1.0 / EXP(VARA))
153        DIT(J,K) = PISPT(K) * EFF     * W12(J,K)
154        DC(J,K) = (5.8197*W12(J,K)/(VLD * DENP1)/(3.0 *
          1            CLD - 1.)) ** ( 1.0/3.0)
155        IF (DC(J,K) .GT. DCMAX)   CLD = 1. / 3. + 4. * W12(J,K)/(3.14159*
          1DENP1 * VLD * DCMAX**3.)
160        IF (DC(J,K).GT.DCMAX)   DC(J,K) = DCMAX
163        CL(J,K) =  CLD *  DC(J,K)
164        W2(J,K) = 1.26*DC(J,K) ** 3.0 * SF/ CSTWR * (2.0 *CLD -1.0)*PC(J)
165    135 IF (C5) 140, 136, 140
166    136 IF (BRC) 138, 137, 138
167    137 TBC = 14.085 * WF*DC(J,K) / PC(J) **0.31
170        GO TO 139
171    138 TBC = WF/2.* DC(J,K) * (PC(J) / BRRP) ** (-BRE)/ BRC
172    139 IF (C1) 145, 140, 145
173    145 WRATIO = 1.0 - W12(J,K) / W11(J,K)
174        IF (ABS(WRATIO) - 0.001) 140, 140, 150
```

```
ISN        SOURCE STATEMENT

175   150 W11(J,K) = W12(J,K)
176       NITER(J,K) = NITER(J,K) + 1
177       GO TO 111
200   112 W12(J,K) = RIT(IDEL) / (PISPT(K) *EFF)
201       DC(J,K) = (5.8197*W12(J,K)/(VLD * DENP1)/(3.0 *
         1          CLD - 1.)) ** ( 1.0/3.0)
202       IF (DC(J,K) .GT. DCMAX)   CLD = 1. / 3. + 4. * W12(J,K)/(5.14159*
         1DENP1 * VLD * DCMAX**3.)
205       IF (DC(J,K).GT.DCMAX)   DC(J,K) = DCMAX
210       DIT(J,K) = RIT(IDEL)
211       CL(J,K) =  CLD *  DC(J,K)
212       W2(J,K) = 1.28*DC(J,K) ** 3.0 * SF/ CSTWR * (2.0 *CLD -1.0)*PC(J)
213   115 IF (C5) 140, 116, 140
214   116 IF (BRC) 118, 117, 118
215   117 TBC = 14.085 * WF*DC(J,K) / PC(J) ** 0.31
216       GO TO 140
217   118 TBC = WF/2.* DC(J,K) * (PC(J) / BRRP) ** (-BRE)/ BRC
220   140 TB(J,K) = TBC
221       CIGSTB(J,K)  =  CI * GS * TB(J,K)
222       AT = DIT(J,K) / (TB(J,K) * PC(J)                    * PISPT(K) *CFGPTR
         1     * 0.96) * REFISP
223       DT = (1.273 * AT ) ** 0.5
224       DE(J,K) = DT * SQRT( EX(K))
225       TLN(J,K) = ( DE(J,K) - DT) /0.728 * (1.0 - SUB) - DC(J,K)/2.
         1            + SQRT( DC(J,K) ** 2.0/4. - (( DE(J,K) - DT ) /0.728
         2            * SUB * 0.364 + DT / 2.0 ) ** 2.0 )
226       CL(J,K) =  DC(J,K) * CLD  +  TLN(J,K)
227       W3(J,K) = 0.431 * (AT ** 2.0 * EX(K) / (1.0 - SUB))** 0.512
230       WIN = 0.00345 * (DC(J,K) ** 2.0 * TB(J,K)/ 1000.0 ) ** .693 * CLD
231       WPY = 0.92 * AT ** 0.5
232       WATT = 0.01 * DC(J,K) ** 2.0
233       W4(J,K) = 0.00175 * DC(J,K) ** 2.0 + DC(J,K) ** 3.0 / 15742.0
         1          + WATT + WIN + WPY
234       W5(J,K) = (W2(J,K) + W3(J,K) + W4(J,K))
235       DELW5(J,K)= 0.16 *  (WPY) +  0.064 *  (W3(J,K) + WIN)
236       W6(J,K) = W5(J,K) - DELW5(J,K)
237       W7(J,K) =  W12(J,K) +    W5(J,K)
240       PWFA(J,K) = W12(J,K) / W7(J,K)
241       WPLWS(J,K) = (WS - W7(J,K)) / WS
242       DELVA(J,K) = PISPT(K) * EFF    * G * (ALOG (WS/(WS-W12(J,K))))
         1                - CIGSTB(J,K)
243       IF  (TB(J,K).LE.ZTB)GO TO 200
246       ZTB = TB(J,K)
247       JN1 = J
250       KN1 = K
251   200 IF  (TB(J,K).GT.YTB)GO TO 210
254       YTB = TB(J,K)
255       JN2 = J
256       KN2 = K
257   210 IF  (PWFA(J,K).LE.ZPWFA)GO TO 220
262       ZPWFA= PWFA(J,K)
263       JN3 = J
264       KN3 = K
265   220 IF  (PWFA(J,K).GT.YPWFA)GO TO 230
270       YPWFA = PWFA(J,K)
```

```
ISN        SOURCE STATEMENT

271        JN4    = J
272        KN4   = K
273   230  IF (C1GSTB(J,K).LE.ZC1GS) GO TO 240
276        ZC1GS = C1GSTB(J,K)
277        JN5 = J
300        KN5 = K
301   240  IF (C1GSTB(J,K).GT.YC1GS)GO TO 250
304        YC1GS = C1GSTB(J,K)
305        JN6   =J
306        KN6   =K
307   250  IF (WPLWS(J,K).LE.ZWPLWS)GO TO 260
312        ZWPLWS = WPLWS(J,K)
313        JN7     = J
314        KN7     = K
315   260  IF (WPLWS(J,K).GT.YWPLWS)GO TO 270
320        YWPLWS = WPLWS(J,K)
321        JN8     = J
322        KN8     = K
323   270  IF (W7(J,K).LE.ZW7)GO TO 280
326        ZW7     = W7 (J,K)
327        JN9     = J
330        KN9     = K
331   280  IF (W7(J,K).GT.YW7)GO TO 290
334        YW7     = W7(J,K)
335        JN10    = J
336        KN10    = K
337   290  IF (DC(J,K).LE.ZDC) GO TO 300
342        ZDC = DC(J,K)
343        JN11= J
344        KN11= K
345   300  IF (DC(J,K).GT.YDC)GO TO 310
350        YDC = DC(J,K)
351        JN12= J
352        KN12= K
353   310  IF (DE(J,K).LE.ZDE)GO TO 320
356        ZDE = DE(J,K)
357        JN13 = J
360        KN13 = K
361   320  IF (DE(J,K).GT.YDE)GO TO 330
364        YDE = DE(J,K)
365        JN14= J
366        KN14= K
367   330  IF (DIT(J,K).LE.ZDIT)GO TO 340
372        ZDIT = DIT(J,K)
373        JN15 = J
374        KN15 = K
375   340  IF (DIT(J,K).GT.YDIT)GO TO 500
400        YDIT = DIT(J,K)
401        JN16 = J
402        KN16 = K
403   500  CONTINUE
405   350  IF (PISPT(  K).LE.ZPISPT)GO TO 360
410        ZPISPT = PISPT(K)
411        KN17 = K
412   360  IF (PISPT(  K).GT.YPISPT)GO TO 370
```

```
ISN        SOURCE STATEMENT
415    .   YPISPT = PISPT (K)
416        KN18 = K
417    370 IF  (EFF      .LE.ZEFF)GO TO  380
422        ZEFF = EFF
423        KN19 =K
424    380 IF (EFF      .GT.YEFF)GO TO 700
427        YEFF = EFF
430        KN20 = K
431    700 CONTINUE
433        KGO = 0
434        IT=N3
435    845 WRITE (IT, 2000)CARD1, CARD2
     C
     C     WRITE MOTOR CONFIGURATION DATA
     C
436        WRITE (IT, 2010)CLD,  SF,  CSTWR, WF,  VLD ,SUB
     C
     C     WRITE MISSION DATA
     C
437        IF (C5.EQ.0.0)GO TO 850
442        IF (IXX.EQ.0) GO TO 847
445        WRITE (IT, 2020)DELVR(IDEL), WS, GS,  C1,  C5
446        GO TO 865
447    847 WRITE( IT,2021) RIT(IDEL), WS, GS, C1, C5
450    850 CALL ATHRUZ  (D5, 5HNUT S)
451        CALL ATHRUZ  (D51,5HPECIF)
452        CALL ATHRUZ  (D52,5HIEC  )
453        IF (IXX.EQ.0) GO TO 852
456        WRITE (IT, 2025)DELVR(IDEL), WS, GS, C1, D5, D51, D52
457        GO TO 865
460    852 WRITE( IT, 2026) RIT(IDEL), WS, GS, C1, D5, D51, D52
     C
     C     WRITE PROPELLANT DATA
     C
461    865 WRITE (IT, 2027)PROPID(LP), PROPID(LP+1), DENP2, DENP1
462        IF (BRC.EQ.0.0) GO TO 866
465        WRITE( IT, 2028) BRE, BRC, BRRP, REFISP, GAM
466        GO TO 867
467    866 WRITE( IT,2029) REFISP, GAM
470    867 IF (NPR.EQ.0) GO TO 868
473        IF (KGO.NE.0)GO TO 866
476        KGO = 1
477        IT = 11
500        GO TO 845
     C
     C     WRITE OUTPUT DATA
     C
501    868 DO 900 K=1, NEX
     C
     C
502        WRITE (IT, 2030)EX(K)
503        WRITE (IT,2040)(J, PC(J), TH(J,K), PISPT(K), EFF,
          1                PWFA(J,K),    DELVA (J,K),  CIGSTB (J,K),
          2                J=1, NP)
510        WRITE (IT,2045)
```

```
ISN        SOURCE STATEMENT

511        WRITE (IT,2050)(J, WPLWS(J,K), W7(J,K), W12(J,K), W2(J,K),
          1                W3(J,K),    W4(J,K), W5(J,K),  W6(J,K), J=1,NP)
     C
516        WRITE (IT,2055)
517        WRITE (IT,2060)(J, DC(J,K),  CL(J,K),  DE(J,K),  TLN(J,K),
          1                DIT(J,K), NITER(J,K), J=1, NP)
     C
524    900 CONTINUE
526    870 WRITE (N3, 2075)ZTB, EX(KN1), JN1, YTB, EX(KN2), JN2,
          1                ZPWFA, EX(KN3), JN3, YPWFA, EX(KN4), JN4
527        IF (C1.EQ.0.0.OR.GS.EQ.0.0)KSTAR=1
532        IF (KSTAR.EQ.0)GO TO 875
535        WRITE (N3,2075)ZC1GS, EX(1), NP, YC1GS, EX(NEX), NP
536        GO TO 880
537    875 WRITE (N3,2080)ZC1GS, EX(KN5), JN5, YC1GS, EX(KN6), JN6
540    880 WRITE (N3, 2085)ZWPLWS, EX(KN7),  JN7, YWPLWS, EX(KN8), JN8,
          1                ZW7, EX(KN9), JN9, YW7, EX(KN10),  JN10
541        IF (KSTAR.EQ.0)GO TO 885
544        WRITE (N3, 2090)ZDC, EX(1), NP, YDC, EX(KN12), NP
545        GO TO 890
546    885 WRITE (N3,2095)ZDC, EX(KN11), JN11,  YDC, EX(KN12), JN12
547    890 WRITE (N3,2100)ZDE, EX(KN13), JN13,  YDE, EX(KN14), JN14
550        IF (KSTAR.EQ.0)GO TO 892
553        WRITE (N3,2105)ZDIT, EX(KN15), NP, YDIT, EX(KN16), NP
554        GO TO 894
555    892 WRITE (N3,2110)ZDIT, EX(KN15), JN15, YDIT, EX(KN16), JN16
556    894 WRITE (N3,2112)ZPISPT, EX(KN17), NP, YPISPT,  EX(KN18), NP
557        WRITE (N3,2114)ZEFF, EX(KN19), NP, YEFF, EX(KN20), NP
560   3210 IF (ICEL.LT.NLELVR)GO TO 1
563        END FILE I1
564        IFILE = IFILE + 1
565        LP = LP+2
566        IF (NC) 99, 3220, 99
567   3220 IF (NPR.EQ.0)GO TO 950
572        WRITE (N3,2115)
573        LP=1
574        DO 3230 J=1, IFILL
575        WRITE (N3,2120) J, PROPID(LP), PROPID(LP+1)
576        LP= LP+2
577   3230 CONTINUE
601        REWIND I1
602        CALL TYPE(36,36HSAVE AND LABEL TAPE ON LOGICAL DRIVE)
603        CALL TYPE  (14, 14H       , S.SUOO, I1)
604        CALL TYPE  (0)
605        CALL TYPE  (34, 34HSPHERICAL PERFORMANCE      E-40310  )
606        CALL TYPE  (20, 20HSAVE TAPE FOR 24HRS.)
607        CALL TYPE  (0)
610    950 CALL TYPE (-1)
611        CALL EXIT
612        GO TO 950
613   2000 FORMAT   (1H1, 46X28HTHICKOL CHEMICAL CORPORATION/53X15HELKTON DIV
          1ISION /53X16HELKTON, MARYLAND //// 45X 33HSPHERICAL PERFORMANCE AN
          2D WEIGHT  //(1X14A5,A1))
     C
614   2010 FORMAT   (//40X24HMOTOR CONFIGURATION DATA///36X34HCASE LENGTH TO
```

```
ISN        SOURCE STATEMENT

          1DIAMETER RATIO  =  F7.3//36X18HCASE SAFETY FACTOR, 13X3H=  F7.3//
          236X34HCASE STRENGTH TO WEIGHT RATIO  =  2PE13.5,2X2HIN//
          336X12HWEB FRACTION, 19X1H= 3XF7.4,7X7HPERCENT//36X26HVOLUMETRIC LO
          4ADING DENSITY, 5X4H=    F7.4,7X7HPERCENT//
          5  36X, 18HNOZZLE SUBMERGENCE 13X 4H=   F7.4, 7X 7HPERCENT///)
    C
615  2020 FORMAT   (40X12HMISSION DATA///36X34HVELOCITY INCREMENT REQUIRED
          1  =  F9.2, 5X6HFT/SEC//36X18HTOTAL STAGE WEIGHT 13X3H=  ,F9.2,
          2 5X3HLBM//36X26HLOCAL GRAVITATIONAL ACCEL.,5X3H=  ,F9.2, 5X,
          3 7HFT/SEC2//36X24HGRAVITY TERM COEFFICIENT, 7X3H=  ,F9.2//36X
          4 19HSPECIFIED BURN TIME,12X,3H=  ,F9.2, 5X3HSEC///)
616  2021 FORMAT   (40X12HMISSION DATA///36X34HTOTAL IMPULSE REQUIRED
          1  =  F9.2, 5X7HLBF-SEC//36X18HTOTAL STAGE WEIGHT 13X3H=  ,F9.2,
          2 5X3HLBM//36X26HLOCAL GRAVITATIONAL ACCEL.,5X3H=  ,F9.2, 5X,
          3 7HFT/SEC2//36X24HGRAVITY TERM COEFFICIENT, 7X3H=  ,F9.2//36X
          4 19HSPECIFIED BURN TIME,12X,3H=  ,F9.2, 5X3HSEC///)
617  2025 FORMAT   (40X12HMISSION DATA///36X34HVELOCITY INCREMENT REQUIRED
          1  =  F9.2, 5X6HFT/SEC//36X18HTOTAL STAGE WEIGHT 13X3H=  ,F9.2,
          2 5X3HLBM//36X26HLOCAL GRAVITATIONAL ACCEL.,5X3H=  ,F9.2,5X,
          3 7HFT/SEC2//36X24HGRAVITY TERM COEFFICIENT, 7X3H=  ,F9.2//36X
          4 19HSPECIFIED BURN TIME,12X,3H=  ,3A5///)
    C
620  2026 FORMAT   (40X12HMISSION DATA///36X34HTOTAL IMPULSE REQUIRED
          1  =  F9.2, 5X7HLBF-SEC//36X18HTOTAL STAGE WEIGHT 13X3H=  ,F9.2,
          2 5X3HLBM//36X26HLOCAL GRAVITATIONAL ACCEL.,5X3H=  ,F9.2, 5X,
          3 7HFT/SEC2//36X24HGRAVITY TERM COEFFICIENT, 7X3H=  ,F9.2//36X
          4 19HSPECIFIED BURN TIME,12X,3H=  ,3A5///)
621  2027 FORMAT   (40X15HPROPELLANT DATA///36X11HDESIGNATION,20X,3H=  ,2A5
          1          //36X16HDENSITY (METRIC), 15X,3H=  ,F10.4,4X5HGM/CC//
          2 36X17HDENSITY (BRITISH) ,14X,3H=  ,F10.4,4X6HLB/IN3)
622  2028 FORMAT   (/ 87X, F7.3 / 36X18HBURN RATE EQUATION, 13X 3H=  F7.4 ,
          1          4H(PC/ F6.1 , 1H) // 36X 26HREFERENCE SPECIFIC IMPULSE
          2          5X, 3H=   , F10.4, 5X  11HLBF-SEC/LBM // 36X  19HSPECIFIC
          3 HEAT RATIO  12X, 3H=  F10.4 )
623  2029 FORMAT  ( //36X 18HBURN RATE EQUATION 14X 3H=  13HNOT SPECIFIED //
          1         36X 26HREFERENCE SPECIFIC IMPULSE 5X 3H=   F10.4, 5X
          2         11HLBF-SEC/LBM // 36X 19HSPECIFIC HEAT RATIO 12X, 3H=
          3         F10.4)
624  2030 FORMAT  (1H1, 57X8HRUN DATA///6X19HEXPANSION RATIO   = F10.3//   3
          1X4HLINE3X16HCHAMBER PRESSURE,4X9HBURN TIME4X15HTHEORETICAL ISP,4X
          214HISP EFFICIENCY 3X10HMASS RATIO  8X18HVELOCITY INCREMENT/4X2HNO,
          387X6HACTUAL , 7X13HGRAVITATIONAL/110X4HLOSS/10X4HPSIA,13X3HSEC,
          413X3HSEC,41X6HFT/SEC, 10X6HFT/SEC/)
    C
625  2040 FORMAT  (4X12,7XF9.2, 7XF9.3, 8XF8.3,  11XF7.4, 7XF7.4, 6XF8.1,
          1          6X, F9.1)
    C
626  2045 FORMAT  (//3X4HLINE3X16HPAYLOAD TO STAGE,4X
          1         23HTOTAL MOTOR  PROPELLANT6X4HCASE,7X6HNOZZLE, 7X4HMISC
          2         10X13HINERT  WEIGHT/4X2HNO,
          3         6X 12HWEIGHT RATIO, 8X6HWEIGHT,2(7X6HWEIGHT),
          4         2(6X6HWEIGHT), 6X7HINITIAL 7X5HFINAL//34X,
          5          3HLBM,9X3HLBM,10X3HLBM,2(9X3HLBM), 2(10X3HLBM)/)
627  2050 FORMAT  (4X12,8XF7.4, 9XF9.2, 4XF9.2, 4XF8.2, 4XF8.2, 4XF8.2,
          1        5XF8.2, 5XF8.2)
```

```
ISN       SOURCE STATEMENT
    C
630  2055 FORMAT  (//3X4HLINE3X13HCASE DIAMETER 8X10HTOTAL CASE 2X
          1       11HNOZZLE EXIT, 4X13HNOZZLE LENGTH 7X13HTOTAL IMPULSE, 9X
          2       5HNITER/4X2HNO,27X6HLENGTH5X8HDIAMETER//16X2HIN,16X2HIN,
          3       11X2HIN,
          4       14X2HIN, 16X7HLBF-SEC/)
631  2060 FORMAT  (4XI2, 5XF9.3, 11XF9.3, 3XF9.3, 7XF9.3, 11XF10.0, 10XI5)
    C
632  2070 FORMAT   (1H1, 53X16HRUN DATA SUMMARY///14X9HPARAMETER, 65X
          1         8HLOCATION/67X15HEXPANSION RATIO,20X,7HLINE NO//
          2         3X22HMAXIMUM BURN TIME ,SEC, 19X3H=  ,F13.3, 9XF10.3,
          3         25XI2//3X22HMINIMUM BURN TIME ,SEC,19X3H=  ,F13.3, 9X,
          4         F10.3,25XI2///3X18HMAXIMUM MASS RATIO,23X3H=  ,F14.4,
          5         8XF10.3,25XI2//3X18HMINIMUM MASS RATIO,23X3H=  ,F14.4,
          6         8XF10.3,25XI2//)
633  2075 FORMAT   (3X34HMAXIMUM GRAVITATIONAL LOSS ,FT/SEC,7X3H=  ,F11.1,
          1         11XF10.3,23X2H1-,I2//3X28HMINIMUM GRAVITATIONAL LOSS ,
          2         6HFT/SEC,7X3H=  ,F11.1,11XF10.3,23X2H1-,I2//)
634  2080 FORMAT   (3X34HMAXIMUM GRAVITATIONAL LOSS ,FT/SEC,7X3H=  ,F11.1,
          1         11XF10.3,25XI2//3X 34HMINIMUM GRAVITATIONAL LOSS ,FT/SEC,
          2         7X3H=  ,F11.1,11XF10.3,25XI2//)
635  2085 FORMAT   (3X37HMAXIMUM PAYLOAD TO STAGE WEIGHT RATIO,4X3H=  ,
          1         F14.4,8XF10.3,25XI2//3X24HMINIMUM PAYLOAD TO STAGE,
          2         13H WEIGHT RATIO, 4X3H=  ,F14.4,8XF10.3,25XI2///3X
          3         31HMAXIMUM TOTAL MOTOR WEIGHT ,LBM,10X3H=  ,F12.2,10X
          4         F10.3,25XI2//3X31HMINIMUM TOTAL MOTOR WEIGHT ,LBM,
          5         10X3H=  ,F12.2,10XF10.3,25XI2//)
636  2090 FORMAT   (3X25HMAXIMUM CASE DIAMETER ,IN,16X3H=  ,F13.3,9XF10.3,
          1         23X2H1-,I2//3X25HMINIMUM CASE DIAMETER ,IN,16X3H=  ,
          2         F13.3,9XF10.3,23X2H1-,I2//)
637  2095 FORMAT   (3X25HMAXIMUM CASE DIAMETER ,IN,16X3H=  ,F13.3,9XF10.3,
          1         25XI2//3X25HMINIMUM CASE DIAMETER ,IN,16X3H=  ,
          2         F13.3,9XF10.3,25X,I2//)
640  2100 FORMAT   (3X32HMAXIMUM NOZZLE EXIT DIAMETER ,IN,9X3H=  ,F13.3,9X
          1         F10.3,25XI2//3X32HMINIMUM NOZZLE EXIT DIAMETER ,IN,
          2         9X3H=  ,F13.3,9XF10.3,25XI2//)
641  2105 FORMAT   (3X30HMAXIMUM TOTAL IMPULSE ,LB-SEC,11X3H=  ,F10.0,12X
          1         F10.3,23X2H1-,I2//3X30HMINIMUM TOTAL IMPULSE ,LB-SEC,11X
          2         3H=  ,F10.0,12XF10.3,23X2H1-,I2//)
642  2110 FORMAT   (3X30HMAXIMUM TOTAL IMPULSE ,LB-SEC,11X3H=  ,F10.0,12X
          1         F10.3,25XI2//3X30HMINIMUM TOTAL IMPULSE ,LB-SEC,11X
          2         3H=  ,F10.0,12XF10.3,25XI2//)
    C
643  2112 FORMAT (3X28HMAXIMUM THEORETICAL ISP ,SEC ,13X3H=  ,F13.3, 9X,
          1       F10.3, 23X2H1-,I2//3X28HMINIMUM THEORETICAL ISP ,SEC ,
          2       13X3H=  ,F13.3, 9X,F10.3, 23X2H1-,I2//)
644  2114 FORMAT (3X22HMAXIMUM ISP EFFICIENCY,19X3H=  ,F14.4,  8X,F10.3,
          1       23X2H1-,I2//3X22HMINIMUM ISP EFFICIENCY,19X3H=  ,
          2       F14.4, 8X,F10.3,23X2H1- ,I2)
    C
645  2115 FORMAT (1H1,10X,29HCONTENTS OF INTERMEDIATE TAPE//12X
          1       7HFILE NO,7X11HDESCRIPTION/)
    C
646  2120 FORMAT (14XI2,10X2A5)
```

REFERENCES TO DEFINED SYMBOLS

VALUE	NAME	STATEMENT NUMBERS
03623	1000S	2062
03636	1001S	2088
03642	1002S	2110
03651	1003S	2135,2152,2173,2191
00202	1004S	2166
00223	1005S	2167,2168
00243	1006S	2186
00536	100S	2390
00413	101S	2350
00460	102S	2347
00463	103S	2345,2346
00512	104S	
00574	111S	2426,2427,2613
01364	112S	2425
01220	115S	
01224	116S	2709
01230	117S	2713
01246	118S	2714,2715
00516	130S	
00523	132S	2383
00531	133S	2382,2384
00764	135S	
00770	136S	2551
00774	137S	2555
01012	138S	2556,2557
01033	139S	2571
01267	140S	2552,2553,2590,2604,2605,2710,2711,2729
01037	145S	2591,2592
01056	150S	2606
00246	1S	3910
03655	2000S	3239
01610	200S	2948
03743	2010S	3249
04152	2020S	3279
04534	2021S	3298
04617	2025S	3336
04675	2026S	3359
05054	2027S	3381
05157	2028S	3400
05265	2029S	3417
05362	2030S	3450
05553	2040S	3458
05614	2045S	3498
06007	2050S	3504
06054	2055S	3542
06210	2060S	3548
06245	2070S	3599
06462	2075S	3655
06561	2080S	3674
06653	2085S	3732

CROSS-REFERENCE DICTIONARY

07032	2090S	3743
07125	2095S	3767
07212	2100S	3790
07301	2105S	3819
01625	210S	2962
07374	2110S	3844
07461	2112S	3866
07554	2114S	3890
07643	2115S	3935
07677	2120S	3950
01642	220S	2976
01657	230S	2990
01674	240S	3004
01711	250S	3018
01726	260S	3032
01743	270S	3046
01760	280S	3060
01775	290S	3074
02012	300S	3088
02027	310S	3102
02044	320S	3116
03425	3210S	
03450	3220S	3923
03511	3230S	
02061	330S	3130
02076	340S	3144
02125	350S	
02140	360S	3184
02153	370S	3196
02164	380S	3207
02113	500S	3158
02175	700S	3217
02207	845S	3437
02276	847S	3271
02320	850S	3266
02372	852S	3328
02420	865S	3291,3352
02465	866S	3394
02477	867S	3412
02514	868S	3426,3431
02733	870S	
03047	875S	3642
03077	880S	3665
03203	885S	3735
03232	890S	3758
03317	892S	3809
03345	894S	3835
02724	900S	
03556	950S	3929,4008
03603	999S	2052
00013	99S	3924,3925
VIRTUAL	ALOG	2928
11157	AT	2773,2774,2840,2866
VIRTUAL	ATHRUZ	3310,3315,3320
07761	BCDLI.	3314,3319,3324,3974,3979,3989,3994

12113	BRC	2123,2554,2586,2712,2744,3391,3403
10473	BRE	2125,2576,2734,3401
10023	BRRP	2127,2574,2732,3405
10030	C1	2068,2428,2569,2750,3286,3335,3343,3366,3629
11656	C1GSTR	2755,2941,3000,3007,3014,3021,3485
11651	C5	2064,2396,2550,2708,3263,3288,3307
11162	CAPG	2288,2301,2363
11164	CAPGA2	2277,2278,2281
13470	CARD1	2054,3241
14417	CARD2	2056,3243
15025	CFOPT	2364,2368
16166	CFOPTR	2302,2371,2765
13243	CFX	2369,2372
13023	CL	2527,2685,2835,3562
13245	CLD	2422,2471,2514,2524,2528,2626,2669,2683,2686,2832,2863,3250
13246	CLD1	2090,2421
14414	CSTWR	2096,2537,2695,3254
16162	D5	3313,3345,3368
10714	D51	3318,3347,3370
13244	D52	3323,3349,3372
10734	DC	2486,2488,2517,2522,2526,2533,2566,2585,2641,2643,2672,2677,2684,2691,2724,2743,2812,2824,2833, 2852,2873,2880,2885,3084,3091,3098,3105,3560
12101	DCMAX	2102,2211,2215,2489,2493,2518,2521,2644,2648,2673,2676
15476	DE	2789,2791,3112,3119,3126,3133,3564
12121	DELVA	2942,3483
10720	DELVR	2200,2434,3280,3337
13507	DELWS	2908,2910
14416	DENP	2129,2380,2385,2387,2391,2393
11653	DENP1	2386,2395,2468,2496,2623,2651,3388
13022	DENP2	2389,2392,3386
10251	DIT	2467,2682,2770,3140,3147,3154,3161,3568
16174	DT	2778,2788,2790,2796
16165	EFF	2119,2436,2462,2614,2933,3203,3209,3213,3219,3479
VIRTUAL	EFTIL.	3914
15716	EX	2161,2313,2367,2779,2843,3451,3603,3610,3617,3624,3653,3660,3678,3685,3706,3713,3720,3727,3746, 3753,3771,3777,3794,3801,3823,3830,3847,3853,3870,3877,3894,3901
VIRTUAL	EXIT	4005
VIRTUAL	EXP	2446
VIRTUAL	FILIL.	3244,3262,3290,3309,3351,3374,3390,3411,3422,3453,3493,3499,3537,3543,3577,3628,3664,3689,3731, 3757,3781,3805,3834,3857,3881,3905,3936,3957
12077	G	2206,2441,2937
10027	GAM	2121,2252,2254,2259,2265,2276,2315,2327,3409,3420
11156	GG	2280,2324
12111	GMIG	2255,2257,2289,2319,2351
16172	GS	2070,2429,2751,3284,3303,3341,3364,3632
VIRTUAL	HNLIL.	2063,2065,2067,2069,2071,2073,2075,2077,2079,2081,2089,2091,2093,2095,2097,2099,2101,2111,2114, 2116,2118,2120,2122,2124,2126,2128,2143,2160,2181,2199,3251,3253,3255,3257,3259,3261,3281,3283, 3285,3287,3289,3300,3302,3304,3306,3308,3338,3340,3342,3344,3346,3348,3350,3361,3363,3365,3367, 3369,3371,3373,3383,3385,3387,3389,3402,3404,3406,3408,3410,3419,3421,3452,3471,3473,3475,3478, 3480,3482,3484,3486,3515,3517,3519,3521,3523,3525,3527,3529,3531,3559,3561,3563,3565,3567,3569, 3571,3601,3604,3606,3608,3611,3613,3615,3618,3620,3622,3625,3627,3652,3654,3656,3658,3661,3663, 3676,3679,3681,3683,3686,3688,3704,3707,3709,3711,3714,3716,3718,3721,3723,3725,3728,3730,3745, 3747,3749,3751,3754,3756,3769,3772,3774,3776,3778,3780,3792,3795,3797,3799,3802,3804,3821,3824, 3826,3828,3831,3833,3846,3848,3850,3852,3854,3856,3868,3871,3873,3875,3878,3880,3892,3895,3897, 3899,3902,3904,3952,3954,3956

```
16203   II       2043,3435,3912,3966,3980
10326   IDEL     2207,2208,2210,2398,3273,3292,3330,3353,3906
15737   IFILE    2047,3916,3918,3941
VIRTUAL IOHAC.   52,54,60,62,81,142,144,533,624,649,1881
VIRTUAL IOHEC.   188
VIRTUAL IOHEF.   64,75,79,86,90,147,257,352,447,538,629,689,749,798,903,936,1050,1087,1169,1198,1322,1376,1421,
                 1514,1565,1610,1655,1706,1751,1802,1851,1873,1883
VIRTUAL IOHFC.   66,77,84,88,163,177,209,223,247,271,290,309,328,342,366,385,404,423,437,461,480,499,518,552,571,
                 590,609,663,682,693,706,711,728,747,777,796,815,910,914,916,922,926,930,934,1057,1061,1065,1069,
                 1073,1077,1081,1085,1176,1180,1184,1188,1192,1243,1247,1265,1269,1288,1292,1310,1314,1333,1337,
                 1361,1365,1387,1391,1409,1413,1432,1436,1457,1461,1480,1484,1502,1506,1525,1529,1550,1554,1576,
                 1580,1598,1602,1621,1625,1643,1647,1666,1670,1691,1695,1717,1721,1739,1743,1762,1766,1787,1791,
                 1813,1817,1838,1842
VIRTUAL IOHHC.   107,112,118,124,133,152,160,169,174,183,192,199,204,213,220,225,232,239,244,251,260,268,275,282,
                 287,294,301,306,313,320,325,334,339,346,355,363,370,377,382,389,396,401,406,415,420,429,434,441,
                 450,458,465,472,477,484,491,496,503,510,515,524,529,541,549,556,563,568,575,582,587,594,601,606,
                 615,620,632,640,645,655,660,667,674,679,686,698,703,708,713,720,725,732,739,744,754,759,762,769,
                 774,781,788,793,799,804,812,821,826,831,836,841,846,851,857,862,867,873,879,884,889,894,899,941,
                 946,951,956,961,966,971,977,982,987,994,1002,1008,1013,1020,1025,1033,1037,1045,1092,1097,1102,
                 1107,1112,1117,1122,1128,1133,1138,1145,1150,1155,1160,1165,1199,1204,1212,1217,1223,1228,1235,
                 1240,1257,1262,1280,1285,1302,1307,1325,1330,1341,1350,1353,1358,1369,1379,1364,1401,1406,1424,
                 1427,1446,1449,1454,1472,1477,1494,1499,1517,1522,1533,1542,1547,1558,1568,1573,1590,1595,1613,
                 1618,1635,1640,1658,1663,1674,1683,1688,1699,1709,1714,1731,1736,1754,1759,1770,1779,1784,1795,
                 1805,1810,1821,1830,1835,1846,1852,1857,1864,1869
VIRTUAL IOHIC.   72,906,1093,1172,1196,1251,1273,1296,1318,1344,1372,1395,1417,1440,1465,1488,1510,1536,1561,
                 1584,1606,1629,1651,1677,1702,1725,1747,1773,1798,1824,1849,1876
VIRTUAL IOHID.   56,115,121,127,128,129,130,136,137,148,149,155,156,157,165,166,179,180,195,196,216,217,235,236,
                 254,255,256,263,264,265,278,279,297,298,316,317,330,331,349,350,351,356,359,360,373,374,392,393,
                 411,412,425,426,444,445,446,453,454,455,468,469,487,488,506,507,520,521,535,536,537,544,545,546,
                 559,560,578,579,597,598,611,612,626,627,628,635,636,637,651,652,670,671,690,695,716,717,735,736,
                 750,751,765,766,784,785,807,808,809,817,818,854,870,876,902,937,938,974,1016,1017,1049,1088,
                 1089,1125,1141,1142,1168,1207,1208,1209,1220,1231,1232,1253,1254,1275,1276,1277,1298,1299,1320,
                 1321,1346,1347,1374,1375,1397,1398,1419,1420,1442,1443,1467,1468,1469,1490,1491,1512,1513,1538,
                 1539,1563,1564,1586,1587,1608,1609,1631,1632,1653,1654,1679,1680,1704,1705,1727,1728,1749,1750,
                 1775,1776,1800,1801,1826,1827,1860,1861,1872
VIRTUAL IOHLP.   69,138,991,995,1034,1042
VIRTUAL IOHRP.   74,146,997,1005,1040,1048
VIRTUAL IOHSF.   186
VIRTUAL IOHXC.   49,57,70,110,116,122,131,139,150,158,167,172,181,190,197,202,207,211,215,223,230,237,242,249,
                 258,266,273,280,285,292,299,304,311,318,323,332,337,344,353,361,368,375,380,387,394,399,406,413,
                 418,427,432,439,448,456,463,470,475,482,489,494,501,508,513,522,527,539,547,554,561,566,573,580,
                 585,592,599,604,613,618,630,638,643,653,658,665,672,677,684,691,696,701,718,723,730,737,742,752,
                 757,767,772,779,786,791,802,810,819,824,829,834,839,844,849,855,860,865,871,877,882,887,892,897,
                 904,908,912,916,920,924,928,932,939,944,949,954,959,964,969,975,980,985,992,1000,1006,1011,1018,
                 1023,1028,1035,1043,1051,1055,1059,1063,1067,1071,1075,1079,1083,1090,1095,1100,1105,1110,1115,
                 1120,1126,1131,1136,1143,1148,1153,1158,1163,1170,1174,1178,1182,1186,1190,1194,1202,1210,1215,
                 1221,1226,1233,1238,1245,1249,1255,1260,1267,1271,1278,1283,1290,1294,1300,1305,1312,1316,1323,
                 1328,1335,1339,1348,1356,1363,1367,1377,1382,1389,1393,1399,1404,1411,1415,1422,1427,1434,1438,
                 1444,1452,1459,1463,1470,1475,1482,1486,1492,1497,1504,1508,1515,1520,1527,1531,1540,1545,1552,
                 1556,1566,1571,1578,1582,1588,1593,1600,1604,1611,1616,1623,1627,1633,1638,1645,1649,1656,1661,
                 1668,1672,1681,1686,1693,1697,1707,1712,1719,1723,1729,1734,1741,1745,1752,1757,1764,1768,1777,
                 1782,1789,1793,1803,1808,1815,1819,1828,1835,1840,1844,1855,1862,1867,1874,1878
16171   IT       3234,3235,3245,3275,3294,3332,3355,3377,3398,3413,3430,3446,3454,3494,3500,3538,3544
14412   IXX      2082,2165,2424,3268,3325
VIRTUAL .EXP3.   2273,2291,2317,2321,2332,2353,2485,2494,2534,2561,2580,2640,2649,2692,2719,2738,2777,2809,281
```

Reproduced from best available copy.

CROSS-REFERENCE DICTIONARY

		2841,2846,2853,2857,2867,2874,2881,2886
11412	J	2409,2417,2953,2967,2981,2995,3009,3023,3037,3051,3065,3079,3093,3107,3121,3135,3149,3163,3177,
		3460,3467,3470,3491,3506,3511,3514,3533,3535,3550,3555,3558,3573,3575,3940,3951,3962,3964
14170	JN1	2954,3605
14167	JN10	3080,3729
14413	JN11	3094,3773
14436	JN12	3108,3779
14660	JN13	3122,3796
15026	JN14	3136,3803
15032	JN15	3150,3849
15254	JN16	3164,3855
10020	JN2	2968,3612
12106	JN3	2982,3619
15027	JN4	2996,3626
10471	JN5	3010,3680
12342	JN6	3024,3687
15733	JN7	3038,3708
10716	JN8	3052,3715
13467	JN9	3066,3722
15740	K	2137,2154,2175,2193,2304,2401,2415,2955,2969,2983,2997,3011,3025,3039,3053,3067,3081,3095,3109,
		3123,3137,3151,3165,3189,3201,3211,3221,3230,3439,3465,3509,3553,3585
10715	KGO	3232,3428,3434
11166	KN1	2956,3587
11163	KN10	3082,3696
11170	KN11	3096,3759
11413	KN12	3110,3737,3761
11652	KN13	3124,3782
11654	KN14	3138,3784
12102	KN15	3152,3811,3836
12105	KN16	3166,3813,3838
12110	KN17	3190,3858
12116	KN18	3202,3860
12341	KN19	3212,3882
14165	KN2	2970,3589
14164	KN20	3222,3884
16173	KN3	2984,3591
11655	KN4	2998,3593
14415	KN5	3012,3666
10022	KN6	3026,3668
12112	KN7	3040,3690
15031	KN8	3054,3692
10472	KN9	3068,3694
15732	KSTAR	2247,3637,3639,3732,3806
VIRTUAL	LITCT.	2041,2209,2212,2253,2260,2266,2292,2311,2322,2341,2354,2381,2451,2455,2473,2480,2509,2530,2598,
		2611,2628,2635,2664,2688,2794,2837,3264,3269,3326,3392,3424,3429,3433,3630,3633,3636,3640,3733,
		3807,3917,3927,3937,3984,3998,3999
11160	LP	2042,2104,3375,3919,3921,3938,3944,3958,3960
VIRTUAL	LTCR2.	
16176	N2	2048,2058,2084,2106,2131,2148,2169,2187
16177	N3	3233,3595,3646,3670,3698,3739,3763,3786,3815,3840,3862,3886,3931,3946
11171	NC	2080,3922
11154	NDELVR	2076,2177,2195,3907
12107	NEX	2074,2156,2307,2404,3442,3644
13247	NITER	2423,2610,2612,3570
12114	NP	2072,2139,2412,3462,3507,3551,3655,3662,3748,3755,3825,3832,3872,3879,3896,3903

Reproduced from best available copy.

CROSS-REFERENCE DICTIONARY

16163	NPR	2078,3423,3926
16175	NTAPES	
12346	PC	2144,2548,2560,2573,2706,2718,2731,2758,3472
11165	PEPC	2336,2337,2348,2352,2365
15736	PEPCD	2249,2320,2338,2349
11415	PISPT	2373,2438,2462,2616,2762,2934,3180,3187,3192,3199,3477
14661	PROPID	2113,2115,3382,3384,3953,3955
15034	PWFA	2917,2972,2975,2986,2993,3481
15734	REFISP	2117,2370,2772,3407,3418
13727	RIT	2182,2619,2680,3299,3365
VIRTUAL	RTNIO.	2057,2083,2103,2130,2147,2164,2185,2203
VIRTUAL	RWTIO.	2045,3968
VIRTUAL	SETFP.	2037
12117	SF	2094,2538,2696,3252
VIRTUAL	S.JXIT	4009
VIRTUAL	SLIIO.	2053,2055
VIRTUAL	SLOIO.	3240,3242
07714	SNGCT.	2205,2214,2227,2229,2231,2233,2235,2237,2239,2241,2243,2245,2248,2250,2256,2262,2290,2328,2344, 2388,2394,2472,2475,2481,2492,2497,2505,2510,2529,2532,2536,2558,2563,2583,2603,2627,2630,2636, 2647,2652,2660,2665,2687,2690,2694,2716,2721,2741,2768,2775,2776,2797,2800,2805,2807,2811,2814, 2825,2839,2844,2849,2851,2854,2856,2860,2865,2870,2872,2877,2879,2882,2884,2889,2903,2906,3920, 3959,3973,3978,3988,3993
VIRTUAL	SQRT	2284,2295,2357,2782,2819
VIRTUAL	STHIO.	3237,3247,3277,3296,3334,3357,3379,3398,3415,3448,3456,3496,3502,3540,3546,3597,3648,3672,3700, 3741,3765,3788,3817,3842,3864,3888,3933,3948
16164	SUB	2130,2793,2802,2836,3265
VIRTUAL	TAPES	2038
15255	TB	2749,2754,2756,2855,2944,2951,2958,2965,3474
12343	TBC	2397,2432,2570,2588,2728,2746,2747
13743	TLN	2831,2834,3566
VIRTUAL	TSHIO.	2050,2060,2086,2108,2133,2150,2171,2189
VIRTUAL	TYPE	3970,3975,3981,3985,3990,3995,4001
VIRTUAL	UTVAR.	2044,2049,2059,2085,2107,2132,2149,2170,2188,3236,3246,3276,3295,3333,3356,3378,3397,3414,3447, 3455,3495,3501,3539,3545,3596,3647,3671,3699,3740,3764,3787,3816,3841,3863,3887,3913,3932,3947, 3967
10017	VARA	2445,2449
14657	VLD	2092,2469,2500,2624,2655,3258
10474	W11	2251,2595,2609
12362	W12	2461,2466,2477,2507,2594,2608,2622,2632,2662,2913,2915,2923,3520
14172	W2	2549,2707,2896,3522
12602	W3	2850,2895,2900,3524
11172	W4	2894,2897,3526
10031	W5	2898,2909,2912,3528
15741	W6	2911,3530
14437	W7	2914,2916,2919,3056,3063,3070,3077,3518
16161	WATT	2878,2891
15475	WF	2098,2569,2582,2727,2740,3256
11414	WIN	2864,2892,2899
11431	WPLWS	2921,3028,3035,3042,3049,3516
12100	WPY	2871,2893,2905
12115	WRATIO	2600,2601
12104	WS	2066,2458,2918,2920,2922,2925,3282,3301,3339,3362
16167	X2GGM	2258,2279,2282
14163	YC1GS	2232,3015,3022,3657,3682
10521	YDC	2238,3099,3106,3750,3775

Reproduced from best available copy.

CROSS-REFERENCE DICTIONARY

15030	YDE	2240,3127,3134,3798
11161	YDIT	2242,3155,3162,3827,3851
12103	YEFF	2246,3214,3220,3898
12345	YPISPT	2244,3193,3200,3874
12120	YPWFA	2230,2987,2994,3621
14171	YTB	2226,2959,2966,3607
10717	YW7	2236,3071,3078,3724
12344	YWPLWS	2234,3043,3050,3710
11155	ZC1GS	2219,3001,3008,3651,3675
14166	ZDC	2222,3085,3092,3744,3768
12076	ZDE	2223,3113,3120,3791
15735	ZDIT	2224,3141,3148,3820,3845
16170	ZEFF	2226,3204,3210,3891
10025	ZPISPT	2225,3181,3188,3867
10016	ZPWFA	2218,2973,2980,3614
16175	ZTAPES	
11167	ZTB	2217,2945,2952,3600
15033	ZW7	2221,3057,3064,3717
10024	ZWPLWS	2220,3029,3036,3703
03571	D.0000	2261,2263,2264,2267,2268,2269,2270,2271,2272,2274,2275,2283,2287,2294,2298,2299,2300,2314,2316, 2318,2323,2325,2326,2329,2330,2331,2333,2334,2335,2339,2340,2356,2360,2361,2362,2430,2431,2435, 2439,2440,2442,2443,2444,2450,2452,2453,2454,2456,2457,2464,2465,2470,2474,2476,2478,2479,2482, 2483,2484,2495,2498,2499,2501,2502,2503,2504,2506,2508,2511,2512,2513,2531,2535,2539,2540,2541, 2542,2543,2544,2545,2546,2562,2564,2567,2568,2575,2577,2578,2579,2581,2587,2596,2597,2617,2620, 2625,2629,2631,2633,2634,2637,2638,2639,2650,2653,2654,2656,2657,2658,2659,2661,2663,2666,2667, 2668,2689,2693,2697,2698,2699,2700,2701,2702,2703,2704,2720,2722,2725,2726,2733,2735,2736,2737, 2739,2745,2752,2753,2759,2760,2763,2764,2766,2767,2769,2771,2786,2787,2792,2795,2798,2799,2801, 2803,2804,2806,2810,2815,2816,2817,2818,2822,2823,2826,2827,2828,2829,2830,2838,2842,2847,2848, 2858,2859,2861,2862,2868,2869,2875,2876,2883,2887,2888,2890,2901,2902,2904,2907,2924,2926,2927, 2931,2932,2935,2936,2938,2939,2940,4000,4004
00256	P.0064	2213
00723	P.0156	2490,2491
00732	P.0161	2519,2520
01154	P.0203	2645,2646
01163	P.0206	2674,2675
01601	P.0244	2947
01616	P.0252	2960,2961
01633	P.0260	2975
01650	P.0266	2988,2989
01665	P.0274	3003
01702	P.0302	3016,3017
01717	P.0310	3031
01734	P.0316	3044,3045
01751	P.0324	3059
01766	P.0332	3072,3073
02003	P.0340	3087
02020	P.0346	3100,3101
02035	P.0354	3115
02052	P.0362	3128,3129
02067	P.0370	3143
02104	P.0376	3156,3157
02133	P.0406	3183
02146	P.0413	3194,3195
02163	P.0420	3206
02171	P.0425	3215,3216

Reproduced from best available copy.

CROSS-REFERENCE DICTIONARY

02247	P.0440	3265
02253	P.0443	3270
02343	P.0454	3327
02444	P.0463	3393
02503	P.0471	3425
02507	P.0474	3430
03015	P.0530	3634
03021	P.0533	3641
03155	P.0542	3734
03266	P.0551	3808
03432	P.0561	3908,3909
03454	P.0570	3928
03013	P.0650	3631
00113	S.0653	2105,3376,3945
00601	S.0655	2399,2618,2679,3274,3293,3331,3354
02752	S.0657	3588
02761	S.0660	3590
02770	S.0661	3592
02777	S.0662	3594
03040	S.0663	3645
03062	S.0664	3667
03071	S.0665	3669
03116	S.0666	3691
03125	S.0667	3693
03134	S.0670	3695
03143	S.0671	3697
03174	S.0672	3738,3762
03216	S.0673	3760
03245	S.0674	3783
03254	S.0675	3785
03301	S.0676	3812,3837
03310	S.0677	3814,3839
03360	S.0700	3859
03367	S.0701	3861
03410	S.0702	3883
03417	S.0703	3885
00154	S.0704	2141
00151	S.0705	2146
00174	S.0706	2158
00171	S.0707	2163
00225	S.0710	2179
00215	S.0711	2184
00241	S.0712	2197
00236	S.0713	2202
00512	S.0714	2306,2312,2366,2378
00515	S.0715	2309
00413	S.0716	2379
02175	S.0717	2403,2437,2615,2761,3179,3186,3191,3198,3227
02203	S.0720	2406
00551	S.0721	3231
02116	S.0722	2411,2547,2559,2572,2705,2717,2730,2757,3174
02124	S.0723	2414
02113	S.0724	2419,2460,2487,2516,2525,2565,2584,2593,2607,2621,2642,2671,2681,2723,2742,2748,2943,2950,2957, 2964,2971,2978,2985,2992,2999,3006,3013,3020,3027,3034,3041,3048,3055,3062,3069,3076,3083,3090, 3097,3104,3111,3118,3125,3132,? 3146,3153,3160,3171

Reproduced from best available copy.

CROSS-REFERENCE DICTIONARY

00565	S.0725	3178
01332	P.0726	2781
02724	S.0727	3441,3476,3582
02732	S.0730	3444
02523	S.0731	3586
02600	S.0732	3464
02552	S.0733	3492
02653	S.0734	3508
02625	S.0735	3536
02722	S.0736	3552
02700	S.0737	3576
03514	S.0740	3942
03470	S.0741	3965
07711	P.0742	4046
07714	P.0743	6
07711	P.0744	4052
07711	P.0745	2136,2153,2174,2192,2303,2400,2408,3438,3459,3505,3549,3939
07712	P.0746	2416,3466,3510,3554
07713	P.0747	3176,3229,3490,3584

REFERENCES TO LOCATION COUNTERS

LC START	NAME	STARTING AND ENDING STATEMENT NUMBERS
00000		1-1
07711	DATCT.	4-4
00000	PLGCT.	4013-4040
00000	PRGCT.	2-2,2036-4012,4041-4042
03603	SFLCT.	3-3,48-90,106-1883,4043-4053
07711	STRCT.	5-47,91-105,1884-2035

NO MESSAGES FOR ABOVE ASSEMBLY

M E M O R Y M A P

SYSTEM, INCLUDING IOCS 00000 THRU 12261

FILE BLOCK ORIGIN 12270

NUMBER OF FILES -

1.	S.FBIN	12270
2.	S.FBOU	12313
3.	S.FBPP	12336
4.	FTC00.	12361
5.	FTC01.	12404
6.	FTC02.	12427
7.	FTC03.	12452
8.	FTC04.	12475

OBJECT PROGRAM 12520 THRU 35410

1.	DECK -MAIN -	*	12520
2.	SUBR -INSYFB-		30730
3.	SUBR -OUSYFB-		30767
4.	SUBR -POSTX -		31026
5.	SUBR -PPSYFB-		31133
6.	SUBR -CNSTNT-	*	31171
7.	SUBR -FC0 -		31201
8.	SUBR -FC1 -		31202
9.	SUBR -FC2 -		31203
10.	SUBR -FC3 -		31204
11.	SUBR -FC4 -		31205
12.	SUBR -FC5 -		31206
13.	SUBR -FC6 -		31207
14.	SUBR -FC7 -		31210
15.	SUBR -IOS -		31211
16.	SUBR -RWD -		31466
17.	SUBR -ACV -		32146
18.	SUBR -ECV -		32176
19.	SUBR -FCV -		32444
20.	SUBR -HCV -		32545
21.	SUBR -ICV -		32650
22.	SUBR -XCV -		32670
23.	SUBR -INTJ -		32711
24.	SUBR -FFC -	*	33225
25.	SUBR -SLI -		33634
26.	SUBR -SLO -		33661
27.	SUBR -EFT -		33726
28.	SUBR -RWT -		33741
29.	SUBR -UTV -		33760
30.	SUBR -ATHRUZ-		34013
31.	SUBR -TYPE -		34035
32.	SUBR -TAPL -	*	34120
33.	SUBR -FPT -		34202
34.	SUBR -XPM -	*	34552
35.	SUBR -XIT -		34763

Reproduced from best available copy.

```
36.  SUBR -XP3   -          34765
37.  SUBR -XPN   -          35036
38.  SUBR -LOG   -          35144
39.  SUBR -SQR   -          35311
```

(* - INSERTIONS OR DELETIONS MADE IN THIS DECK)

INPUT - OUTPUT BUFFERS 73770 THRU 77776

UNUSED CORE 35411 THRU 73753

OBJECT PROGRAM IS BEING ENTERED INTO STORAGE.

E. SAMPLE OUTPUT

THIOKOL CHEMICAL C ORATION
ELKTON DIVISION
ELKTON, MARYLAND

SPHERICAL PERFORMANCE AND WEIGHT

SAMPLE DATA SET TO DESIGN A
200000 LBF-SEC TOTAL IMPULSE MOTOR USING PB-AP-AL PROPELLANT

MOTOR CONFIGURATION DATA

CASE LENGTH TO DIAMETER RATIO	=	1.000	
CASE SAFETY FACTOR	=	1.400	
CASE STRENGTH TO WEIGHT RATIO	=	11.00000E 05	IN
WEB FRACTION	=	60.0000	PERCENT
VOLUMETRIC LOADING DENSITY	=	95.0000	PERCENT
NOZZLE SUBMERGENCE	=	40.0000	PERCENT

MISSION DATA

TOTAL IMPULSE REQUIRED	=	200000.00	LBF-SEC
TOTAL STAGE WEIGHT	=	2100.00	LBM
LOCAL GRAVITATIONAL ACCEL.	=	0.00	FT/SEC2
GRAVITY TERM COEFFICIENT	=	0.00	
SPECIFIED BURN TIME	=	NOT SPECIFIED	

PROPELLANT DATA

DESIGNATION	-	TPH-3062	
DENSITY (METRIC)	=	1.7326	GM/CC
DENSITY (BRITISH)	=	0.0626	LB/IN3
BURN RATE EQUATION	=	0.3100(PC/1000.0) 0.29	
REFERENCE SPECIFIC IMPULSE	=	245.0000	LBF-SEC/LBM
SPECIFIC HEAT RATIO		1.1600	

Reproduced from best available copy.

RUN DATA

EXPANSION RATIO = 10.000

LINE NO	CHAMBER PRESSURE PSIA	BURN TIME SEC	THEORETICAL ISP SEC	ISP EFFICIENCY	MASS RATIO	VELOCITY INCREMENT ACTUAL FT/SEC	VELOCITY INCREMENT GRAVITATIONAL LOSS FT/SEC
1	300.00	40.004	267.205	0.9700	0.9446	3818.8	0.0
2	400.00	36.802	267.205	0.9700	0.9444	3818.8	0.0
3	500.00	34.496	267.205	0.9700	0.9427	3818.8	0.0
4	600.00	32.719	267.205	0.9700	0.9402	3818.8	0.0
5	700.00	31.289	267.205	0.9700	0.9372	3818.8	0.0
6	800.00	30.100	267.205	0.9700	0.9338	3818.8	0.0
7	900.00	29.089	267.205	0.9700	0.9303	3818.8	0.0
8	1000.00	28.214	267.205	0.9700	0.9266	3818.8	0.0

LINE NO	PAYLOAD TO STAGE WEIGHT RATIO	TOTAL MOTOR WEIGHT LBM	PROPELLANT WEIGHT LBM	CASE WEIGHT LBM	NOZZLE WEIGHT LBM	MISC WEIGHT LBM	INERT WEIGHT INITIAL LBM	INERT WEIGHT FINAL LBM
1	0.6110	816.93	771.64	11.92	18.88	14.48	45.29	43.56
2	0.6109	817.06	771.64	15.90	15.32	14.20	45.42	43.97
3	0.6102	818.54	771.64	19.87	13.03	14.00	46.90	45.63
4	0.6092	820.74	771.64	23.84	11.41	13.85	49.10	47.96
5	0.6079	823.39	771.64	27.82	10.20	13.73	51.75	50.71
6	0.6065	826.32	771.64	31.79	9.26	13.63	54.68	53.72
7	0.6050	829.45	771.64	35.77	8.50	13.55	57.81	56.91
8	0.6035	832.72	771.64	39.74	7.87	13.47	61.08	60.24

LINE NO	CASE DIAMETER IN	TOTAL CASE LENGTH IN	NOZZLE EXIT DIAMETER IN	NOZZLE LENGTH IN	TOTAL IMPULSE LBF-SEC	NITER
1	29.154	35.078	11.182	5.924	200000.	0
2	29.154	34.537	10.096	5.383	200000.	0
3	29.154	34.149	9.327	4.995	200000.	0
4	29.154	33.852	8.743	4.697	200000.	0
5	29.154	33.613	8.277	4.459	200000.	0
6	29.154	33.416	7.894	4.262	200000.	0
7	29.154	33.249	7.571	4.095	200000.	0
8	29.154	33.105	7.293	3.950	200000.	0

RUN DATA SUMMARY

PARAMETER			LOCATION	
			EXPANSION RATIO	LINE NO
MAXIMUM BURN TIME ,SEC	=	40.004	10.000	1
MINIMUM BURN TIME ,SEC	=	27.111	80.000	8
MAXIMUM MASS RATIO	=	0.9446	10.000	1
MINIMUM MASS RATIO	=	0.9019	80.000	1
MAXIMUM GRAVITATIONAL LOSS ,FT/SEC	=	0.0	10.000	1- 8
MINIMUM GRAVITATIONAL LOSS ,FT/SEC	=	0.0	80.000	1- 8
MAXIMUM PAYLOAD TO STAGE WEIGHT RATIO	=	0.6433	80.000	4
MINIMUM PAYLOAD TO STAGE WEIGHT RATIO	=	0.6035	10.000	8
MAXIMUM TOTAL MOTOR WEIGHT ,LBM	=	832.72	10.000	8
MINIMUM TOTAL MOTOR WEIGHT ,LBM	=	749.07	80.000	4
MAXIMUM CASE DIAMETER ,IN	=	29.154	10.000	1- 8
MINIMUM CASE DIAMETER ,IN	=	28.014	80.000	1- 8
MAXIMUM NOZZLE EXIT DIAMETER ,IN	=	30.391	80.000	1
MINIMUM NOZZLE EXIT DIAMETER ,IN	=	7.293	10.000	8
MAXIMUM TOTAL IMPULSE ,LB-SEC,	=	200000.	10.000	1- 8
MINIMUM TOTAL IMPULSE ,LB-SEC,	=	200000.	80.000	1- 8
MAXIMUM THEORETICAL ISP ,SEC	=	301.172	80.000	1- 8
MINIMUM THEORETICAL ISP ,SEC	=	267.205	10.000	1- 8
MAXIMUM ISP EFFICIENCY	=	0.9700	10.000	1- 8
MINIMUM ISP EFFICIENCY	=	0.9700	80.000	

RUN DATA

EXPANSION RATIO = 80.000

LINE NO	CHAMBER PRESSURE PSIA	BURN TIME SEC	THEORETICAL ISP SEC	ISP EFFICIENCY	MASS RATIO	VELOCITY INCREMENT ACTUAL FT/SEC	VELOCITY INCREMENT GRAVITATIONAL LOSS FT/SEC
1	300.00	38.439	301.172	0.9700	0.9019	3707.8	0.0
2	400.00	35.363	301.172	0.9700	0.9094	3707.8	0.0
3	500.00	33.147	301.172	0.9700	0.9128	3707.8	0.0
4	600.00	31.440	301.172	0.9700	0.9139	3707.8	0.0
5	700.00	30.065	301.172	0.9700	0.9137	3707.8	0.0
6	800.00	28.923	301.172	0.9700	0.9126	3707.8	0.0
7	900.00	27.952	301.172	0.9700	0.9109	3707.8	0.0
8	1000.00	27.111	301.172	0.9700	0.9088	3707.8	0.0

LINE NO	PAYLOAD TO STAGE WEIGHT RATIO	TOTAL MOTOR WEIGHT LBM	PROPELLANT WEIGHT LBM	CASE WEIGHT LBM	NOZZLE WEIGHT LBM	MISC WEIGHT LBM	INERT WEIGHT INITIAL LBM	INERT WEIGHT FINAL LBM
1	0.6385	759.08	684.61	10.58	50.47	13.43	74.47	70.74
2	0.6415	752.81	684.61	14.10	40.94	13.15	68.20	65.13
3	0.6429	750.01	684.61	17.63	34.81	12.96	65.40	62.75
4	0.6433	749.07	684.61	21.15	30.49	12.82	64.46	62.12
5	0.6432	749.25	684.61	24.68	27.26	12.70	64.64	62.52
6	0.6428	750.16	684.61	28.21	24.73	12.60	65.54	63.61
7	0.6421	751.57	684.61	31.73	22.70	12.52	66.96	65.17
8	0.6413	753.35	684.61	35.26	21.03	12.45	68.74	67.07

LINE NO	CASE DIAMETER IN	TOTAL CASE LENGTH IN	NOZZLE EXIT DIAMETER IN	NOZZLE LENGTH IN	TOTAL IMPULSE LBF-SEC	NITER
1	28.014	48.330	30.391	20.316	200000.	0
2	28.014	46.550	27.440	18.535	200000.	0
3	28.014	45.259	25.350	17.245	200000.	0
4	28.014	44.263	23.762	16.248	200000.	0
5	28.014	43.460	22.496	15.445	200000.	0
6	28.014	42.793	21.455	14.779	200000.	0
7	28.014	42.227	20.576	14.212	200000.	0
8	28.014	41.737	19.821	13.722	200000.	0

RUN DATA

EXPANSION RATIO = 53.000

LINE NO	CHAMBER PRESSURE PSIA	BURN TIME SEC	THEORETICAL ISP SEC	ISP EFFICIENCY	MASS RATIO	VELOCITY INCREMENT ACTUAL FT/SEC	VELOCITY INCREMENT GRAVITATIONAL LOSS FT/SEC
1	300.00	38.674	295.732	0.9700	0.9138	3723.3	0.0
2	400.00	35.578	295.732	0.9700	0.9192	3723.3	0.0
3	500.00	33.349	295.732	0.9700	0.9212	3723.3	0.0
4	600.00	31.631	295.732	0.9700	0.9214	3723.3	0.0
5	700.00	30.248	295.732	0.9700	0.9204	3723.3	0.0
6	800.00	29.099	295.732	0.9700	0.9186	3723.3	0.0
7	900.00	28.122	295.732	0.9700	0.9164	3723.3	0.0
8	1000.00	27.276	295.732	0.9700	0.9138	3723.3	0.0

LINE NO	PAYLOAD TO STAGE WEIGHT RATIO	TOTAL MOTOR WEIGHT LBM	PROPELLANT WEIGHT LBM	CASE WEIGHT LBM	NOZZLE WEIGHT LBM	MISC WEIGHT LBM	INERT WEIGHT INITIAL LBM	INERT WEIGHT FINAL LBM
1	0.6367	762.94	697.20	10.77	41.39	13.58	65.74	62.59
2	0.6388	758.45	697.20	14.36	33.57	13.31	61.25	58.64
3	0.6396	756.82	697.20	17.95	28.55	13.12	59.61	57.37
4	0.6397	756.72	697.20	21.54	25.00	12.97	59.51	57.52
5	0.6393	757.54	697.20	25.13	22.35	12.85	60.34	58.53
6	0.6386	758.97	697.20	28.72	20.28	12.75	61.76	60.11
7	0.6377	760.81	697.20	32.32	18.62	12.67	63.61	62.07
8	0.6367	762.96	697.20	35.91	17.25	12.60	65.76	64.32

LINE NO	CASE DIAMETER IN	TOTAL CASE LENGTH IN	NOZZLE EXIT DIAMETER IN	NOZZLE LENGTH IN	TOTAL IMPULSE LBF-SEC	NITER
1	28.185	44.537	24.887	16.351	200000.	0
2	28.185	43.077	22.471	14.892	200000.	0
3	28.185	42.025	20.760	13.840	200000.	0
4	28.185	41.215	19.458	13.030	200000.	0
5	28.185	40.564	18.422	12.379	200000.	0
6	28.185	40.024	17.569	11.839	200000.	0
7	28.185	39.566	16.850	11.381	200000.	0
8	28.185	39.170	16.231	10.985	200000.	0

RUN DATA

EXPANSICN RATIO = 30.000.

LINE NO	CHAMBER PRESSURE PSIA	BURN TIME SEC	THEORETICAL ISP SEC	ISP EFFICIENCY	MASS RATIO	VELOCITY INCREMENT ACTUAL FT/SEC	VELOCITY INCREMENT GRAVITATIONAL LOSS FT/SEC
1	300.00	39.048	287.306	0.9700	0.9271	3748.9	0.0
2	400.00	35.923	287.306	0.9700	0.9301	3748.9	0.0
3	500.00	33.672	287.306	0.9700	0.9305	3748.9	0.0
4	600.00	31.937	287.306	0.9700	0.9295	3748.9	0.0
5	700.00	30.541	287.306	0.9700	0.9276	3748.9	0.0
6	800.00	29.381	287.306	0.9700	0.9252	3748.9	0.0
7	900.00	28.395	287.306	0.9700	0.9224	3748.9	0.0
8	1000.00	27.540	287.306	0.9700	0.9194	3748.9	0.0

LINE NO	PAYLOAD TO STAGE WEIGHT RATIO	TOTAL MOTOR WEIGHT LBM	PROPELLANT WEIGHT LBM	CASE WEIGHT LBM	NOZZLE WEIGHT LBM	MISC WEIGHT LBM	INERT WEIGHT INITIAL LBM	INERT WEIGHT FINAL LBM
1	0.6314	774.11	717.65	11.09	31.54	13.83	56.46	53.93
2	0.6326	771.58	717.65	14.78	25.59	13.56	53.93	51.83
3	0.6327	771.25	717.65	18.48	21.76	13.36	53.60	51.78
4	0.6323	772.10	717.65	22.18	19.06	13.21	54.44	52.83
5	0.6316	773.65	717.65	25.87	17.03	13.10	56.00	54.53
6	0.6306	775.68	717.65	29.57	15.46	13.00	58.02	56.67
7	0.6295	778.02	717.65	33.26	14.19	12.92	60.37	59.12
8	0.6283	780.60	717.65	36.96	13.14	12.85	62.95	61.77

LINE NO	CASE DIAMETER IN	TOTAL CASE LENGTH IN	NOZZLE EXIT DIAMETER IN	NOZZLE LENGTH IN	TOTAL IMPULSE LBF-SEC	NITER
1	28.458	40.355	18.905	11.897	200000.	0
2	28.458	39.277	17.070	10.819	200000.	0
3	28.458	38.503	15.770	10.045	200000.	0
4	28.458	37.909	14.781	9.451	200000.	0
5	28.458	37.432	13.994	8.974	200000.	0
6	28.458	37.037	13.346	8.579	200000.	0
7	28.458	36.703	12.800	8.245	200000.	0
8	28.458	36.414	12.330	7.956	200000.	0

APPENDIX B

PARAMETRIC STUDY

APPENDIX B

PARAMETRIC STUDY

SET I (Figure B-1 through B-17)

Configuration - Spherical

Volumetric Loading Density - 95%

Web Fraction - 60%

Nozzle Submergence - 40%

Case Material - Titanium ($\frac{\sigma}{\rho_c} = 1.1 \times 10^6$)

Case Safety Factor - 1.4

Chamber Pressure - 300 to 1500 psia

Expansion Ratio - 10 to 80

Total Impulse - 50,000 to 800,000 lbf-sec

Propellants - PB-AP-AL (TP-H-3062)

PB-AP-BE (TP-H-1092)

PB-HAP-AL (no designation)

PB-HAP-BE (no designation)

SET II (Figures B-18 through B-21)

Configuration - Spherical

Volumetric Loading Density - 95%

Web Fraction - 60%

Nozzle Submergence - 40%

Case Material - Titanium ($\frac{\sigma}{\rho_c} = 1.1 \times 10^6$)

Steel ($\frac{\sigma}{\rho_c} = 0.707 \times 10^6$)

Case Safety Factor - 1.1, 1.25, 1.4

Chamber Pressure - Optimum

Expansion Ratio - 53

Total Impulse - 50,000 to 800,000 lbf-sec

Propellants PB-AP-AL (TP-H-3062)
PB-AP-BE (TP-H-1092)

E191-67-05

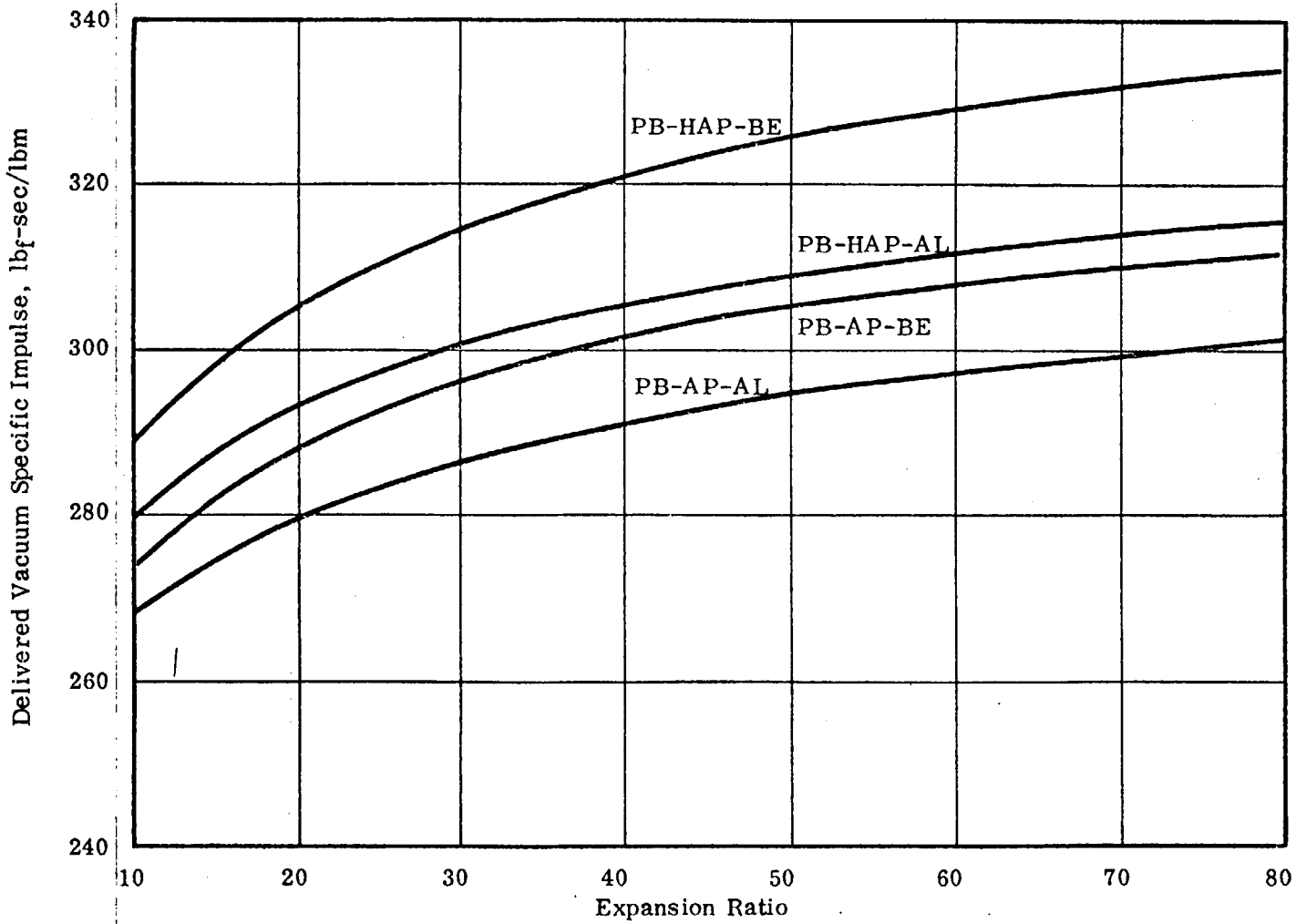

FIGURE B-1. DELIVERED VACUUM SPECIFIC IMPULSE VERSUS EXPANSION RATIO

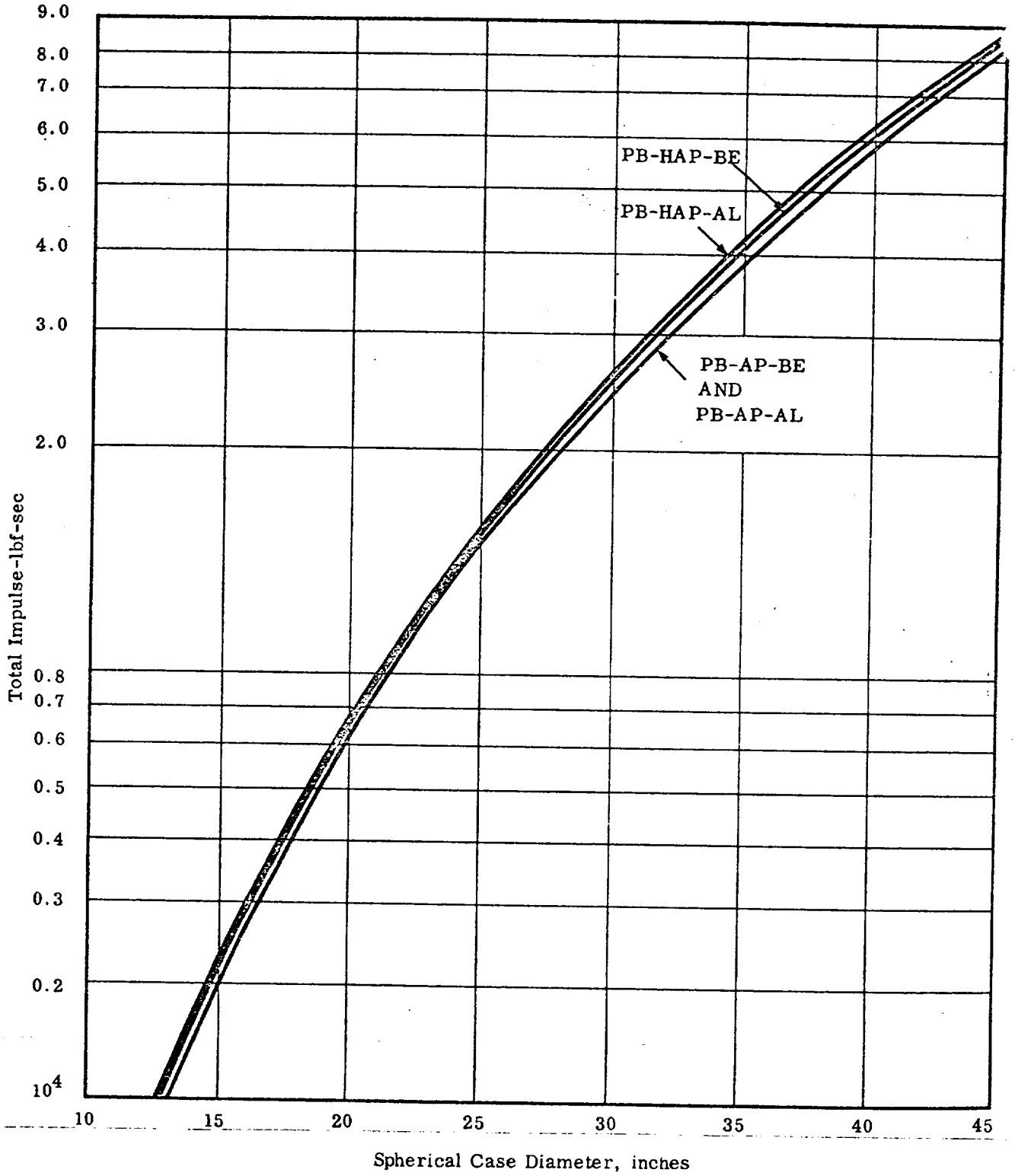

FIGURE B-2. TOTAL IMPULSE VERSUS SPHERICAL CASE DIAMETER
EXPANSION RATIO = 53:1

E191-67-07

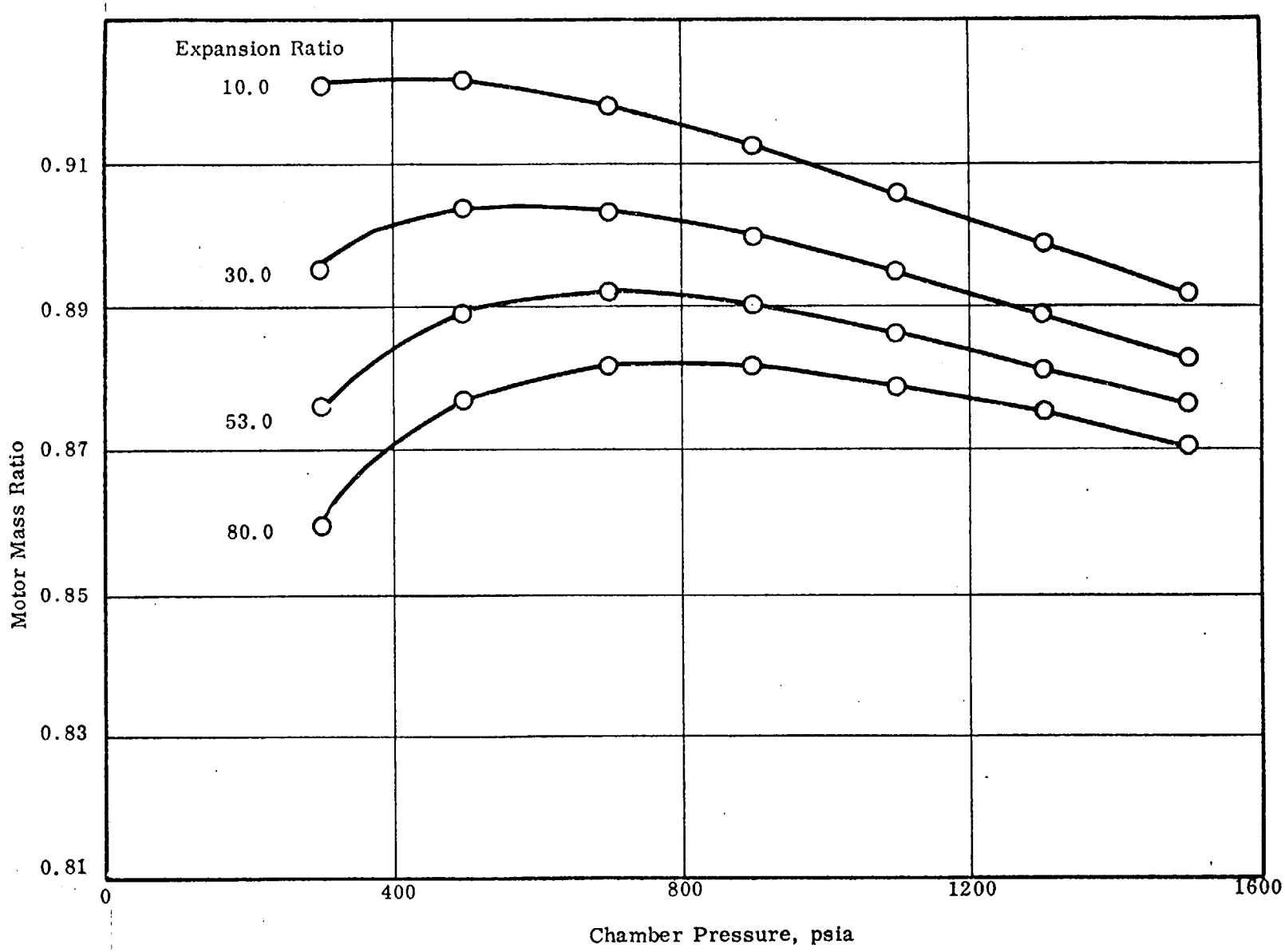

FIGURE B-3. MOTOR MASS RATIO VERSUS CHAMBER PRESSURE

PB-AP-BE PROPELLANT
I_T = 50,000 lbf-sec

E191-67-08

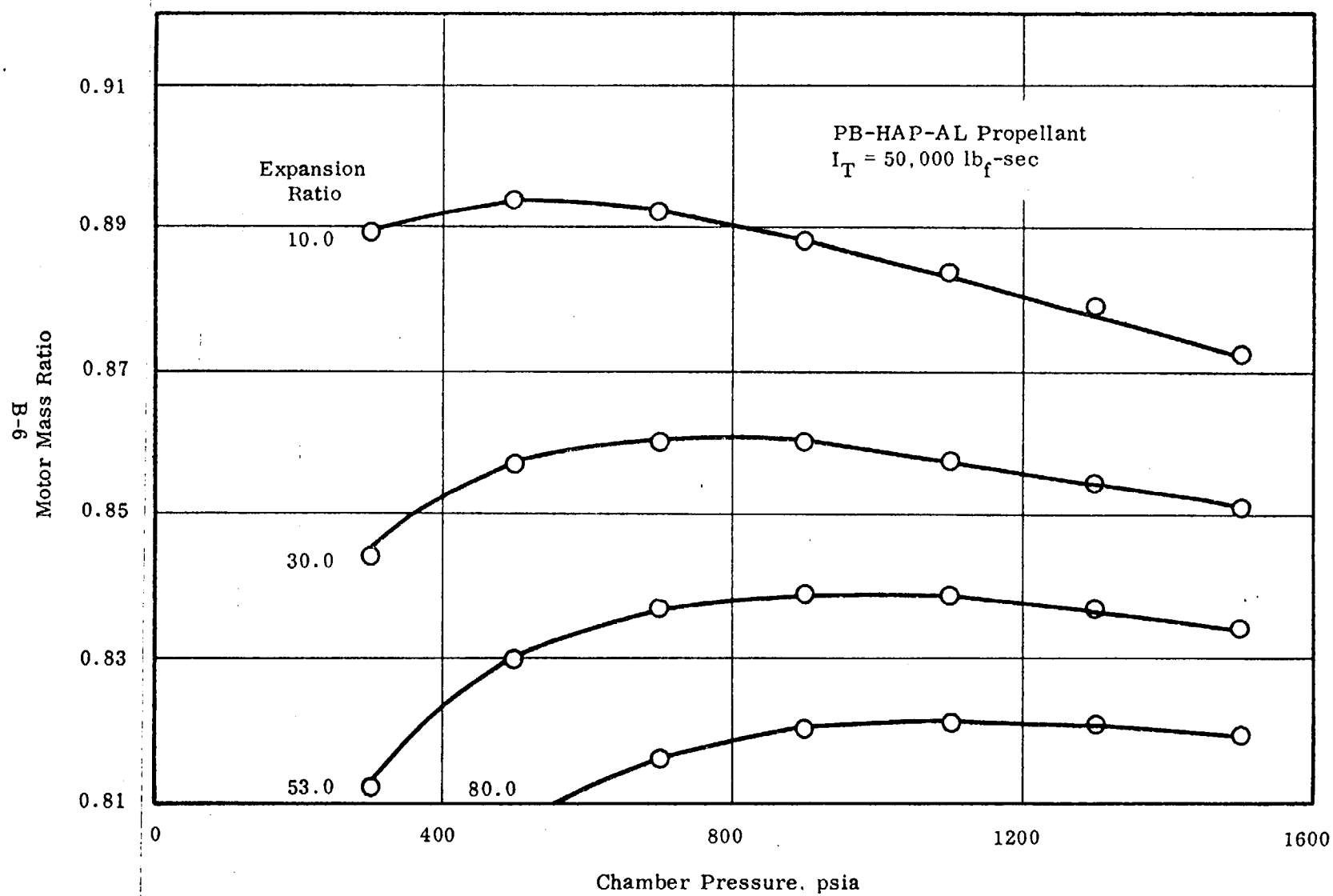

FIGURE B-4. MOTOR M' ^S RATIO VERSUS CHAMBER PRESSURE

E191-67-09

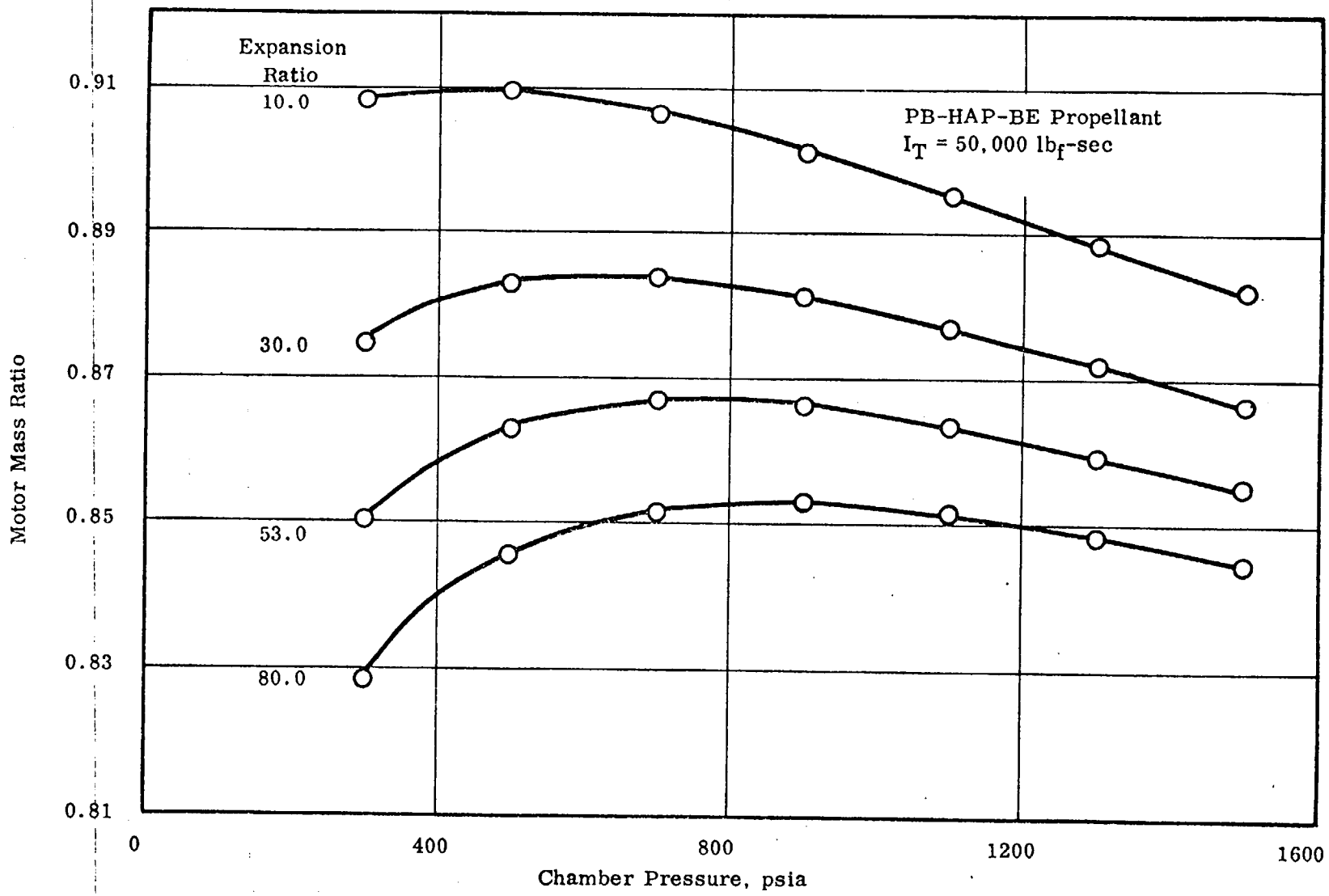

FIGURE B-5. MOTOR MASS RATIO VERSUS CHAMBER PRESSURE

E191-67-10

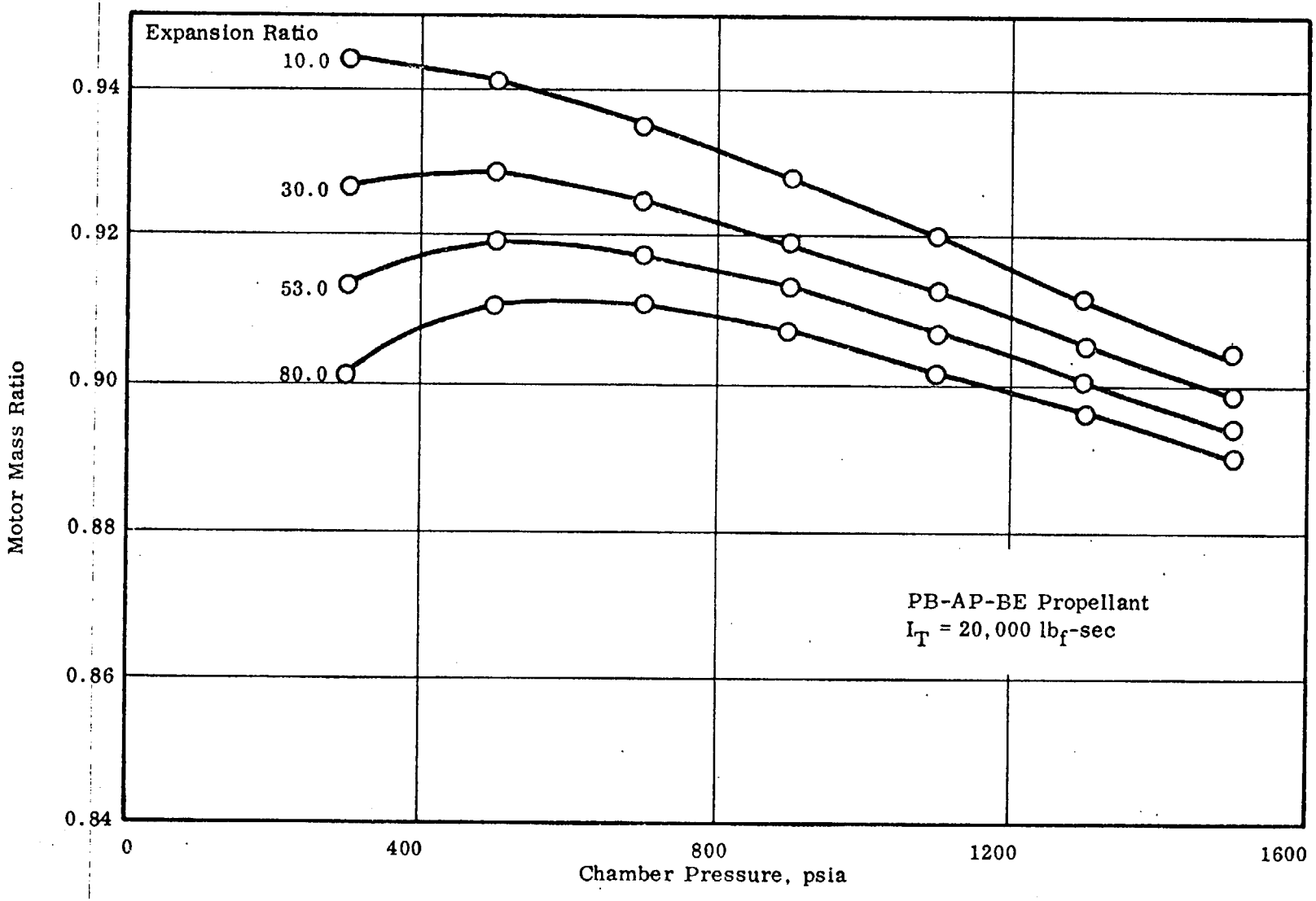

FIGURE B-6. MOTOR MASS RATIO VERSUS CHAMBER PRESSURE

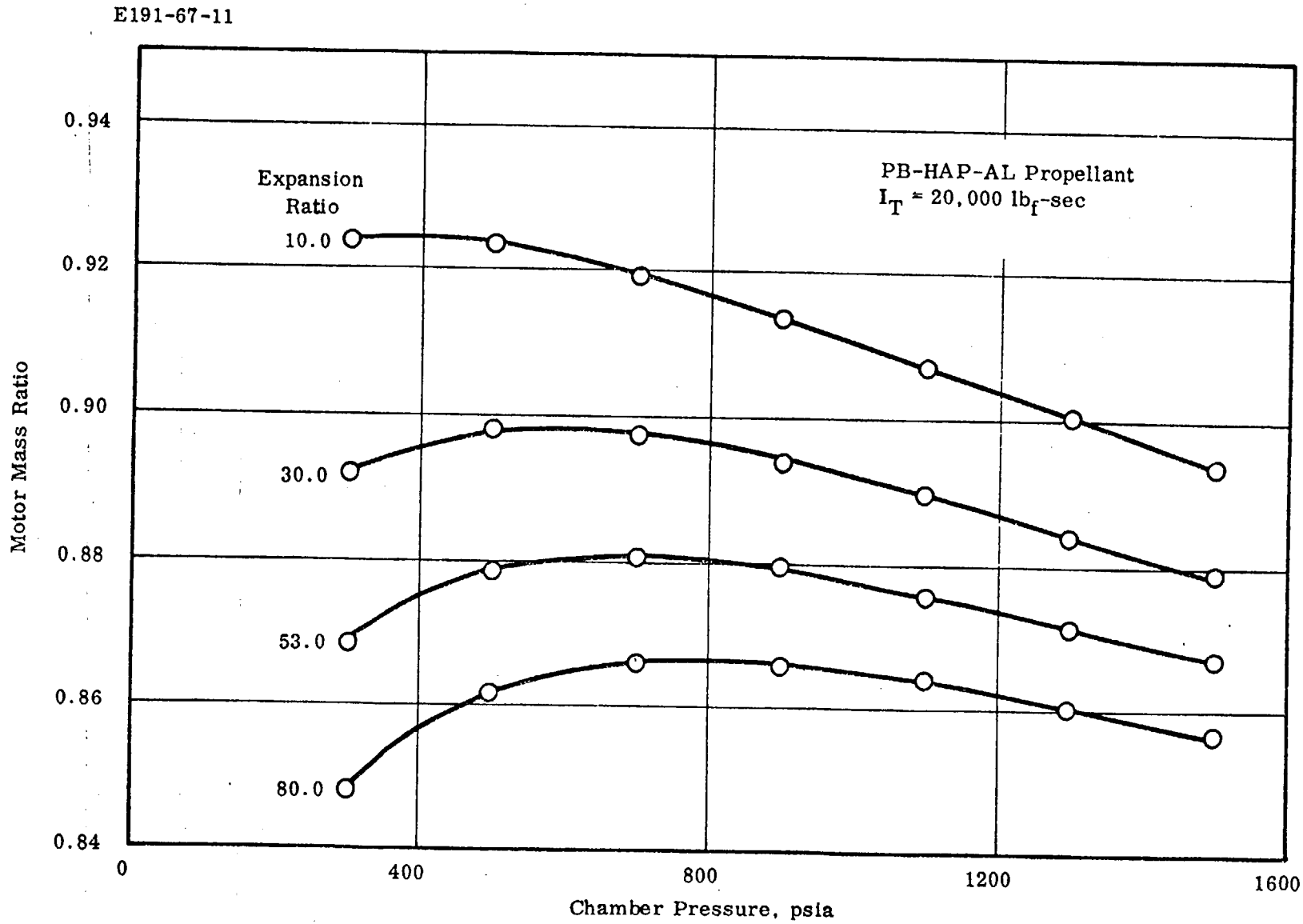

FIGURE B-7. MOTOR MASS RATIO VERSUS CHAMBER PRESSURE

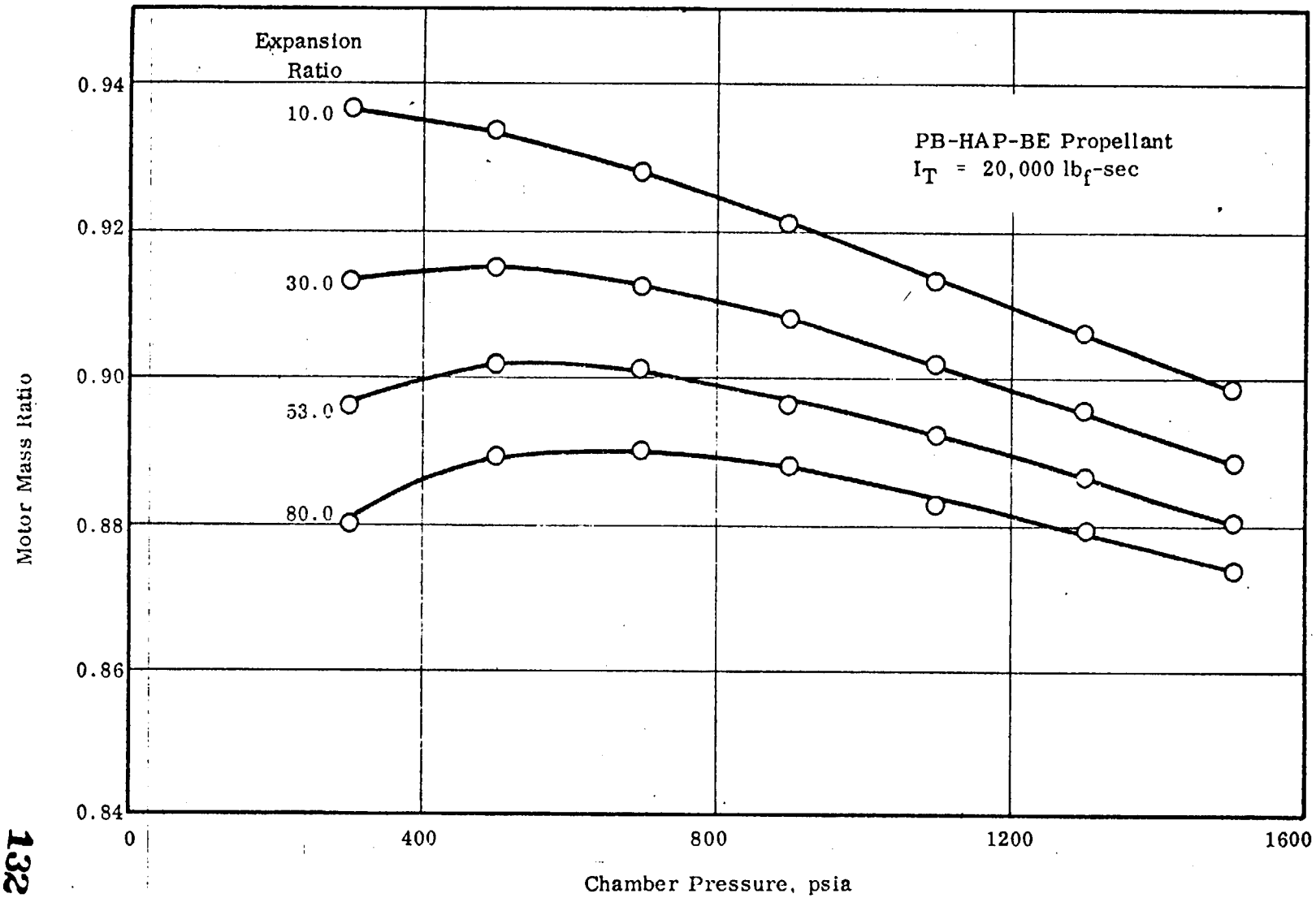

FIGURE B-8. MOTOR MASS RATIO VERSUS CHAMBER PRESSURE

E191-67-13

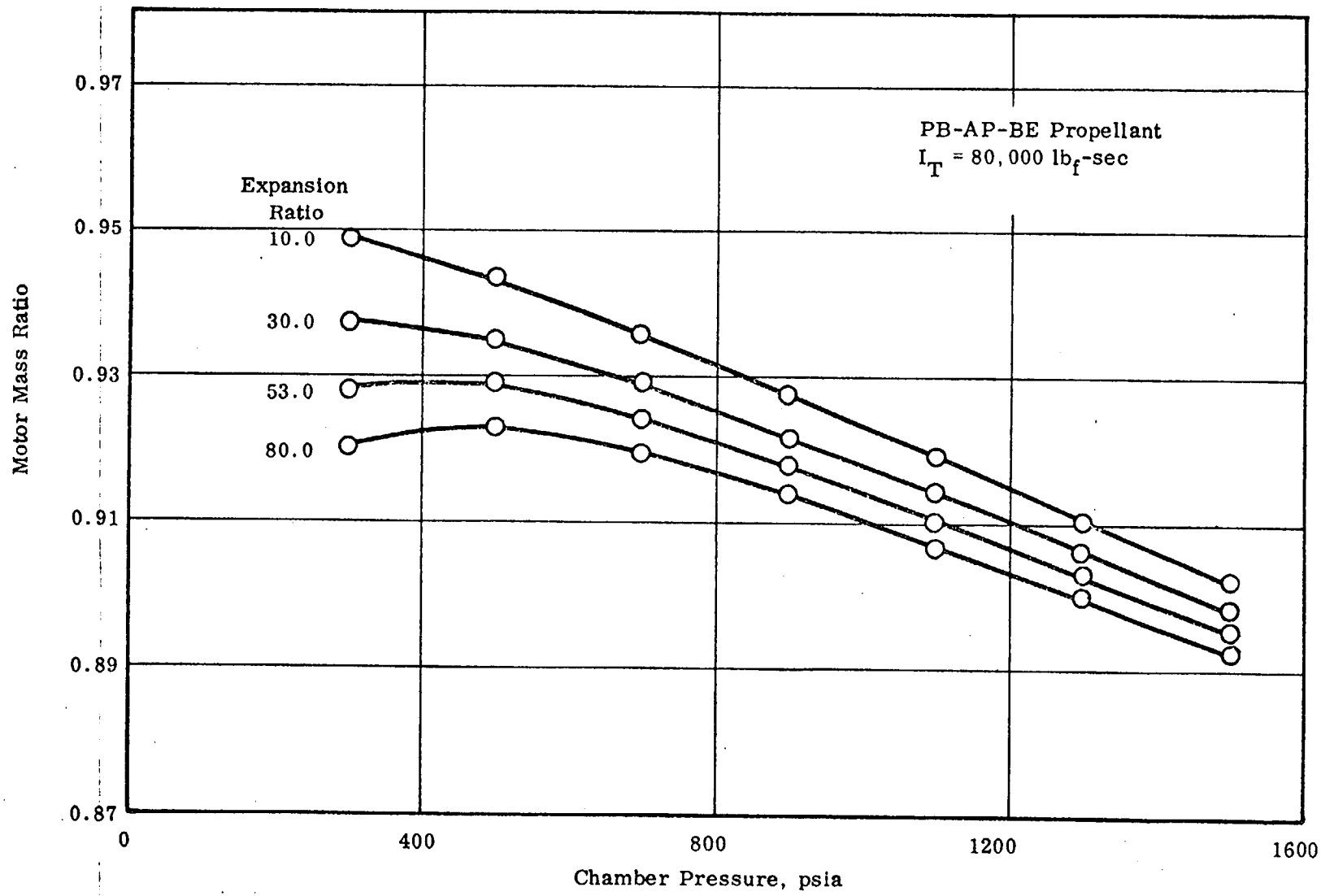

FIGURE B-9. MOTOR MASS RATIO VERSUS CHAMBER PRESSURE

E191-67-14

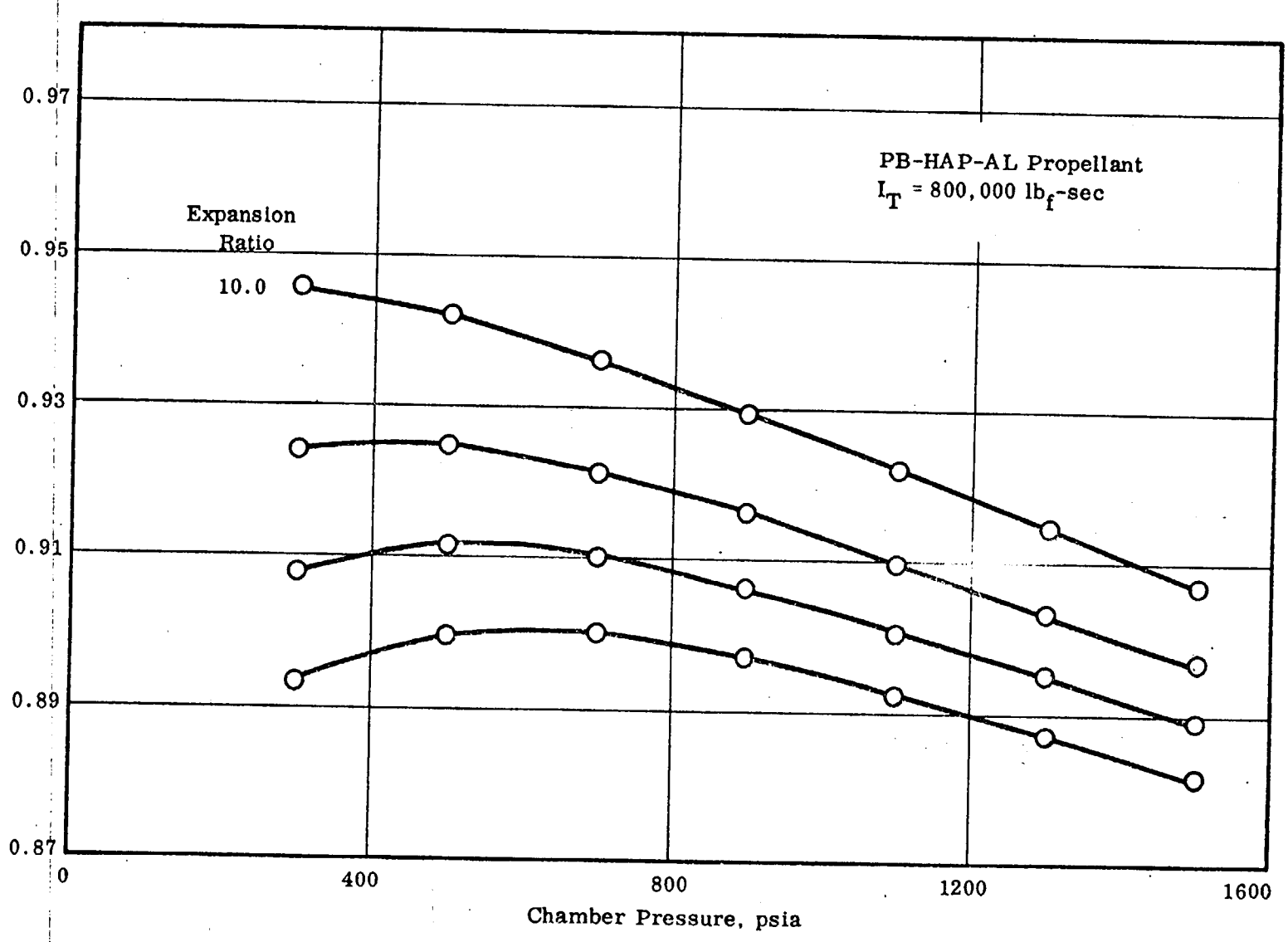

FIGURE B-10. MOTOR MASS RATIO VERSUS CHAMBER PRESSURE

E191-67-15

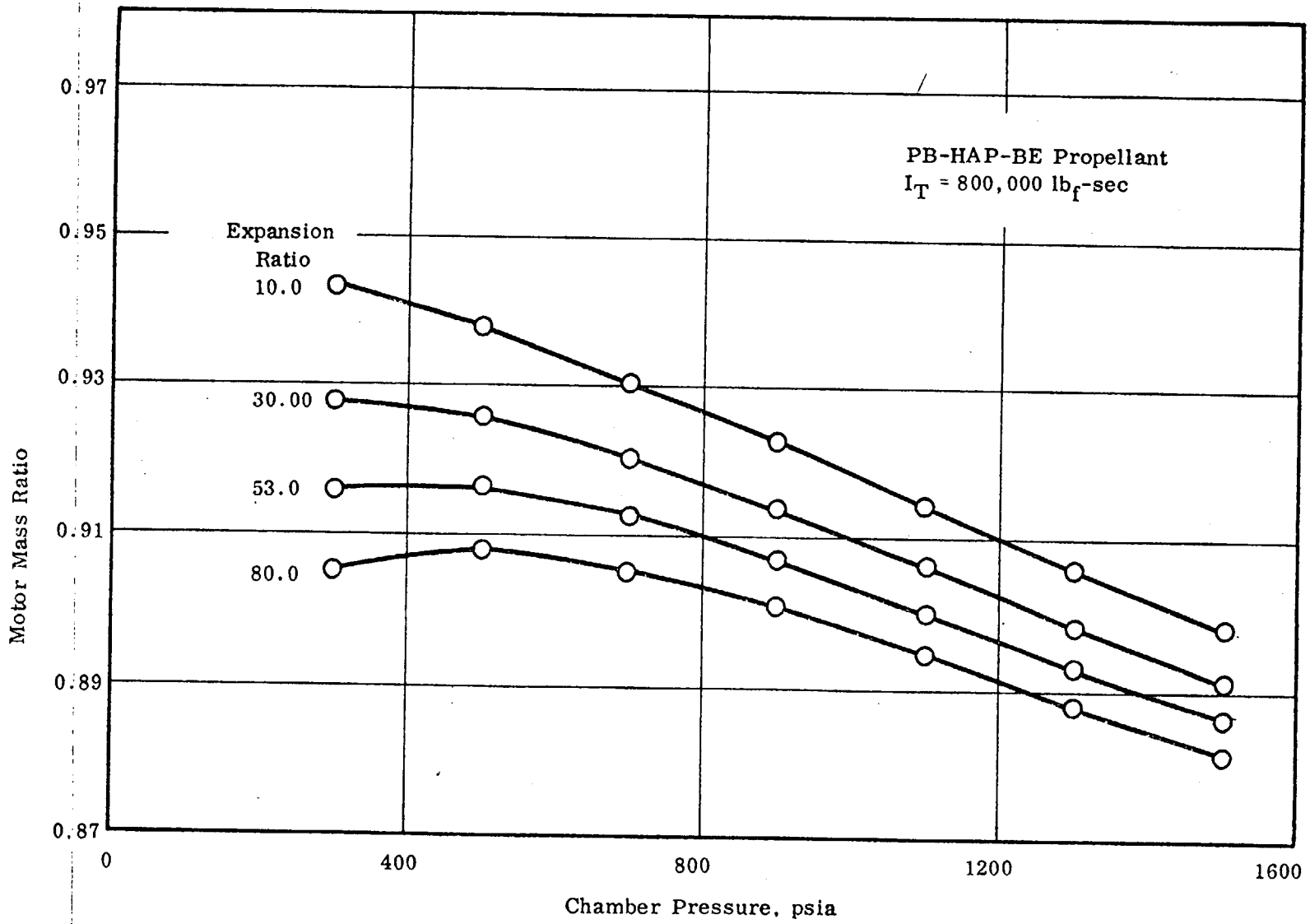

FIGURE B-11. MOTOR MASS RATIO VERSUS CHAMBER PRESSURE

E191-67-16

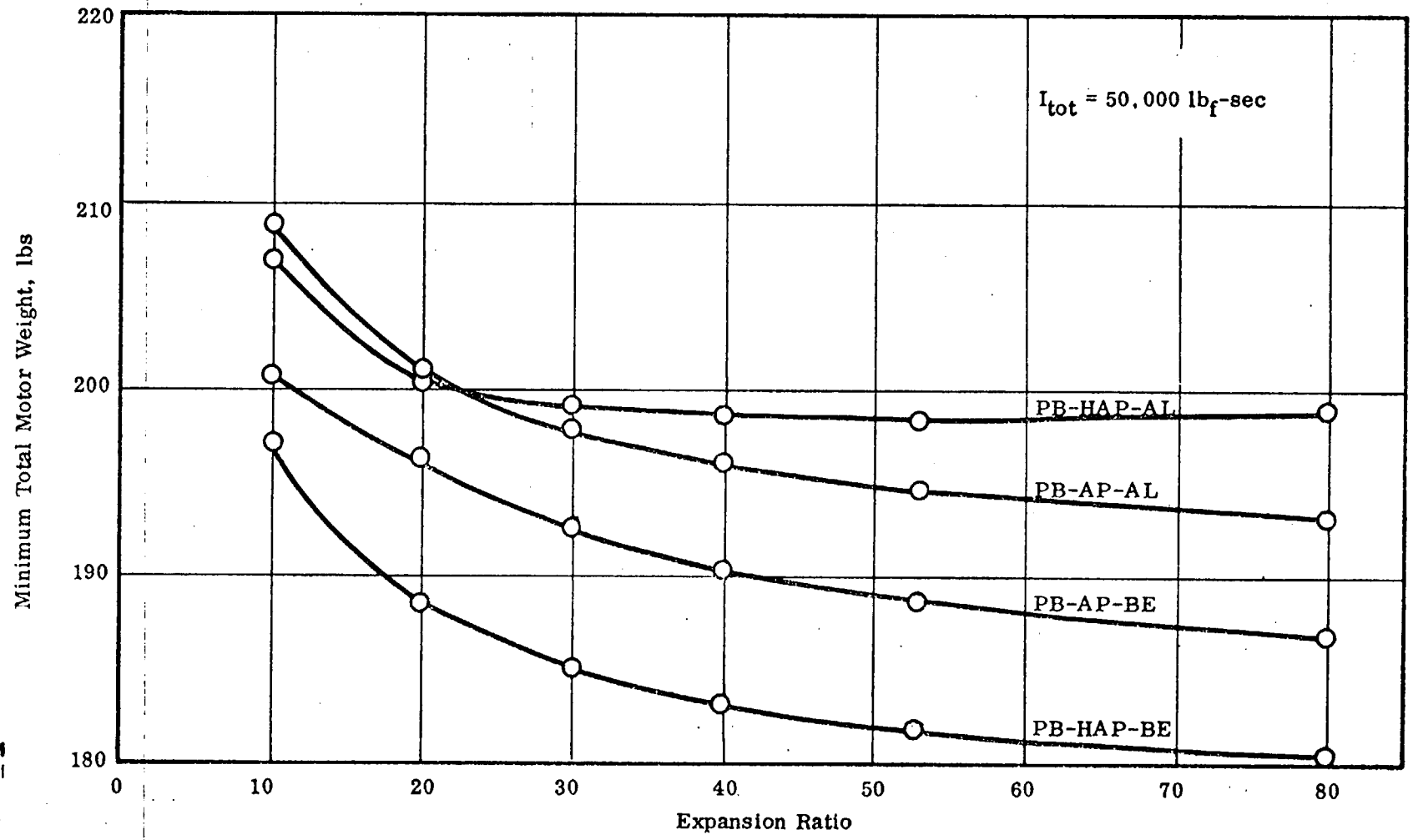

FIGURE MINIMUM TOTAL WEIGHT VERSUS EXPANSION RATIO

E191-67-17

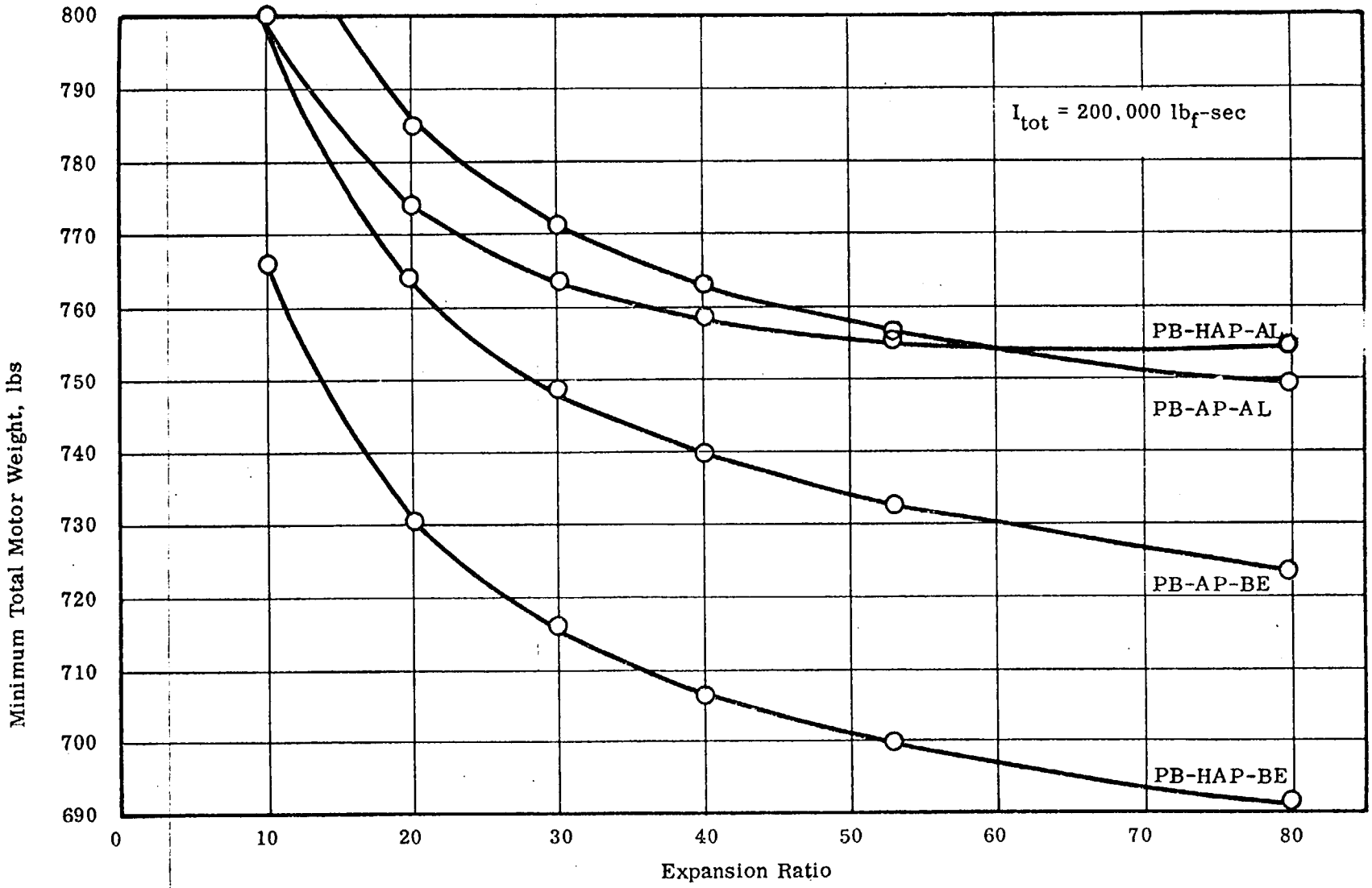

FIGURE B-13. MINIMUM TOTAL WEIGHT VERSUS EXPANSION RATIO

E191-67-18

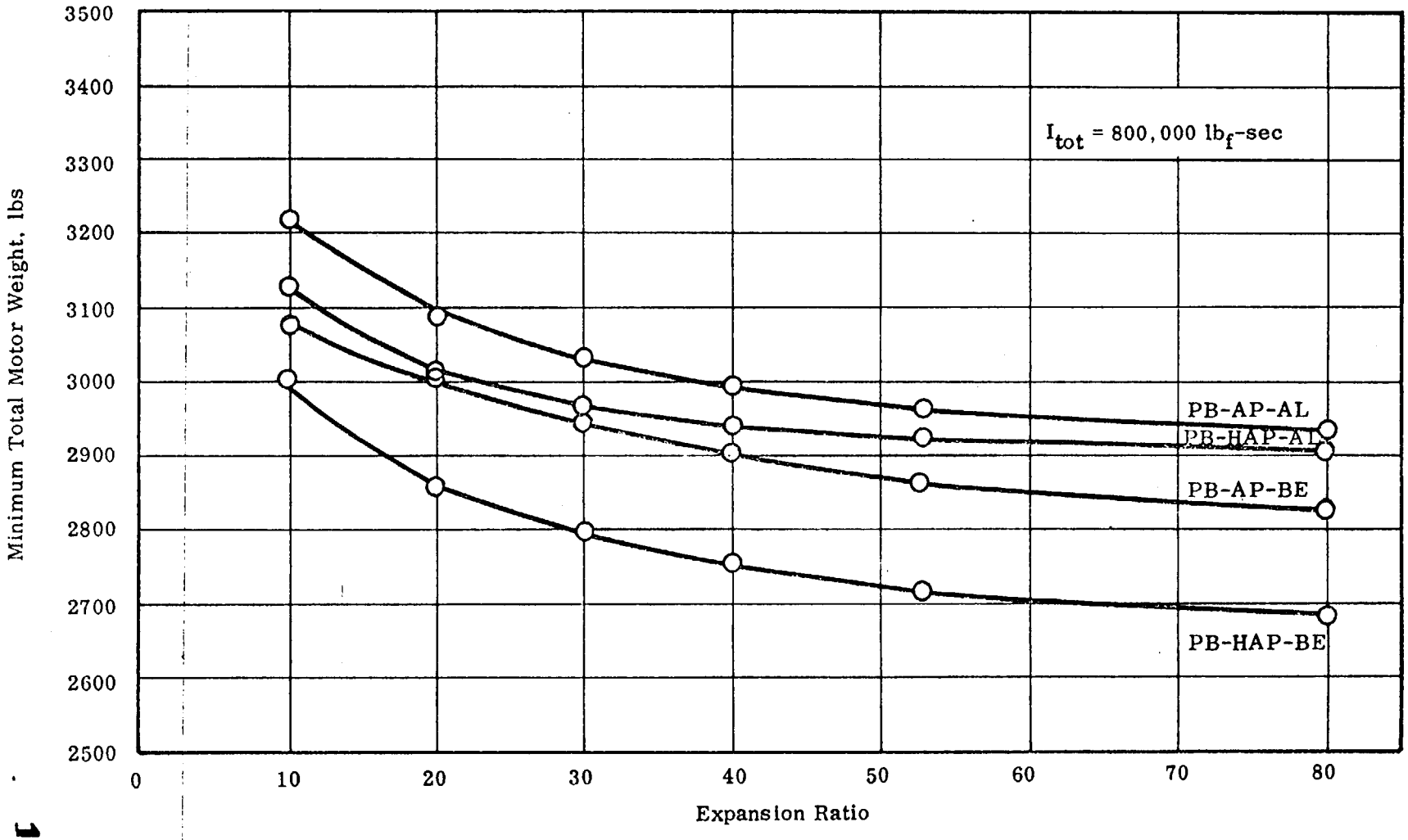

FIGURE B-14. MINIMUM TOTAL WEIGHT VERSUS EXPANSION RATIO

E191-67-19

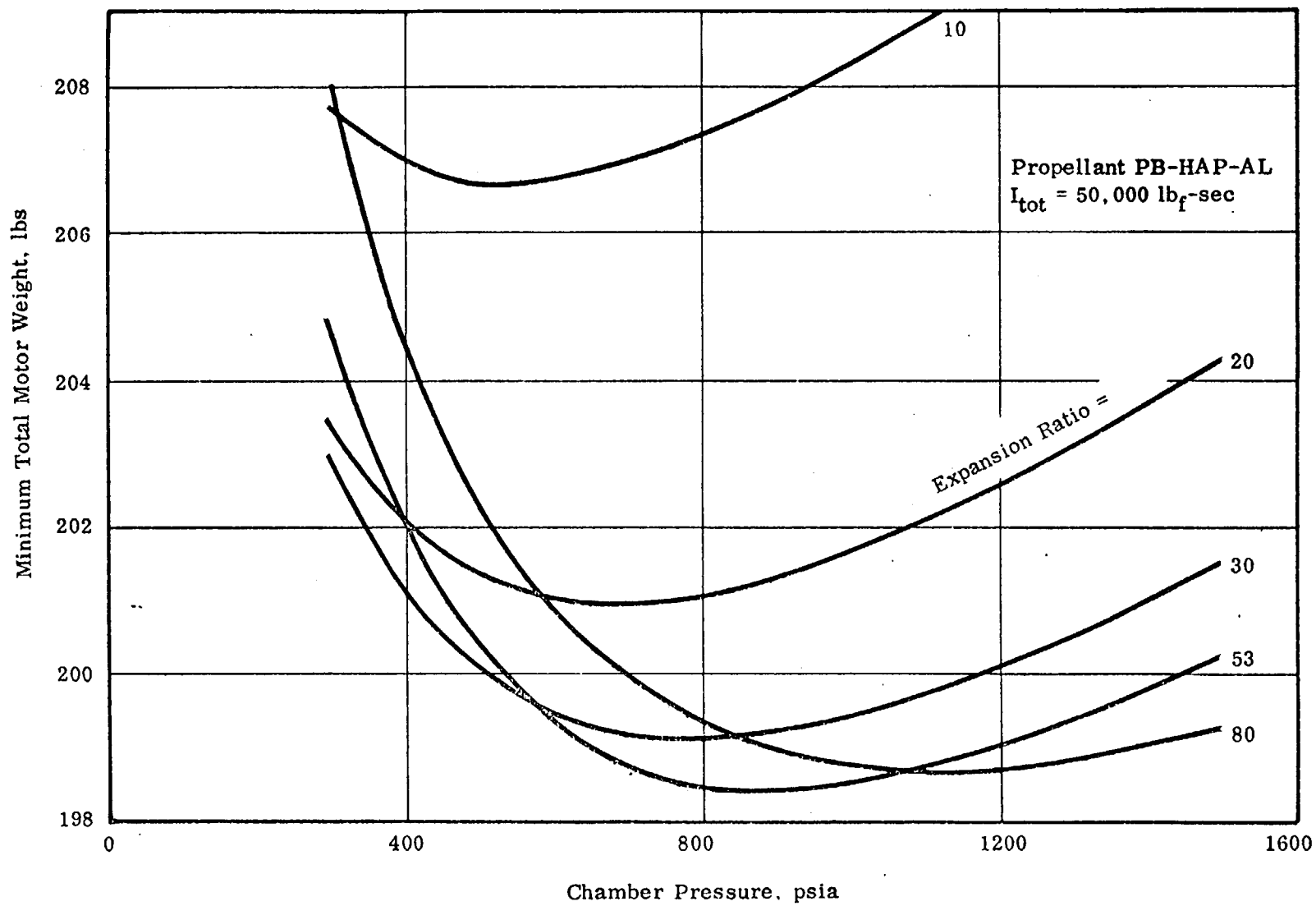

FIGURE B-15. TOTAL MOTOR WEIGHT VERSUS CHAMBER PRESSURE

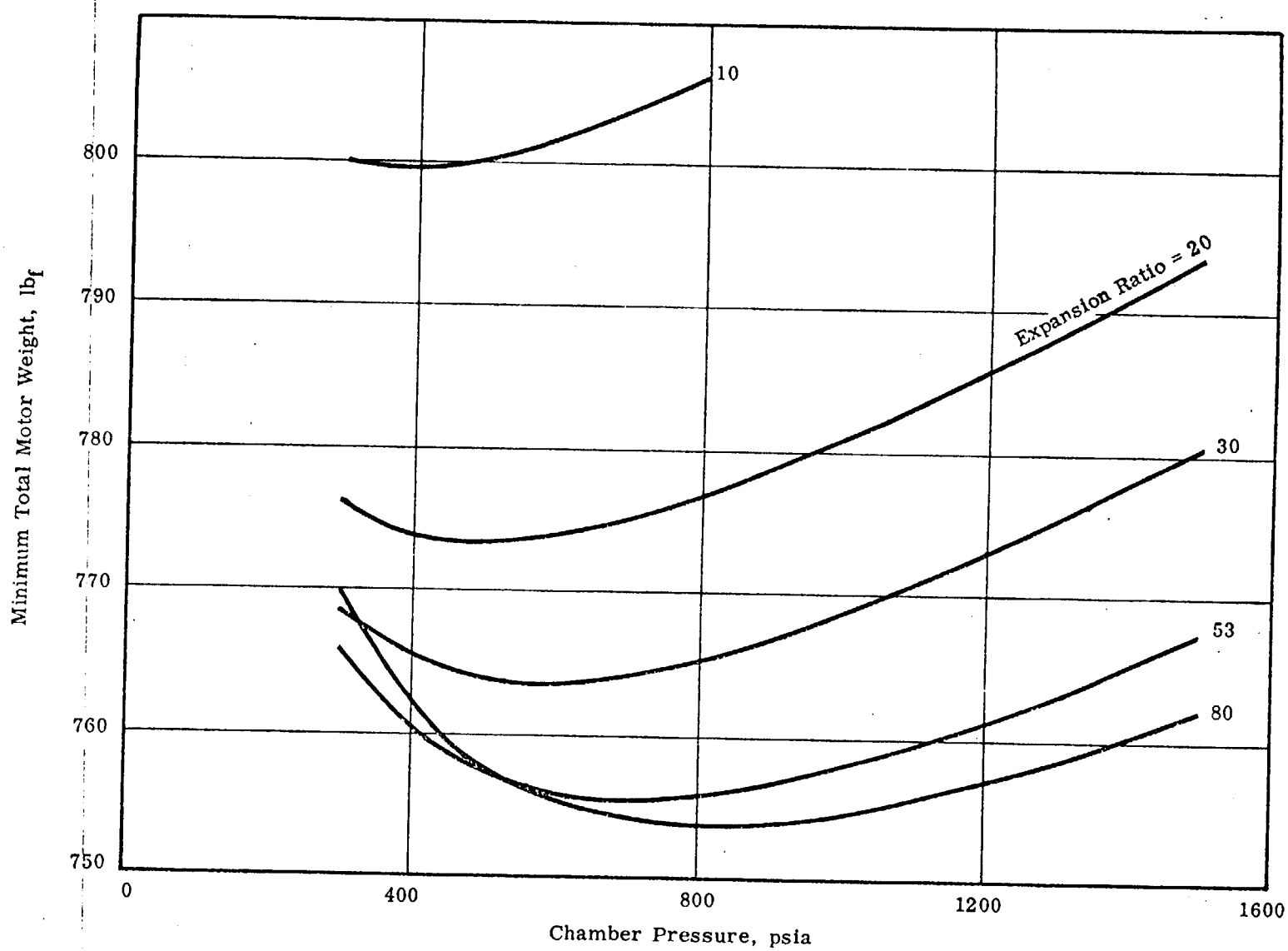

FIGURE B-16. TOTAL MOTOR WEIGHT VERSUS CHAMBER PRESSURE
PROPELLANT PB-HAP-AL
I_{TOT} = 200,000 LB_F - SEC

E191-67-21

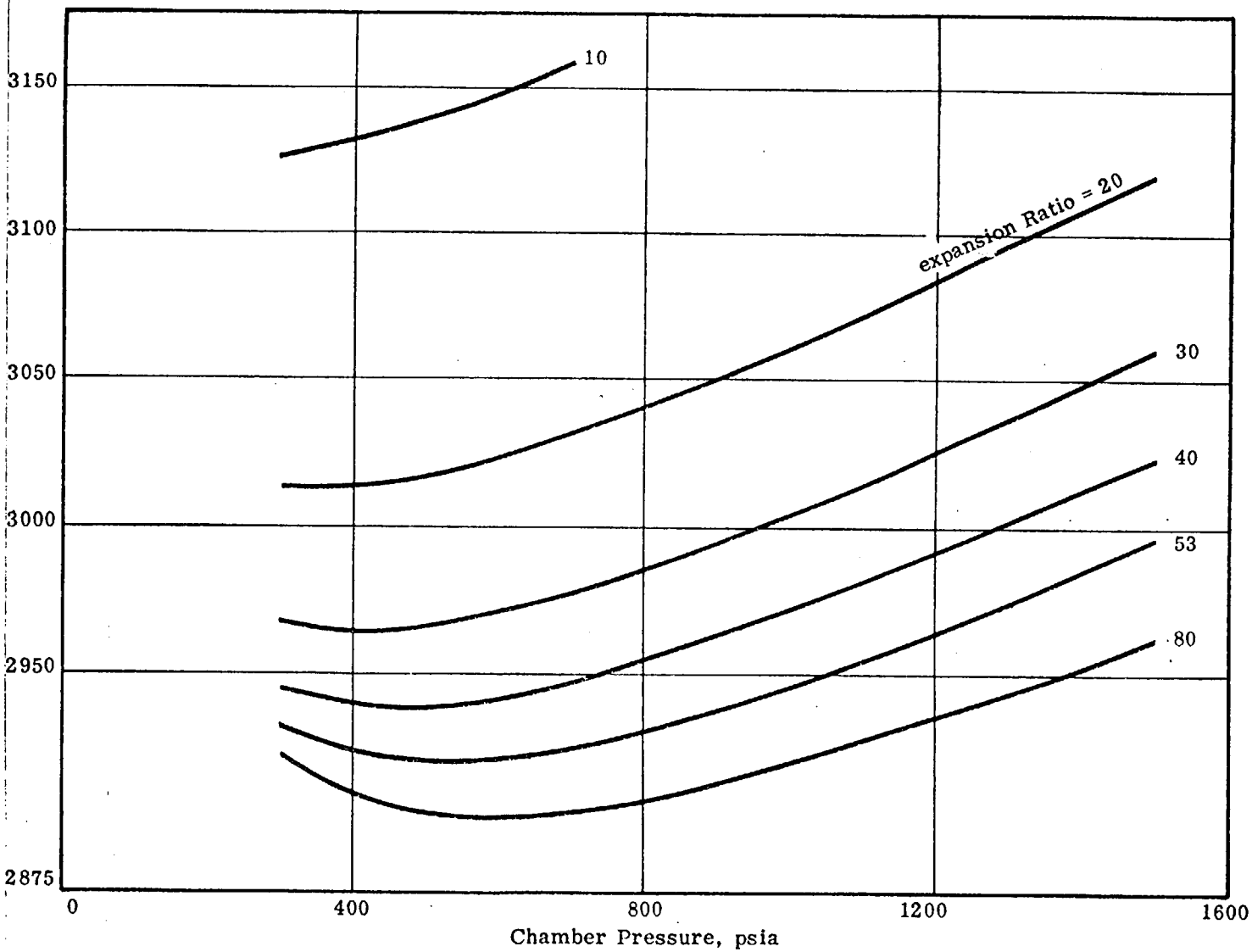

FIGURE B-17. TOTAL MOTOR WEIGHT VERSUS CHAMBER PRESSURE
PROPELLANT PB-HAP-AL
I_{TOT} = 800,000 LB_F - SEC

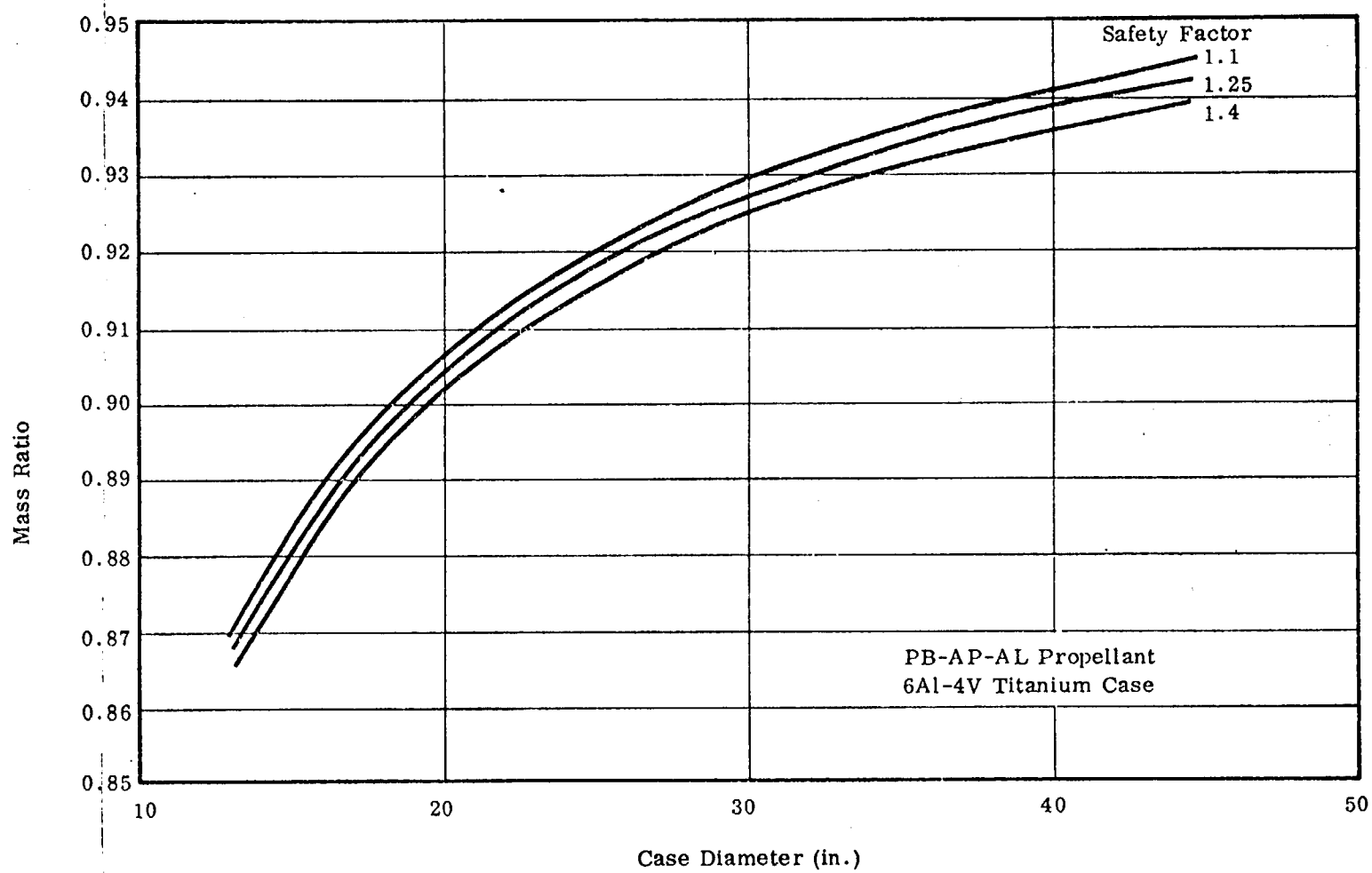

FIGURE B-18. MOTOR MASS RATIO VERSUS CASE DIAMETER

E191-67-23

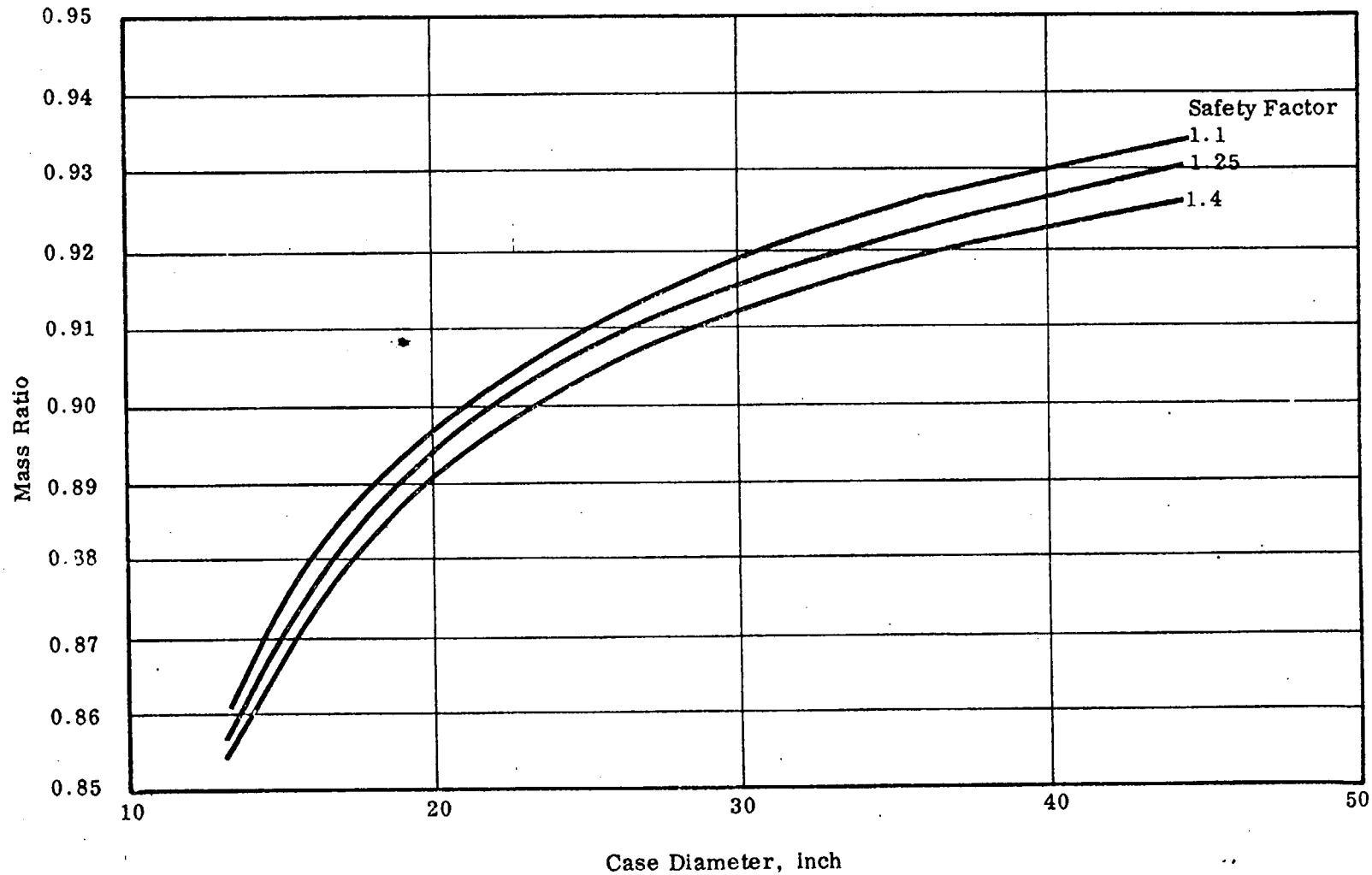

FIGURE B-19. MOTOR MASS RATIO VERSUS CASE DIAMETER
PB-AP-AL Propellant

E191-67-24

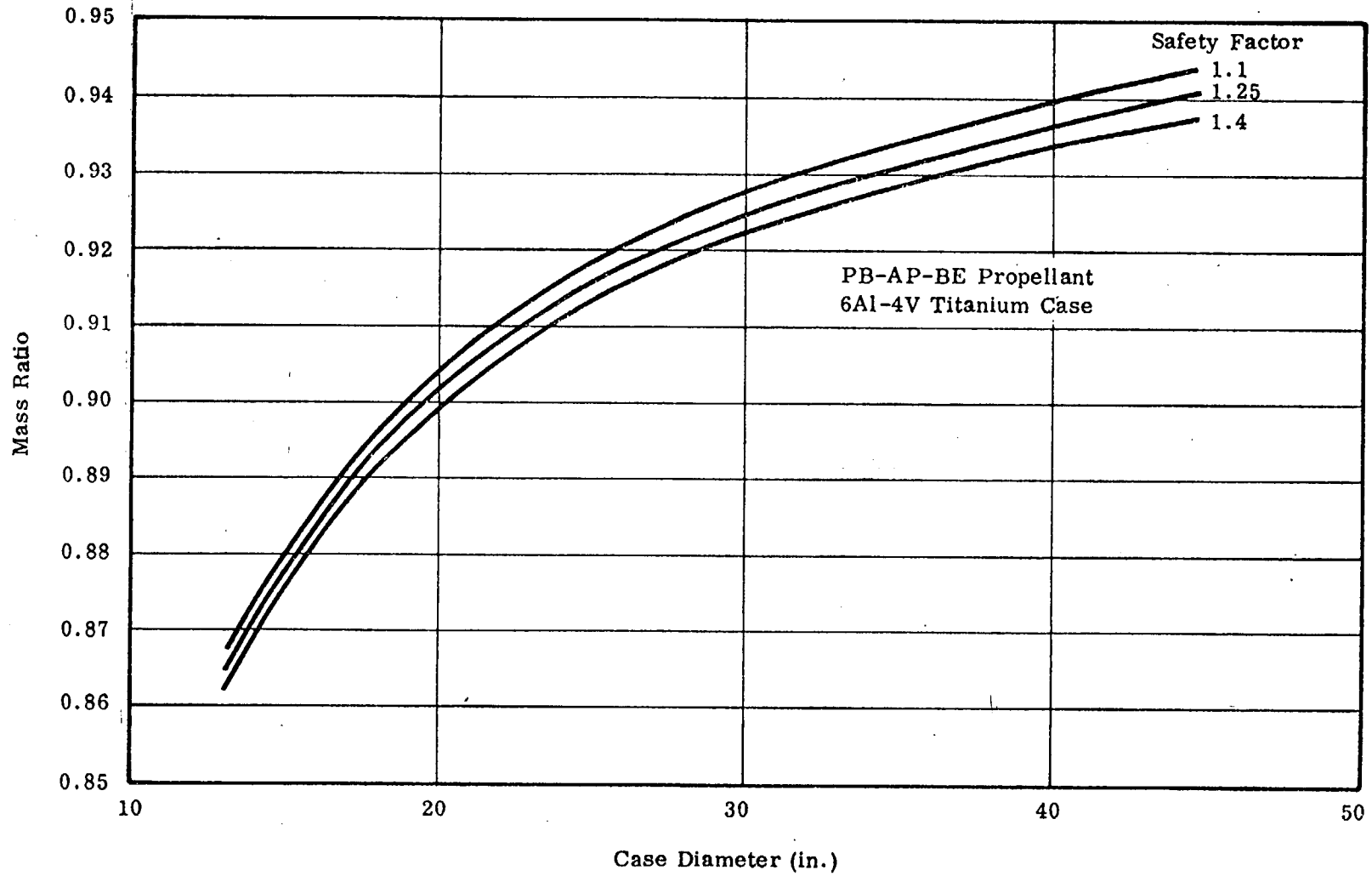

FIGURE B-20. MOTOR MASS RATIO VERSUS CASE DIAMETER

E191-67-25

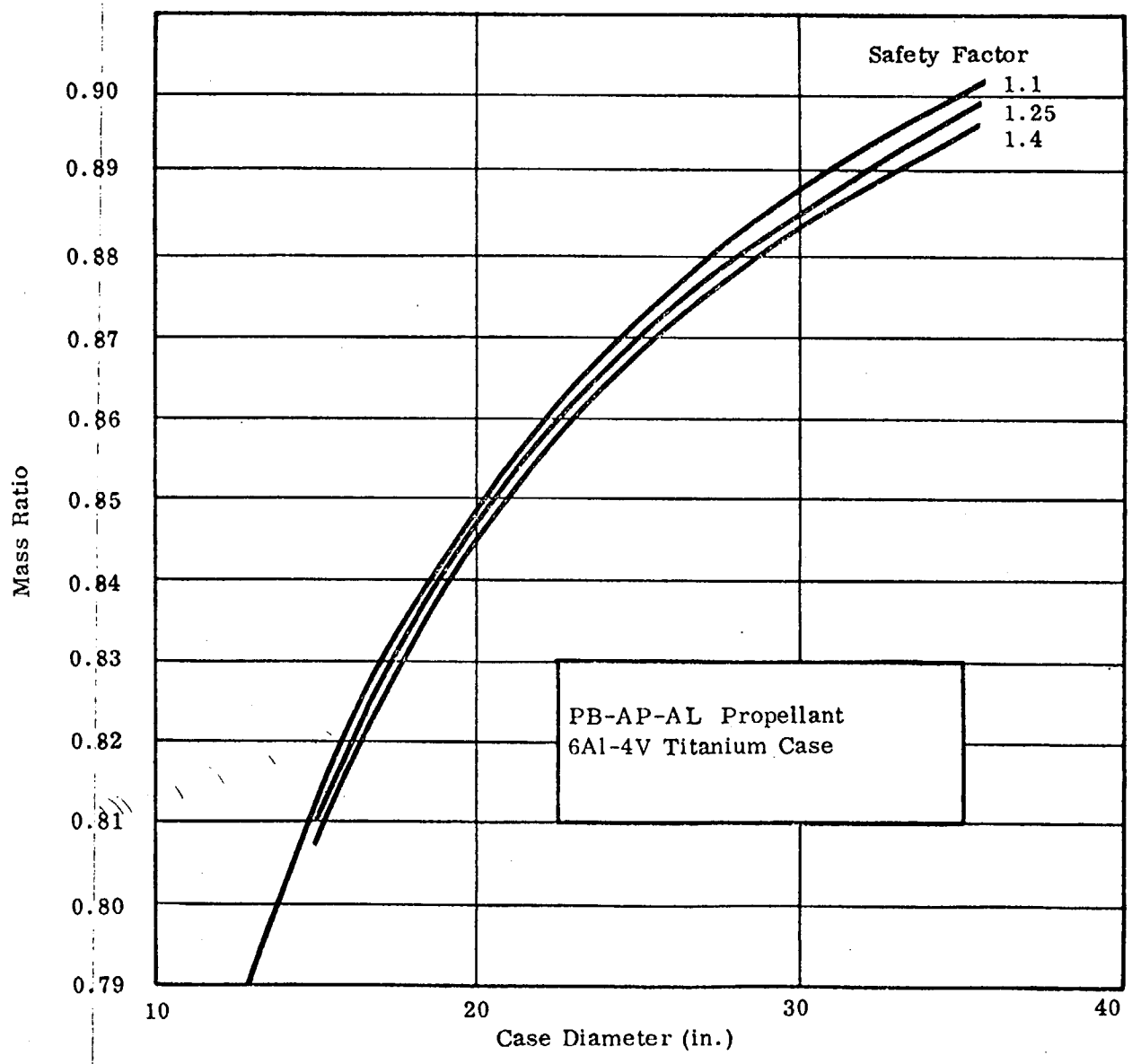

FIGURE B-21. MOTOR MASS RATIO VERSUS CASE DIAMETER

APPENDIX C

SURVEYOR MAIN RETROGRADE MOTOR NOZZLE ALIGNMENT PROCEDURE

OP. NO.	OPERATION	QC/PROD. SIGN OR STAMP DATE
II.	NOZZLE ALIGNMENT	
10.0	Check that the motor that is to be checked for nozzle centerline has no "hold" tags, has cleared QC inspection since the last major operation, and that it is approved for further assembly. Do not proceed with the nozzle centerline determination without a QC representative present. The equipment to be used in the nozzle centerline measurement run is called out by Thiokol Engineering Drawings: E-18731 Nozzle Alignment Arrangement; E-15767 Thrust Alignment Fixture Assembly; Forward Case Flange Target (Brunson No. 4793); Nozzle Target Fixture Assembly (Brunson No. 4300); E-18732 Support Ring Assembly. a) Place motor, head end down on felt pad on large tire. Remove Handling Ring and attach Support Ring Assembly in accordance with Operations 2.0b, 2.0c, and 2.0d. b) Obtain the nozzle assembly used in the preload operations for this motor. c) Lubricate O-ring (E11843-01) with Cosmoline 615 (MIL-G-4343 lubricant) and place on the	

OP. NO.	OPERATION	QC/PROD. SIGN OR STAMP DATE
	nozzle closure. Do not stretch O-ring while lubricating. d) Weigh the nozzle assembly and record the weight, drawing number and serial number on the C.G. Data Sheet, QCI-535 and Nozzle Centerline Sheet QCI-534. Weigh nozzle attachment hardware and O-ring. Record on C.G. Data Sheet and Nozzle Centerline Sheet. e) Remove covering from the aft end of the motor. Remove the cap screws and casting sleeve. Lubricate nozzle bore with MIL-G-4343 lubricant. f) Using no less than 2 operators, carefully place nozzle on the motor oriented correctly with respect to the match marks made during the preload operations. Initially place 4 nozzle assembly bolts 90° apart into nozzle closure and gradually seat nozzle by turning each bolt one-half turn at a time. This method rolls the O-ring into place. Remove the four bolts. g) Secure the nozzle assembly in place by means of 44 bolts (E-14614-01) lubricated with MIL-T-5544, plus 44 washers (E-14615-01), ballast (E-) as required in preload operations for this motor.	

OP. NO.	OPERATION	QC/PROD. SIGN OR STAMP DATE
	NOTE: These washers are directional - the flat part of the washer goes against the closure -- the washer counter bore must be against the bolt head.	
	Torque bolts to 250 ± 25 in./lbs.	10.0_____
10.5	(Ref b 10.0) Verify that the nozzle assy E18219-01 S/N ___ was mated to this motor during pre-load operations.	
	(Ref d 10.0) Verify the weight of nozzle, attaching hardware, and O ring is as recorded on QCI-534.	
	(Ref g 10.0) Verify that the nozzle is assembled per OP 10.0 and that bolts are torqued.	10.5_____
11.0	a. Install the Brunson Nozzle Target Fixture Assembly Number 4300 into the nozzle. Center the exit cone target by carefully checking the dial indicator and adjusting the legs of the holding spider until a centered condition exists. Make a small mark on the lip of the nozzle so that during dial indicator rotation, the plunger can be set in the same place each time. Use a felt point pen for marking. Care should be exercised to prevent distorting nozzle when adjusting the legs.	

OP. NO.	OPERATION	QC/PROD. SIGN OR STAMP DATE
	Lift the motor from the tire and rotate 180° on the pivot trunnion. Recheck centering of the Fixture Assembly No. 4300 and adjust if necessary. Record dial indicator readings on Data Sheet QCI-534. Measure gap between pin and exit cone target and record on Data Sheet QCI-534. b. Install inverted motor assembly into nozzle alignment tool per E18731. c. Once the Support Ring Assembly is resting on the ball spacers, the assembly may be moved slightly by sliding the assembly until all three feelers, (E15769-5) are held between the mandrels and the feeler bases (E15769-6). (Reference Thrust Alignment Fixture Assembly Drawing E15767). These feelers must always remain in place throughout the entire operation.	11.0_____
11.5	Verify that the Nozzle Target fixture Assembly is centered and that the readings are as recorded on QCI-534. Verify that the gap between the pin and exit cone target is as recorded on QCI-534.	11.5_____

150

PM 2-16

OP. NO.	OPERATION	QC/PROD. SIGN OR STAMP DATE
12.0	Level the motor by means of the adjusting nuts using the Paragon Level. a. Place a Paragon Level Assembly, made up of items 12, 13, 15, 16, and 17 of the Nozzle Alignment Arrangement E18731, at a predetermined 7 foot distance from the motor. b. Attach a 40" Wyteface Optical Tooling Scale to the upper flat surface of a mandrel nut (E15643) using a Scale Holding Magnet to hold the scale in a fixed position. Level the motor by means of the adjusting nuts (E15771) using the paragon level. c. Remove Wyteface scale and magnet from the mandrel nut. Place the scale and magnet on each of the other two nuts in order and repeat leveling operations until complete. The differences in the level readings must not exceed 0.001 inch. d. Install 18" flange target assembly (Brunson No. 4793) and level. Measure gap between target assembly and 18" flange where indicated on Data Sheet QCI-534. The differences in the level readings must not exceed 0.001 inch. With Paragon Level, take height readings of a mandrel nut and the 18" flange target. Record gap and height reading on Data Sheet QCI-534.	

OP. NO.	OPERATION	QC/PROD. SIGN OR STAMP DATE
	e. A production operator and a quality control inspector should at this point make simultaneous, but independent readings of each of the three "Lufkin" micrometers that are integral with the micrometer bases E15770. Once the motor is in place and set, the micrometers are to be advanced two ratchet clicks beyond initial contact with the mandrels. Record these readings on Data Sheet, QCI-534. Read micrometers to the nearest ten thousandth of an inch.	12.0_____
12.5	(Ref. e 12.0) Verify the micrometer readings recorded in Operation 12.0 by making an independent reading of the Lufkin micrometers. Verify that the readings do not vary by more than .001 inch. (Ref. d, 12.0) Verify the measurement and record of the gap between the 18" flange and target assembly. Verify that the level height readings are as recorded on QCI-534.	12.5_____
13.0	a. Proceed by moving the jig transit assembly (described by Items 2-10 of E-18731, Nozzle Alignment Arrangement) into place over the level, inverted motor.	

OP. NO.	OPERATION	QC/PROD. SIGN OR STAMP DATE
	b. Once the jig transit assembly is locked in place and leveled, line up transit by reading 1.5 inches on the scale near 3 and the scale opposite. Autocollimate the jig transit with the Paragon level described by items 12-17 of E-18731. Refer to drawing E-18731 to approximate the autocollimated condition. c. After the jig transit is collimated by using the Paragon level, recheck the reading on the two scales. The transit should read 1.5". If it does not, it should be made to do so by use of micrometer dial on the transit and rotating the transit slightly about its vertical axis. Do not try to make the adjustment by using the transverse slides because the transit will require additional autocollimation if this is done. By pointing the transit down at the 18" payload flange and nozzle targets, their displacement parallel to the Y axis can be measured by using the micrometer dial on the transit to the nearest 0.0005". Enter the jig transit Y axis readings and the color of the graduations on the Data recording Sheet QCI-534.	13.0

OP. NO.	OPERATION	QC/PROD. SIGN OR STAMP DATE
13.5	Verify that the jig transit Y axis readings and color are as recorded on form QCI-534.	13.5
14.0	a. Repeat Operations 13.0 b and 13.0 c, but use the two scales at right angles to the scales used previously. The transit must be rotated 90° about its vertical axis. After the transit is collimated and lined up, the displacement of the targets paralleled to the Z axis can be measured. Enter jig transit Z axis readings and the color of the graduations on Data Recording Sheet QCI-534. b. Record on Data Sheet QCI-534 enough time and temperature readings to get a representative time temperature profile. Effort should be made to keep temperature uniform and near 70°F.	14.0
14.5	a. Verify that the jig transit Z axis readings and color are as recorded on form QCI-534. b. Verify that times and temperatures have been recorded on QCI-534.	14.5
15.0	Remove case flange target (Brunson No. 4793) and store in Tooling case.	15.0

OP. NO.	OPERATION	QC/PROD. SIGN OR STAMP DATE
16.0	Lift the motor from the Thrust Alignment Fixture; move to an open working area, rotate motor 180° on the pivot trunnion and place the motor on a felt covered tire.	16.0_____
17.0	Remove Nozzle Target Fixture Assembly (Brunson No. 4300) and store in tooling case.	17.0_____
III.	IGNITION SYSTEM	
18.0	Installation (Install either while the motor is suspended on handling beam or after placement on Center of Gravity Tooling). a) Obtain the ignition system (P/N E-19582) assigned to this motor. Record Serial Number ____. b) Ensure that the threads and O-ring surface of the case and Ignition Assembly are clean and undamaged before installing Ignition Assembly. Lubricate an "O"-ring (E-11878-01). Place O-ring into the 2.405 inch diameter O-ring groove at the head end of the Ignition Assembly (E19582). Do not stretch O-ring while installing. Lubricate the O-ring mating surface with Cosmoline 615 (Silicone grease MIL-G-4343). Very carefully, thread the Ignition Assembly into the head end of the TE-364-3 Motor Assembly (Drawing E-18518.)	

155

RSVP* PROPULSION

(RESTARTABLE, VARIABLE PULSE)
LOCKHEED PROPULSION COMPANY

MTO-837-F
COPY NO. 3

CHARACTERISTICS OF FLUID-CONTROLLED SOLID (RSVP) MOTORS FOR SPACE PROPULSION SYSTEMS (U)

Prepared for the

SPACE-GENERAL CORPORATION

by

LOCKHEED PROPULSION COMPANY

P.O. 1069-P-76407

Prime Contract No. NAS 7-519

.0 July 1967

Prepared by:

N. S. Cohen, Project Engineer

Approved:

D. E. Taylor, Manager
Engineering Research Dept.

Approved:

D. E. Taylor for
J. H. Bonin
Director of Research

157

1.0 INTRODUCTION

The objective of this program is to furnish information regarding the characteristics of fluid-controlled solid (RSVP)* motors for space propulsion systems. These characteristics include the following:

a) Physical description

b) Operational description

c) Performance (Isp)

d) Weight (mass fraction)

e) Development status

f) Reliability

g) Cost

h) Influence of operational requirements

- -storability
- -number of restarts
- -throttling ratio
- -sterilization

This information will be utilized by the Space-General Corporation in the evaluation of various propulsion concepts for NASA applications. Where indicated, it is to be treated as LOCKHEED PROPRIETARY INFORMATION.

Lockheed Propulsion Company (LPC) is presently under contract with the National Aeronautics and Space Administration Office of Advanced Research and Technology to conduct both theoretical and experimental studies of the RSVP motor (Contract NAS 7-444). This work began in January 1966. Company-sponsored efforts began in late 1964 and have continued since. Beginning with the feasibility demonstration

* Restartable Solid, Variable Pulse motor, using the fluid-injection principle.

in 1964 and continuing through the present programs, over 100 test firings of experimental RSVP motors have been made. These tests have provided data regarding operational characteristics which can be used to substantiate preliminary design predictions. However, it must be recognized that there are limitations in the context of the present requirements, which arise from the following considerations:

a) All testing has been made with subscale hardware, which inherently have low values of L* (even at burnout) and short burn time.

b) All testing has been made with heavyweight hardware.

c) Exhaustive testing for the purpose of obtaining statistical reproducibility data has not been an objective to date; testing has been of a research and technology nature.

d) There has never been an RSVP development program for a specific application.

e) Detailed design efforts have not been substantiated by flightweight fabrication.

f) An RSVP motor has never been flown.

Consequently, there are little data available for making accurate predictions of scaling effects to motor sizes of interest in this study, or for predicting the cost and reliability of an actual flightweight system. As a result, much of the information must be based upon best estimates. Fortunately, it thus far appears that the RSVP involves little else but the mating of an ordinary (but relatively small) single liquid component system to an ordinary solid rocket motor. This assumption will be utilized in attempting to cover the unknown aspects, and should be kept in mind by Space-General in conducting the evaluation. LPC is, of course, in the solid propulsion business, but has also acquired liquid component experience

as a result of conventional hybrid and RSVP programs which have continued at an appreciable level of effort since 1959. (Refs. 1-10).

Because of the present development status of the RSVP, it will not be possible to simply adhere to the Space-General format for tabulating information as presented in Report SGC 1069 QR-2. Also, there is no "baseline system" except what may be arbitrarily conceived. Consequently, this format will have to be supplemented by more or less detailed discussion of the various items. The format for an arbitrary baseline system will be included as an Appendix, citing the pertinent discussions where they appear in the text. It is anticipated that this method of presentation meets with contractor approval.

2.0 GENERAL DISCUSSION

2.1 General System Description

2.1.1 Physical Description

A schematic sketch of the RSVP motor is shown in Figure 2.1. The motor consists of a conventionally-oxidized, castable solid propellant, which differs from an ordinary solid propellant only in its tailored ballistic properties for controllability: high burning rate-pressure sensitivity, and ease of extinguishment. The nozzle throat area is sufficiently large that combustion of this solid propellant is incapable of generating sufficient pressure to sustain itself. This mass flow deficiency is made up by injecting an additional source of mass flow, e.g. hypergolic liquid or monopropellant decomposition gases, either of which is also capable of igniting the solid propellant. Throttling is achieved by modulating the control fluid injection rate, and termination is achieved by shutting off the flow.

There are no unusual requirements with respect to the liquid control system, and

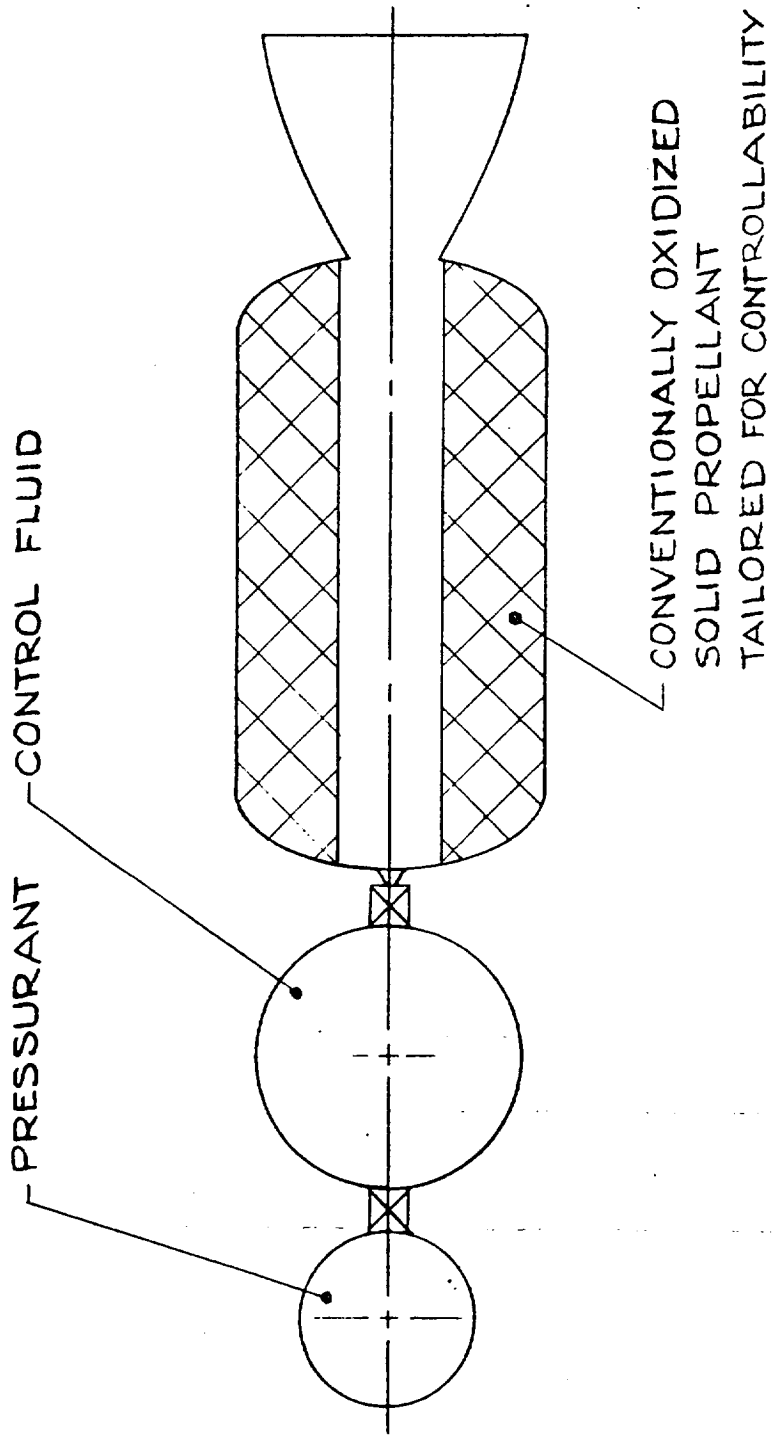

SCHEMATIC OF FLUID-CONTROLLED SOLID (RSVP) MOTOR

FIG. 2-1

conventional liquid technology (and advances therein) are directly applicable. Because the weight ratio of liquid-to-solid is small, nominally about 0.5 for reasons to be explained later, development of certain liquid components should be facilitated and inert gas pressurization will not impose a heavy weight penalty. Similarly, for the solid portion (including the nozzle), conventional solid technology is directly applicable. No evidence to refute these contentions has been encountered in the work to-date.

A conceptual design of an RSVP motor for a space application is presented in Figure 2.2. The sizing of the motor corresponds to an upper-stage application studied by Lockheed Missiles and Space Company (LMSC) under Contracts NAS 7-375 and NAS 7-449 (10, 11). The design illustrates the excellent packaging flexibility of the RSVP, with respect to location and numbers of tanks and solid motor configuration (spherical or otherwise), to best meet envelope requirements. It also indicates the inherent compactness of the RSVP resulting from the high propellant densities (solid propellant specific gravity = 1.72, Compound A specific gravity = 1.75 and, where cryogenic liquid is allowed, liquid fluorine specific gravity = 1.55). Because the NASA has been expressing interest in motors of low L/D, packaging of the liquid and pressurant is shown at the aft end of the solid motor. For higher L/D, packaging can be "in line" with either multiple or single tanks.

Liquid injection occurs at four places, equally spaced around the annulus of the neutral-configured spherical conocyl grain design. Consequently, some plumbing is required to bring the liquid to this near-forward position of the motor. Use of in-line liquid packaging (higher L/D) and one injector for a single-port

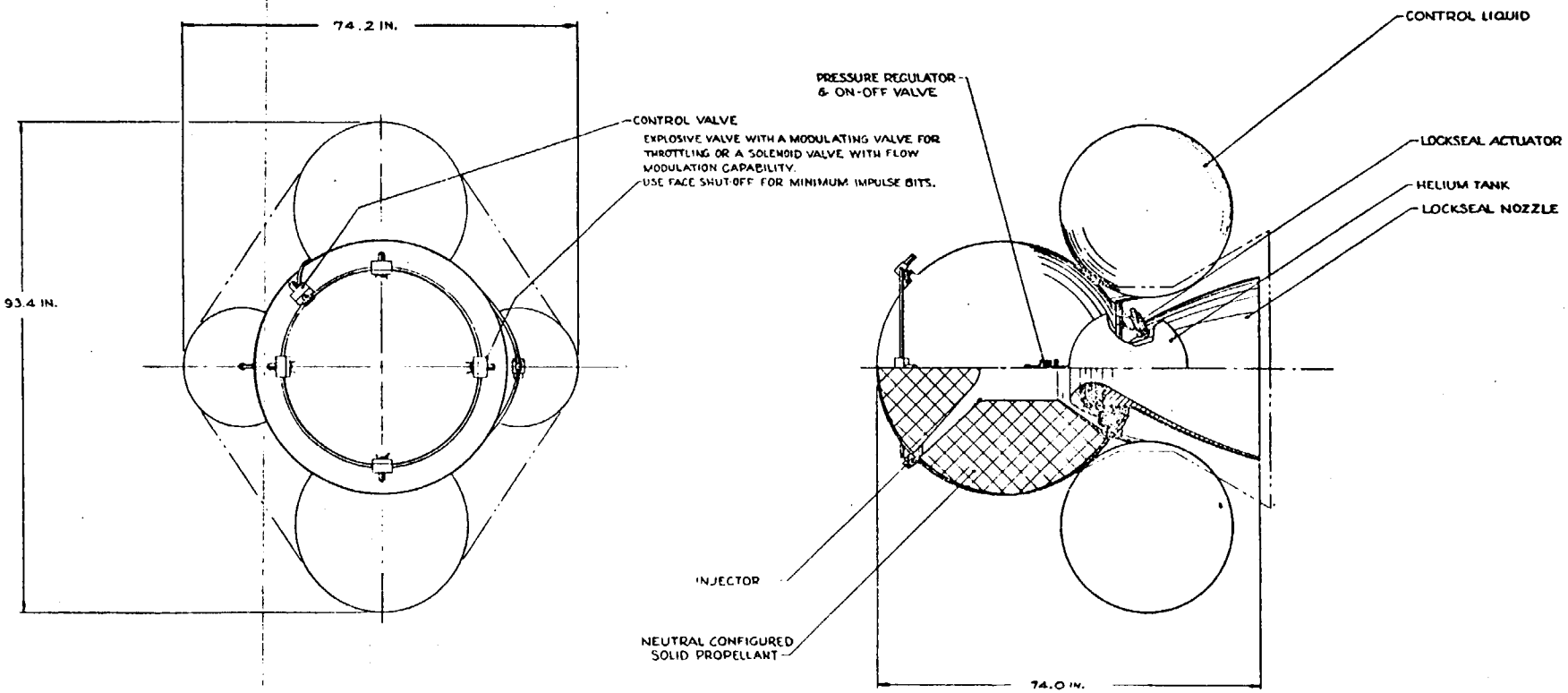

SGC P.O. 1609-P-76407 LOW L/D RSVP LPC 10 JULY 67

cylindrical grain design (heavier case) would simplify the plumbing. To eliminate residual line flow for minimum impulse bit and clean termination, each injector has its own control valve for close-proximity shut-off. The particular mission in question required two restarts, for which explosive-actuation in a single body can be achieved at present state-of-the-art. For more restarts, more explosive valves could be incorporated in parallel, or resort to a solenoid valve could be made (but which is more susceptible to leak). Each of the four valves is fed from a redundant main control valve which, again, can either be an explosive valve or a solenoid valve. For throttling, this main control valve can also be equipped with flow modulation capability; at present, sophisticated variable injectors do not appear to be necessary in the RSVP because of the efficiency demonstrated at low pressure in small motors of low L*. The two helium tanks are tied to one main pressure regulator with an integral valve to arm the motor. Positive expulsion of the liquid can be achieved with either a bladder or ullage rockets.

Omnidirectional thrust vector control is provided by the LPC LOCKSEAL nozzle technique; two actuators are sufficient to provide control in any plane, and there is sufficient room for the necessary angular movement of the nozzle without touching any of the tankage. A contoured nozzle is practical because of the low metal content of the solid propellant, most of which burns to gaseous metal fluoride when fluorinated liquid is used for control.

Changing the type of control fluid will not affect the RSVP configuration. For the same total propellant weight and fluid/solid ratio, replacing Compound A with liquid fluorine will necessitate an increase in insulation and nozzle weights owing to higher combustion temperatures, and the cryogenic liquid may require its own insulation from the environment; differences in tank diameters owing to the

reduced density will be small. Replacing Compound A with hydrazine will result in a noticeable increase in tank diameters (specific gravity = 1.00), but insulation and nozzle weights will be much less owing to the lower combustion temperature. With low metal content in the solid, a contoured nozzle can still be used efficiently. Use of hydrazine will also require decomposition chambers at each injector so as to take advantage of the monopropellant properties for motor ignition. Presumably, supplementary pyrogen igniters could be incorporated, but at a penalty to operational packaging flexibility where a large or not-predetermined number of restarts are desired. For small thrusters, use of gaseous fluorine as injectant can be considered; components associated with liquid feed are eliminated, rendering such a controllable motor attractive from the standpoint of simplicity. For sufficiently small size, the gaseous fluorine-controlled solid motor also becomes competitive from a weight standpoint.

2.1.2 Operational Description

Thrust magnitude and stop-restart control of conventionally oxidized solid propellants by injection of fluids is predicated on two essential facts.

1) Motor pressure is a function of propellant mass flow rate, and can therefore be varied by modulating the liquid injection rate. Because the regression rate of solid propellants is pressure dependent, variations in liquid injection rate will also evoke a response in the solid which increases with burning rate pressure exponent.

2) Solid propellants exhibit a threshold pressure below which combustion cannot be sustained. The value of the threshold pressure depends upon propellant composition. If the nozzle throat area is sufficiently large,

the pressure will fall to ambient upon shutting off the augmenting liquid injection. If ambient pressure is below the propellant deflagration limit, combustion is terminated.

Facilitating the ballistic design procedure is the experimental finding that the solid propellant regression rate and its pressure dependence, under fluid-controlled operation, is essentially unchanged from that in conventional solid operation or when burned as strands. Consequently, grain design flexibility for envelope tailoring, maximum volumentric loading, or for minimum combustion chamber inert weights, exists as in a normal solid.

With the RSVP, regardless of control fluid, the mass balance equation for pressure can be written as:

$$\rho a P^n A_b + \dot{m}_l = \frac{g}{C^*(F/S)} P A_t \qquad (2\text{-}1)$$

or

$$1 + F/S = \frac{g}{C^*(F/S)} \frac{P^{1-n}}{\rho a K_n} \qquad (2\text{-}2)$$

where
- ρ = solid propellant density
- a, n = constants in the solid propellant regression law
- A_b = burning surface area
- A_t = nozzle throat area
- P = pressure
- $\dot{m}_l$ = liquid injection rate
- g = gravitational constant
- F/S = fluid/solid flow rate ratio
- $C^*(F/S)$ = characteristic velocity as a function of F/S
- K_n = A_b/A_t

It is seen that for steady-state operation, $F/S > 0$, the nozzle throat must be sized larger than for conventional solid operation at a given pressure. Hence,

when F/S = 0 by shutting off the fluid flow, the pressure must fall to some new level. If the propellant is sufficiently responsive, i.e., high n, the pressure will fall all the way to ambient.

It is of interest to examine the special case n=1. It is noted from Eq. (2-2) that F/S can then be chosen independent of pressure, and will remain constant regardless of the duty cycle; the solid combustion rate becomes directly proportional to liquid injection rate. When the fluid is shut off, F=0, and the imbalance in the equation obviously forces the pressure down to ambient. This is shown graphically in Figure 2-3. Note that both the nozzle discharge line and the solid input line are straight lines. The slope of the discharge is governed by the choice of F/S. Figure 2-4 illustrates the point that this ideal condition becomes more difficult to achieve as n becomes significantly less than unity. Note the curvature existing in the solid input line, which places a lower limit on the slope of the discharge line (upper limit on K_n) to achieve termination . This curvature also causes F/S to vary with pressure. However, this effect is of little practical concern as long as n is greater than about 0.75, unless there is a requirement for random wide throttling in which case the F/S variation will detract from full utilization of propellants; stop-restart operation can still be conveniently achieved. It is with high n (n=1) that wide throttling is most efficiently achieved as well. No destructive instability problems are evident with n=1 propellants, with fluid-injection, because of the stabilizing influence of the fluid which effectively reduces the value of n as defined for the liquid-solid system.

2.1.3 Differences from a Hybrid

While there are obvious similarities between the RSVP motor being herein described and what is known as a "conventional hybrid", there are also important differences.

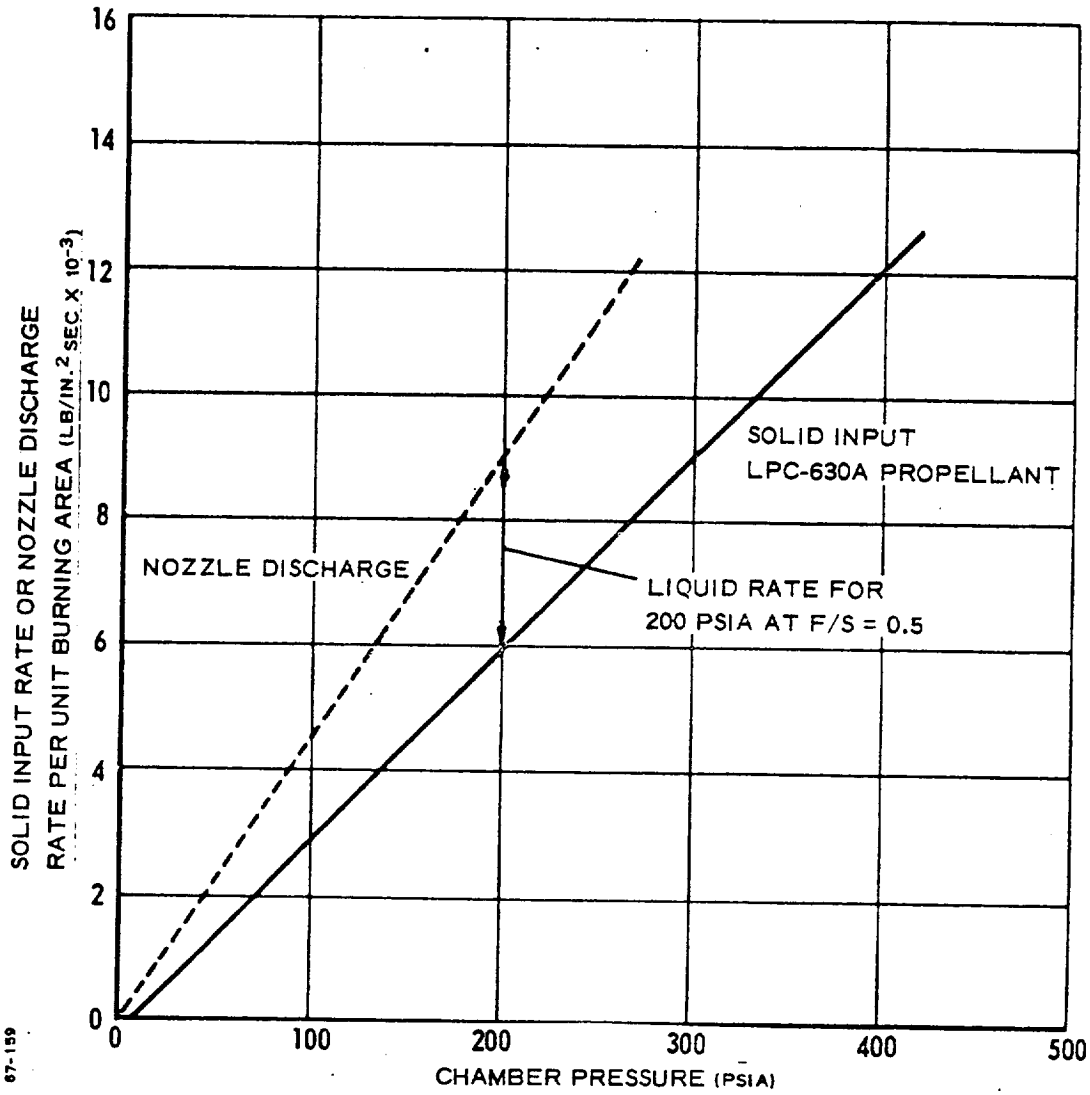

Figure 2-3 Mass Input and Nozzle Discharge Rate Curves for LPC-630A Propellant (n = 1.0)

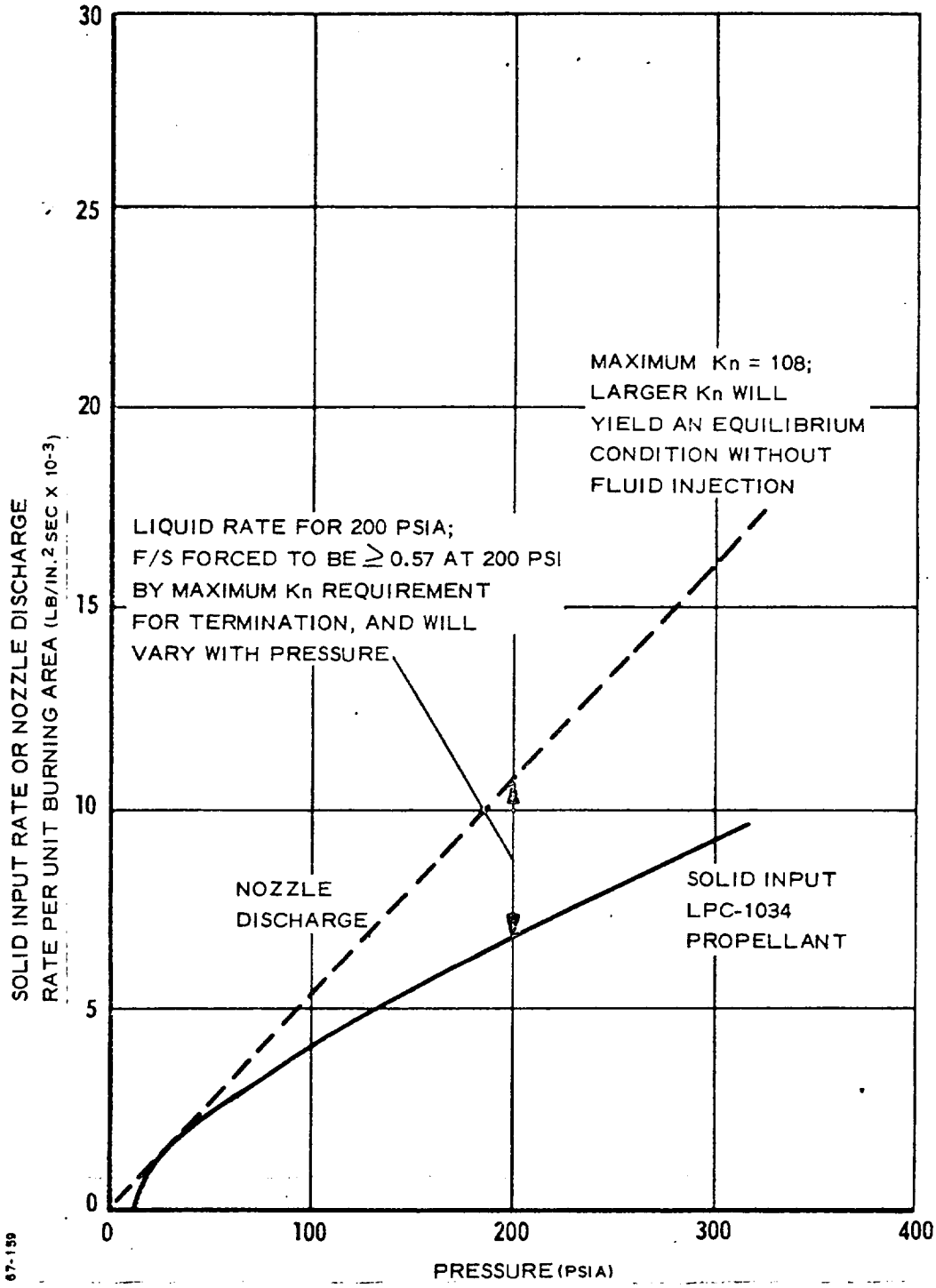

Figure 2-4 Mass Input from Combustion and Nozzle Discharge Ratios for LPC-1034 Propellant (n = 0.76)

The essential similarity is that both are generally thought of as liquid-solid systems, although both can be all-solid systems as well through the use of dual-chamber motors. The essential difference is in the combustion mechanism and interior ballistics of operation.

In the conventional hybrid, the fuel and oxidizer are completely segregated. The oxidizer is generally a liquid, employing oxygenated and/or fluorinated compounds; the solid fuel consists of a hydrocarbon binder containing a large quantity of thermogen powder, generally lithium or lithium hydride. Additives may be included in the solid for combustion tailoring. This combination of ingredients provides high specific impulse but at very high combustion temperatures, particularly with lithium-fluorine systems. Oxidizer/fuel ratios are comparable to those of liquids, but the solid fuel density is generally quite low. Because the fuel and oxidizer are segregated, the combustion mechanism is quite different from that of ordinary solid propellants (12-15). The mechanism is found to involve a turbulent boundary layer mixing process, coupling convective heat transfer and kinetic effects. Regression rates are low and strongly dependent upon grain geometry and injection rate, which effects generally impose restrictions upon grain design in order to meet thrust-time requirements and yet maintain stoichiometry. These restrictions are compounded if there is the additional requirement for deep throttling. The net effect is either reduced volumetric solid loading and mass fraction, or reduced Isp and propellant utilization resulting from off-design operation. Mixing devices or multiport grain design, and partial aft-end oxidizer injection, have been used to improve efficiency of operation but introduce additional cost and reliability factors. The highly metallized fuels are not conveniently castable, and combustion can produce considerable slag. Consequently, the ordinary hybrid has involved much more than the simple mating of liquid and solid components.

In the RSVP, the solid consists of a conventionally oxidized, castable solid propellant whose combustion mechanism is essentially unaffected by fluid injection.

The burning rate is a function of pressure, which is modulated by variations in the fluid mass injection rate. For reasons previously discussed, the main requirement for the solid propellant is that its burning rate should have a high pressure sensitivity. Fluid control can then be provided with liquid/solid ratios far below that of hybrids, minimizing the amount of liquid needed for controllable propulsion and promoting full utilization of propellants in random operation. Using the same kind of liquid oxidizers as do hybrids, specific impulse can be almost as high but, in addition, density is excellent. Grain design flexibility exists as in ordinary solids, and supplementing devices to promote efficiency of operation are not necessary. Finally, because stoichiometry is not primarily involved in RSVP operation, the fluid injectant need not be an oxidizer.

In summary, the conventional hybrid can be thought of as a special case of fluid-controlled solid, the case where the fuel and oxidizer are completely segregated. With the development of controllable solid propellants and solid propellant extinguishment technology in recent years, the essential purpose of this segregation as e.g. suggested in 1956 (16) has become obsolete. Consequently, in application studies covering a wide spectrum, the more general forms of hybrid or controllable solid propulsion should be considered as well as the presently more well-known special case.

2.1.4 Development Status

Since the fall of 1964, approximately $500 K has been spent on theoretical and experimental RSVP research at LPC. These funds include NASA contractual support and Company sponsorship. Over 100 firings have been made using available injection equipment and motors containing from 1-25 pounds of solid propellant. The purpose of these tests has been to study ignition, stability, combustion, transient response (and throttling), efficiency and extinguishability. The objectives of these tests and of concurrent analytical efforts have been successfully met. Of equal significance, it appears that the RSVP involves nothing more than a

combined liquid/solid system, which implies that its development status can draw upon the extensive backgrounds of both liquid and solid technologies. Plans for additional follow-on work possibly to begin later this year, include scaled-up testing to motor sizes which begin to conform to potential NASA applications.

Specific accomplishments to-date are summarized as follows.

Initial Efforts

Lockheed Propulsion Company demonstrated thrust control of solid propellants by fluid injection as early as 1959 (1). Liquids used included hydrazine, nitrogen tetroxide, ethylene oxide and water. However, the solid propellants employed were not suited to controllability, i.e. the values of n were low, and hence the degree of thrust modulation was not very great nor was termination achieved upon liquid cut-off. But these early tests do point out one very important facet of the RSVP concept. It involves nothing really new, requires no advances in state-of-the-art, and readily makes use of developments in solid, liquid or hybrid technology.

The most important development, which is what renders the RSVP attractive as a controllable motor, is the result of recent propellant development and combustion studies related to the single-chamber (pintle) and dual-chamber (solid-solid) controllable solid motors. These and related programs led to the development of reasonably good performance solid propellants with high burning rate pressure exponent, and to an understanding of factors governing extinguishability of solid propellant combustion. This work did not really involve any advances in propellant state-of-the-art, but rather the proper use of already available propellant ingredients. Lockheed Propulsion Company made some of the initial contributions in these areas (17-20), and has continued in propellant formulation studies with the objectives of achieving pressure exponents $0.9 < n \leq 1$, high augmented performance, and physical properties etc. consistent with normal solid propellant requirements.

THIS PAGE CONTAINS COMPANY PROPRIETARY INFORMATION

AND HAS BEEN DELETED EXCEPT FOR REPORTS LIMITED TO

RESTRICTED DISTRIBUTION

THIS PAGE CONTAINS COMPANY PROPRIETARY INFORMATION

AND HAS BEEN DELETED EXCEPT FOR REPORTS LIMITED TO

RESTRICTED DISTRIBUTION

These studies revealed the RSVP to have significant performance and operational advantages over competing controllable propulsion systems. Motor design studies were initiated with very favorable results in both volume-limited and weight limited applications, owing to high density-impulse and high mass fraction.

Through the same time period, advances were reported in the areas of throttleable liquid injectors, warm gas expulsion, positive expulsion bladders, fluorinated oxidizer technology, etc. (21). All of these advances are directly applicable to RSVP, with the note that the RSVP will require the smallest liquid component system. Similarly, advances in solid motor construction, insulating materials and nozzle structure and TVC are directly applicable.

Results Under Contract NAS 7-444

The NASA was quick to recognize the potential of the RSVP for applications requiring random controllability. The first technology program was awarded in January 1966, a follow-on program was awarded in July 1966, and a second follow-on is being jointly planned at present. Program accomplishments are summarized as follows (cf. Ref. 9 for details).

1) It was determined experimentally that fluid injection suppresses low pressure L^* instability; i.e. for increasing values of fluid/solid ratio, F/S, the L^* instability will not occur until lower pressures and lower values of L^*. However, the instability was not eliminated entirely. These results confirm the theoretical analysis. Whether or not the instability can be eliminated entirely depends upon the combustion properties of the solid propellant. By suppressing the instability, wide throttling can be maintained with high n since the motor can operate stably at lower pressures.

2) Random command controllability, and extinguishment upon fluid cut-off in vacuum, were again demonstrated in connection with the L^* tests. As many as nine stop-restart tests were achieved with a single motor.

3) Hypergolic ignition delay time was found to vary inversely with the square of the parameter.

$$\frac{\text{Mass flow rate of fluid}}{\text{Nozzle throat area}}$$

This parameter is an index of motor pressurization by the fluid prior to propellant ignition, which is important according to ignition theory.

4) Vacuum ignition limit was successfully defined with Compound A injection, conforming to theoretical predictions relative to chlorine trifluoride and fluorine. UTC reported difficulties with chlorine trifluoride as hypergol under vacuum conditions, and difficulties have been reported with low volatility liquid systems in vacuum (21), which are predictable from the LPC analysis. Compound A has a much higher vapor pressure and much lower heat of vaporization than these other liquids, e.g. CTF, N_2O_4, N_2H_4, N_2F_4; thus it is favorable for pre-pressurizing a motor above the threshold level for ignition without flooding or ignition aids.

5) C^* efficiency in 25-pound motors varied between 90% and 95% with chlorine trifluoride injection. Specific impulse efficiency varied between 83% and 89%. Efficiency was found to decrease with increasing F/S and reduced L^*.

6) With gaseous fluorine injection in the 25-pound motor, C^* efficiency was measured to be between 95% and 100% and specific impulse efficiency to be 90-96% at pressures ranging from 100 psi-900 psi. The difference in the results between the liquid and gas injection can be attributed to the poor vaporization properties of chlorine trifluoride and the limited droplet

THIS PAGE CONTAINS COMPANY PROPRIETARY INFORMATION AND HAS BEEN DELETED EXCEPT FOR REPORTS LIMITED TO RESTRICTED DISTRIBUTION

THIS PAGE CONTAINS COMPANY PROPRIETARY INFORMATION

AND HAS BEEN DELETED EXCEPT FOR REPORTS LIMITED TO

RESTRICTED DISTRIBUTION

2.1.4 Space-Flight History

A controllable solid, RSVP or a conventional hybrid, has never been completely flightweight-developed let alone flown in space. One possible exception is the Northrup-Carolina dual-chamber (solid-solid) controllable motor, which is undergoing qualification for the Army RMP mission (22). Using solid gas generator control can be construed as a form of RSVP.

2.2 Prediction Techniques

Prediction techniques regarding the RSVP motor are still in their infancy, simply because of a lack of sufficient quantitative information to be of a statistical nature. Although sufficient data have been obtained to guide design efforts, there are no established formulas for weights, costs, reliability, reproducibility, etc.

Weight equations have not been developed at this stage because their universal applicability would be open to question; a multiple of factors and sub-factors are involved. Rather, for any specific application, preliminary and/or detailed designs were prepared which were then subjected to weight analysis in each instance. Sufficient excercises of this nature have been performed over a range of motor sizes to construct a rough weight equation and reasonably accurate mass fraction curves for general evaluation purposes; however, no RSVP motors have been built. A cost and reliability excercise has been performed only once for a specific application, but which cannot be supported by actual development, production or flight experience save that from conventional liquid or solid components. RSVP testing to-date has been technology oriented, not amenable to statistical analyses of reproducibility. On the positive side, analytical methods to predict steady-state and transient RSVP interior ballistics have proven satisfactory, and realization of theoretical performance potential and operational characteristics have been demonstrated in testing.

2.2.1 General Ranges

Data are presented, in the main, for RSVP motors using Compound A as control fluid. Thrust levels considered are in the range from 750-20000 lb., corresponding to total propellant weights from 100-10000 lb. An optimum chamber pressure has been roughly established at about 400 psi, considering inert weight, minimum wall thicknesses and insulation requirements; this can vary, depending upon the mission and envelope requirements. With n=1 solid propellant, the burn time is inversely proportional to pressure to the first power. Expansion ratios considered vary from 30 to 45. The designs assume a requirement of two restarts with a very short time between restarts, and no throttling. More restarts, long shut-down times, and deep throttling will of course affect weight, cost and reliability. Effects of throttling and multiple restart will be discussed to the extent possible. Minimum impulse bit will also be discussed and results of analytical computations presented. Specific impulse is presented over a range of fluid/solid (F/S)ratio, and mass fraction is presented as a function of F/S and motor size. Cost data are presented for a motor containing 1000 lbs. of propellant.

2.2.2 Subsystem Design Alternatives

Theoretical performance data are presented for propellant systems suited for long-term space storability or sterilizability, and for those which are not sterilizable and suited only for relatively short-duration space applications (less than six months). Similarly, data are presented for solid propellants of very high pressure exponent (for random wide throttling), not so high a pressure exponent (adequate for stop-restart), for currently-developed systems and for growth potential systems.

Motor design data are presented, for illustrative purposes, wherein liquid fluorine, gaseous fluorine, or hydrazine is used as control fluid. Results can be compared with the more general Compound A data.

The weight benefits to be gained with alternative materials and by replacing inert gas pressurization with a warm gas generator is examined for one case. For the same reason that the RSVP can use inert gas pressurization with little weight penalty (compared to the bi-liquid or even the ordinary hybrid), so it is that resort to advanced pressurization techniques does not save a considerable amount of weight; the chief savings is in volume. At current state of the art, inert gas pressurization is preferred for random, multiple stop-restart requiring rapid response. The suitability of certain materials of construction with fluorinated liquids is open to question.

2.2.3 Prediction Confidence Level

For reasons mentioned in the introductions to this report and to this section, it will not be possible to assign quantitative numbers for prediction confidence levels concerning the various items. A qualitative description, based upon the extent of pertinent related experience, would be more realistic.

3.0 STEADY-STATE AND TRANSIENT RSVP PERFORMANCE

To best conform to the format of SGC 1069 QR-2 Table 2, this section will present the following:

a) Theoretical specific impulse

b) Incorporation of NAS 7-444 efficiency data to define delivered Isp

c) Equations of transient RSVP ballistics

d) Method to predict throttled performance

e) RSVP throttling potential

f) Analysis of minimum impulse bit, impulse bit reproducibility, and shut-off impulse accuracy.

THIS PAGE CONTAINS COMPANY PROPRIETARY INFORMATION AND HAS BEEN DELETED EXCEPT FOR REPORTS LIMITED TO RESTRICTED DISTRIBUTION

THIS PAGE CONTAINS CLASSIFIED

INFORMATION AND IS PRESENTED

IN VOLUME V

THIS PAGE CONTAINS CLASSIFIED

INFORMATION AND IS PRESENTED

IN VOLUME V

THIS PAGE CONTAINS CLASSIFIED

INFORMATION AND IS PRESENTED

IN VOLUME V

THIS PAGE CONTAINS CLASSIFIED

INFORMATION AND IS PRESENTED

IN VOLUME V

THIS PAGE CONTAINS COMPANY PROPRIETARY INFORMATION AND HAS BEEN DELETED EXCEPT FOR REPORTS LIMITED TO RESTRICTED DISTRIBUTION

Table 3.2

TABLE OF SYMBOLS

a	Solid regression rate equation constant
A_b	Solid burning surface area
A_t	Nozzle throat area
c^*	Characteristic velocity; $c^* = \frac{1}{\Gamma}\sqrt{\frac{R_o T_c}{M}}$
K	Constant in the liquid supply rate equation
L^*	Characteristic length: $L^* = \frac{V_c}{A_t}$
M	Molecular weight
m_l	Mass in the combustion chamber originating from the liquid
m_s	Mass in the combustion chamber originating from the solid
m_t	Total mass in the combustion chamber
n	Exponent in the solid regression rate relation
P_c	Combustion chamber pressure
P_t	Liquid supply tank pressure
R_o	Universal gas constant (mass units)
t	Time
T_c	Combustion chamber pressure
V_c	Combustion chamber volume
γ	Ratio of specific heats
Γ	Function of γ: $\Gamma = \sqrt{\gamma}\left(\frac{2}{\gamma+1}\right)^{\frac{\gamma+1}{2(\gamma-1)}}$
θ	Reduced time: $\theta = \frac{t}{\bar{\tau}}$
ρ_c	Density of gas in the combustion chamber
ρ_s	Propellant mass density
τ_t	Characteristic time, $\tau_t = \frac{L^*}{\Gamma^2 c^*}$

NOTE: "bar" values are steady-state values.

The mass in the chamber is identified as originating from either injected fluid, m_l, or from the solid, m_s, so that

$$m_t = m_l + m_s \tag{3.2}$$

The rate of change of pressure in the chamber, from which the rate of change of thrust can be calculated, is obtained by combining equations (3.1) and 3.2 and differentiating with respect to time:

$$dP/dt = (R_o T_c/V_c M)(d m_l/dt + d m_s/dt) + m_t d (R_o T_c/V_c M)/dt \tag{3.3}$$

For convenience, it will be assumed that V_c and M are constant, and that T_c varies with the mixture ratio, m_l/m_s, as it would under steady-state conditions.

The mass originating as injected fluid, m_l, is assumed to change with time according to equation (3.4)

$$d m_l/dt = K (P_t - P_c)^{1/2} - (m_l/m_t)(g_c P_c A_t/c^*) \tag{3.4}$$

where

$$c^* = \frac{1}{\Gamma}\sqrt{R_o T_c/M} \tag{3.5}$$

The first terms on the right hand side of equation 3.4 represents the rate of injection, and the second term represents the rate of discharge through the nozzle. If the fluid is a gas injected through a sonic orifice, the first term reduces to KP_t.

The mass originating from the solid, m_s, is assumed to change with time according to equation (3.6).

$$d m_s/dt = \rho_s A_b a P_c^n - (m_s/m_t)(g_c P_c A_t/c^*) \tag{3.6}$$

Equations (3.3) (3.4) and (3.6) can be nondimensionalized for convenience in computation by employing the steady-state quantities $\overline{m_t}$, $\overline{m_l}$, $\overline{m_s}$, $\overline{c^*}$, $\overline{K}$, and $\overline{P_c}$, and the steady-state time constant for the chamber,

$$\tau_c = L^*/\Gamma^2 c^* \tag{3.7}$$

Using these quantities yields the following definitions for the nondimensional variables:

$$P_r = P_c/\overline{P}_c$$
$$L_r = m_l/\overline{m}_l$$
$$S_r = m_s/\overline{m}_s$$
$$c_r^* = c^*/\overline{c}^*$$
$$\theta = t/\tau_c$$
$$\xi = m_l/m_s$$
$$\overline{\xi} = \overline{m}_l/\overline{m}_s$$

This set of equations then can be combined with equations (3.3), (3.4), (3.5) and (3.6) to yield the following nondimensionalized equations:

$$d\,P_r/d\theta = (c_r^*)^2(1 + 1/\xi)^{-1}\,d\,L_r/d\theta + (c_r^*)^2(1 + \overline{\xi})^{-1}\,d\,S_r/d\theta + (1/c_r^*)(2\,P_r)\,d\,c_r^*/d\theta \qquad (3.8)$$

$$d\,L_r/d\theta = K_r\,(P_t/\overline{P}_c - P_r)^{1/2}/(P_t/\overline{P}_c - 1)^{1/2} - (P_r/c_r^*)(1 + 1/\overline{\xi})/(1 + 1/\xi) \qquad (3.9)$$

$$d\,S_r/d\theta = P_r^{\,n} - (P_r/c_r^*)(1 + \overline{\xi})/(1 + \xi) \qquad (3.10)$$

In the following equation, c^* is expressed as a function of ξ by a third order polynominal:

$$c^* = C_o + C_1\xi + C_2\xi^2 + C_3\xi^3 \qquad (3.11)$$

The rate of change of c^* can be expressed nondimensionally in terms of ξ, L_r, and S_r, as follows:

$$d\,c_r^*/d\theta = \{C_1/\overline{c}^* + (2\,C_2/\overline{c}^*)(\xi) + (3\,C_3/\overline{c}^*)\,\xi^2\}\,\{S_r\,\overline{\xi}\,d\,L_r/d\theta - \xi\,d\,S_r/d\theta\} \qquad (3.12)$$

Equations (3.8), (3.9) (3.10) and (3.12), along with an equation for the control valve function,

$$K_r = f(\theta) \qquad (3.13)$$

have been programmed for simultaneous solution by finite difference methods on an IBM Systems 360 computer. They have also been linearized for analytical solution. To include ignition transients, and flow before ignition, the program has been modified in that F/S, ξ , has been changed to the fluid fraction of the total flow, F/T. This avoids the infinity when the solid mass input is zero.

3.2.2 Application of the Model to Experimental Transients

The analysis of experimentally-obtained RSVP transients has been performed only to a limited extent to-date. Typical examples wherein the analytical model has been applied is presented as follows. At this time, the ability of the model to predict the experimental transients can only be rated as fairly good.

Sinusoidal Response

Calculations have been made for both the amplitude and phase response of the motor pressure to sinusoidal variation of the control fluid injection rate. This type of modulation has been proposed as a technique to achieve effective throttling. These initial calculations were made to compare predicted response with actual data from a gaseous fluorine/LPC-615A test firing. During this test, the fluorine control valve cycled on-and-off producing a nearly sinusoidal variation in the pressure upstream of the injector. This produced a cyclic variation in the fluorine injection rate and also in the motor pressure. Figures 3.4 and 3.5 present the amplitude and phase data obtained from this firing along with the predicted response. The measured amplitude response is seen to agree fairly with the predicted purves; however, the measured phase lag was somewhat greater than predicted. This phase discrepancy is most likely due to the assumption made in the derivation of the mathematical model that the burning rate adjusts instantaneously to variations in pressure according to the rate law $r = aP^n$, whereas in actuality there is a lag between burning rate and pressure variations (Ref. 19).

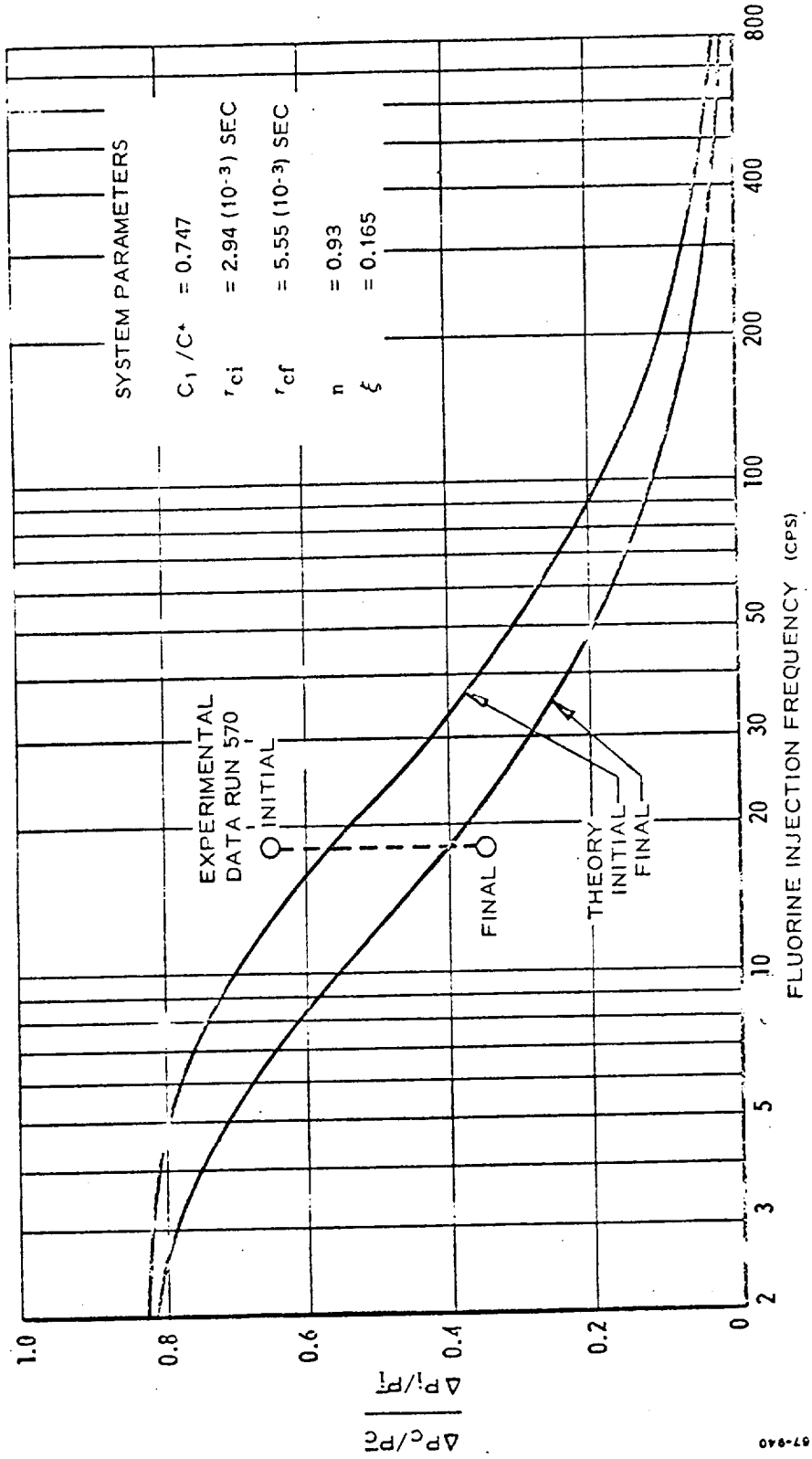

Figure 3.4 Comparison of Experimental Data with Theory for the Motor Response to Sinusoidal Control Fluid Injection

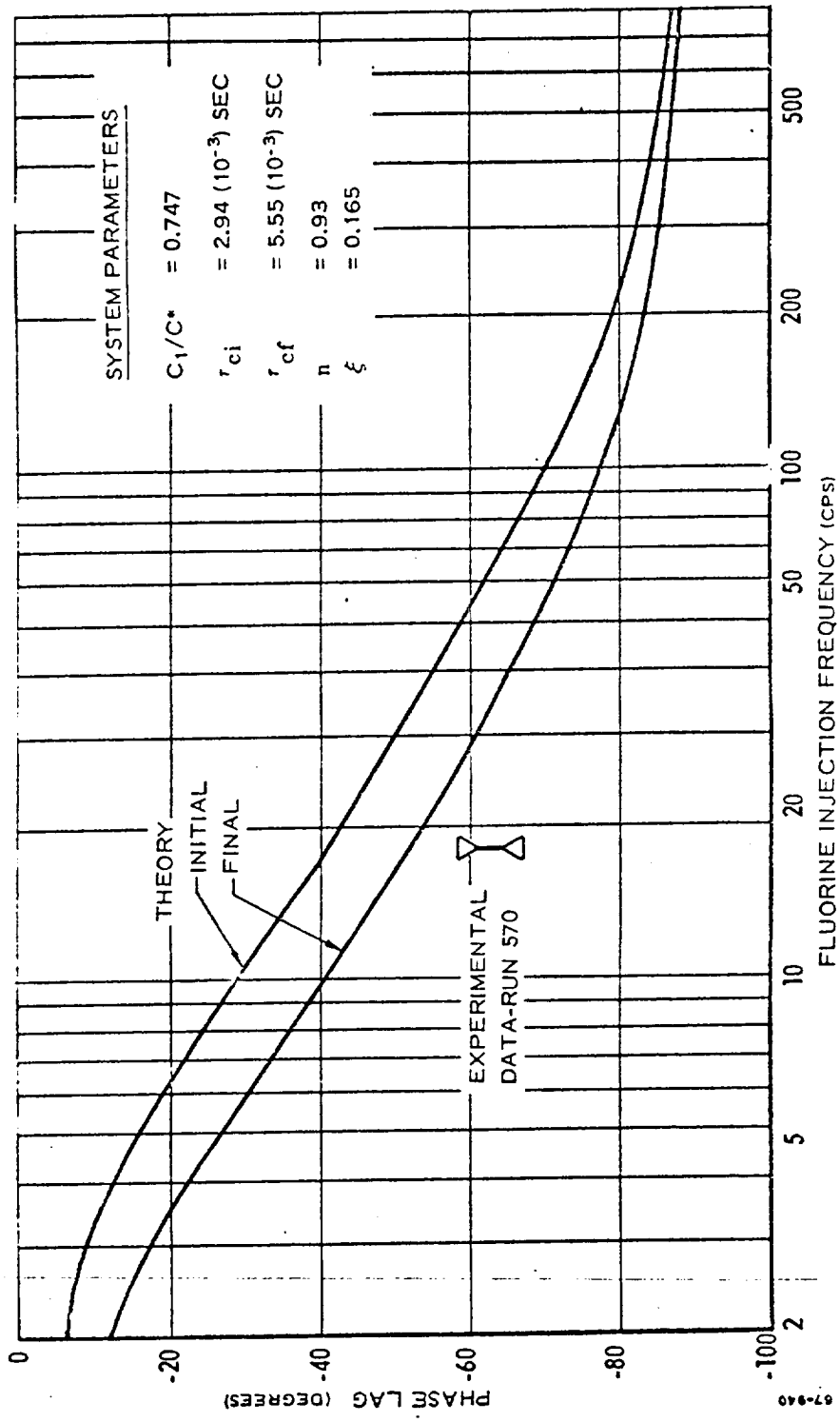

Figure 3.5 Comparison of Experimental Data with Theory for the Motor Response to Sinusoidal Control Fluid Injection

Thrust Tail-off

A result comparing predicted and experimental thrust tail-off is shown in Fig. 3.6. The predicted tail-off has generally been somewhat fast, which is attfibuted to the residual liquid between the valve and injector that exists from the test set-up. The model accounts for the recorded motion of the valve, but assumes no more liquid flow once the valve is shut. Modifying the apparatus to provide close-proximity or face shut-off would enhance the agreement.

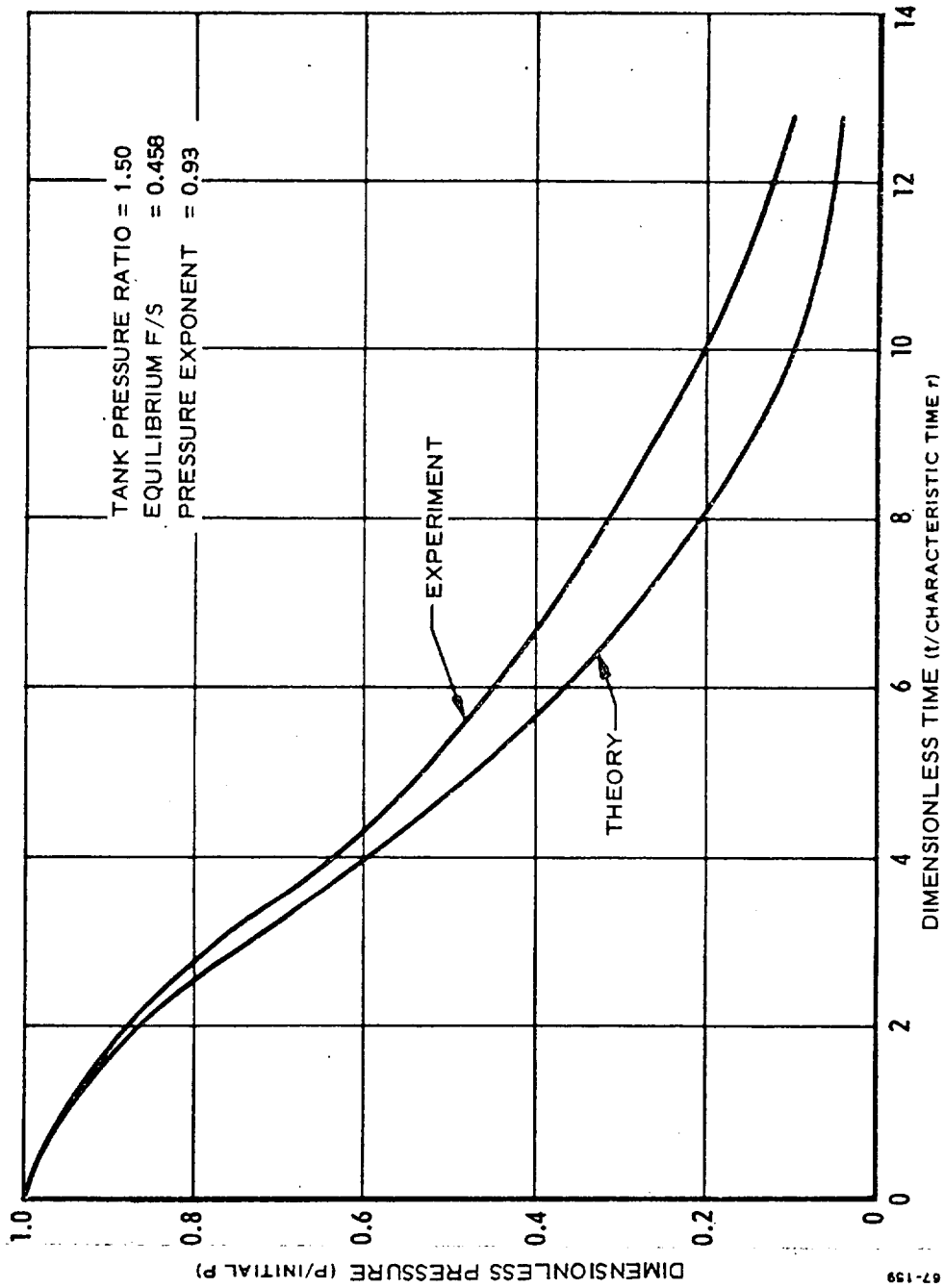

Figure 3-6 Comparison of Theoretical and Experimental Pressure Decay During Valve Command Close

3.3 Performance Under Random Throttling Conditions

The previous section presented the equations used to describe modulation transients themselves. This section will present a system of equations that can be used to predict the total impulse delivered by the propulsion system for a completely random throttled duty cycle. A duty cycle efficiency factor can be defined as follows:

$$\eta_{cy} = \frac{\text{Total Delivered Impulse}}{\text{Total Propellant Wt x Design Point Theoretical Isp}}$$

This efficiency factor takes into account performance losses over the duty cycle due to ordinary loss factors, pressure variations, and any departure from full utilization of propellants.

Total impulse is expressed as:

$$I = \int_0^{t_b} \eta \, I_{sp} dt \tag{3.14}$$

Where I = total impulse

t_b = burn time

Isp = theoretical Isp

η = Isp efficiency

and

$$I_{sp} = I_{sp}(F/S,P) \tag{3.15}$$

$$\eta = (0.96-0.07F/S)xf(P) \tag{3.16}$$

Specific impulse is a function of F/S and pressure. Efficiency is a function of F/S as shown, and should also be a function of pressure at sufficiently low pressure. A small effect of pressure on efficiency has been observed in tests conducted under NAS7-444 down to 60 psi chamber pressure. More data are required for a quantitative functional description.

The burn time, t_b, is established depending upon whether liquid or solid is used up first. For the liquid,

$$M_f = \int_0^{t_{bf}} \dot{m}_f dt \tag{3.17}$$

and for the solid,

$$M_s = \int_0^{t_{bs}} \dot{m}_s dt = \int_0^{t_{bs}} \frac{\dot{m}_f}{F/S} dt \tag{3.18}$$

where M_f = weight of liquid

$\dot{m}$ = flow rate of liquid

M_s = weight of solid

$\dot{m}_s$ = flow rate of solid

t_{bf} = time to deplete liquid

t_{bs} = time to deplete solid

Consequently, t_b is the lesser of t_{bf} or t_{bs}.

The flow rates are determined from the RSVP equations. The continued development will assume that the transients comprise a negligible portion of the firing, i.e., the throttling is between discrete steady-state thrust

levels. Instantaneous thrust is related to $\dot{m}_f$ and F/S as follows:

$$F = \dot{m}_f \left(\frac{1+F/S}{F/S} \right) \eta I_{sp} \tag{3.19}$$

which reduces to a function of pressure for a particular design. $\dot{m}_f$ and F/S are related to pressure as follows:

$$\dot{m}_f + \rho A_b a P^n = \frac{g}{C^*} P A_t \tag{3.20}$$

$$F/S = \left(\frac{g}{\rho a K_n} \right) \frac{P^{1-n}}{C^*} - 1 \tag{3.21}$$

where symbols have been defined previously, and

$$C^* = C^*(F/S, P) \tag{3.22}$$

Consequently, a stipulated thrust variation corresponds to a unique pressure variation from which, in turn, the other quantities are defined. Then given a thrust-time function, F(t), Eqs. (3.15), (3.16), and (3.19)-(3.22) represent six equations for the unknowns Isp, C*, η, P, $\dot{m}_f$ & F/S as functions of time. Knowing $\dot{m}_f$ and F/S serves to establish t_b and I from Eqs. (3.14) - (3.16).

For continuous thrust modulation, i.e. random wavy or pulsed thrust-time programs, the transient equations developed in Section 3.2 would have to be used. The computer output would include a running integral of impulse and weight expended until either fluid or solid is depleted.

With the special case of n=1 F/S remains constant. In this case, everything simplifies and the only losses in impulse are those expressed by η(F/S,P) in Eq. (3.16). Propellant utilization is full. A major effort under Contract NAS7-444, and in supplementary Company-sponsored work, has been devoted to the achievement of n=1 solid propellants.

3.4 RSVP Throttleability Potential

The throttleability of the RSVP is limited only by the lowest pressure at which combustion can be sustained stably (i.e. without erratic chuffing). Consequently, rather than perform series of demonstrations of deep throttling, LPC under Contract NAS7-444 concentrated on characterizing low pressure stability limits for a particular rubber base propellant. It was determined that the low pressure stability limit decreased with increasing motor L^*, much as has been reported for unaugmented solid propellants (23). An additional factor was found to be the F/S ratio; with increasing F/S, the pressure-L^* instability boundary was shifted to lower values of pressure and L^*. This stabilizing effect of fluid injection was also explained theoretically, essentially by the same mechanism which reduces the effective pressure exponent (n) of the system below that of the solid itself (19).

Knowing the low pressure stability limit, throttling ratio is then determined by acceptable mass fraction penalty, i.e. allowable high-thrust maximum pressure. Obviously, throttling ratio can be tripled by allowing the maximum pressure to be 1200 psi instead of 400 psi; however, it would be more desirable if stable combustion could be achieved e.g. down to 20 psia rather than limited to 60 psia.

Stability results obtained under Contract NAS 7-444 are shown by the solid lines in Figure 3.7. The F/S=0.5 line is extrapolated, by the dashed line, to values of L^* corresponding to initial and final values for the motor sizes considered in this study. For the 100 lb motor, if the extrapolation is correct, it is seen that operation at 20 psia will be stable throughout the burn time of the motor. With the nominal design pressure of 400 psi, the

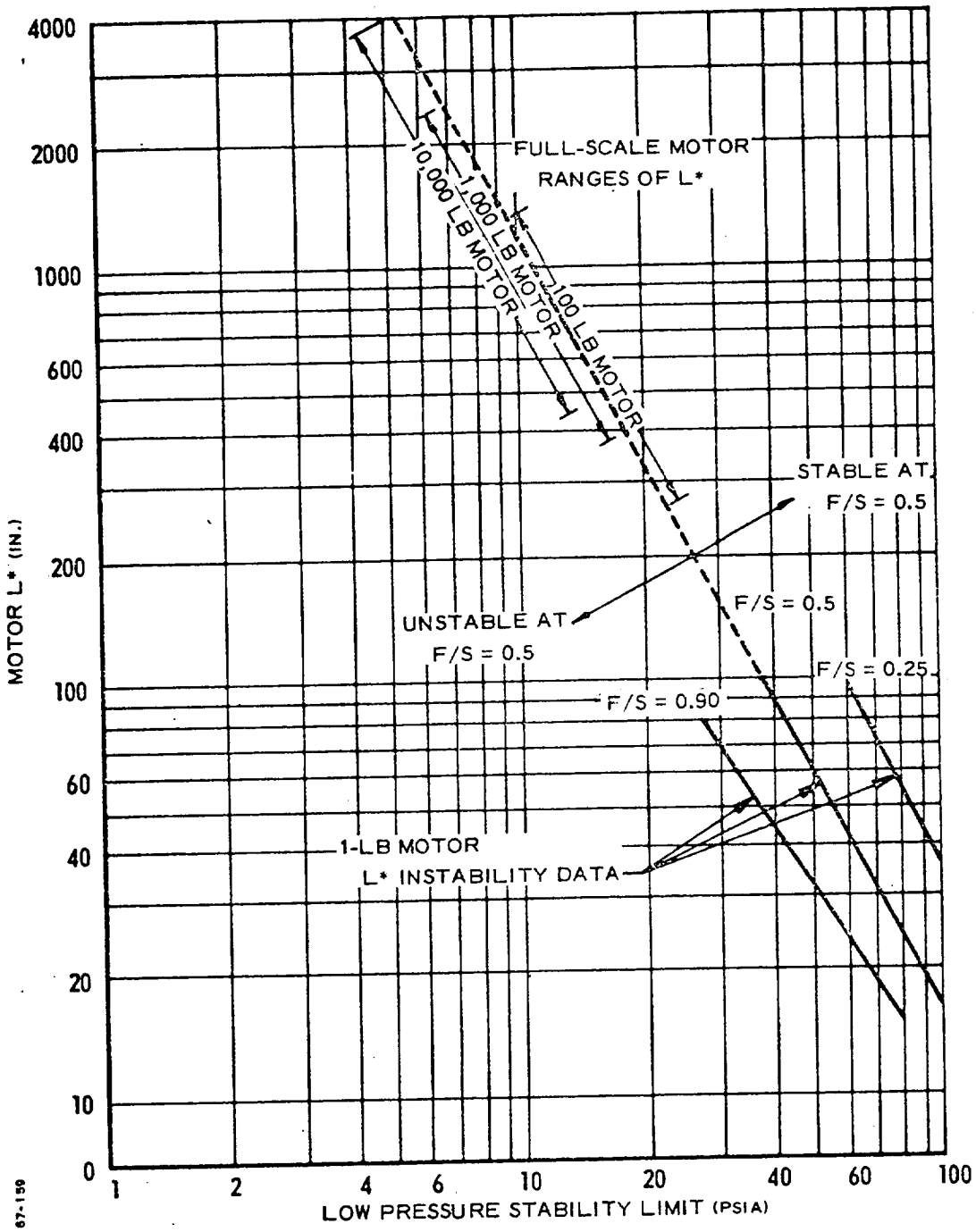

Figure 3-7 L* Instability Data from Contract NAS 7-444, and Extrapolation to Full-Scale Motors

throttling ratio would be roughly 20=1 with no additional mass fraction penalty.

A few demonstration-type throttling tests have been made at LPC with either a dual-manifold injector or by modulation of the valve or supply pressure. Either way, the liquid flow rate can be modulated, but the dual injector presumably has the advantage of maintaining good atomization at the lower flow rate. However, the question of injector design and sophistication in throttling devices is not likely to be as serious with the RSVP as it is with liquids and hybrids. The combustion process is dominated by the efficient combustion of the solid in a zone very close to the propellant surface. The desired secondary reactions with the injectant in the motor cavity add 10%-20% to the performance of the solid alone, whereas in a bi-liquid or a conventional hybrid the liquid injection accounts for 100% of the performance of the system.

Demonstrated throttling ratios from 1000 psi in 25 lb. motors have not been in excess of 20:1 to date, limited by low L* and available equipment from previous LPC hybrid programs. Efficient deep throttling in the hybrid is limited by the large mixture ratio excursions that result. Step-throttling occurred with rapid response, and the solid did not extinguish in the course of the rapid depressurization transient.

3.5 Minimum Impulse Bit

LPC has been investigating the question of minimum impulse bit associated with a main thruster, as it has bearing upon both military and NASA

applications of current interest. Studies to-date have been analytical in nature, using the transient ballistics computer programs and performing an error analysis on the results to qualify impulse bit error. This section will introduce possible modes of operation to achieve impulse bits, and then present results for two illustrative modes as applied to the preliminary designs developed in this study. Presumably, experimental study of minimum impulse bit will occur in the course of RSVP technology development, wherein the analyses will serve as a useful guide.

3.5.1 Methods to Achieve Minimum Impulse Bit

Use of the main thruster to provide small impulse bits can be accomplished by operating the flow control valve in several possible ways. These techniques are summarized in Figure 3-8.

One general technique is a valve-control mode, that operates independently of the motor ballistics which ensue as a result of the valve operation. One can control the valve action time (time to open or close) t_v, the percentage of the fully-open position that the valve is allowed to reach, h, and the duration that this valve position is maintained before command to close, t_o. The smaller each of these parameters are made, the smaller the impulse bit. This technique has the advantage of being able to supply extremely small impulse bits, approaching zero, but at the disadvantage of no ballistically coupled control and consequently larger error.

A second general technique is ballistic (pressure or thrust) feedback control to command the valve to close. That is, the valve opens, and when, e.g., a certain fraction of equilibrium pressure is reached in the motor, a

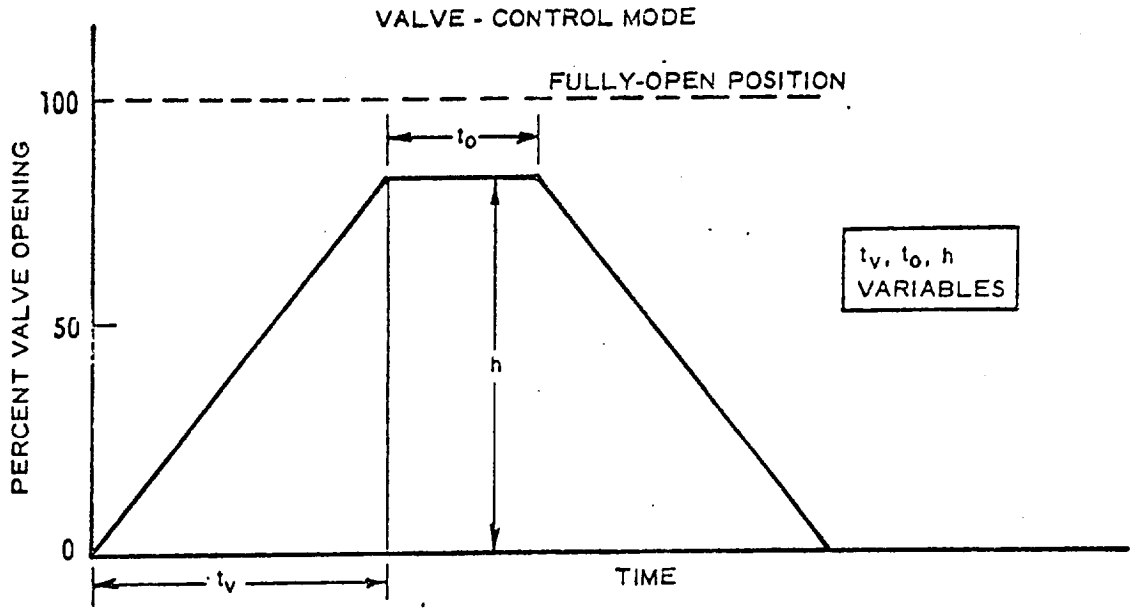

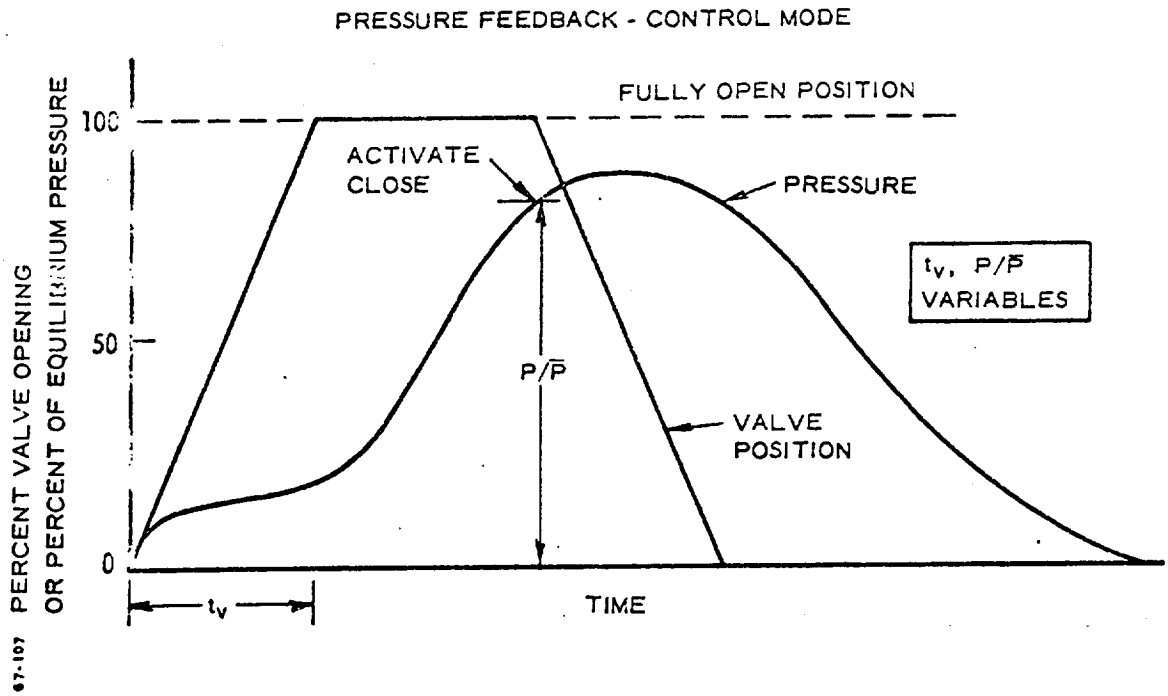

Figure 3-8 Methods of Achieving Minimum Impulse Bit

pressure-switch signal commands the valve to close. In this mode of operation, one can control the valve action time, t_v, and the percent of equilibrium pressure to be reached ($P/\bar{P}$) for command shut-off. While this technique will not yield as small an impulse bit as can potentially be achieved by valve on-off control, unless $P/\bar{P}$ is made to be very small, it has the advantage of providing ballistically coupled control to enhance reproducibility.

3.5.2 Results of a Parametric Analysis

The results of analysis of two special cases are discussed as illustrative examples.

(1) In the pressure-feedback control mode, the valve is commanded to close when 90 percent of equilibrium pressure is achieved. Valve action time, t_v, is varied as a parameter. The effect of variations in ignition delay time (t_{ig}) is also examined.

(2) In the valve-control mode, the valve is taken to be fully open (h=100 percent), and the time that the valve remains fully open is zero (t_o=0). In other words, the valve simply opens and shuts. Valve action time, t_v, is varied as a parameter, and the effect of variations in ignition delay time also is examined. In this mode of operation, ignition delay time and reproducibility assumes maximum importance when attempting to minimize impulse bit.

In mode 1 of operation, the impulse bit was studied as a function of θ_v (valve open or close time, nondimensionalized by the L^*-governed characteristic time of the chamber: $\theta_v = t_v/\tau$), with F/S and n as variable parameters. The dimensionless ignition delay time was found to have negligible effect because, in this mode of operation, the valve has to wait for 90% of

equilibrium pressure to be reached anyway and the impulse produced by pre-ignition Compound A vapor is negligible. Sufficient results were obtained over the spectrum so as to evaluate effects of errors in the governing parameters. Essential results are summarized as follows:

(a) With decreasing F/S, impulse bit increases and its error becomes more sensitive to errors in the governing parameters.

(b) As the valve time increases as a proportion of the chamber characteristic time(increasing θ_v), impulse bit increased and errors in the valve became increasingly significant. On this basis it can be expected that valve errors will be most significant for the low L* liquid engines.

(c) Impulse bit does not tend to zero as the valve time approaches zero. Even if the valve is infinitely fast, the pressurization to 90 percent equilibrium and the subsequent depressurization to zero will occur over a finite time as governed by the L^* of the chamber. In fact, this condition is pretty well reached when the valve time is equal to the characteristic time of the chamber ($t_v/\tau=1$). A valve faster than this will show no significant effect.

(d) With a fast valve (low θ_v) and at high F/S, impulse bit decreases as n increases. With a slow valve and at low F/S, impulse bit decreases as n decreases. Errors in n were found to have a significant effect on impulse bit error.

With a nominal value of F/S=0.5, and n=0.9, an error envelope is constructed as a function of θ_v as shown in Figure 3.9. For the pressure-feedback

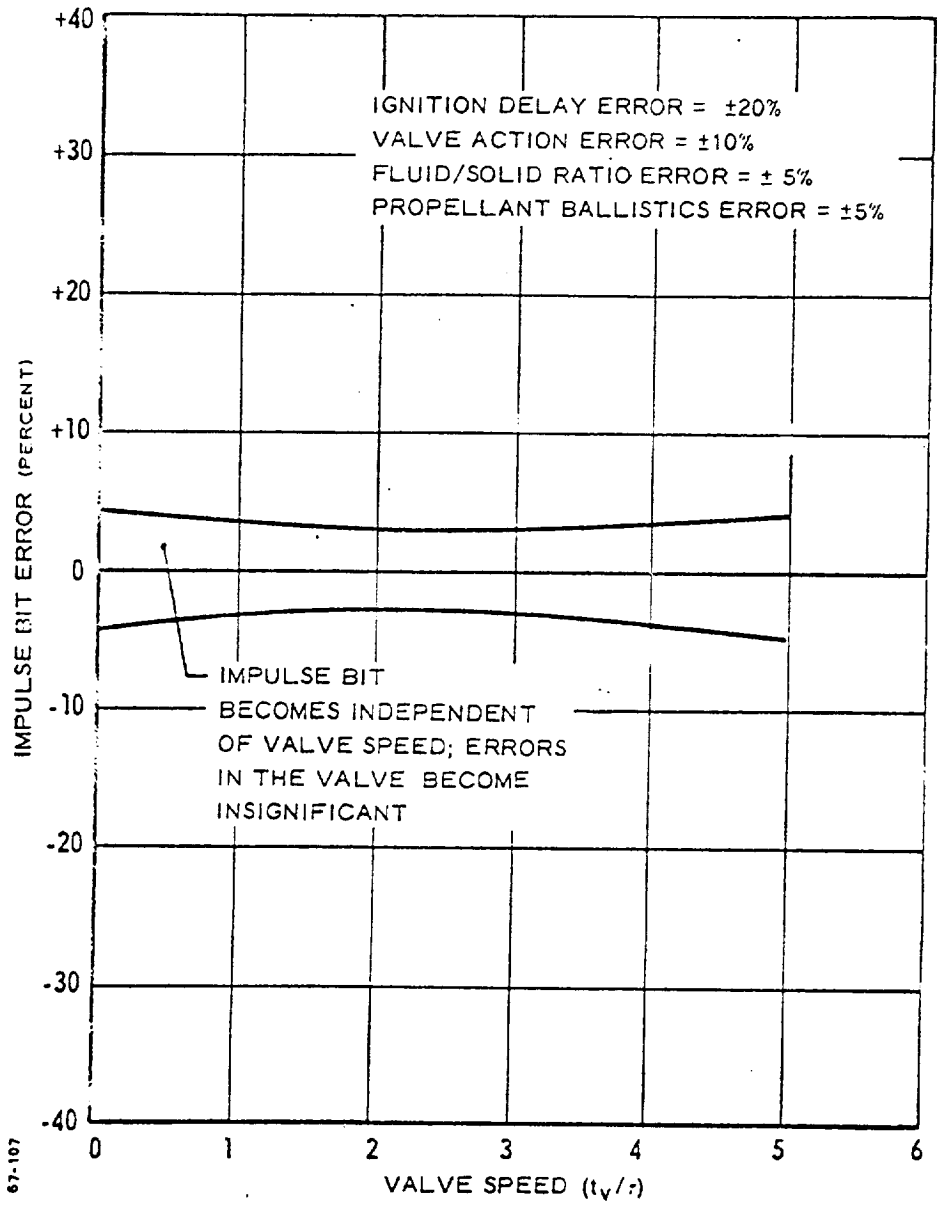

Figure 3-9 Effect of Valve Speed on Minimum Impulse Bit Reproducibility in the "90% Equilibrium Pressure" Pressure-Feedback Controlled Mode of Operation

control mode of operation, and with the sources and magnitudes of errors shown in the figure, the impulse bit error is seen to be within ± 5 percent. For the very fast valve ($t_v/\tau \rightarrow 0$), the effect of error in the valve time becomes insignificant but errors in the ballistic quantities, particularly n, are found to have a little greater effect. For the slower valve (increasing t_v/τ), the error in the valve begins to be the dominant source of impulse bit error. A minimum error of ± 2.5 percent appears in the neighborhood of $t_v/\tau = 2$.

In mode 2 of operation, i.e. the rapid on-off ballistically uncoupled mode, the following trends were noted:

(a) Impulse bit decreases with increasing F/S, n and ignition delay time. Indeed, if the ignition delay is greater than the time required for the valve to cycle, there would theoretically be no ignition; the impulse bit is then produced by the oxidizer vapor. This is a nebulous situation, particularly with the presence of hypergolic vapor in the chamber which could eventually produce an uncontrolled chuff.

(b) Impulse bit decreases as the valve action time becomes a smaller fraction of the chamber characteristic time (reduced θ_v). Examples of computer outputs illustrating this effect are shown in Figure 3-10. A similar trend would be noted by fixing the valve time and increasing the ignition delay time.

An error envelope analogous to that presented in Figure 3.9 is shown for mode 2 in Figure 3.11. In this mode of operation, it is found that the impulse bit error becomes very large as the impulse bit magnitude tends

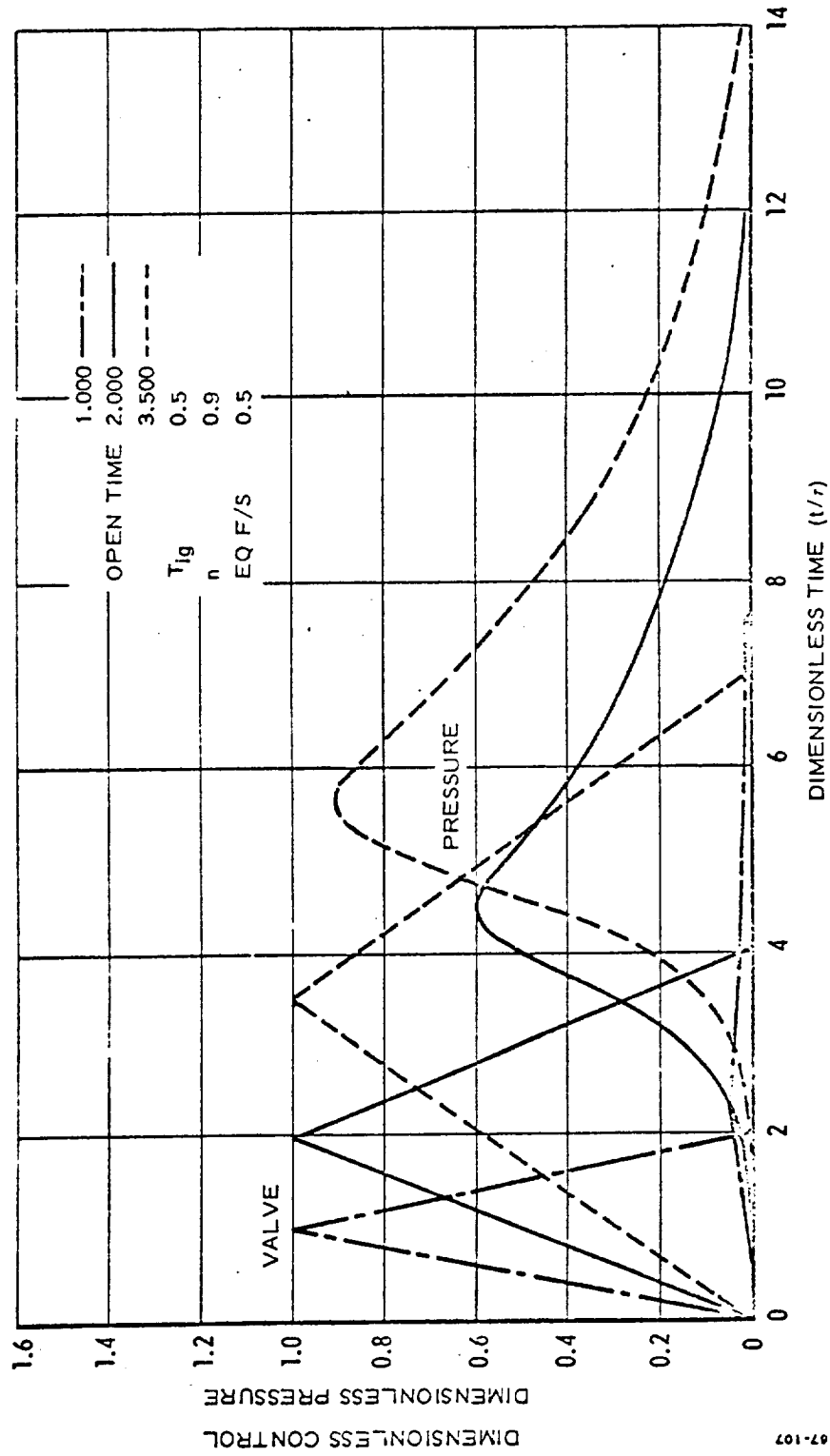

Figure 3-10 Effect of Valve Open Time on Rapid On-Off Impulse Bit

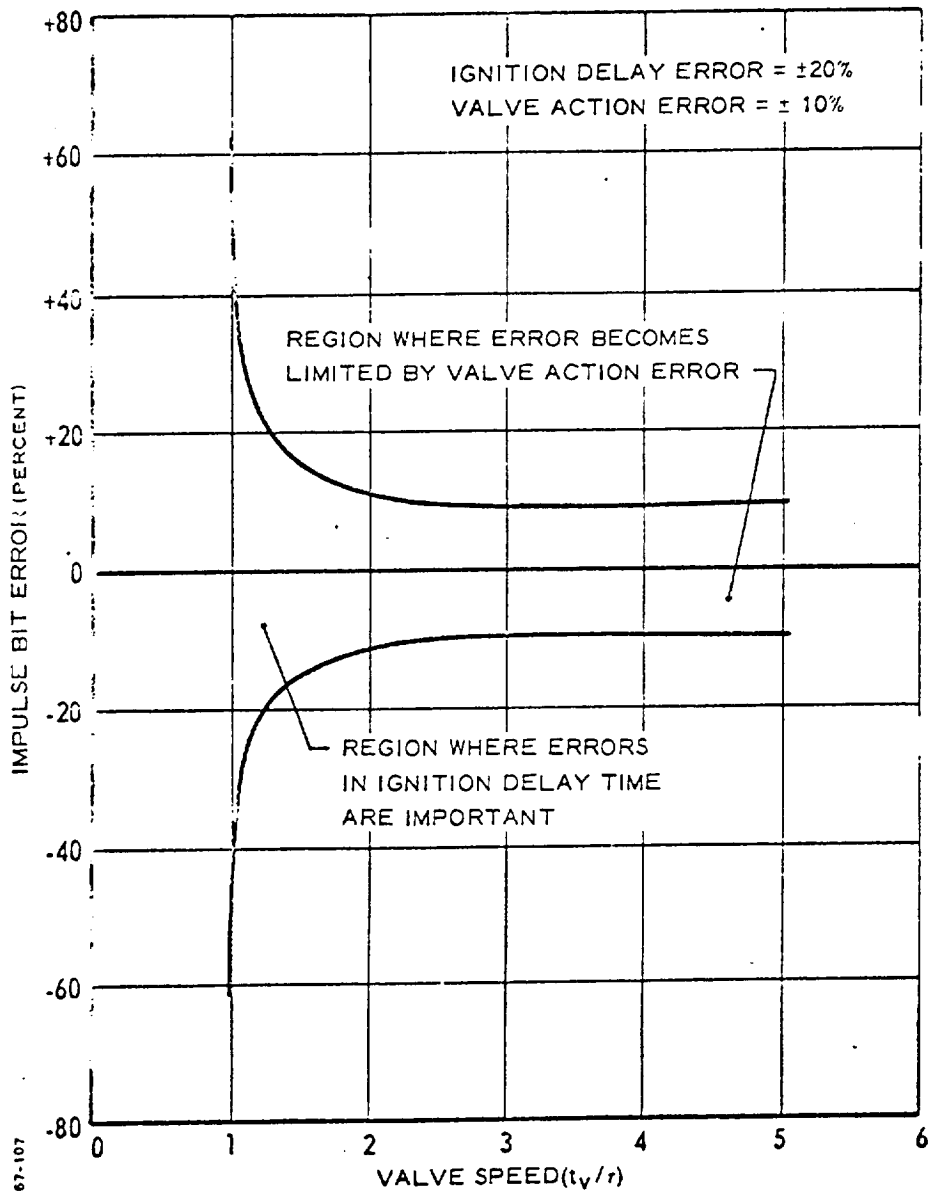

Figure 3-11 Effect of Valve Speed on Minimum Impulse Bit Reproducibility in the Rapid On-Off Mode of Valve Operation

toward zero (faster and faster valve). This is due to the eventually enormous effect of errors in ignition delay, i.e. will the solid ignite or not. Consequently, even though the magnitude of the impulse bit can be very small in this region, this region may have to be avoided in practice because the errors are so great. Note the rapidity at which the impulse bit error approaches a limiting value of $\pm$ 10 percent as the valve slows down beyond $t_v/\tau=2$. This error is still much larger than exists with pressure-feedback control. Being ballistically coupled to the motor operation, pressure-feedback control minimizes effects of ignition delay error and valve error.

With hot gas control (e.g. hydrazine decomposition products), impulse bit magnitude in either mode is generally a little larger because of the C^* of hydrazine gases relative to Compound A prior to ignition of the solid.

3.5.3 Numerical Results for Designs in Question

The dimensionless parametric results were quantified corresponding to the preliminary designs studied in this program. Dimensional inputs are summarized in Table 3.3. and assumed errors are summarized in Table 3.4. The values of L^* and τ correspond to the actual designs; the other values were assumed based upon available information. The parametric study encompassed the entire range of dimensionless numbers of interest.

Results for the pressure-feedback control mode of operation (mode 1 cited above) are presented in Figure 3.12. Impulse bit is plotted vs total propellant weight and corresponding to initial and final values of L^*; F/S is taken as 0.5 and n as 0.9. The design (equilibrium) performance values of the different sized motors are presented in Table 4.1 in

TABLE 3.3 DIMENSIONAL INPUTS FOR RSVP IMPULSE BIT CALCULATIONS

Total Propellant Weight (lb)	F/S	Initial L^*(in.)	Final L^*(in.)	t_v(msec)	τ (msec)	tig(msec)
100	0.25	360	---	20	13.3	40
100		---	1500	20	55.3	
1000		560	---	40	20.7	
1000		---	3000	40	111	
4000		650	---	60	24.0	
4000		---	4500	60	166	
10000		680	---	80	25.1	
10000		---	5000	80	185	
100	0.50	260	---	20	9.6	20
100		---	1300	20	48.0	
1000		400	---	40	14.8	
1000		---	2500	40	92.3	
4000		460	---	60	17.0	
4000		---	3800	60	140	
10000		480	---	80	17.7	
10000		---	4200	80	155	
100	1.00	200	---	20	7.4	
100		---	1000	20	36.9	20
1000		300	---	40	11.1	
1000		---	1800	40	66.5	
4000		350	---	60	12.9	
4000		---	2800	60	104	
10000		360	---	80	13.3	
10000		---	3000	80	111	

TABLE 3.4 ASSUMED ERRORS FOR IMPULSE BIT REPRODUCIBILITY DETERMINATION

Total Propellant Weight (lb)	t_v/τ Error* %	F/S Error %	Error in Burn Rate %	Error in n %	Error in Ignition Delay (%)
100	± 11.2	± 5	± 5	± 5	± 20
1000	± 8.9	± 4	± 4	± 4	± 20
4000	± 6.7	± 3	± 3	± 3	± 20
10000	± 5.4	± 2	± 2	± 2	± 20

* Combines error in t_v with error in L^*.

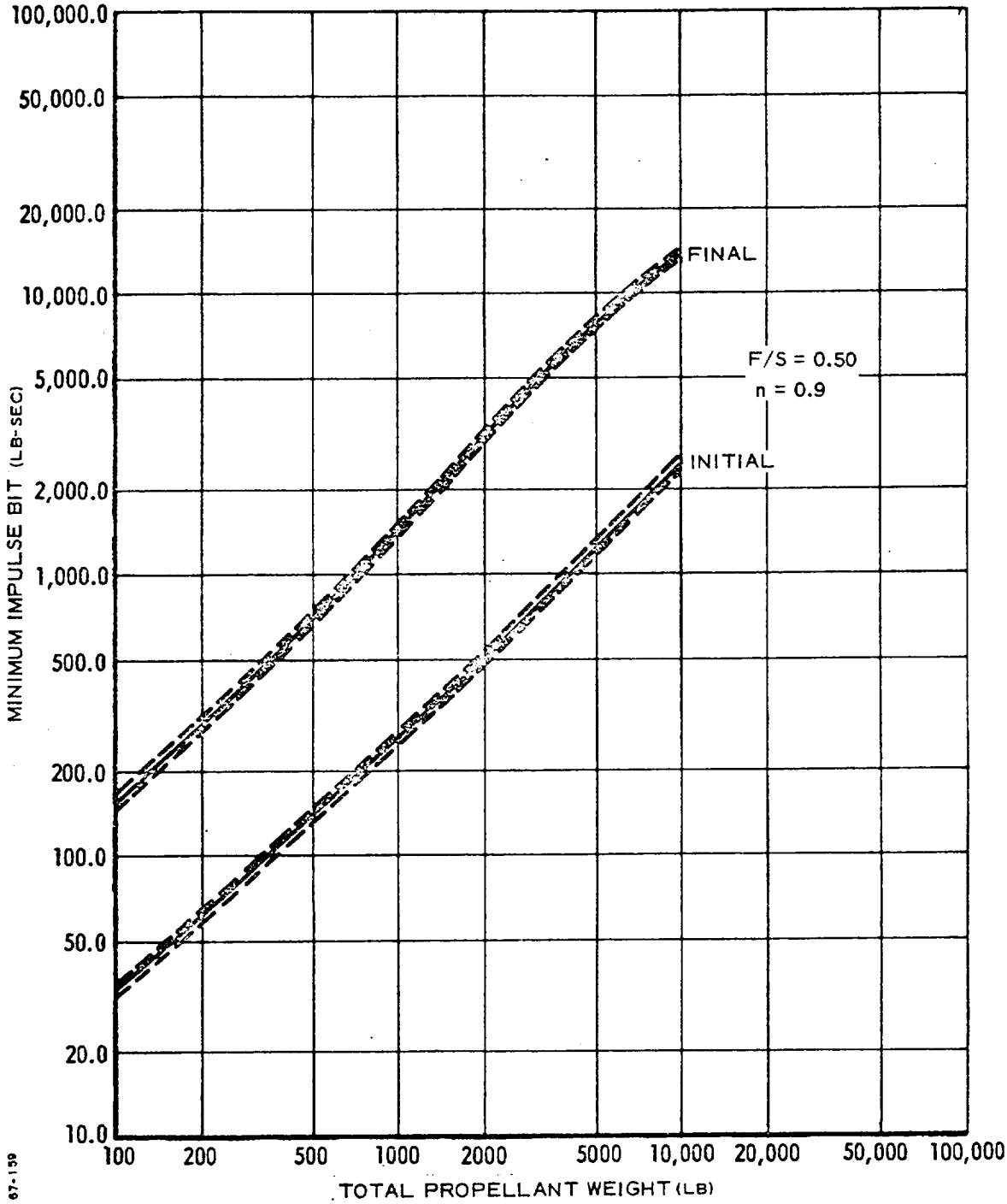

Figure 3-12 Minimum Impulse Bit Magnitude and Error as a Function of Motor Size: Pressure-Feedback Control Mode

Section 4, in connection with weight information. Error envelope is dashed.

The impulse bit error is found to remain fairly constant at about ± 4%. With increasing motor size, the absolute errors in the governing parameters are smaller. However, because of the values assumed for the valve time in relation to the chamber characteristic time, θ_V increases with motor size and is in the range where the error influence coefficient increases with θ_V. Consequently, the impulse bit error need not necessarily decrease with increasing motor size. From the early part of the firing to near the end of the firing, the value of θ_V within a motor decreases substantially; hence, errors due to the valve are decreased. However, because of errors in burning rate, there is introduced an uncertainty in the time at which the motor free volume reaches a certain value. The introduction of this error tends to make the impulse bit error less sensitive to time within the firing. Impulse bit magnitude and error for F/S=1.0 was found to be only slightly smaller than reported for F/S=0.5. However, for F/S=0.25, impulse bit magnitude increased by about 15 percent and the error envelope averaged out to be about ± 10 percent.

Results for the rapid on-off mode of operation are presented in Figure 3.13. Impulse bit error varies from about ± 7% to ± 11% at the initial portion of the firing, and from about ± 15% to ± 20% near burn-out. The reduction in impulse bit magnitude in the course of the firing is a natural consequence of the increased sluggishness of the chamber as its free volume increases.

Note that the initial impulse bit in this mode of operation is about 2/3 that in the pressure-feedback-control mode; this difference is not great considering the difference in penalty to reproducibility. The error in

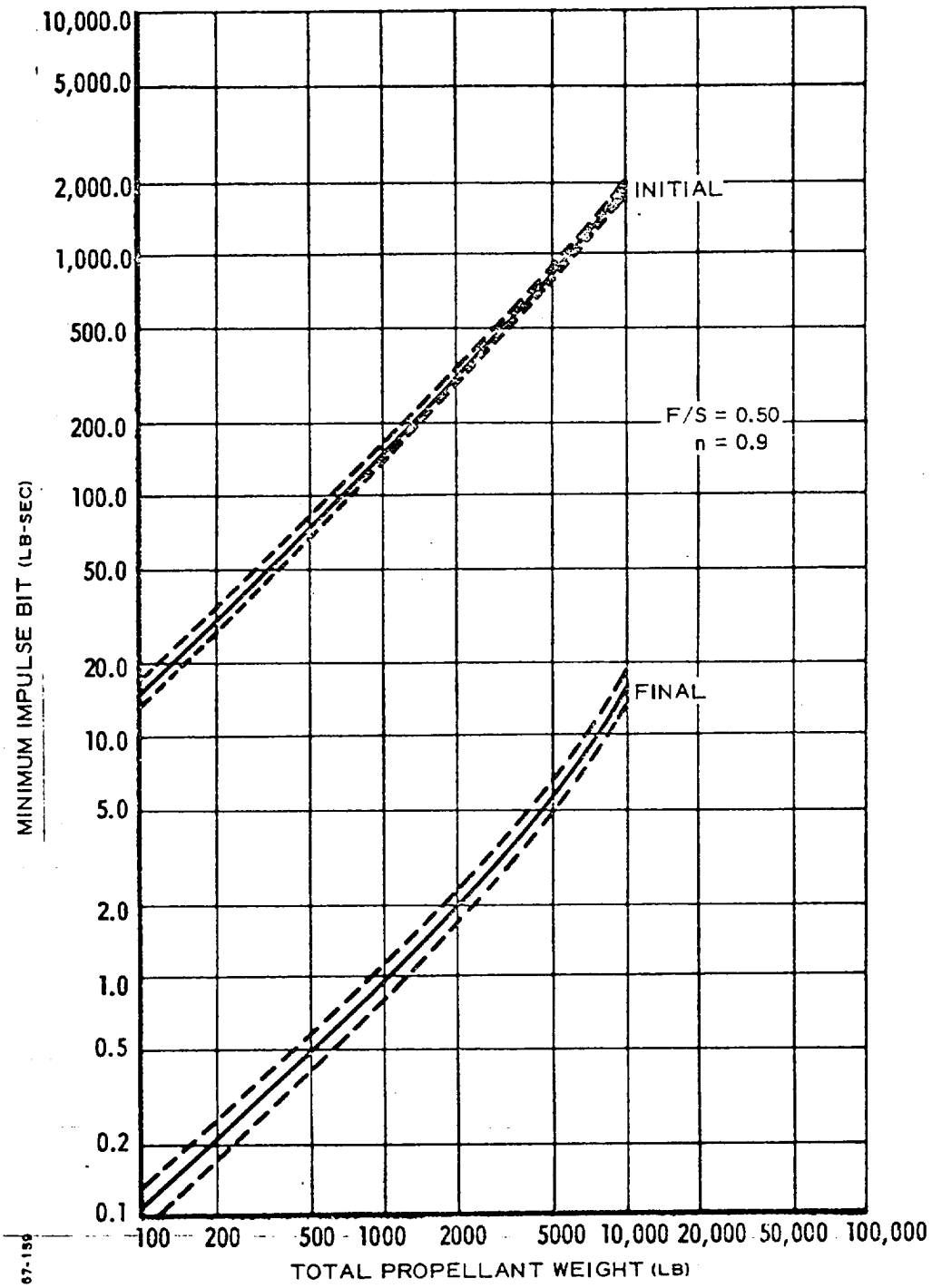

Figure 3-13 Minimum Impulse Bit Magnitude and Error as a Function of Motor Size: Rapid On-Off Mode

ignition delay time, particularly as the value of θ_v gets small and t_{ig} gets long, can assume serious proportions regardless of propulsion concept. However, for the quantitative inputs used (Tables 3.3 and 3.4), the errors did not get as large as potentially indicated by Figure 3.11.

The error envelopes in Figs. 3-9 and 3-11 are also illustrative of how reproducibility varies with varying impulse bit magnitude for a given motor size (i.e., by changing valve speed for a fixed initial or final L*). This effect is shown for both modes of operation in Fig. 3-14. The illustrative example in this figure is for the 1000 lb. motor design at its initial L*. Corresponding to Fig. 3-9 for mode 1 of operation note that the magnitude of the error in this mode is comparatively small and relatively independent of valve speed (or impulse bit magnitude). Similarly, corresponding to Fig. 3-11 for mode 2, the magnitude of the per cent error is larger and starts to increase considerably with reduction in bit magnitude - particularly as t_v/τ approaches unity. Note, also, that as the valve becomes sufficiently slow, both modes of operation provide nearly the same impulse bit magnitude.

3.5.4 Concluding Remarks

Although pressure-feedback control produces larger values of impulse bit than with rapid on-off valve operation, the impulse bit is much more reproducible at a given valve action time and motor L* (t_v/τ) with feedback control. To reduce the impulse bit magnitude with feedback control, the effect of reducing $P/\overline{P}$ should be examined; e.g. command the valve to close when $P/\overline{P}$=0.5 instead of 0.9. It is anticipated that as $P/\overline{P}$ is reduced, the reproducibility will be poorer; however, there may be some threshold $P/\overline{P}$ above which reproducibility is still good.

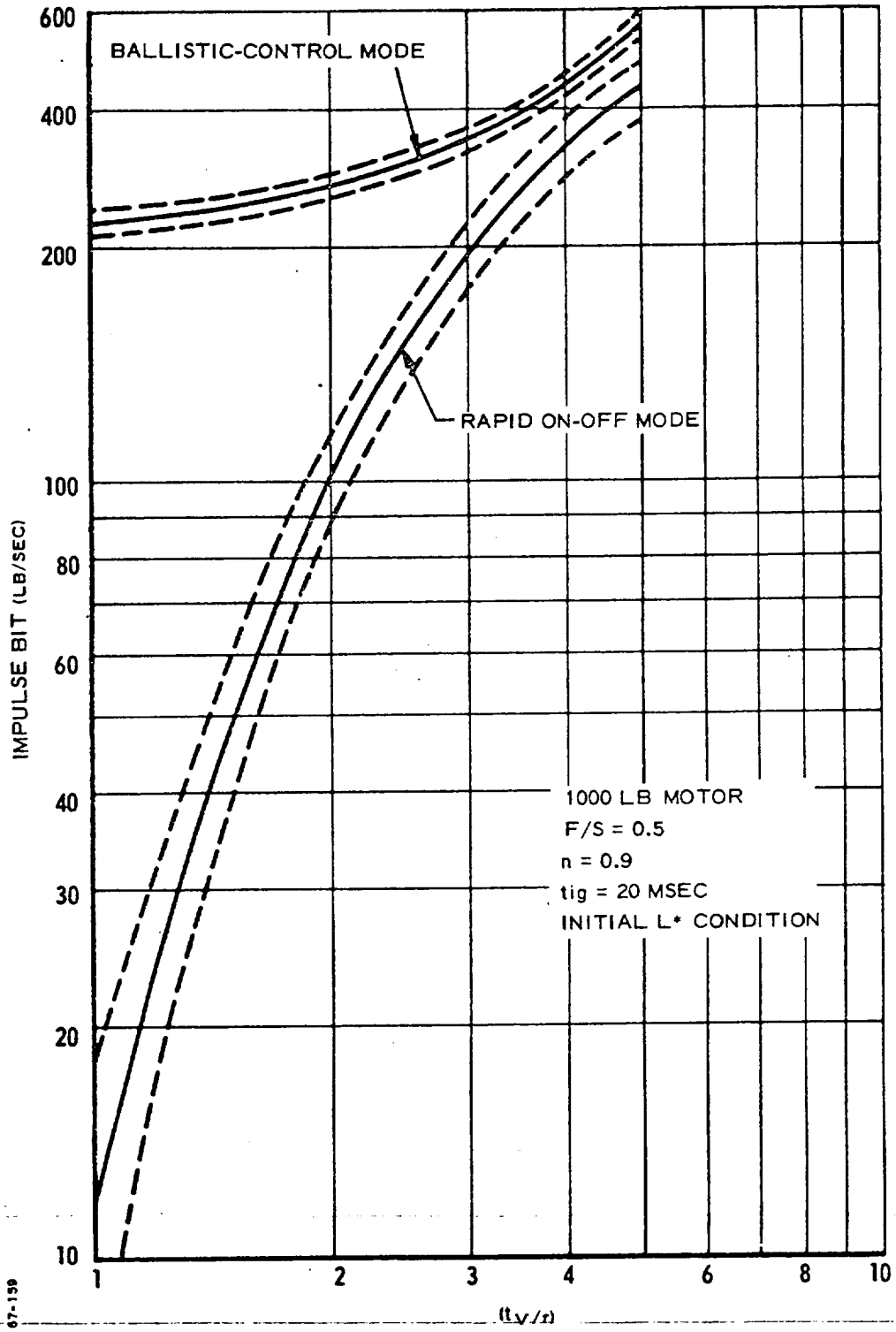

Figure 3-14 Minimum Impulse Bit and Error as a Function of Valve Action Time for a Given Motor Size

Similarly, in the valve-control mode, it is anticipated that reproducibility will improve by allowing the valve to remain open for a finite time. But this will increase the impulse bit magnitude.

By a thorough parametric analysis of the modes of operation, it will be possible through trade-offs to converge on the minimum impulse bit of acceptable reproducibility.

It is also necessary to investigate the magnitudes of the individual sources of error as input to the error analysis, e.g., valve manufacturer certification and observed test performance, batch-to-batch reproducibility of propellants to be tested, reproducibility in achieving design fluid/solid ratio at steady-state, and ignition delay reproducibility. All of these tasks should be a part of any controllable motor evaluation program.

4.0 RSVP COMPONENT WEIGHTS

4.1 Effect of Motor Size and Fluid/Solid Ratio

A parametric preliminary design study of the effect of motor size and design F/S ratio on RSVP mass fraction was conducted under Contract NAS 7-449, leading to a detailed design for a particular application (10). The present preliminary design study has made use of the results of the former, extending the range of sizes in question and correcting the parametric results based upon information from the detailed design.

A tabulation of component weights, over a wide range of motor sizes for an RSVP using Compound A as control fluid, is presented in Table 4.1. Corresponding performance quantities are also included. Based upon these data, an approximate weight equation was constructed as given in Table 4.2. 250 grade 18% nickel maraging steel (Vanadium Corporation of America) has been assumed for all tankage. It is a high-strength steel which has been used in solid rocketry, has good workability and weldability, and promises to be compatible with fluorinated liquids.

THIS PAGE CONTAINS CLASSIFIED

INFORMATION AND IS PRESENTED

IN VOLUME V

TABLE 4.2 APPROXIMATE WEIGHT EQUATION TERMS COMPOUND A/SOLID RSVP

Residual Propellant =	$W_1 = 0.017W$	
Filled Helium Tank =	$W_2 = 0.062 \frac{F/S}{1+F/S} W \left(\frac{P_{He}}{4500}\right)$	
Liquid Tank =	$W_3 = 0.030 \frac{F/S}{1+F/S} W \left(\frac{P_L}{600}\right)$	$t \geq 0.02$ in.
	$W_3 = 0.155\left(\frac{F/S}{1+F/S} W\right)^{0.67}$	$t < 0.02$ in.
Expulsion Bladder =	$W_4 = 0.027\left(\frac{F/S}{1+F/S} W\right)^{0.67}$	
Plumbing =	$W_5 = 4.20 \left(\frac{F/S}{1+F/S} \dot{W}\right)^{0.5}$	
Solid Rocket Chamber =	$W_6 = 0.019 \frac{1}{1+F/S} W\left(\frac{P_s}{400}\right)$	$t \geq 0.02$ in.
	$W_6 = 0.195\left(\frac{1}{1+F/S} W\right)^{0.67}$	$t < 0.02$ in.
Insulation =	$W_7 = 0.138\left(\frac{1}{1+F/S} W\right)^{0.67} t_b$	
Lockseal Nozzle =	$W_8 = 0.10F^{0.67} t_b\left(\frac{\epsilon}{45}\right)^{0.2}$	
Lockseal Actuation	$W_9 = 0.017 F^{0.8}$	
Mounting =	$W_{10} = 0.27W^{0.5}$	

W = total propellant weight (lb.)
F/S = fluid/solid ratio
P = pressure (psi)
F = thrust (lb.)
t_b = burn time (minutes)
$\dot{W}$ = total flow rate (lb/sec)
t = minimum wall thickness

The use of titanium with Compound A is questionable, considering existing information with both Compound A and chlorine trifluoride (24). Because of the possibility of leaking onto adjacent vessels which might otherwise be constructed of titanium or filament-wound, the maraging steel was used throughout. There is need for more extensive compatability and storability studies than have been performed to date.

A curve of mass fraction as a function of motor size for a particular F/S ratio is presented in Figure 4.1. The boundaries indicate expected accuracy. The increased accuracy shown for the 5500 lb. size is indicated because this size corresponds to the detailed design of Ref. (10). Use of titanium tankage and a filament-wound solid motor (particularly for small motors) will improve mass fraction as indicated by the dashed line. Additional improvement through resort to warm gas pressurization is also indicated. The sharp curvature in the lines begin to result from minimum gage considerations; the titanium and filament winding continue to be efficient to smaller motors than does the maraging steel. As motor size is reduced further, the miscellaneous components assume increased significance which enhances the steepness of the line. Compatible aluminum alloys would be attractive in this range.

Figure 4.2 shows the effect of variations in design F/S ratio on mass fraction for a particular size. Given a particular mission, then, the optimum F/S ratio can be determined by combining these curves or the weight equation with the effect of F/S ratio on specific impulse (e.g. Figure 3.1).

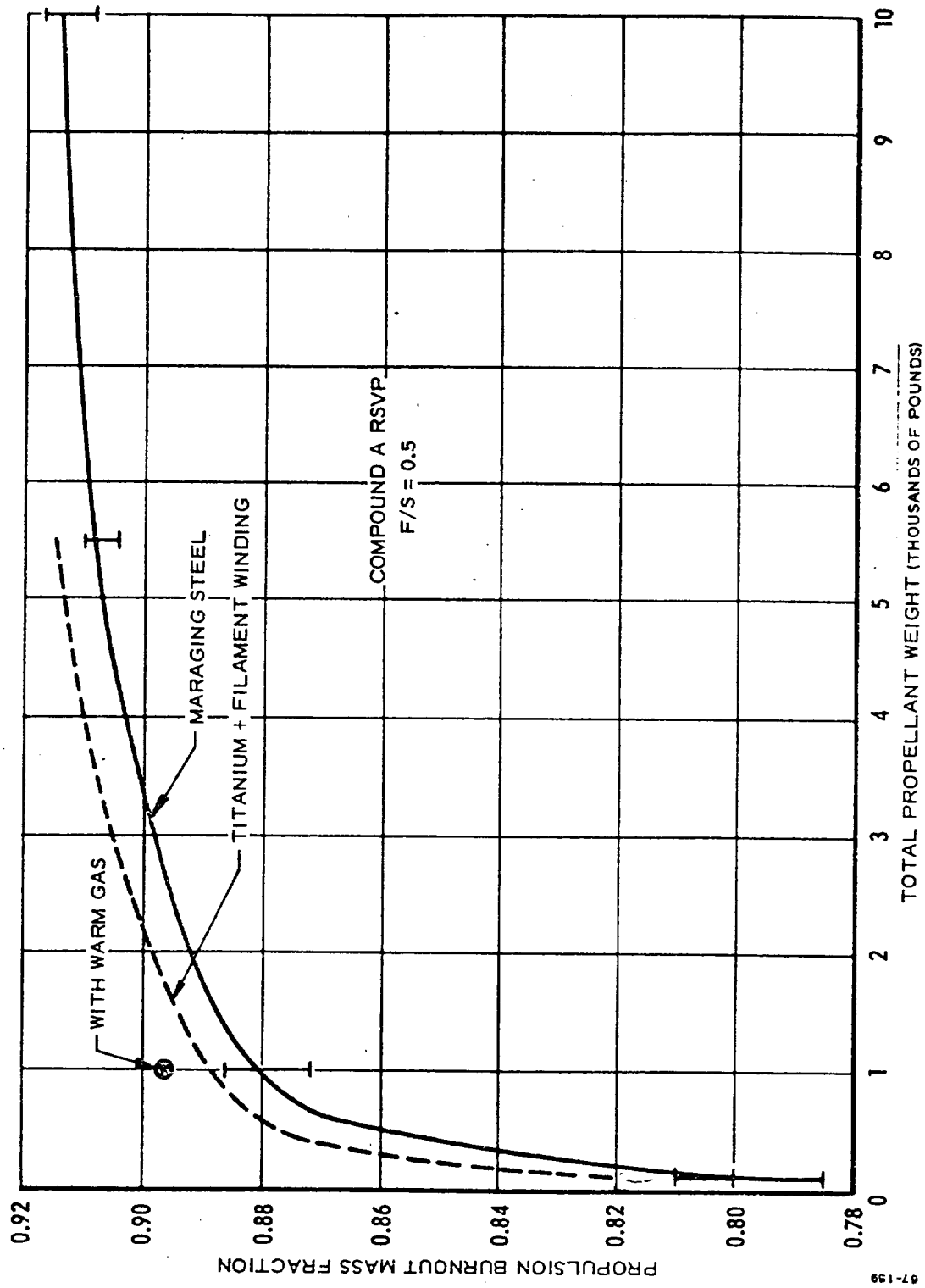

Figure 4-1 Mass Fraction Scaling

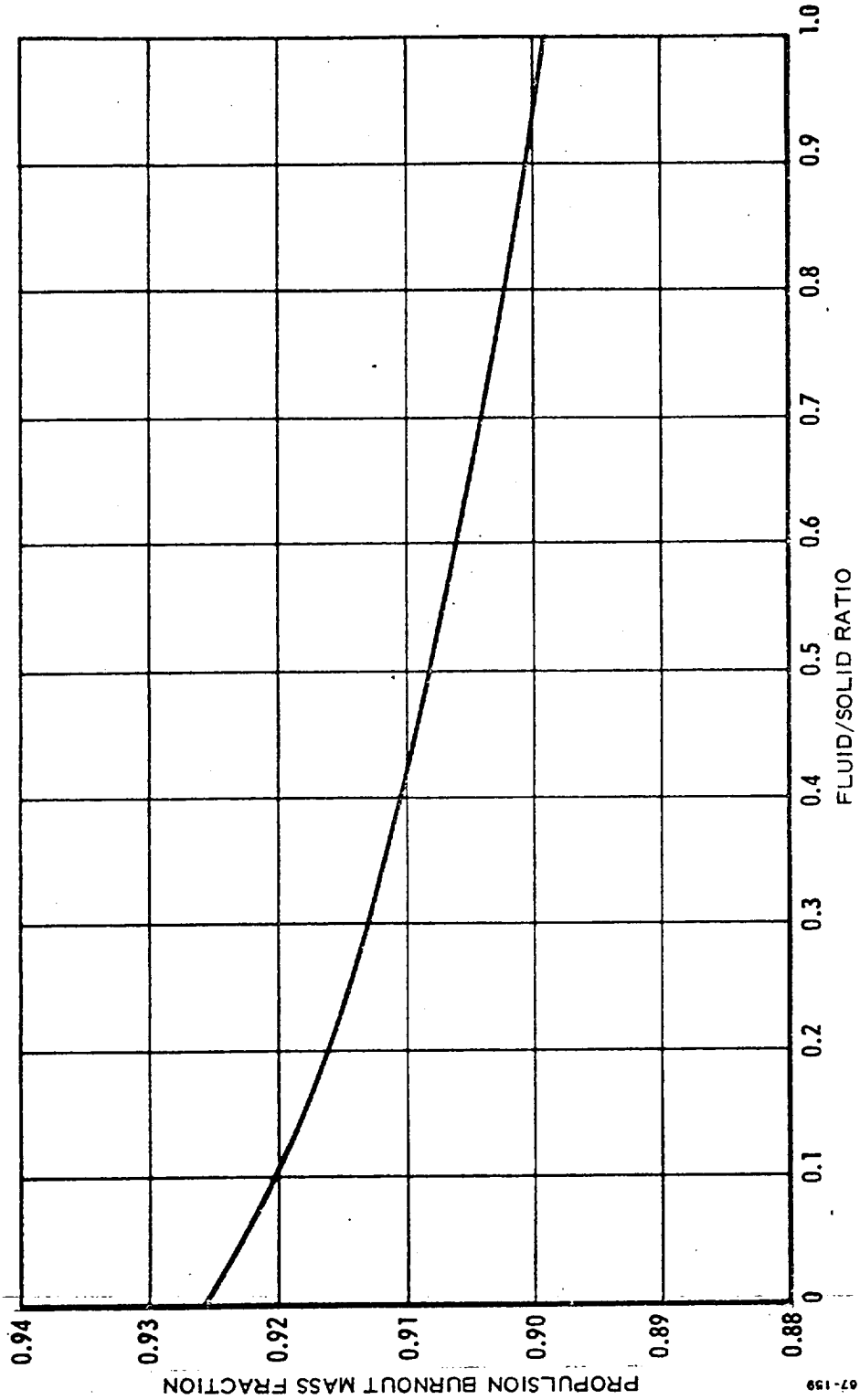

Figure 4-2 Effect of Fluid/Solid Ratio on Mass Fraction: Compound A RSVP, 5500 lb Motor

4.2 Alternate RSVP Versions

A weight breakown comparing hydrazine control with Compound A control is presented in Table 4.3. Hydrazine is more state-of-the-art than fluorinated liquid, has better storability potential, and can be tapped for state-of-the-art attitude or vernier monopropellant control. The hydrazine RSVP is shown to operate at lower F/S, because of performance dilution with increasing F/S. A similar breakdown comparing Compound A control with liquid fluorine control is shown in Table 4.4. These results, for hydrazine in Table 4.3 and for fluorine in Table 4.4, can be used to modify the influence coefficients as presented in Table 4.2 for Compound A. At a given F/S, the weight differences arise mainly from differing liquid densities and insulation requirements.

Use of gaseous fluorine as control fluid provides the ultimate in control system simplicity. The only control components are a pressure regulator and a valve, and even the regulator can be eliminated if blowdown operation is satisfactory. For application to large motors, the mass fraction would be lower than for an equivalent Compound A system but not necessarily prohibitive; the chief disadvantage would probably be the prospect of handling large tanks containing considerable weights of the gas at high pressure at the launch site. For small motors, however (e.g. < 100 lbs total propellant) not only is this hazard reduced to potentially acceptable levels but the difference in mass fraction from the equivalent Compound A system is reduced. Indeed, for sufficiently small sizes where the liquid plumbing and pressurization weights become proportionately large, the mass fraction of the gaseous fluorine system becomes greater. Although long-term

THIS PAGE CONTAINS CLASSIFIED

INFORMATION AND IS PRESENTED

IN VOLUME V

THIS PAGE CONTAINS CLASSIFIED

INFORMATION AND IS PRESENTED

IN VOLUME V

THIS PAGE CONTAINS CLASSIFIED

INFORMATION AND IS PRESENTED

IN VOLUME V

storability of pressurized fluorine gas in flightweight systems is presently unknown, strong consideration should be given to this concept for small motor applications. A weight breakdown in two sizes is shown in Table 4.5. The fluorine tank safety factor is 2.0, as compared to 1.5 used for helium and 1.25 used for liquid and solid vessels.

5.0 RELIABILITY

Component failure modes and effects, and failure rate data, are presented in tabular form in the Appendix. These tables conform to SGC 1069 QR-1 Table 4-8 as the format for SGC 1069 QR-2 Table 4, and to SGC 1059 QR-2 Table 5.

Failure rate data were obtained from a similar study in association with General Dynamics/Convair, which applied failure rate data for liquid components. The data simply list failure rates for pertinent liquid and solid components; it is assumed that matching the two constitute no additional failure.

THIS PAGE CONTAINS COMPANY PROPRIETARY INFORMATION AND HAS BEEN DELETED EXCEPT FOR REPORTS LIMITED TO RESTRICTED DISTRIBUTION

THIS PAGE CONTAINS COMPANY PROPRIETARY INFORMATION

AND HAS BEEN DELETED EXCEPT FOR REPORTS LIMITED TO

RESTRICTED DISTRIBUTION

THIS PAGE CONTAINS COMPANY PROPRIETARY INFORMATION AND HAS BEEN DELETED EXCEPT FOR REPORTS LIMITED TO RESTRICTED DISTRIBUTION

THIS PAGE CONTAINS COMPANY PROPRIETARY INFORMATION AND HAS BEEN DELETED EXCEPT FOR REPORTS LIMITED TO RESTRICTED DISTRIBUTION

THIS PAGE CONTAINS COMPANY PROPRIETARY INFORMATION AND HAS BEEN DELETED EXCEPT FOR REPORTS LIMITED TO RESTRICTED DISTRIBUTION

THIS PAGE CONTAINS COMPANY PROPRIETARY INFORMATION

AND HAS BEEN DELETED EXCEPT FOR REPORTS LIMITED TO

RESTRICTED DISTRIBUTION

materials attack at high temperature levels. The latter appears to be the most critical area requiring technology improvement, simply because of a present lack of information. Continuation of solid propellant sterilizability characterization with appropriate development would be a close second, however; binder development is the most critical area here.

7.2 Influences on Operating Conditions

By causing a change in propellants and inert weights, it is possible that sterilization can affect optimum operating conditions. However such a change would not appear to be necessitated by sterilization.

7.3 Influences on Materials Selection

As mentioned above, reactive liquid attack on its container at high temperature is an important question requiring study.

Another effect of the sterilization might be the selection of ultra-high strength pressure vessel materials, where otherwise not economically justifiable; the effect of the temperature cycling on strength should be investigated.

Sterilization may also require development in the area of bonding and liner materials, similar to propellant binder development. Still other factors include hydraulic system components, nozzle insulation materials temperature cycling and LOCKSEAL element integrity, temperature cycling of fittings and joints, expulsion bladder apart from liquid attack, and electrical components as they pertain to choice of materials.

7.4 Influences on Weight

The prospect of sterilization would make the advanced techniques of a hot gas generator or main tank injection for liquid pressurization more attractive for the RSVP, than it otherwise might, from a weight standpoint. Of course, for a liquid or ordinary hybrid, the volume of liquid in question causes a significant penalty with inert gas pressurization even without sterilization.

Apart from the increased pressure and introduction of different thermal stresses caused by the sterilization, with associated conservative design, sterilization can influence weight by affecting choice of materials for chemical and thermal cycle compatibility. Pertinent study is recommended.

7.5 Influences on Reliability

The reliability of an RSVP motor, from an in-flight mission standpoint, would appear to be enhanced by the sterilization process. Not only would there be conservative design and choice of materials to withstand the sterilization cycle over and above the actual in-flight duty cycle, but also the sterilization offers an additional quality control test as a by-product. For example, the ability of the materials in contact with Compound A to withstand the temperature cycling would virtually assure long-term storage compatability in the mission. The ability of structures to withstand loads under high temperature (e.g. the helium tank, or the liquid tank holding vapor pressure) would add assurance to their functioning in the mission. Choice of the solid motor case material for strength after cycling can serve to reduce some effects of insulation failure modes, as would also be the case for nozzle components. Absence of leaking following sterilization would add assurances that leaking would be minimized during the mission. Hermetic

sealing for isolation purposes (bacterial and vacuum) would be necessary.

Because complete isolation of the unit is a part of the sterilization process, some thought should be given to techniques for remote detection of potential failure modes as brought about by sterilization prior to flight. This can be done to some extent by the instruments suggested in Table 4 of the Appendix, which can telemeter information and/or institute remedial action in space, but there may be other techniques which can be used while the system is still on the ground (e.g. X-ray). Having satisfactorily withstood sterilization, there would appear to be added assurance for in-flight success.

7.6 Influences on Development Time and Cost

It would appear that the demonstration of sterilizable solid propellant in the course of research and technology programs would be prerequisite for system development for a particular application. Consequently, no additional development time or costs need be incurred by the sterilization requirement in the course of propellant development.

It is difficult to assess, at this time, what sterilization will really do to component development time and cost. Conceivably, costs could come down in certain areas. For example, the sterilization requirement could dictate a choice of materials which although heavier may be easier to forge, form or machine. Compound A may not be suitable; an alternate liquid may be much cheaper although less energetic. Questions of this nature are yet to be resolved. Undoubtedly, sterilization introduces additional design problems which will increase design time and cost. Effects on production

costs will be a function of the sophistication of the design solutions and the choice of materials; here, labor costs will probably predominate and could increase or decrease depending upon the results. Certainly, additional testing and qualification would be necessary, which may turn out to be the major source of increased time and dollars as brought about by sterilization.

Costing exercise based upon design studies which account for sterilization are recommended so as to obtain information of a quantitative nature.

REFERENCES

(1) Campbell, P. and Woodward, J. "Chemical Thrust Modulation of Solid Rockets", Bulletin of the 17th NASA-JANAF Solid Propulsion Conference, pp. 247-264 (May 1961)

(2) "Hybrid Propulsion Research Program", Series of Progress Reports under Contracts DA-04-495-ORD-3577 (1962-1964) and DA-04-495-AMC-218(Z) (1965), Lockheed Propulsion Company

(3) "Feasibility Demonstration of Hybrid Propulsion System", Final Report on Contract DA-04-495-AMC-1632(Z) (Aug 1966), Lockheed Propulsion Company

(4) Panelli, G.C., "A Study of Hybrid Propulsion Systems for Apollo Lunar Landings and Takeoffs", Bulletin of the 19th Interagency Solid Propulsion Conference (Vol I, pp. 145-164, July 1963).

(5) Shea, D.C. and Hartzell, W.C., "Design Study of a Throttleable Hybrid Motor", Bulletin of the 20th Interagency Solid Propulsion Conference (July 1964).

(6) "A Study of Storable Prepackaged Hybrid Propulsion Systems", Final Report on Contract AF 04(611)-9893, Report AFRPL-TR-65-37, Lockheed Propulsion Company (Mar 1965)

(7) Coates, R.L., Cohen, N.S. and Bonin, J.H., "Thrust Magnitude and Restart Control of Solid Propellants by Injection of Hypergolic Fluids", J. Spacecraft & Rockets 4, pp. 354-359 (Mar 1967)

(8) Cohen, N.S. and Fuller, W.F., "Liquid-Controlled Motors for Post Boost Control Applications", to be presented at the 9th ICRPG Liquid Propulsion Conference, St. Louis, (Oct 1967)

(9) "Study of Fluid-Controlled Solid Propellant Rocket Motors (RSVP Motor)", Series of Progress Reports Under Contract NAS 7-444, Lockheed Propulsion Company (1966-1967)

(10) "Design of a Fluid-Controlled Solid Rocket Motor for a Space Application", Report 740-6-3861 on LMSC P.O. ITA 24-16080, Contract NAS 7-449, Lockheed Propulsion Company (Aug 1966)

(11) "Solid and Hybrid Propulsion for Near Future NASA Missions, Part 1, Upper Stage Applications", Final Report on Contract NAS 7-375, Lockheed Missiles & Space Company (Dec 1965)

REFERENCES (Cont'd.

(12) Smoot, L. D. and Price, C. F., "Regression Rates of Metalized Hybrid Fuel Systems", J. AIAA 4, 910-915 (May 1966)

(13) Smoot, L. D. and Price, C. F., "Regression Rate Mechanisms of Non-metalized Hybrid Fuel Systems", J. AIAA 3, 1408-1413 (Aug. 1965)

(14) Smoot, L. D., Price, C. F. and Mihlfeith, C. M., "The Pressure Dependence of Hybrid Fuel Regression Rates", J. AIAA 5, 102-106 (Jan. 1967)

(15) Fuller, W. F. and Taylor, D. E., "A Design Procedure for Selection of Hybrid Fuel Grains for Mission Applications", Bulletin of the First Joint AIAA/ICRPG Solid Propulsion Conference, Wash., D.C. (July 1966)

(16) Berman, K. and Moore, G. E., "A Solid-Liquid Rocket Propellant System", Jet. Prop. 26, 965-969 (Nov. 1956).

(17) Coates, R. L., Polzien, R. and Price C. F., "Design Procedures for Combustion Termination by Nozzle Area Variation", J. Spacecraft & Rockets 3, pp. 419-425 (1966)

(18) Coates, R. L. and Cohen, N. S., "Correlation of Solid Propellant Extinguishment Data", Proceedings of the Third ICRPG Combustion Conference (CPIA Pub. 138, Vol 1, pp. 213-219, October 1966)

(19) Coates, R. L., Cohen, N. S. and Harvill, L. R., "An Interpretation of L* Combustion Instability in Terms of Acoustic Combustion Instability Theory", ibid., pp. 291-303.

(20) Coates, R. L. et al., "Composition and Burning Characteristics of Solid Propellants for Controllable Motors", AIAA Propulsion Joint Specialist Conference, Wash. D. C., (July 1967)

(21) Various Papers Presented at the 7th and 8th ICRPG Liquid Propulsion Conferences (CPIA Publications 72 and 121, 1965 and 1966)

(22) Frazer, A. C. and Todd, M. A., "Development Status Report - A Controllable Solid Rocket for Post Boost Payload Deployment", Proceedings of the First Joint AIAA/ICRPG Solid Propulsion Conference (Vol 1, pp. 85-125, 1966)

(23) Anderson, F. A., Strand, L. D. and Strehlow, R. A., "Low Pressure Rocket Extinction", J. AIAA 1, 2669-2671 (Nov. 1963)

(24) "Compatability of Structural Materials with Hybaline A-5 and Compound A", Report AFML-TR-64-391, Pennsalt Chemical Co., King of Prussia, Pa. (1964); also, recent private communications with H. Miller of Pennsalt.

APPENDIX: TABULATION OF INFORMATION ACCORDING TO SGC 1069 QR-2 FORMAT

The following series of tables will attempt insofar as possible to follow the Space General format as presented in its report SGC 1069 QR-2. However, as discussed in the text, there is no RSVP "baseline" system save what may be arbitrarily defined. This has been done to some extent through physical description, performance and weights in the text, within the limitations of the RSVP development status as discussed in the text. The motor for which the most complete set of data are supplied corresponds to the 1000 lb CompoundA/Solid RSVP, as summarized in the second column of Table 4.1 in the text. The motor size depicted in Figure 2.2, however, corresponds to 5500 lbs of propellant, but is configured the same way.

Much of the tabulated information requires and makes reference to discussions in the text. It is hoped that these discussions will be included as necessary supplements in the report to the NASA.

SGC 1069 QR-2 TABLE 1 - GENERAL SYSTEM DESCRIPTION

Refer to sections in the text for the indicated descriptions.

- Physical Characteristics - Section 2.1.1
- Operational Description - Section 2.1.2
- Development Status - Section 2.1.3
- Description of General Ranges for Data - Section 2.2.1
- Subsystem Design Alternatives - Section 2.2.2
- Prediction Confidence Level - Distributed thru Sections 1 and 2

THIS PAGE CONTAINS CLASSIFIED

INFORMATION AND IS PRESENTED

IN VOLUME V

SGC 1069 QR-2 TABLE 3 - SUBSYSTEM AND COMPONENT WEIGHT DATA*

System Description	Dry Weight for Base System (lb)	Burnout Weight for Base System	Predicted Weight for Base System	Prediction Methods	Prediction Limitations	Expected Accuracy of Predicted Weight
100 lb Propellant Compound A/Solid	24.2	25.0	125.9	Preliminary Design	Particular design; cf. tables in Sect. 4	Fairly good
100 lb Propellant Gaseous Fluorine/Solid	34.7	36.8	138.3	As above	As above	Fairly good
1000 lb Propellant Compound A/Solid	125.2	135.6	1142.2	As above	As above	Fairly good
1000 lb Propellant N_2H_4/Solid	114.7	129.2	1134.7	As above	As above	Fairly good
5500 lb Propellant Compound A/Solid	514.2	562.0	6107.7	Detailed Design	As above	Good
5500 lb. Propellant Liquid Fluorine/Solid	557.3	604.4	6156.1	Detailed Design	As above	Good
10,000 lb Propellant Compound A/Solid	860	943	11,030	Preliminary Design	As above	Fairly good

*See Section 4 in text for discussion, weight breakdowns, approximate weight equation and curves.

SGC 1069 QR-2 TABLE 4 - COMPONENT FAILURE MODES AND EFFECTS

Component	Failure Mode	Failure Cause	Failure Effect	Failure Detection	Remedial Action	Mode Elimination or Rate Reduction
1) He tank to store pressurant	1) Leakage 2) Rupture	1) Diffusion through imperfections 2) Overpressure, excessive stress	1) Ranges from 0 to mission failure 2) Mission failure	1) Instrumental monitoring 2) Instrumental monitoring	1) Bleed in additional gas from supplementary tank 2) Vent	1) Carry excess gas; hermetic sealing 2) Conservative design & test
2) He fill valve to fill with pressurant	1) Failure to actuate during fill 2) Leakage during flight	1) Imperfections 2) Diffusion	1) None on mission 2) Ranges from 0 to mission failure	1) Pre-launch 2) Instrumental monitoring	1) Replace at launch pad 2) Actuate redundant valve or bleed in excess gas from supplementary tank	1) Quality control 2) Quality control, carry excess gas, hermetic sealing
3) High pressure He lines and fittings to transmit pressurant	Per He tank	Per He tank	Per He tank	Per He tank	Per He tank	Per He tank; also redundant plumbing in parallel
4) Explosive valve to arm liquid	Failure to operate	Squib failure or valve jam	Ranges from mission degradation to failure	Instrumental monitoring	Actuate alternate initiator or valve	Redundant initiator or valve in paralle Quality control
5) Pressure regulator to control liquid pressurization	Does not transmit design pressure	Poor setting, imperfect mechanism	Ranges from mission degradation to failure	Instrumental monitoring	Cut out bad regulator and employ standby regulator	Redundant regulator. Quality control
6) Liquid tank to store liquid	Rupture	1) Corrosion 2) Overpressure	1) Ranges from mission degradation to failure 2) Mission failure	1) —— 2) Instrumental monitoring	1) —— 2) Vent excess gas	1) Materials development; conservative design & test 2) Conservative design & test

SGC 1069 QR-2 TABLE 4 (continued)

Component	Failure Mode	Failure Cause	Failure Effect	Failure Detection	Remedial Action	Mode Elimination or Rate Reduction
7) Liquid fill valve	Per He fill valve	Per He fill valve; corrosion in flight	Per He fill valve	Per He fill valve; liquid vapor detector in hermetic seal	Per He valve; carry excess liquid	Per He fill valve; carry excess liquid
8) Expulsion bladder to provide positive liquid expulsion	Rupture	Bad welding or bonding; improper motion; corrosion; overpressure	Ranges from mission degradation to failure	Liquid vapor detection in ullage space	Design for positive expulsion to be supplied by acceleration to complete the pulse. The next pulse will require ullage rockets if alternate thrustors are available.	Conservative design & test Redundancy in e.g. attitude control or vernier motors
9) Liquid flow control valves: n number of starts, with or without throttling	1) Failure to operate 2) Leakage	1) Valve imperfection, bad signal or coil 2) Corrosion, improper seal; damage from tank corrosion	Ranges from mission degradation to failure	Instrumental monitoring	Use alternate circuit or redundant valve	Quality control Carry excess liquid. Filter liquid. Redundant valves
10) Liquid lines, fittings	Per He lines	Per He lines	Per He lines	Per He lines; liquid vapor detector	Vent, redundant plumbing in parallel	Hermetic sealing Excess liquid Redundant plumbing
11) Liquid Injector	1) Burn-up 2) Clogging 3) Commutative leak (throttling)	1) Thermal & chemical attack 2) Recirculation of condensed combustion products 3) Poor seal	Ranges from mission degradation to failure	1) Temperature sensor 2) Flow rate sensor 3) Flow rate sensor	---------	1) Conservative design, insulation 2) Filter liquid 3) Quality control

SGC 1069 QR-2 TABLE 4 (continued)

Component	Failure Mode	Failure Cause	Failure Effect	Failure Detection	Remedial Action	Mode Elimination or Rate Reduction
12) Filters to remove foreign material	Blockage	Tank corrosion, chipped materials, insoluable foreign matter in liquid	Ranges from none to mission failure	Flow rate sensor	----------	Control of syste and liquid cleanness; materials development to avoid corrosion
13) Control system to activate control functions	No signal or signal in error	Broken elements or distortion	Mission degraded or failed	Signal telemetry	Redundancy	Redundancy
14) Control system to institute remedial action	As above	As above	As above only if component fails	As above	As above	As above; required only if component fails
15) Cryogenic insulation (liquid fluorine)	Overpressure	Liquid boiling	Mission failure	Instrumental monitoring	Vent, carry excess liquid	Conservative insulation design
16) Decomposition chamber (for N_2H_4)*	1) No reaction 2) Rupture	1) Catalyst poisoning 2) Thermal stresses, clogging, overpressure	Ranges from mission degradation to failure	Instrumental monitoring	Institute redundant system	Redundant system; conservative design and test
17) Solid propellant	1) Grain cracking 2) Unbonding 3) Failure to extinguish	1) Hard ignition, poor mechanical properties 2) Poor processing 3) Leakage into chamber	1,2) Chamber overpressure; degrades mission, or mission failure if burst 3) Mission degradation	Instrumental monitoring	--------- --------- 3) Redundant valve	1) Continuous check & control of propellant properties durin manufacture; ignition development to avoid hard start 2) X-ray inspection after fabrication 3) Redundancy

*For gaseous fluorine, replace helium with fluorine in Items 1-3; eliminate Items 4, 6, 7, 8, 10, 11 and possibly 5.

SGC 1069 QR-2 TABLE 4 (continued)

Component	Failure Mode	Failure Cause	Failure Effect	Failure Detection	Remedial Action	Mode Elimination or Rate Reduction
.8) Solid Propellant Combustion Chamber	Rupture	Overpressure	Mission failure	Instrumental monitoring	Shut off liquid at certain pressure level until cause is determined	Conservative design and test
.9) Chamber insulation	1) Burnthrough leading to burst 2) High backside temperature	Unbonding, thin areas, materials degradation & charring in multiple stop-restart	Mission degradation	Thermocouple instrumentation of case material	Shut off liquid to avoid case rupture	Conservative design & test. X-ray inspectio
20) Nozzle structure						
a) Subsonic approach	Disintegration	High ablation rate, poor material, cracking due to thermal & pressure stresses	Mission degradation	Sensors	--------	Conservative design & test; material qualit control
b) Nozzle throat (pyrolytic graphite)	1) Ejection 2) Erosion	1) Thermal & pressure stresses 2) Combustion products flow	Mission degradation	Interior ballistics monitoring	--------	Conservative design & test; material quality control
c) Throat backing heat sink	Cracking	Thermal stress	Poor conduction of heat away from nozzle approach & throat; possible mission degradation	Sensors	--------	Conservative design & test; materials quali control
d) Nozzle exit cone	Rupture	Overpressure; inadequate insulation	Mission degradation	Accelerometer	--------	Conservative design & test for pressure & insulation requirements

SGC 1069 QR-2 TABLE 4 (continued)

Component	Failure Mode	Failure Cause	Failure Effect	Failure Detection	Remedial Action	Mode Elimination or Rate Reduction
e) Lockseal element for TVC	1) Unbonding of Lockseal elements 2) Cracking or disintegration of boot	1) Pressure & temperature stresses 2) Excessive ablation; thermal and pressure stresses; material defect	1) Mission degradation 2) Only in the resultant effect on the elements	Position indicator	If possible, coordinate an attitude control system with the main thrust	Conservative design & test
21) TVC actuation	Poor actuation or retraction	1) Hydraulic pump jam 2) oil leaks	1) Ranges from mission degradation to failure 2) Mission degradation	1)Position indicator 2) Hydraulic indicator	Per 20e	1) Quality control 2) Quality control, carry excess oil; consider electric drive actuator

SGC 1069 QR-2 TABLE 5 - SUBSYSTEM AND COMPONENT FAILURE RATES AND DEVELOPMENT FACTORS

Component	Failure Rate Motor on (per 10^6 Hrs.)	Failure Rate Motor Off (per 10^6 Hrs.)	Failures per 10^6 Cycles	Expected Operating Failure Rates After "N" Test Seconds
He Tank and Lines	100	100		
Filter	50	50		
Pressure Regulator	1250	1250		
Burst Diaphragms	100	100		
Fill Valves	3	3		
Ground Connections	3	3		
Liquid Tank and Diaphragm	500	500		
Solid Motor and Nozzle	32374	405		
Servo Actuators	12324	12324		
Control Valves	700	700		
Explosive Valve			100	
Hydraulic Pump	607	607		Use pertinent liquid and solid information where available.
TVC Actuators	3140	3140		
Liquid Lines	360	360		
Hydraulic Lines	360	360		

THIS PAGE CONTAINS COMPANY PROPRIETARY INFORMATION

AND HAS BEEN DELETED EXCEPT FOR REPORTS LIMITED TO

RESTRICTED DISTRIBUTION

THIS PAGE CONTAINS COMPANY PROPRIETARY INFORMATION AND HAS BEEN DELETED EXCEPT FOR REPORTS LIMITED TO RESTRICTED DISTRIBUTION

SGC 1069 QR-2 TABLE 8 - SUMMARY OF STERILIZATION CONSIDERATIONS

Refer to qualitative discussion in Section 7 of the text.

No quantitative data are available

HYBRID AND SOLID PROPULSION

UNITED TECHNOLOGY CENTER

UTC 2280 - FR

DESIGN CRITERIA FOR (HYBRID) SPACE PROPULSION SYSTEMS (U)

FINAL REPORT

Prepared for
Space-General Corporation
Under Contract No.
P. O. 1069-P-77818

July 1967

Prepared by:

Engineering Department
UNITED TECHNOLOGY CENTER
Division of United Aircraft Corporation
Sunnyvale, California

Report Submitted By:

J. O. Spano
Liquid/Hybrid Advanced Design Section

L. E. Fischer
Liquid/Hybrid Advanced Design Section

Approved By:

T. D. Myers, Project Engineer

B. R. Felix, Project Manager

CONTENTS

Section

FOREWARD

ABSTRACT

1.0 INTRODUCTION

2.0 HIGH ENERGY HYBRID PROPULSION SYSTEM
- 2.1 Hybrid Base System Design
- 2.2 Hybrid Propulsion System Component System Description
  - 2.2.1 Oxidizer valve
  - 2.2.2 Injector
  - 2.2.3 Hybrid Fuel
  - 2.2.4 Combustion Case and Liner
  - 2.2.5 FLOX Oxidizer
  - 2.2.6 Oxidizer Feed System
- 2.3 Hybrid Motor Performance
- 2.4 Hybrid Subsystem and Component Weight Data
- 2.5 Hybrid System Analysis (Description and Reliability Hybrid Prediction)
- 2.6 System Development and Production Costs

3.0 FW-4S SOLID PROPULSION SYSTEM
- 3.1 Solid Propellant Base System Description
- 3.2 Parametric Solid Motor Performance Data
- 3.3 Solid Motor System Analysis (Description and Reliability)
  - 3.3.1 Motor Success Diagram and Reliability Model Summation
  - 3.3.2 Ignition Subsystem
  - 3.3.3 Case Subsystem
  - 3.3.4 Nozzle Subsystem
  - 3.3.5 Attach Hardware Subsystem
  - 3.3.6 Propellant Reliability
  - 3.3.7 Reliability Growth of the FW-4S Solid Motor
- 3.4 Solid Motor System Development and Production Costs

4.0 VOYAGER MISSION ANALYSIS

5.0 SUMMARY AND CONCLUSION

REFERENCES

TABLES

List of Tables

2-I 3rd Stage Delta Hybrid Propulsion Requirement
2-II Composition of High Energy Hybrid Fuels
2-III UTC Hybrid Motor Performance Evaluation
2-IV Hybrid Motor Performance
2-V Hybrid Subsystem and Component Weight Data
2-VI High Energy Hybrid Propulsion System Weight Summary
2-VII First Unit Production Cost
2-VIII High Energy Hybrid Propulsion System Costs

3-I UTC Solid Propellant Performance Evaluation
3-II Solid Propellant Subsystem and Component Weight Data
3-III Inherent Design Reliability for Scout Motor
3-IV Ignition Subassembly Failure Modes
3-V Motor Care Subassembly Failure Modes
3-VI Nozzle Subassembly Failure Modes
3-VII Attach Hardware Subsystem Failure Modes
3-VIII Propellant Performance Reliability
3-IX Propellant Subsystem Failure Modes
3-X FW-4S System Development and Production Cost Summary
3-XI FW-4S Development Cost Breakdown

FIGURES

List of Figures

2-1 Base Hybrid Grain Design (3 Spoke Cartwheel Fuel grain Configuration.
2-2 Base Hybrid Stage Design
2-3 Oxidizer Throttle Valve
2-4 Typical Hybrid Injector Assembly
2-5 High Energy Upper Stage Hybrid Propulsion System Flow Schematic
2-6 Normalized Combustion Efficiency of a Throttling Hybrid Motor
2-7 ODIE Theoretical Pefformance vs. Chamber Pressure
2-8 Kinetic Specific Impulse vs. Chamber Pressure (F=2K)
2-9 Kinetic Specific Impulse vs. Chamber Pressure (F=6.9K)
2-10 Kinetic Specific Impulse vs. Chamber Pressure (F-20K)
2-11 Hybrid Mass Fraction vs. Total Impulse (ΔV=5000 ft/sec)
2-12 Hybrid Mass Fraction vs. Total Impulse (ΔV=10000 ft/sec)
2-13 Hybrid Mass Fraction vs. Total Impulse (ΔV=15000 ft/sec)
2-14 Hybrid Mass Fraction vs. Total Impulse (N_2H_4 Gas Generator Pressurization)
2-15 Payload Weight vs. Liftoff Weight with Thrust Fixed
2-16 Payload Weight vs. Liftoff Weight with F/W Fixed
2-17 Hybrid Propulsion System Functional Success Diagram
2-18 Pressurization System Functional Success Diagram
2-19 Oxidizer Tankage Functional Success Diagram
2-20 Oxidizer Control Valve Functional Success Diagram
2-21 Electrical Control Unit Functional Schematic
2-22 Case and Insulation Functional Success Diagram
2-23 Nozzle Assembly Functional Success Diagram
2-24 Failure Mode Analysis
2-25 Hybrid Propulsion System Reliability Growth Potential
2-26 Hybrid First Unit and R&D Cost vs. Propellant Weight
2-27 Hybrid R&D Cost vs. Number of Equivalent Hardware Units.
2-28 Hybrid 1st Unit Production Cost per pound of Payload

3-1 Cutaway View of the UTC FW-4S Solid Motor
3-2 FW-4S Pertinent Motor Dimensions
3-3 FW-4S Motor Case
3-4 FW-4S Nozzle
3-5 FW-4S Igniter
3-6 FW-4S Ballistic Performance Summary at Vacuum Conditions
3-7 FW-4S Motor Ignition Transient
3-8 FW-4S Chamber Pressure and Thrust vs. Time Vacuum Conditions-200 RPM (70°F)
3-9 FW-4S Chamber Pressure and Thrust vs. Time Vacuum Conditions-0 RPM (70°F)
3-10 FW-4S Motor Temperature vs. Time
3-11 FW-4S Payload Acceleration vs. Time (0 RPM at 70°F)
3-12 FW-4S Payload Acceleration vs. Time (200 RPM at 70°F)
3-13 FW-45 Motor Weight Breakdown
3-14 FW-4S Motor Weight vs. Time
3-15 FW-4S Rocket Motor Mass Properties Sequential Breakdown
3-16 FW-4S Longitudinal Center of Gravity vs. Time
3-17 FW-4S Moment of Inertia vs. Time

List of Figures (Continued)

3-18 FW-4S Motor Limit Load Diagram
3-19 FW-4S Motor Cutaway, showing Internal Components
3-20 FW-4S Pertinent Internal Dimensions
3-21 FW-4S Vacuum Specific Impulse and Nozzle Weight vs. Nozzle Length
3-22 FW-4S Vacuum Specific Impulse vs. Burning Time
3-23 FW-4S Missile Attach Structures
3-24 FW-4S Propellant Weight vs. Case Length
3-25 FW-4S Average Nozzle Expansion Ratio and Throat Diameter vs. Case Length
3-26 FW-4S Specific Impulse vs. Case Length
3-27 FW-4S Total Impulse vs. Case Length
3-28 FW-4S Total Motor Weight vs. Case Length
3-29 FW-4S Mass Fraction vs. Case Length
3-30 FW-4S Motor Weight vs. Case Length
3-31 FW-4S Specific Impulse vs. Nozzle Expansion Ratio
3-32 FW-4S Nozzle Length vs. Nozzle Expansion Ratio
3-33 FW-4S Nozzle Diameter vs. Nozzle Expansion Ratio
3-34 FW-4S Nozzle Weight Change vs. Nozzle Length
3-35 Solid Motor Reliability Success Diagram
3-36 Ignition Subsystem Reliability Diagram
3-37 Case Subsystem Reliability Model
3-38 Nozzle Subsystem Reliability Model
3-39 Attach Hardware Subsystem Reliability Model
3-40 Total Impulse Reliability vs. Cutoff Accuracy
3-41 Solid Motor Reliability Growth vs. System Firings
3-42 Normalized Production Cost of FW-4S as a Function of Propellant Weight

1.0 INTRODUCTION

Unmanned space missions planned for the next 15 to 20 years include a wide range of propulsion system design requirements. High energy hybrid propulsion systems offer propellant specific impulse comparable to high energy bipropellant liquid propulsion systems while requiring approximately 40 percent fewer components in a typical application. The space storability of the hybrid propulsion system is excellent since only one liquid propellant tank is required, thus precluding a possible system failure from an insulation breakdown between two high energy liquid propellant such as fluorine and hydrogen. The fewer hybrid propulsion system components relative to a comparably performing bipropellant liquid propulsion system offers higher inherent system reliability and lower development costs. Hybrid propulsion systems are capable of thrust management and throttleability adequate for many mission requirements.

In order to allow realistic evaluations of the hybrid propulsion system performance for future space applications, parametric design data have been prepared and compiled under this subcontract. The hybrid design data compiled under this contract is to be used by NASA to evaluate the relative performance of liquid, hybrid, and solid propulsion systems for future unmanned space missions.

The hybrid performance, cost, reliability, and weight data were to be based primarily on the UTC throttleable, high energy hybrid development program performed under Contract NAS 7-475. The hybrid design covers a thrust range from 2000 to 20,000 pounds, a nozzle expansion area ratio range from 20 to 70 and a chamber pressure range from 75 to 500 psia.

Since hybrid propulsion systems are in the development stage much of the pertinent data relating to flight performance, reliability, and cost had to be predicted.

A parallel study was also to be completed for the Scout FW-4S solid motor. This study used existing design brochures, available cost information, and reliability studies. The solid motor data is for a single chamber pressure and grain configuration. Increases and decreases in total impulse were calculated by varying the case length and using the appropriate throat diameter to maintain the nominal 700 psia pressure. Data was readily available only for the solid propellant motor, hence no staging information was given in this study. The thrust range covered was from 3000 to 11,000 pounds.

Hybrid propulsion system design information for the Voyager program was not included in this report due to lack of available hybrid preliminary design study for this mission. A comparison of a solid propellant de-orbit motor for the Voyager vehicle calculated from the parametric FW-4S design data compiled under this contract and a separate UTC preliminary design study was included in this report.

2.0 HYBRID PROPULSION SYSTEMS

2.1 HYBRID PROPULSION SYSTEM

Under phase VII of NASA Contract No. NAS7-311, United Technology Center (UTC) provided design and analytical support to Douglas Aircraft Company (DAC), Missile and Space System Division, in a design study conducted to evaluate hybrid propulsion systems for upper-stage applications. The major application considered was the third-stage Delta designated DSV3E propulsion system.

Tradeoff design studies conducted by UTC and DAC resulted in optimum design specifications for the thrust chamber assembly (TCA)* of the third-stage Delta propulsion system. The design specifications are listed in Table 2-I. The resultant hybrid TCA design was chosen as the base system for generating parametric design data for this report. The design was based on a three-spoke cartwheel fuel grain configuration as shown in figure 2-1. The three-spoke design was chosen because more test data was available and good internal mixing was achieved with this number of fuel ports. However, variations of the base design can use a different number of spokes without significantly changing the grain ballistics or motor performance. The base stage design used for this report is sketched in figure 2-2. Descriptions of the motor and stage components are presented in the following paragraphs.

---

*The thrust chamber assembly of a hybrid propulsion system consists of the oxidizer control valve, oxidizer distribution manifold and injector assembly, fuel grain, combustion chamber, insulation, and exit nozzle.

TABLE 2-I

THIRD-STAGE DELTA HYBRID PROPULSION REQUIREMENTS

Parameter	Value
Chamber pressure, psia	250
Burning time, sec	110
Expansion ratio	52
Thrust, lb	6900
Grain diameter, in.	27.5
Fuel	HFX 2081
Oxidizer	80/20 FLOX
Mixture ratio	3.5
Number of starts (maximum)	5

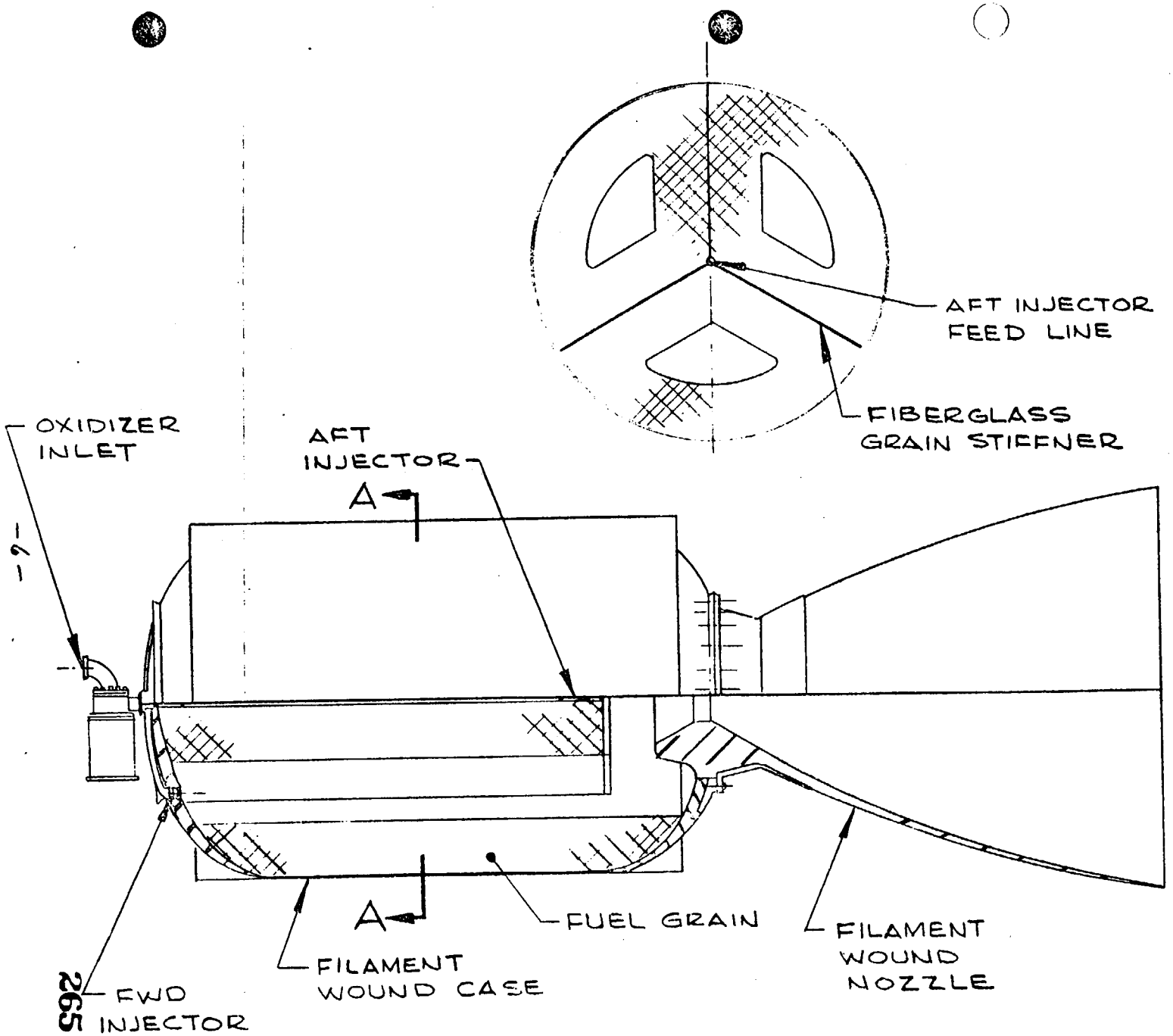

Figure 2-1 Base Hybrid Grain Design
(73 Spoke Cartwheel Fuel Grain Configuration)

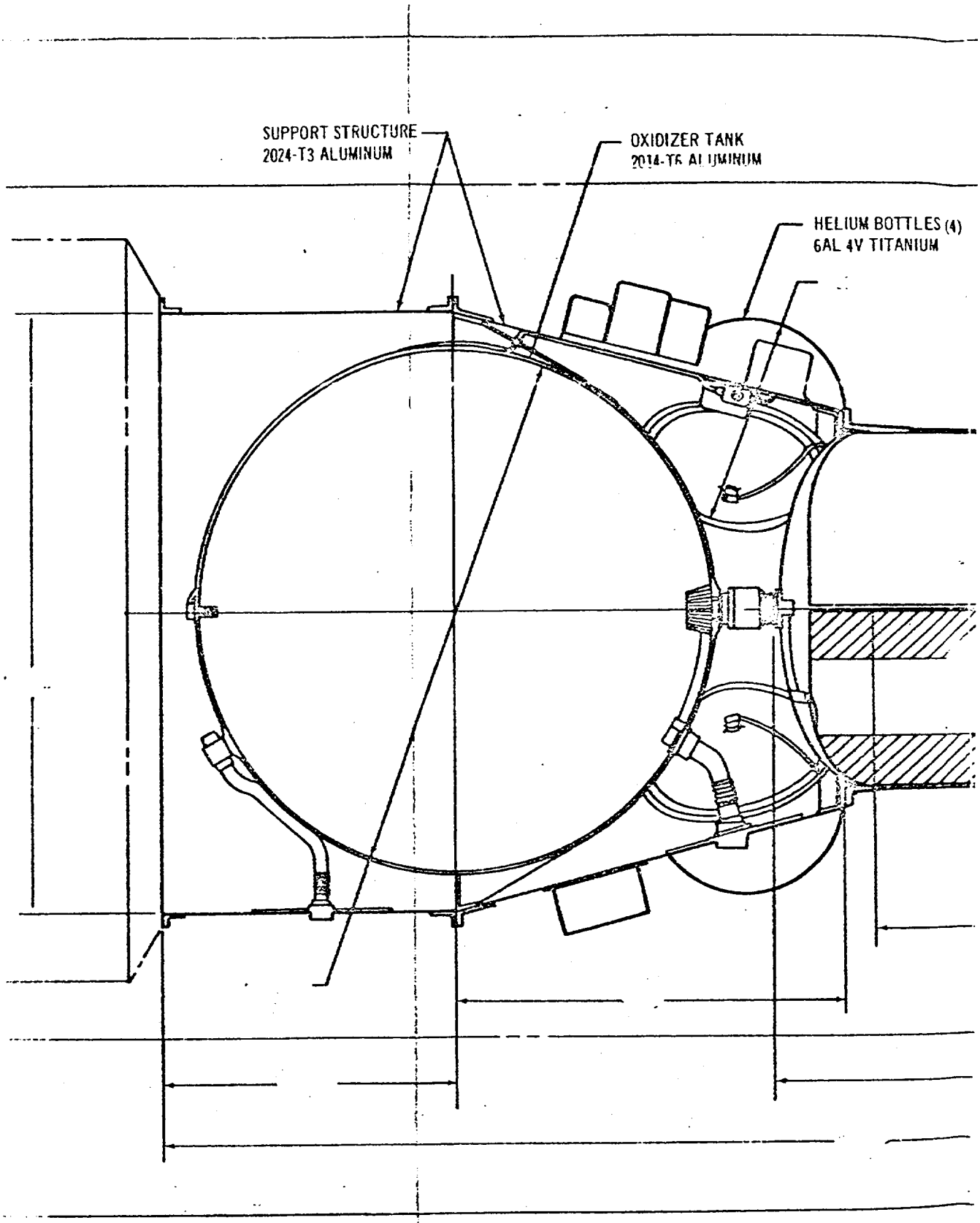

Figure 2-2 Base Hybrid Stage Desig

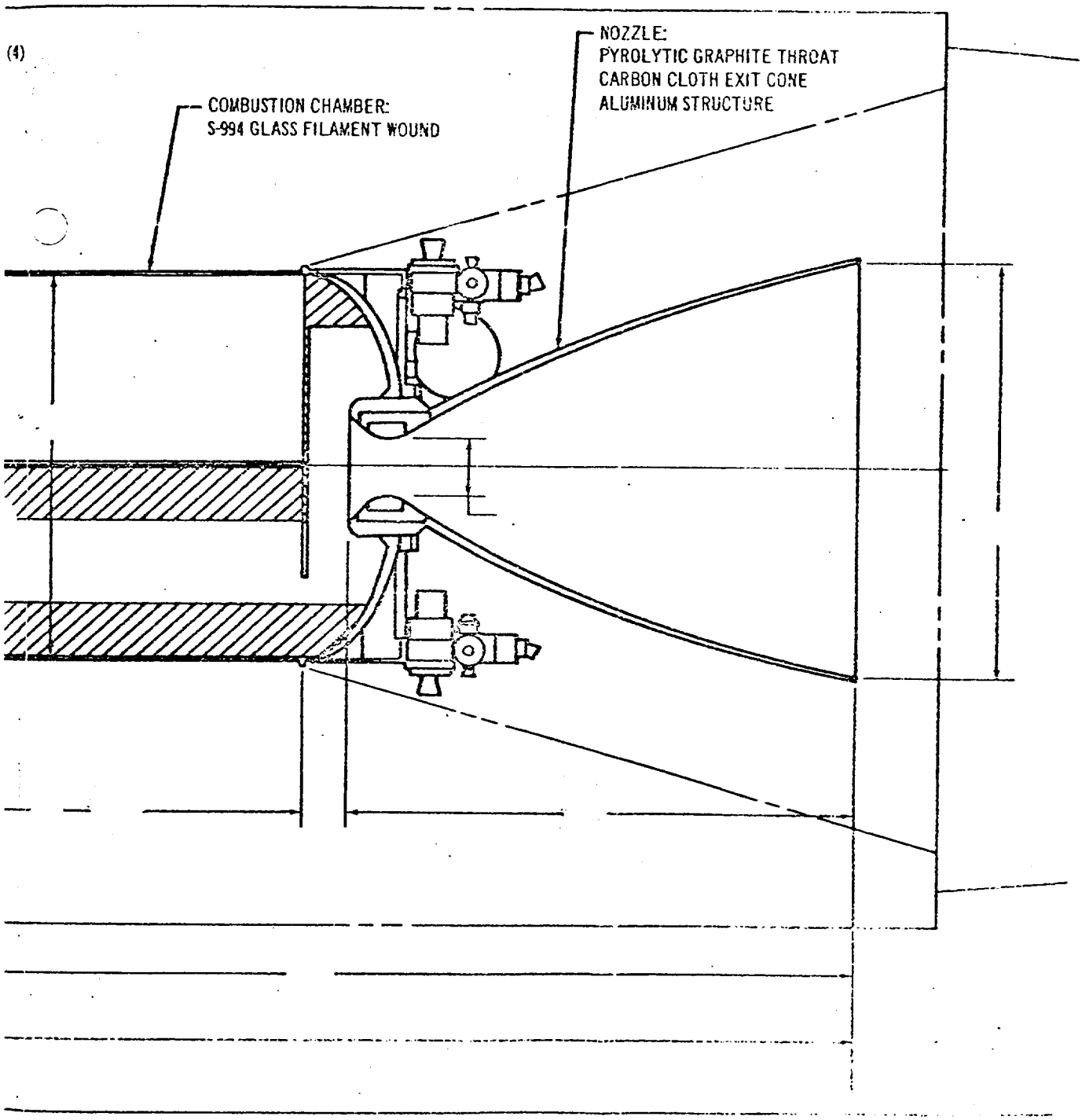
(4)
NOZZLE:
PYROLYTIC GRAPHITE THROAT
CARBON CLOTH EXIT CONE
ALUMINUM STRUCTURE
COMBUSTION CHAMBER:
S-994 GLASS FILAMENT WOUND

2.2 HYBRID PROPULSION SYSTEM COMPONENT DESIGN

2.2.1 Oxidizer Valve

An electrically actuated flow control valve based on redundant torque motors driving a translating pintle through a ball screw drive was selected for this application. This valve was selected over a pilot-operated solenoid valve, which was the next most promising valve, for two reasons: (1) substantial experience has been acquired with the torque motor valve configuration with FLOX and (2) high reliability can be achieved with this valve using triple redundant torque motors so that failure of any one actuator does not prevent the valve from operating. With solenoid valves; separate series parallel valves would be required to achieve comparable reliability. The oxidizer valve assembly is shown in Figure 2-3.

Aluminum was selected for the valve body material, resulting in a valve weight of only 6 lb. This weight corresponds to the valve weights of experimental units now being evaluated at UTC.

2.2.2 Injector

The oxidizer distribution manifold and injector assembly is an integral aluminum unit which also forms the polar boss and forward closure of the combustion chamber. One injector unit is provided at the forward end of the grain at the center of each fuel grain port. The injectors are fixed orifice spray nozzles. In addition, a centrally located wide-angle spray nozzle is incorporated in the aft face of the fuel grain. Approximately 10% of the total oxidizer flow rate is diverted to the aft end of the motor to improve combustion efficiency and to provide a means for preselecting lower thrust levels should this be desirable for alternative payload weights. By changing injector orifice sizes, the head and aft flow

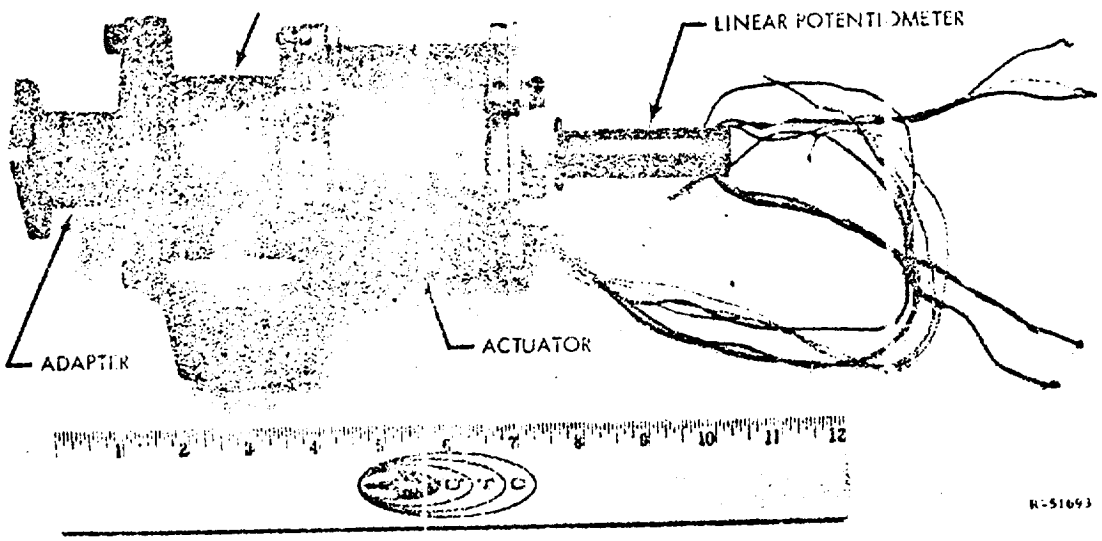

ASSEMBLED

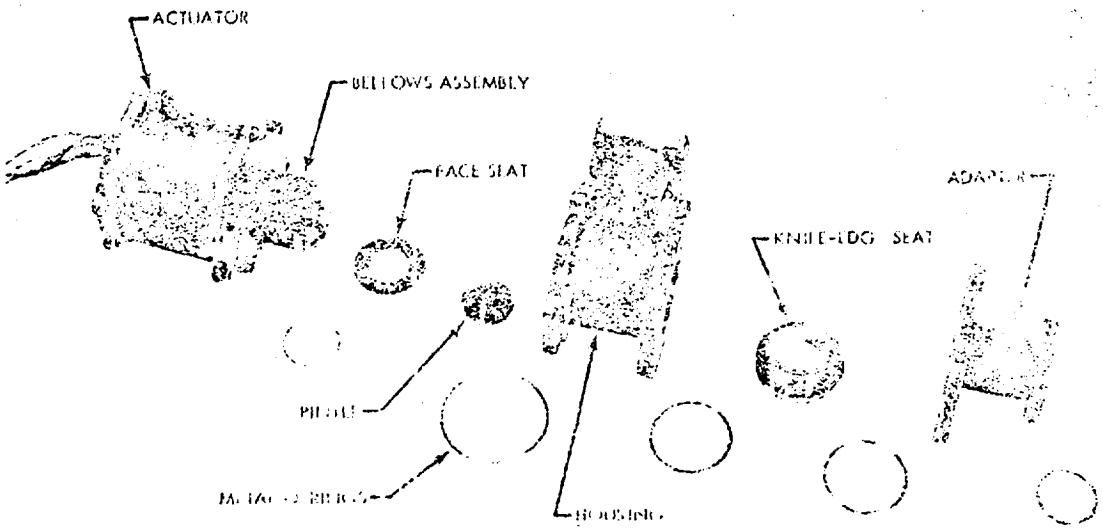

DISASSEMBLED

Figure 2-3 Oxidizer Throttle Valve

Reproduced from best available copy.

distribution can be adjusted to maintain the optimum propellant mixture ratio while operating at reduced thrust. A typical hybrid injector assembly is shown in Figure 2-4.

2.2.3 Hybrid Fuel Grain

A family of hybrid fuels based on high energy alkaline metals have been developed and extensively tested at UTC over the last four years. These fuels also simplify grain design because of their relatively high regression rates. The composition of five currently operational fuels, designated HFX 2080 through HFX 2084 are shown in Table 2-II.

TABLE 2-II

COMPOSITION OF HIGH ENERGY FUELS

(PROPRIETARY & CLASSIFIED)

The UTC fuel HFX 2080 was the first lithiated formulation tested in small motors. This formulation is not suitable for applications requiring restart, however, since it sustains combustion after oxidizer flow is terminated because of a reaction between the lithium metal and the binder. The fuels HFX 2081, 2, and -3 were subsequently formulated. These non-sustaining fuels vary only in binder composition. In HFX 2084, however, the binder level was increased to improve performance with OF_2 or (70/30 FLOX) by providing additional carbon for reaction with the oxygen in the oxidizer. This fuel is the optimum formulation for restartable (nonsustaining) operation with OF_2. In addition, HFX 2084 is

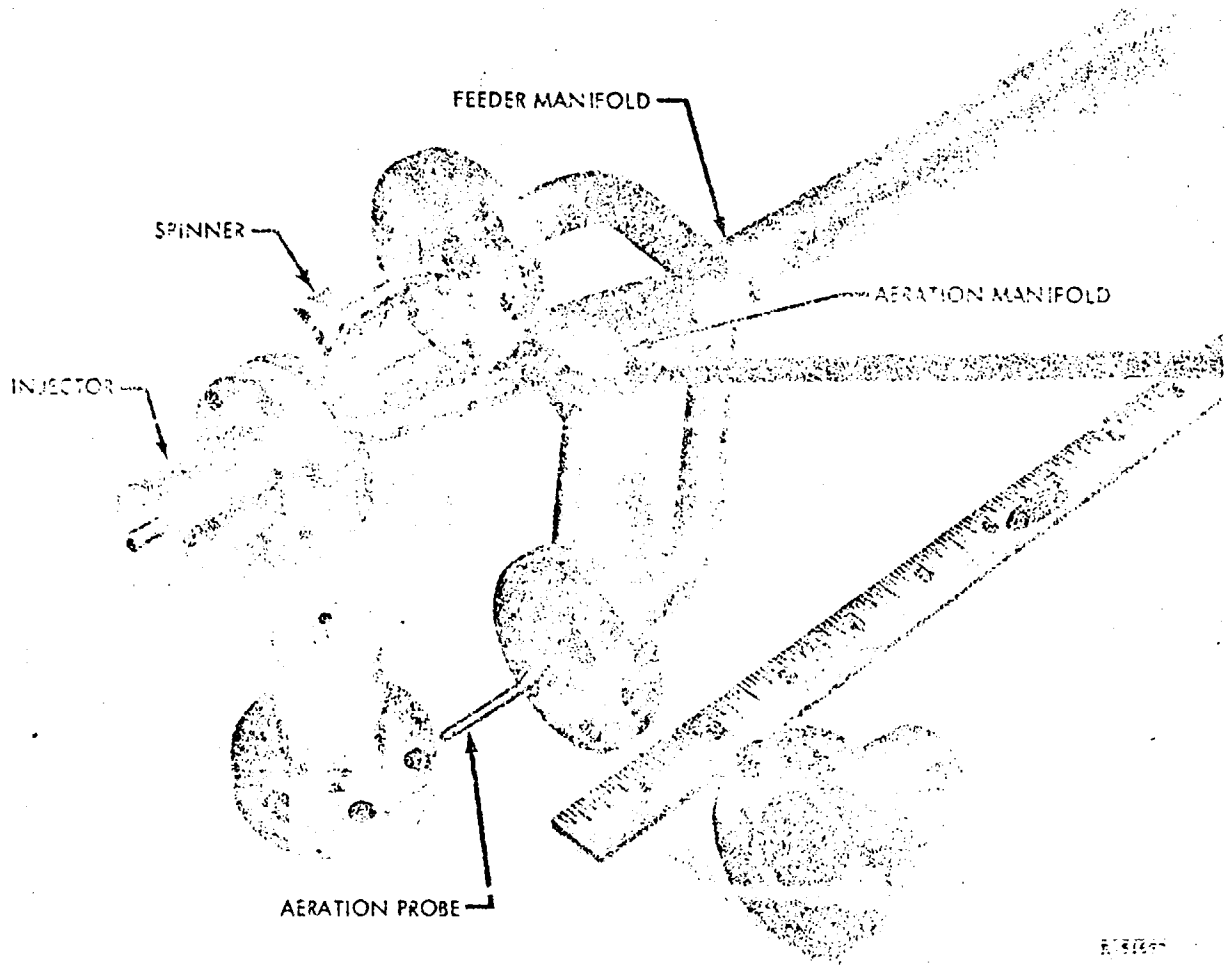

Figure 2-4 Typical Hybrid Injector Assembly

Reproduced from best available copy.

readily processed and cast by the conventional grain fabrication methods and cures into a tough rubbery fuel with excellent mechanical properties.

2.2.3.1 Grain Internal Ballistics

The internal ballistics behavior of lithiated fuel systems has been extensively characterized over a range of oxidizer mass flux values of to lb/in.^{2}-sec. It has been found that the regression rate of these fuel systems is accurately correlated by the following equation:

$$\dot{r} = A\, G_o^{\,n}$$

For this hybrid propellant system A =

n =

where

$\dot{r}$ = instantaneous regression rate, in/sec

G_o = instantaneous oxidizer mass flux lb/in^2-sec

A = constant characteristic of the particular system

2.2.3.2 Impact Sensitivity

Tests to determine the impact sensitivity of typical lithium containing fuels were conducted because the quantity of energy available from the lithium-hydrocarbon reaction indicated the possibility of shock-induced hazardous behavior. The impact sensitivities were measured under an argon atmosphere at standard conditions. No sparking, deflagration, or detonation were noted under an inert atmosphere with impacts up to 300 kg-cm, although sparking was noted at 60 kg-cm impact in normal atmosphere. The nature of the sparking suggested that metallic lithium was being ignited by friction from the striker. From these tests it was concluded that impact hazard is not a problem with these fuels. In addition, when some samples were ignited in air, they exhibited a low-order smoldering which was readily extinguished. No detonation has ever occurred.

2.2.3.3 Moisture Sensitivity

An indication of the susceptibility of lithium fuels to atmospheric moisture was provided by experiment. Slab samples of typical lithium fuels were stored at 40°C in air saturated with water vapor. Weight gains for the samples ranged from 4×10^{-6} lb/in^{2}hr. to 6×10^{-6} lb/in^2 hr. gain with time was asymptotic rather than linear reflecting a decreasing lithium concentration in the surface layers.

The lithium based fuel grains can be handled for short periods in a normal atmosphere because even under the severe test conditions, the weight gain was not significant during the first hours of exposure. Weighing and mixing of the fuel ingredients, however, are normally carried out under dry argon.

Experience obtained on the NASA contract (NAS7-311) with both subscale and fullscale motors has shown that these lithium fuel grains can be stored for up to six months without any degradation in performance. For instance, cast subscale fuel grains have been stored 4 to 5 months before motor assembly, restored another 4 to 5 months and operated satisfactorily in static test firings. Two fullscale 17-inch diameter fuel grains were cast into filament wound shells and assembled into a fiberglass flightweight type motor and stored 3 months before testing. One of these motors was stored another 5 months and again was successfully static fired. All the motors were stored in the same manner by placing three or four desiccant bags inside the assembly and sealing the nozzle and injector holes.

2.2.3.4 Vacuum Storage

Samples of typical lithium containing fuels have been subjected to

high vacuum in order to determine its behavior in space conditions such as those which typically occur during coast periods. Test samples were subjected to vacuum conditions at 150 miles simulated altitude. One set of samples was subjected to ten days storage at ambient temperature whereas the second set was subjected for a similar period of time but at +165°F. At the end of the test period, weight loss determinations were made as well as tensile testing to determine if any changes occurred in physical properties. No significant weight loss or mechanical property variation was noted in any of the samples.

2.2.3.5 Effects of Radiation

Several fuel samples have been subjected to radiation doses from a colbalt-60 source followed by testing on an Instron machine. Doses up to 9.3×10^6 rads which is representative of the maximum expected in two years space storage were imposed. The results of this radiation study indicated that almost no change in physical properties occurs. There appeared to be a small increase in maximum stress levels without changing the elongation properties, an effect similar to that of aging.

2.2.3.4 Vacuum Ignition

Ignition studies were conducted on lithiated fuels to demonstrate the vacuum hypergolic ignition characteristics of the system with FLOX and OF_2. A total of 15 motor starts, three with OF_2 and 12 with FLOX, were conducted at conditions simulating altitudes over 115,000 ft. Ambient pressure appeared to have little effect on ignition delay of this system, probably because the thrust chamber is pressurized by the vaporization of the oxidizer prior to any reaction. The major parameter affecting delay time appeared to be the oxidizer mass flux. At an oxidizer mass flux value of 0.025 lb/in^2-sec, which is lower than that which would exist during a restart with the proposed propulsion system, the ignition delay was

approximately 250 milliseconds with FLOX at -310°F. It is interesting to note that FLOX was found to be two to three times as reactive as OF_2.

2.2.4 Combustion Chamber

2.2.4.1 Case and Liner

The combustion chamber case was a glass filament-wound epoxy-resin structure with isotensoid end domes. The case design was based on a composite material strength of 128,000 psi and a safety factor of 1.25. The base design operating pressure was 250 psia. Equal polar opening diameters were employed to provide a constant wrap angle for the helical windings.

The case would be fabricated by wrapping over the preassembled and lined fuel grain and the fore and aft closure insulation. Helical windings would be applied to a thickness of 0.0132 in., prefabricated attach skirts bonded to the case, and additional hoop windings applied to provide a wall thickness of 0.0336 in. in the cylindrical section of the case.

An epoxy versamid liner 0.03 in. thick would be applied to the fuel grain and cured prior to wrapping the case. This liner protects the case for approximately three seconds should the fuel grain burn through locally when the fuel is nearly consumed.

2.2.4.2 Case Insulation

Nylon cloth phenolic was selected for the forward and aft closure insulation material. This material was selected because test data have shown it to have a moderate, even erosion rate with very little char formation. The maximum average erosion rate (near the nozzle) for this design would be approximately 0.0073 in/sec, based on test data.

Other insulation materials are available with lower erosion rates, however, these form a heavy char layer which radiates excessive thermal energy back to the fuel grain at shutdown. Such radiation deteriorates the aft face of the grain during coast periods.

The insulation was sized with 20% excess material to provide a margin of safety if uneven erosion occurs.

2.2.4.3 Nozzle

The exit nozzle is an uncooled design with a nozzle expansion area ratio of 52:1. The nozzle shape is a 70% bell contour.

The throat section is comprised of CARB-I-TEX with annealed pyrolytic graphite rings at the throat. The pyrolytic graphite rings are oriented to provide high thermal conductivity normal to the exposed material surface to prevent excessive erosion of the throat. Annealed pyrolytic graphite rings are employed to minimize axial growth of the rings.

The exit cone material is tape-wound graphite phenolic which has shown excellent resistance to erosion in tests with similar propellant combinations.

The base design assumes the most severe case of heat soak between engine restarts. In this case, the maximum thermal penetration occurs during coast and it is assumed that no significant amount of cooling has taken place prior to the next restart. Dependent on the duty cycle required of the motor, it may be possible to reduce the nozzle weight from 100 lb to approximately 60 lb, substantially increasing the motor mass fraction.

2.2.5 FLOX Oxidizer

Mixtures of fluorine and oxygen yield a very reactive oxidizer

with excellent performance. The physical properties of the two chemicals are very similar. One significant difference is found in their vapor pressures. These differences result in different boil-off rates which can result in a change in the composition of the remaining liquid if the boil-off gases are vented to the atmosphere. These composition changes can be completely precluded by including a condenser in the ground support equipment to recycle the boil-off gases back into the flight tank. Although the flight tank is insulated and loading takes place at the last practical time, some hold capability is necessary. In case of a test delay, even relatively long hold periods such as 10 days are feasible. This combination of requirements necessitates the use of a recirculating closed system rather than an atmosphere vent.

Both the NASA and Air Force programs conducted over the past four years have conducted extensive test firings with FLOX and Li/LiH/Binder fuel systems. In no instance has this combination resulted in a catastrophic incident or even uncontrolled combustion. For example, a pressure tap failure in one test stand control valve allowed a stream of FLOX to spurt through a ½ inch line under a pressure of 1000 psi. The stream happened to be directed upward in range of the recording cameras and was consequently recorded and studied. It was noted that even this large flow of liquid vaporized within a few feet of its entrance into the atmosphere. The resultant cloud of reactive oxidizer swirled about the motor test stand and quickly dissipated. No combustion occurred with the motor or on any of the test stand components.

2.2.6 Oxidizer Feed System

The liquid feed system includes the oxidizer tank with insulation, pressurization system and the associated feed lines, valves and fittings.

A flow schematic of the proposed system is presented in Figure 2-5 and a description of the principal items is presented in the following sections.

2.2.6.1 Oxidizer Tankage and Insulation

Type 2014-T6 aluminum was selected as the primary candidate material for oxidizer tank construction. The tank is fabricated in hemispheres and welded together. The material has a room temperature ultimate strength of 68,000 psi and a density of 0.100 lb/in.^{3}

The oxidizer tankage is insulated to preclude venting of the oxidizer to the atmosphere due to boil-off. The primary source of heat transfer to the oxidizer is through conduction at the points where the tankage and its support structure come into contact and through feed lines. Special design considerations were assumed for the study to minimize the effect of these paths.

A vent switch and valve assembly were used with the oxidizer tankage as a safety feature.

2.2.6.2 Pressurization System

Four spherical tanks were employed for the high-pressure helium supply. These vessels were designed for a rated pressure of 5250 psia, 750 psi above the nominal value. The tank material was 6Al 4V titanium alloy with an ultimate strength of 170,000 psi and a safety factor on the rated pressure of 1.5.

A two-stage pressure regulator was used between the helium supply and the oxidizer tank to provide a constant oxidizer tank pressure of 350 psia during motor operation.

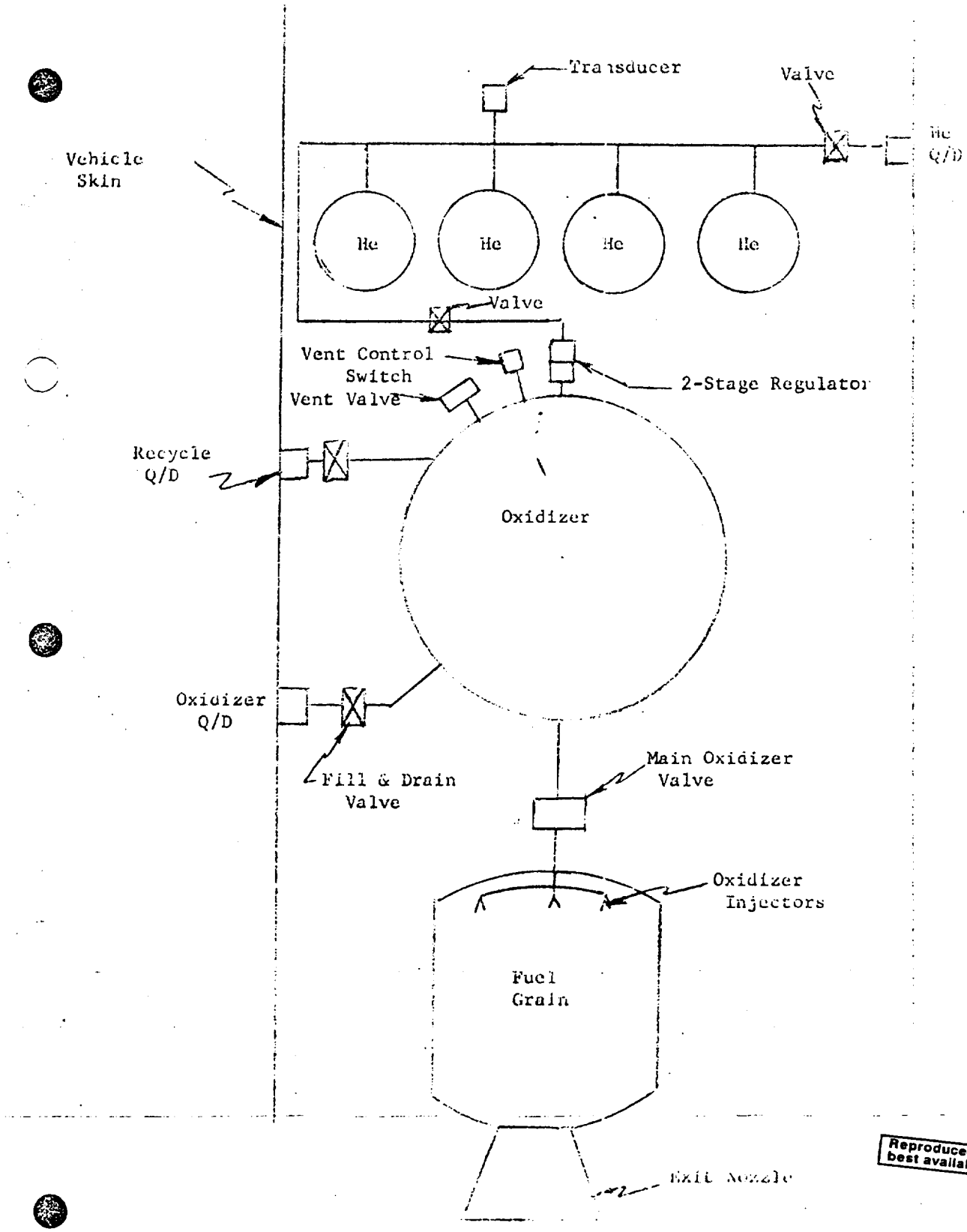

Reproduced from best available copy.

HIGH ENERGY UPPER STAGE [illegible] PROPULSION SYSTEM

Figure 2-5

Several alternate approaches to pressurization which can reduce pressurization system weight were considered. These systems were, (1) a turbopump feed system, (2) a helium pressurization system with the helium passing through a heat exchanger located in the exit nozzle prior to entering the oxidizer tank, and (3) a solid propellant augmented system wherein the solid propellant combustion gases are added to the helium pressurization system for the purpose of adding heat, and (4) monopropellant hot gas generator. These approaches were not selected for the base propulsion system primarily because it is believed that they would significantly add to development cost and time. They could be considered for an uprated stage.

2.3 HYBRID MOTOR PERFORMANCE

High-energy propellant systems, such as the systems of interest in this study, are characterized by high combustion chamber temperatures and theoretical equilibrium performance. The high temperatures encountered in the combustion of these propellant systems cause substantial dissociation of the combustion products. The rapid expansion os these exhaust products in conventional rocket nozzle contours does not allow equilibrium recombination of the dissociated species. As a result, a performance loss is encountered in the expansion process. Both chamber pressure and propellant mixture ratio affect the loss, due to their effects on reactant concentrations. This nonequilibrium or kinetic loss has been evaluated through the use of the Bray sudden freezing criteria in a UTC computer program . (Ref. 2-1)

Additional performance losses are experienced in a hybrid motor due to poor reactant mixing, local mixture ratio deviations, incomplete combustion, heat transfer, friction, divergence, two phase flow and possible weak shocks in the nozzle. The losses encountered in the engine can be measured by the

combustion efficiency η_{c*} and the nozzle stream efficiency η_{cf}. These losses are defined as follows:

$$\eta_{c*} = \text{Combustion efficiency} = \frac{C^* \text{ delivered}}{C^* \text{ shifting equilibrium}}$$

$$\eta_{c_s} = \text{Nozzle stream efficiency (vacuum conditions only)} = \frac{C_f \text{ delivered}}{C_f \text{ ideal}}$$

The η_{c*} efficiency is a measure of the efficiency of a selected injector and chamber design and accounts for all chamber losses due to incomplete combustion, poor mixing, and heat transfer. In the NAS7-311 program, UTC demonstrated combustion efficiencies in excess of 96% with FLOX-Lithium propellants. If the engine is throttled the combustion efficiency tends to decrease with thrust as shown in Figure 2-6. The combustion efficiency was measured for a 22-inch motor and has been normalized with respect to the fixed thrust efficiency.

The nozzle stream efficiency accounts for divergence, heat transfer, friction, two phase flow, and other acrodynamic flow losses which occur in the nozzle. This quantity is nearly independent in magnitude of the kinetic loss in the nozzle; therefore, the nozzle thrust coefficient $C_{f\ ideal}$ is the maximum thrust coefficient available to the engine after the kinetic loss has occurred. Then

$$C_{F_K} = \frac{I_{s_k}\, g}{c^*} = \text{Kinetic thrust coefficient}$$

therefore

$$C_{f_d} = \eta_{c_s} \cdot C_{F_K} = \text{Delivered thrust coefficient.}$$

The nozzle stream loss (η_{cs}) has been calculated for supersonic flow in bell nozzles with program such as that described in reference 2-2. These losses are as follows for two conventional bell nozzles:

K+E 10 TO ½ INCH 46 1473
10 INCHES MADE IN U.S.A.
KEUFFEL & ESSER CO.

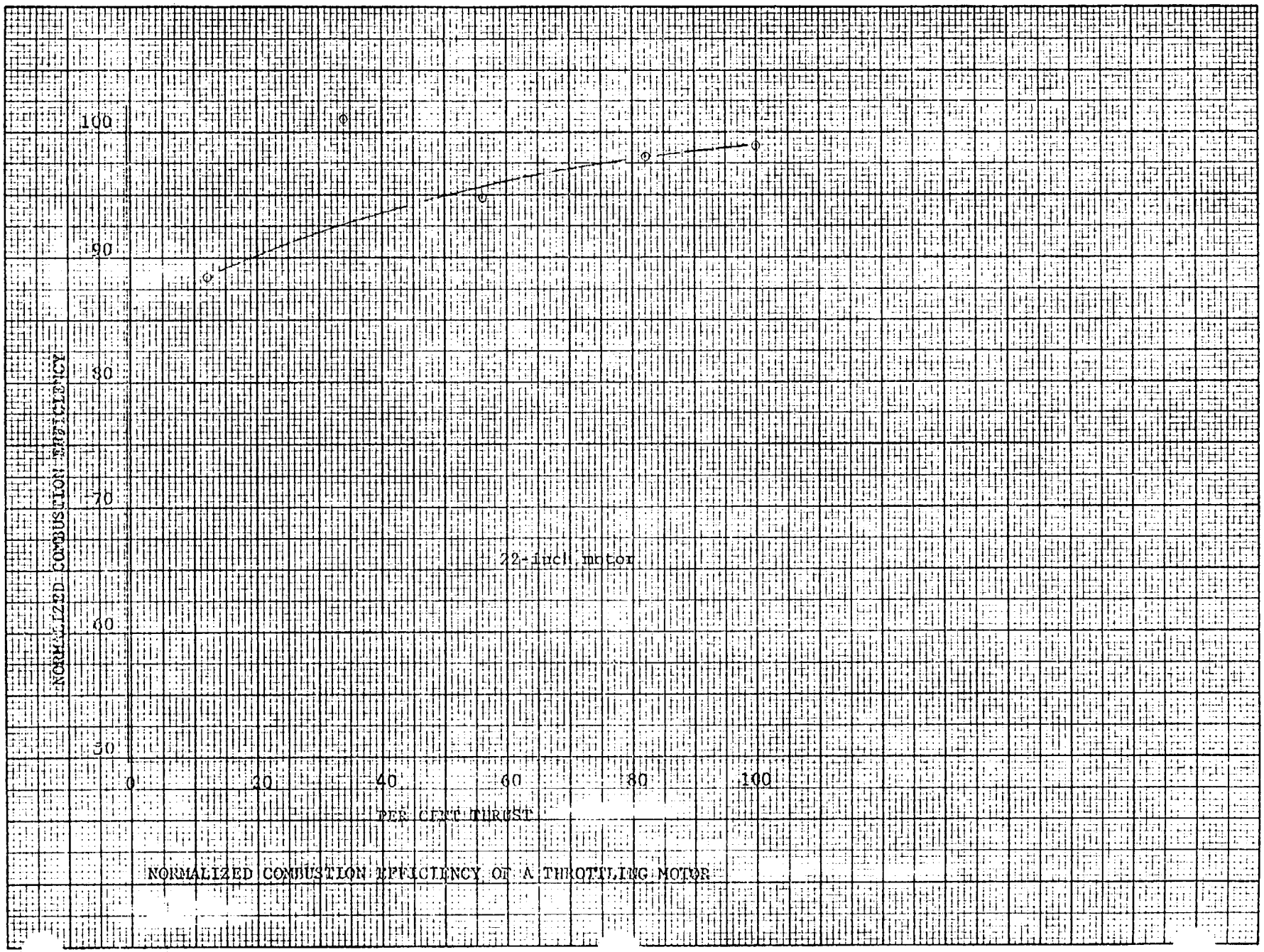

NORMALIZED COMBUSTION EFFICIENCY OF A THROTTLING MOTOR

Figure 2-6

	70% bell, ϵ = 40	80% bell, ϵ = 40
Divergence losses	1.5%	1.0%
Heat and friction losses	1.2%	1.2%
Nozzle stream efficiency	97.3%	97.8%

The performance model used to predict the delivered specific impulse is described as follows:

1. Performance losses are independent of each other.
2. Performance is calculated by

$$I_{sp} = I_{sp_{ODIE}} - \Delta I_{sp_{c*}} - \Delta I_{sp_K} - \Delta I_{sp_N} - \Delta I_{sp_\phi} - \Delta I_{sp_\epsilon}$$

where:

$I_{sp_{ODIE}}$ = theoretical shifting equilibrium specific impulse

$\Delta I_{sp_{c*}}$ = $I_{sp_{ODIE}} (1 - \eta_{c*})$ combustion loss

ΔI_{sp_K} = the kinetic specific impulse at the theoretical combustion temperature (η_{c*} = 100%)

ΔI_{sp_N} = $I_{sp_{ODIE}} (1 - \eta_{cs})$ = nozzle loss

$I_{sp_{2\phi}}$ = $I_{sp_{ODIE}} (1 - \eta_{2\phi})$ = two-phase flow loss

ΔI_{sp_ϵ} = $I_{sp_{ODIE}} (1 - \eta_\epsilon)$ = nozzle expansion area ratio loss (duty cycle).

This independent evaluation of the losses gives a straightforward method of predicting real engine performance. The model assumes that the interactions between the various performance losses are negligible. The method begins with the calculation of ODIE performance and combustion product composition and physical properties. The energy release performance losses are calculated and comprise the combustion losses. The kinetic losses are then calculated, based on the kinetics and thermodynamics of the recombination reactions of dissociated species.

Finally, the boundary layer and gas particle flow losses are summed to give the combined nozzle flow losses. The combustion, kinetic, and nozzle flow losses are summed to give a total I_{sp} loss which is subtracted from the ODIE performance to give the predicted delivered specific impulse. Mixture ratio variations are not included in the predictions, since they have not been established for the hybrid motor.

The predicted performance losses of the UTC hybrid motor are outlined in Table 2-III. The expected accuracy of the predicted performance is $\pm$ 10 seconds which is limited primarily by the accuracy of present kinetic rate constant data for fluorinated propellant systems.

Tests by UTC indicate that pulse mode operation of the high energy hybrid engine is currently not practical. Due to the variation of chamber volume with burn time the minimum impulse bit of the engine is predicted to vary between 700 and 2,000 lb-sec depending on the burn time. This and other pertinent performance data are summarized in Table 2-IV for the base system under consideration.

Parametric equilibrium and kinetic specific impulse data are presented in Figures 2-7 - 2-10. This data can be used to predict engine performance at various chamber pressures, expansion ratios, and thrust level by using the independent prediction technique. The combustion and nozzle flow losses can be considered to nearly/be constant over the ranges under consideration.

TABLE 2-III

UTC HYBRID MOTOR PERFORMANCE EVALUATION

Design Parameters

P_c	= 250 psia	M.R.	= 3.5
ϵ	= 52.0	F	= 6900 lb
% Bell	= 70		

Efficiency

Combustion (c*)	96%
Kinetic	Bray criteria
Nozzle flow	97.3% (98.5 divergence, 98.8 heat and friction)

Predicted I_s

$$I_{s_p} = I_{s_{pODIE}} - \Delta I_{s_{pK}} - \Delta I_{s_{pN}} - \Delta I_{s_{pc*}}$$

Propellant		FIOX/HFX 2080
Mixture Ratio		3.5
I_{s_p} ODIE		417 seconds
$\Delta I_{s_{pC*}}$	(Combined combustion chamber losses)	-16
$\Delta I_{s_{pK}}$	(Nonequilibrium loss)	-14
$\Delta I_{s_{pN}}$	(Combined nozzle losses)	-10
I_{s_p}	(Delivered specific impulse)	377

2-IV HYBRID MOTOR PERFORMANCE

Parameter	Measured Value (for "base" system)	Predicted Value (for "base" system)	Prediction Methods (Equations, Tables, Graphs, etc.) For New Systems	Limitations of Prediction Method (Thrust range, P_c range, throttle range, etc.)	Expected Accuracy of Predicted Performance
Steady State Isp Pulse mode Isp if applicable		377 sec @ E = 52.0 NA	Section 2.3	2000 - 20,000# 75 - 500 psia ε=20 - 70	± 10 sec
Minimum Impulse Bit		700 - 2000 Lb-sec			———
Reproducibility of Impulse Bit		Varies By 300%			± 100%
Total Impulse Cutoff Accuracy		.7%			± .3%
Throttled Performance		See Figure 2-6		8:1	± 2%
Thrust Vector Alignment		2 mrad			± 1 mrad
Thrust Centerline Offset					

K+E SEMI-LOGARITHMIC 46 4973
3 CYCLES X 70 DIVISIONS MADE IN U.S.A.
KEUFFEL & ESSER CO.

Reproduced from best available copy.

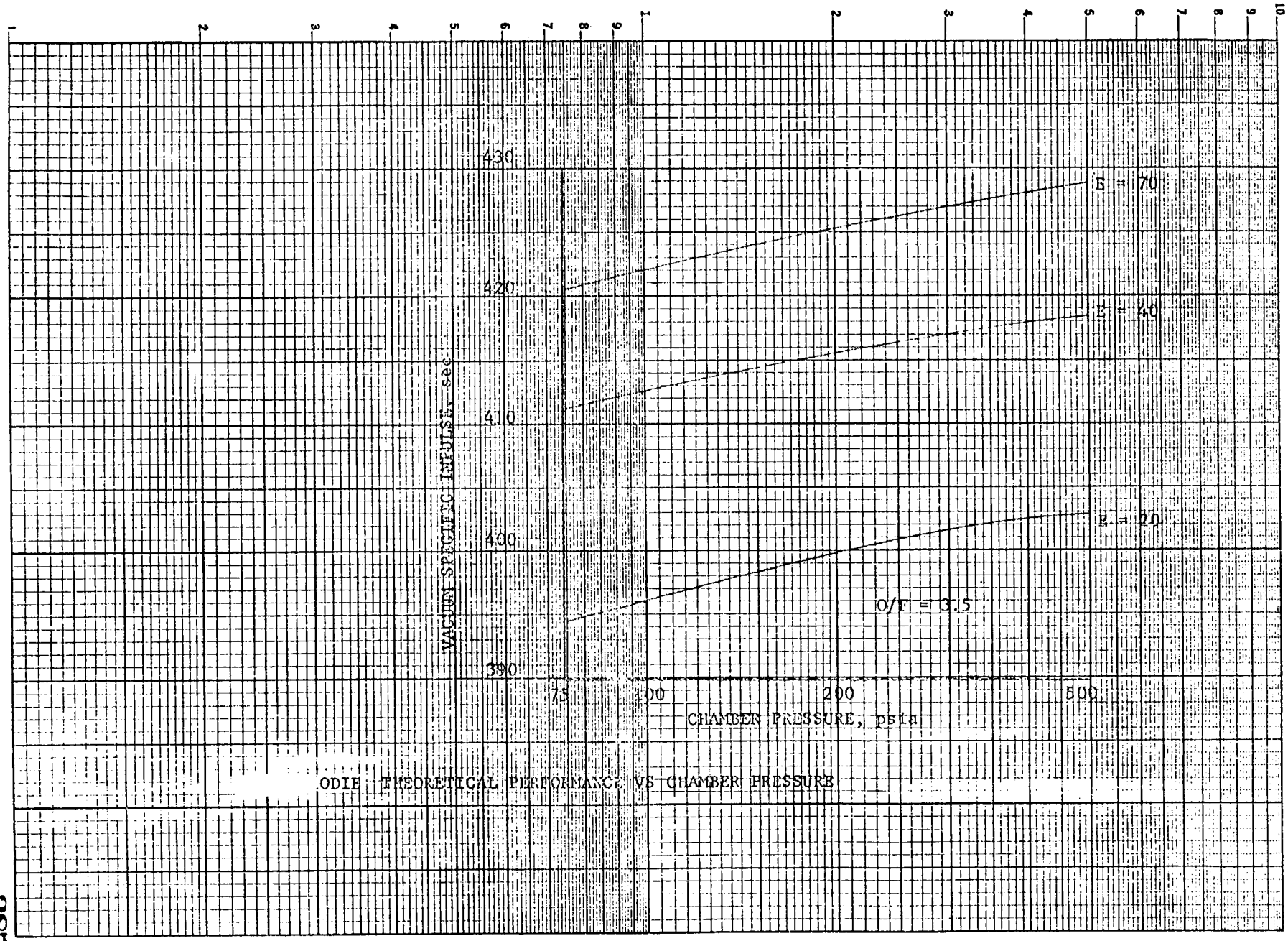

ODIE THEORETICAL PERFORMANCE VS CHAMBER PRESSURE

Figure 2-7

K+E LOGARITHMIC 46 4973
CYCLES X 70 DIVISIONS MADE IN U.S.A.
KEUFFEL & ESSER CO.

Reproduced from best available copy.

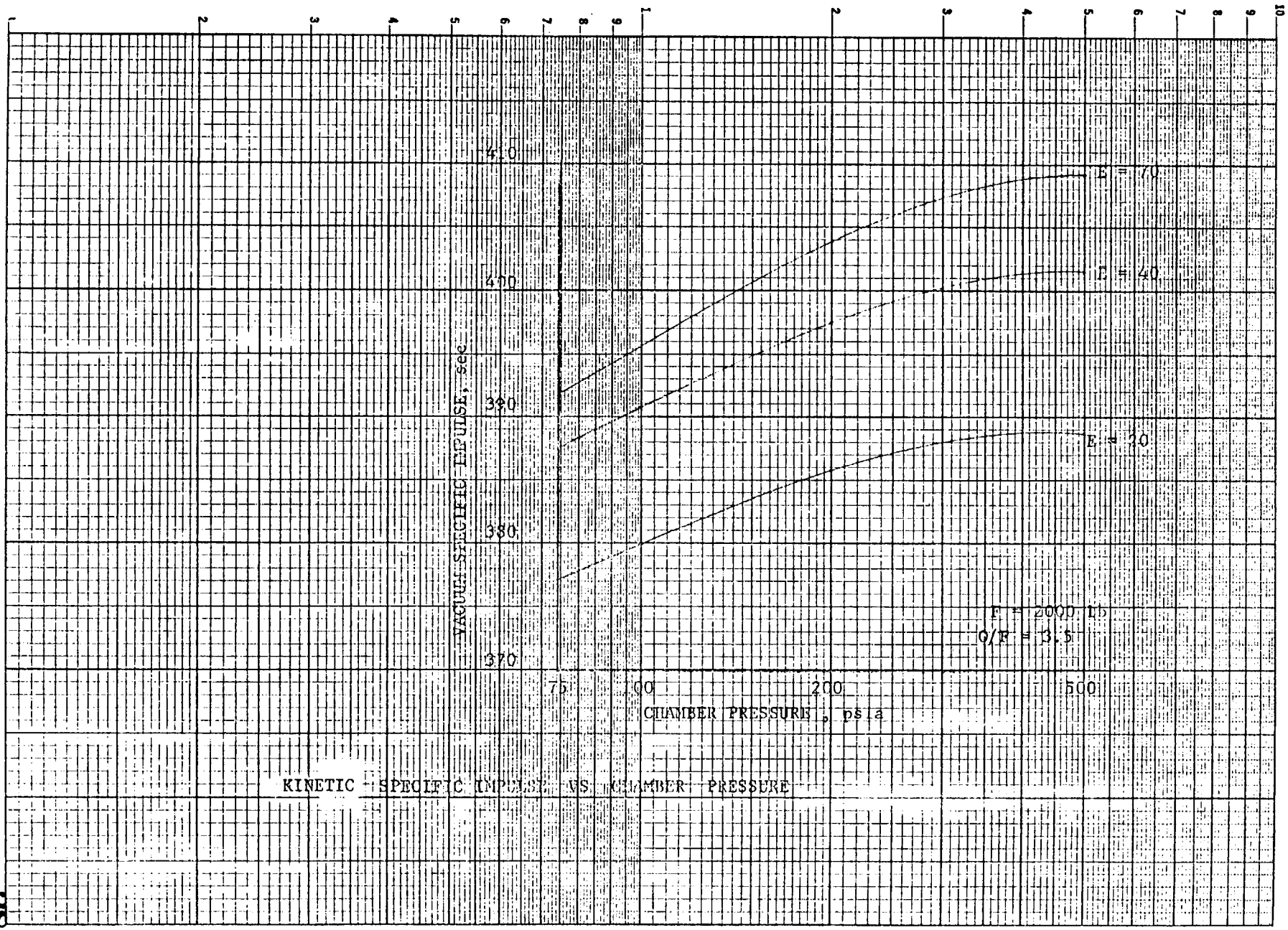

KINETIC SPECIFIC IMPULSE VS CHAMBER PRESSURE

Figure 2-8

K+E LOGARITHMIC 46 4973
2 CYCLES X 70 DIVISIONS MADE IN U.S.A.
KEUFFEL & ESSER CO.

Reproduced from best available copy.

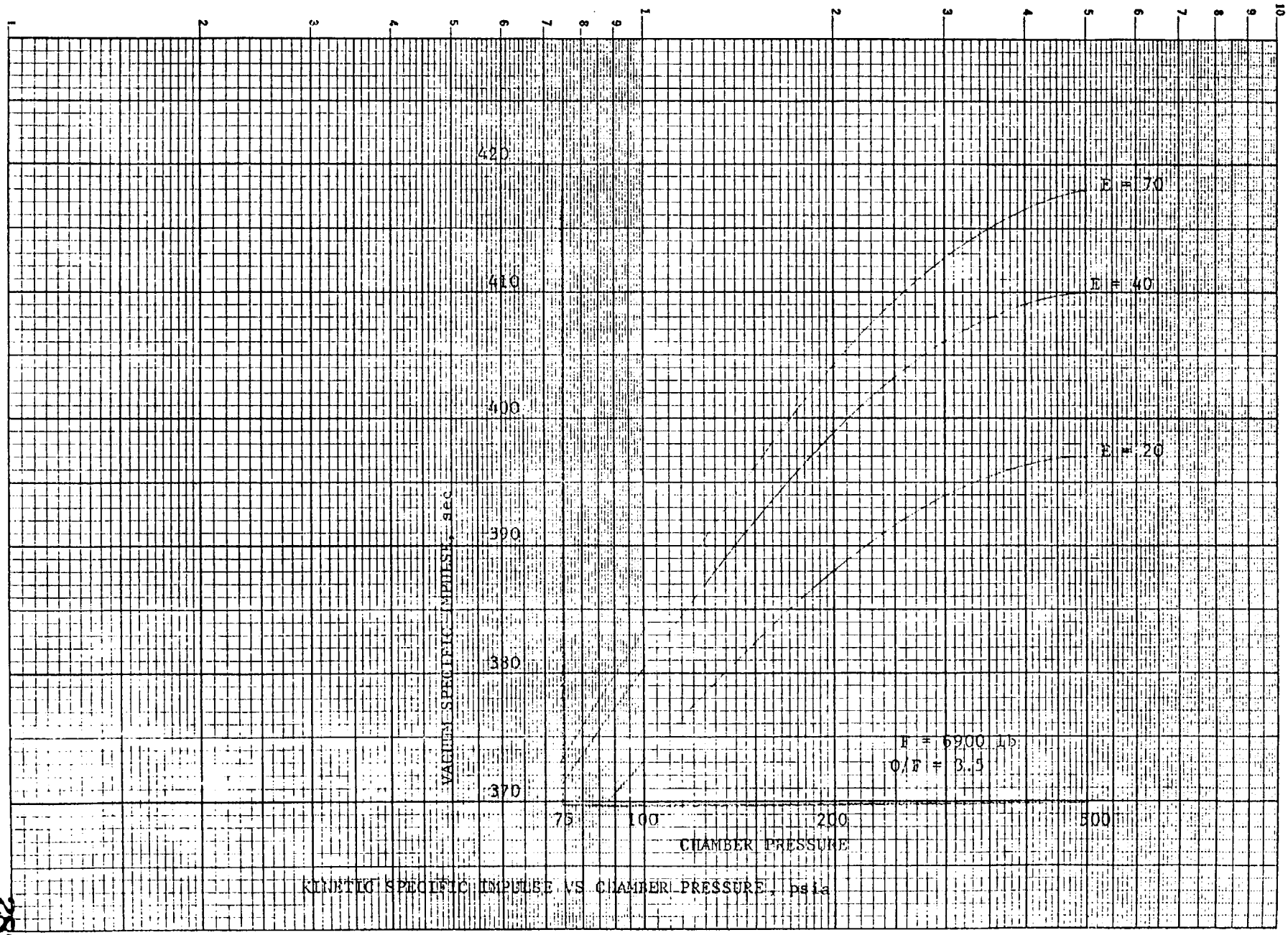

KINETIC SPECIFIC IMPULSE VS CHAMBER PRESSURE, psia

Figure 2-9

K+E S' LOGARITHMIC 46 4973
2 ES X 70 DIVISIONS MADE IN U.S.A.
KEUFFEL & ESSER CO.

Reproduced from best available copy.

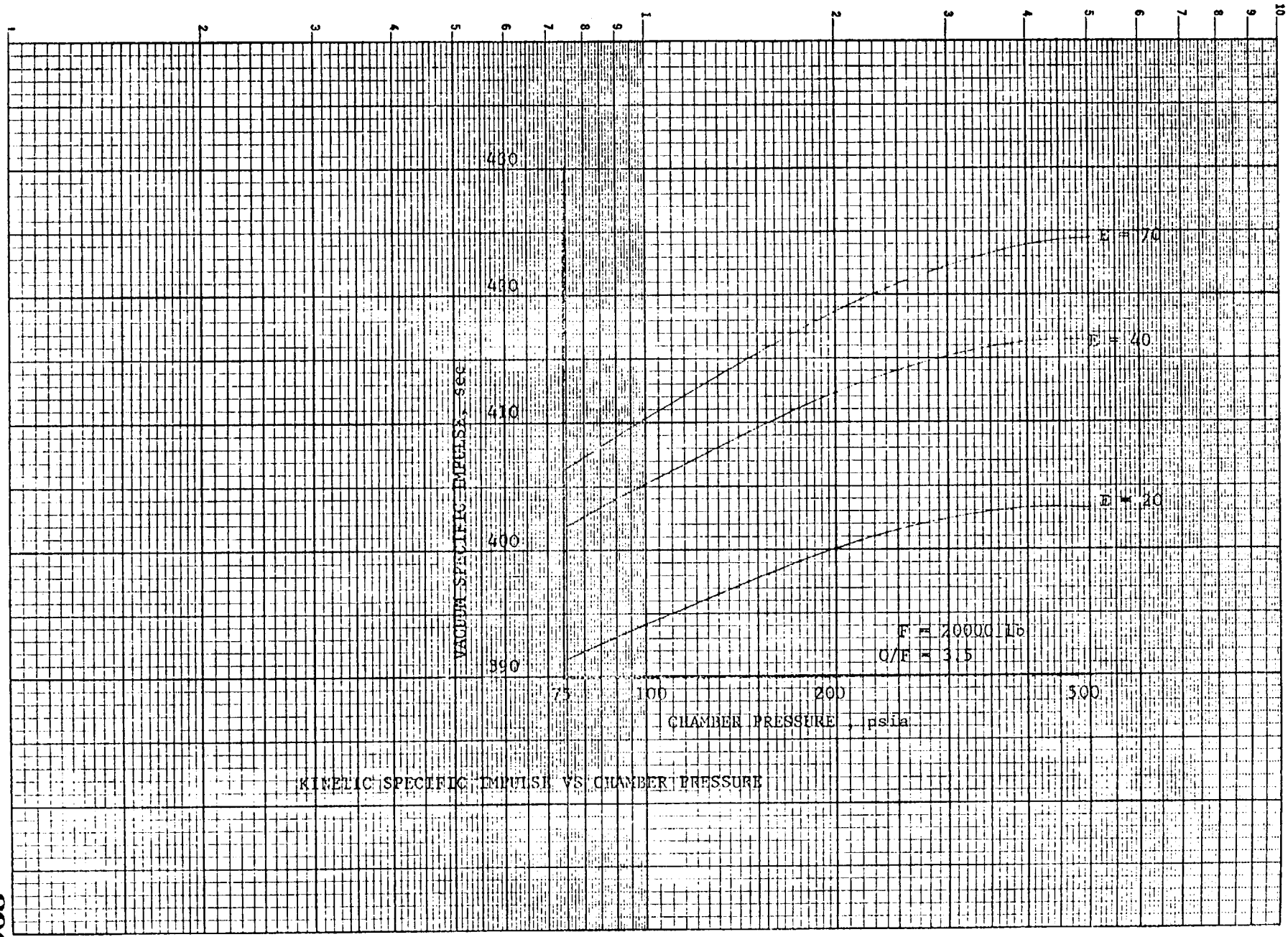

KINETIC SPECIFIC IMPULSE VS CHAMBER PRESSURE

Figure 2-1

2.4 SUBSYSTEM AND COMPONENT WEIGHT DATA

The component and subsystem weights were calculated with a computer program (HSWOP) developed at UTC over the past several years. HSWOP is a computerized method of calculating parametric design information for hybrid propulsion systems. The program allows an evaluation of the interactions and relative merits of the numerous design options such that the design resulting in optimum stage performance can be selected relatively rapidly and efficiently.

The basic propulsion system design criteria options available in the program are:

1) Specify lift off weight and payload weight.
2) Specify velocity increment and payload weight.
3) Specify lift off weight and velocity increment.
4) Specify lift off weight and weight of usable propellant.
5) Specify total impulse and velocity increment.
6) Specify total impulse and payload weight.
7) Specify usable propellant and velocity increment.

With any of above options specified the program calculates the hybrid propulsion system design parameters.

The program also defines the geometry of the nozzle and calculates the engine performance. With the nozzle geometry described by the length, expansion area ratio, percent bell, and exit diameter, the program defines the contour of the nozzle in X and Y coordinates and calculates the weight and balance.

The hybrid fuel grain is designed in accordance with the latest UTC hybrid grain design technology. The grain case is also calculated as a function of geometry, materials of construction and safety factor.

Finally, the weights for all the various subsystems and components of the stage such as the oxidizer tank, oxidizer tank pressurization system, the injector, oxidizer valve, and various other components are calculated. The expected accuracy of the dry weight calculations is within $\pm$ 10% for each component and $\pm$ 5% for the total propulsion system.

The weights of the thrust chamber assembly include the oxidizer control valve, oxidizer distribution manifold, injector assembly, fuel grain, combustion case, insulation, and nozzle. The oxidizer assembly includesthe feed and fill systems, oxidizer tank, oxidizer, and pressurization system. The weights of the propulsion system (thrust chamber assembly, oxidizer assembly) and the typical high energy hybrid stage (propulsion system, guidance electronics, support structure, miscellaneous) are tabulated in Table 2-V for the base system and Table 2-VI for the parametric design data. The motor and stage mass fractions are plotted in figures 2-11 through 2-13 for cold gas pressurization and Figure 2-14 for monopropellant pressurization. The mass fractions are defined as follows:

$$\text{Motor Mass Fraction} = \frac{\text{Usable Propellant Weight}}{\text{Propulsion System Weight}}$$

$$\text{Stage Mass Fraction} = \frac{\text{Usable Propellant Weight}}{\text{Hybrid Stage Weight}}$$

The expected accuracy of the stage mass fraction calculation is within $\pm$ ½%. The payload capabilities of several typical cold gas pressurized hybrid stages are plotted in figures 2-15 and 2-16 for $\epsilon = 40$ and $P_c = 150$ psia. A detailed description of HSWOP and several output listings appear in Appendix A which is proprietary.

TABLE 2V- SUBSYSTEM AND COMPONENT WEIGHT DATA
HYBRID

"BASE" SUBSYSTEM OR COMPONENT DESCRIPTION:	Dry Weight (for "base" subsystem) (Predicted)	WET Weight (for "base" subsystem) (Predicted)	Predicted Weight for the "base" system	Prediction Methods (Tables, Graphs, Equations, etc.) For New Subsystems	Limitations of Prediction Techniques (Thrust range, P_c range, etc.)	Expected Accuracy of Predicted Weight
TCA Assembly	185	643.		HSWOP	F= 2000-20000# P_c= 75-500 psia	± 5% on dry wt.
Oxidizer Assembly Design Alternative 1	154	1741.				
Propulsion System	339	2384				
Delta High Energy Stage	570	2630				

TABLE 2-VI

HIGH ENERGY HYBRID PROPULSION SYSTEM WEIGHT SUMMARY
(ϵ = 40, F/W_o = 1.92 ΔV = 10,000 ft/sec)
Dry Wt. Accuracy $\pm$ 5%
on Propulsion System

THRUST LEVEL lb_f	CHAMBER PRESSURE psia	DRY TCA ASSEMBLY lb_m	WET TCA ASSEMBLY lb_m	DRY OX ASSEMBLY lb_m	WET OX ASSEMBLY lb_m	WET PROPULSION SYSTEM lb_m	HYBRID STAGE lb_m
2,000	75	126	265	23	505	770	867
	150	84	222	32	501	723	856
	300	83	218	53	526	745	863
	500	87	222	82	556	779	897
6,900	75	264	737	60	1644	2381	2681
	150	200	669	98	1633	2303	2640
	300	171	632	170	1613	2246	2658
	500	172	630	270	1613	2244	2759
10,000	75	379	1065	84	2466	3532	3829
	150	281	961	139	2507	3468	3766
	300	246	914	244	2583	3497	3798
	500	250	914	388	2726	3641	3946
20,000	75	688	2046	158	4876	6923	7368
	150	498	1844	267	4955	6799	7247
	300	427	1750	475	5104	6854	7306
	500	433	1748	759	5389	7137	7595

K+E 10 X 10 TO ½ INCH 46 1473
7½ X 10 INCHES MADE IN U.S.A.
KEUFFEL & ESSER CO.

Reproduced from best available copy.

HYBRID MASS FRACTION VS. TOTAL IMPULSE (ΔV=5000 ft/sec)

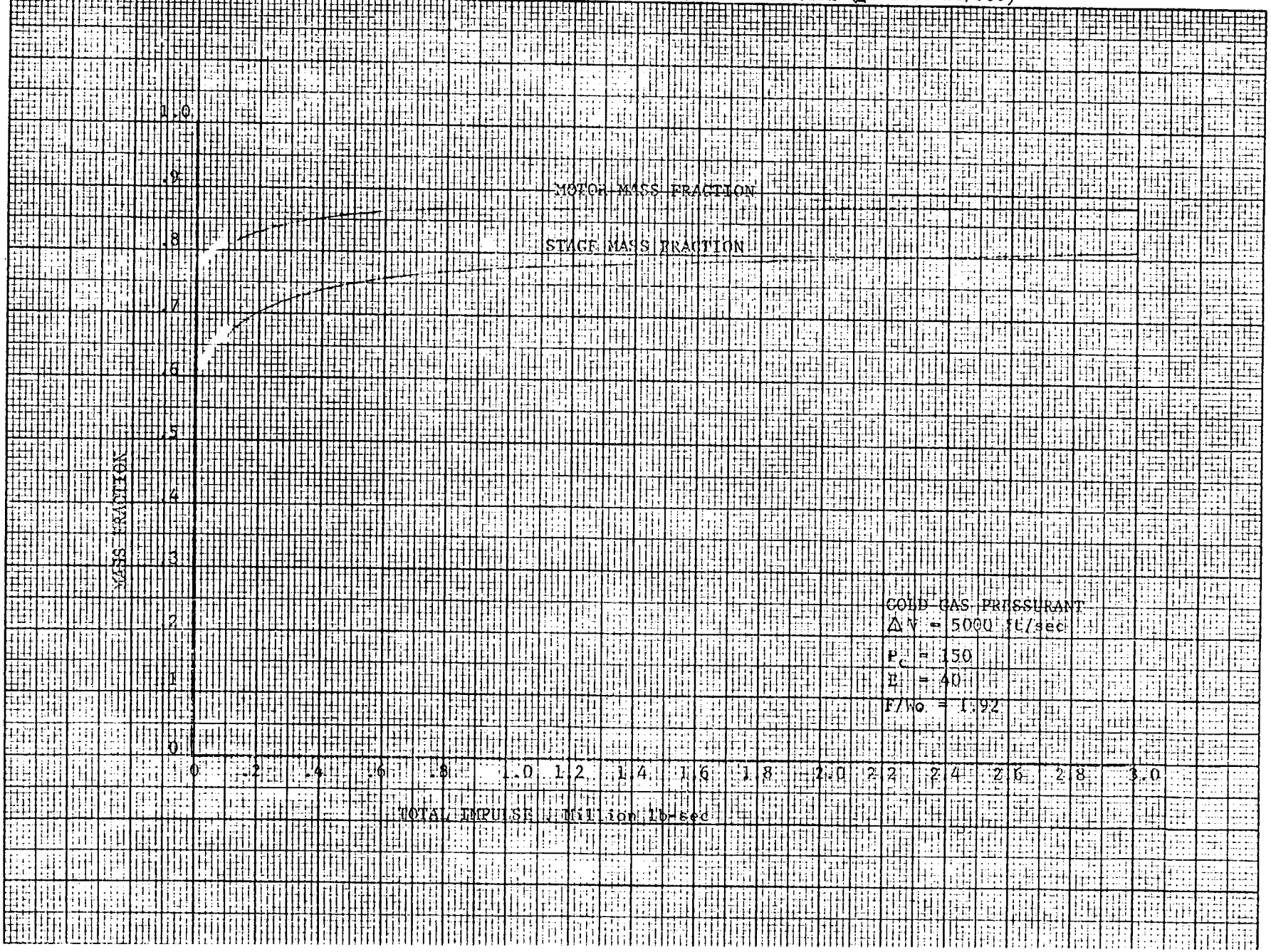

Figure 295

K+E 10 TO ½ INCH 46 1473
10 INCHES MADE IN U.S.A.
KEUFFEL & ESSER CO.

Reproduced from best available copy.

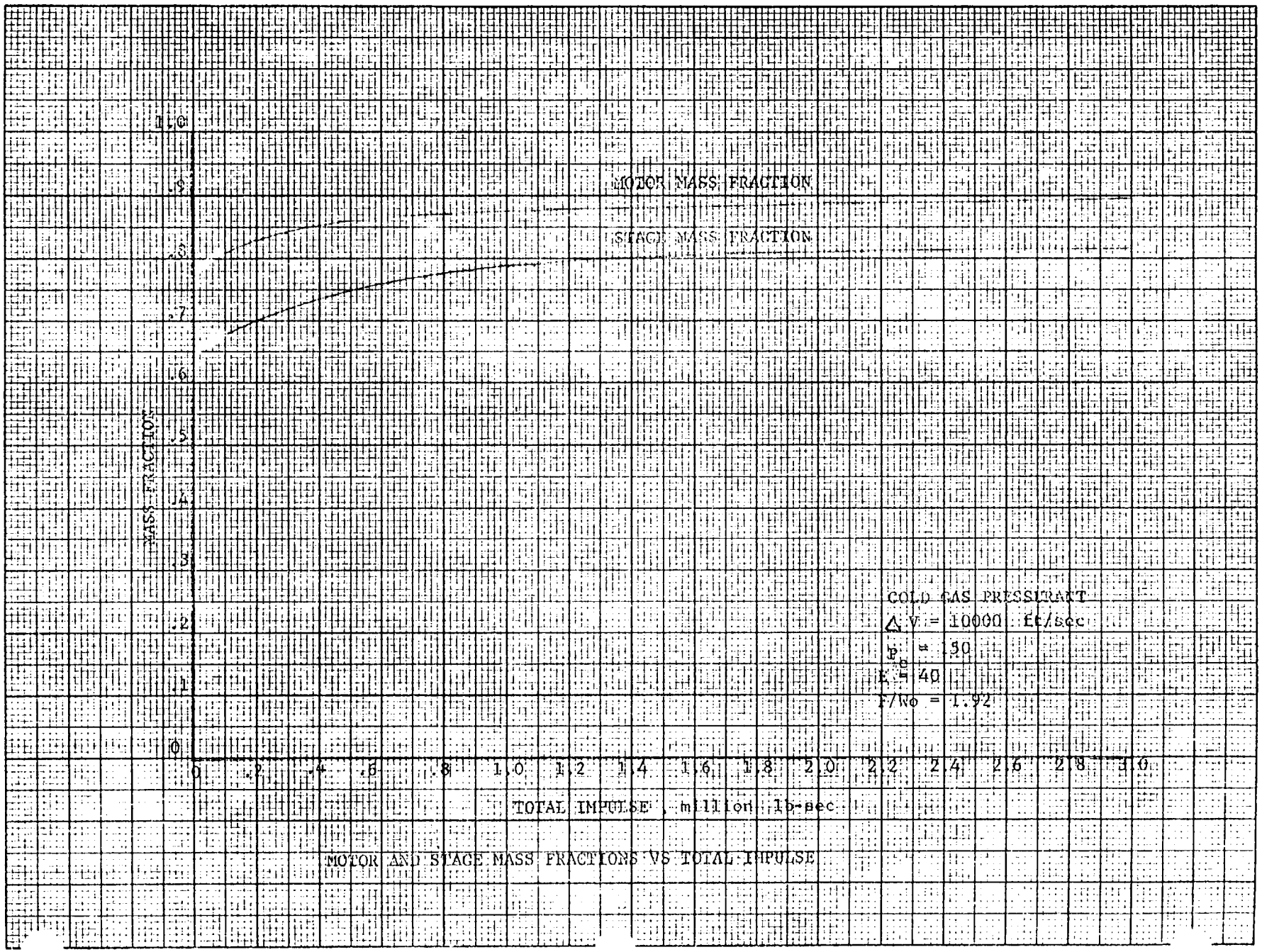

MOTOR AND STAGE MASS FRACTIONS VS TOTAL IMPULSE

Figure 2296

K+E X 10 TO ½ INCH 46 1473
X 10 INCHES MADE IN U.S.A.
KEUFFEL & ESSER CO.

Reproduced from best available copy.

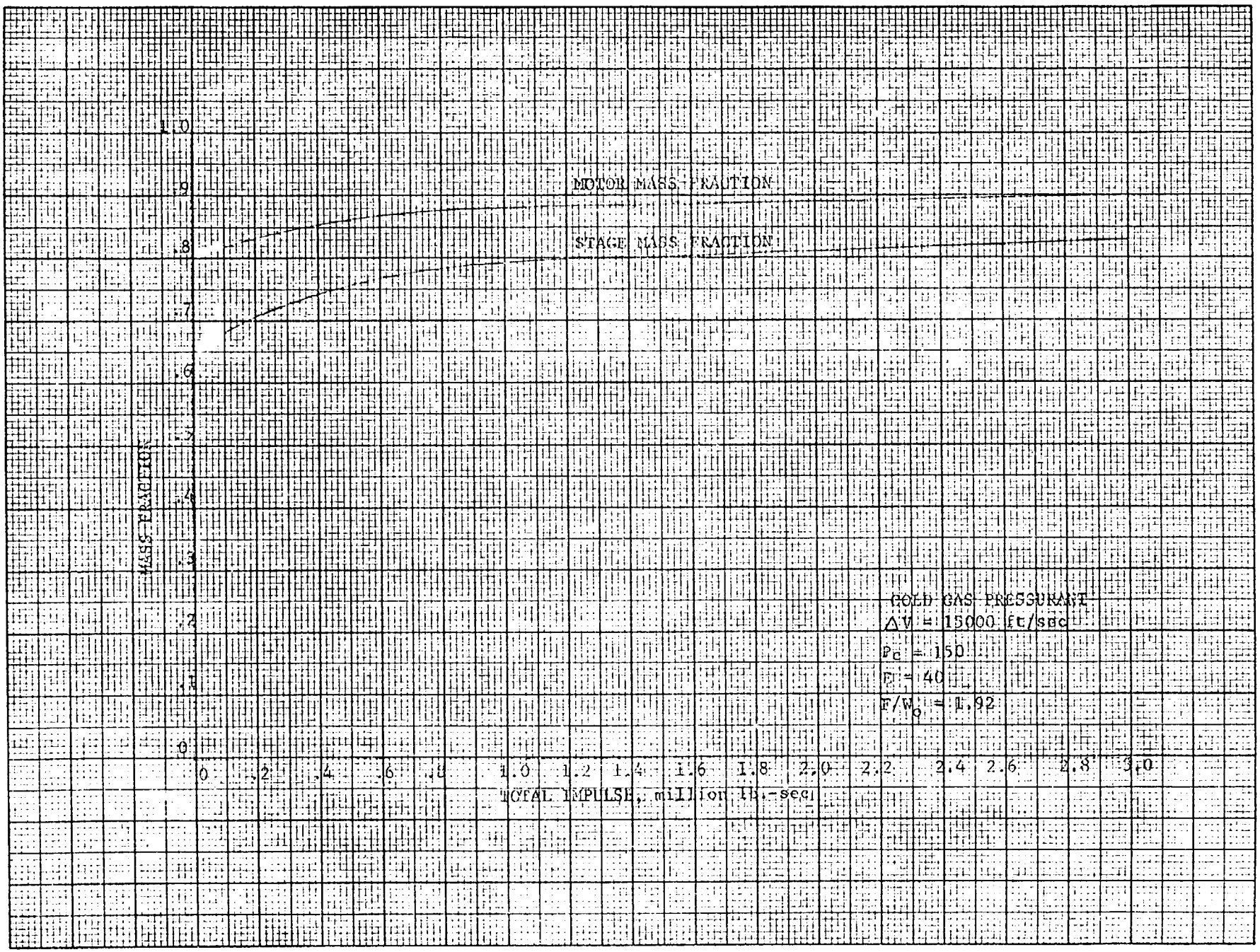

Figure 2-13

K+E 10 TO ½ INCH 46 1473
10 INCHES MADE IN U.S.A.
KEUFFEL & ESSER CO.

Reproduced from best available copy.

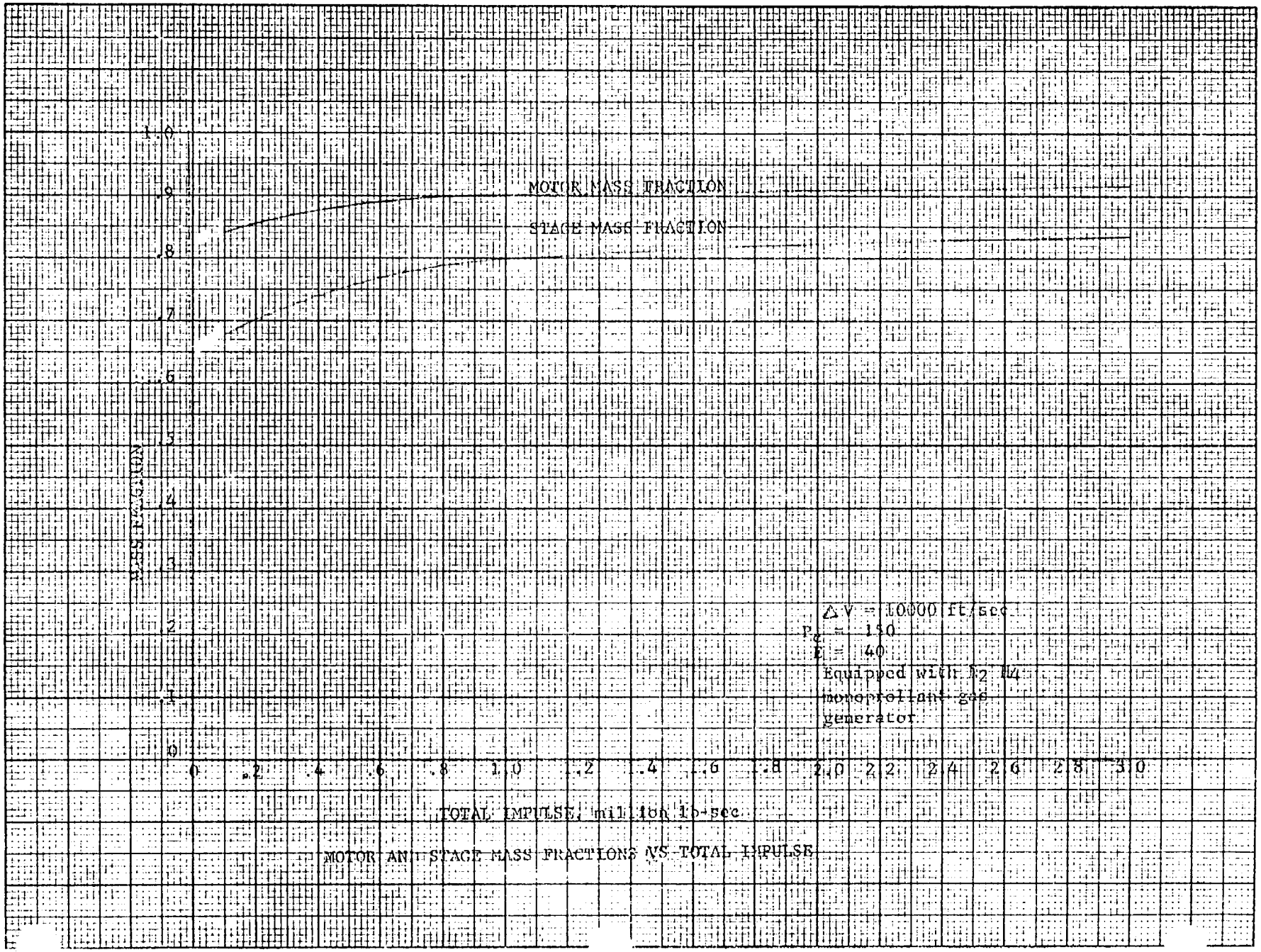

Figure 2 MOTOR AND STAGE MASS FRACTIONS VS TOTAL IMPULSE

K+E 10 X 10 TO ½ INCH 46 1473
7½ X 10 INCHES MADE IN U.S.A.
KEUFFEL & ESSER CO.

Reproduced from best available copy.

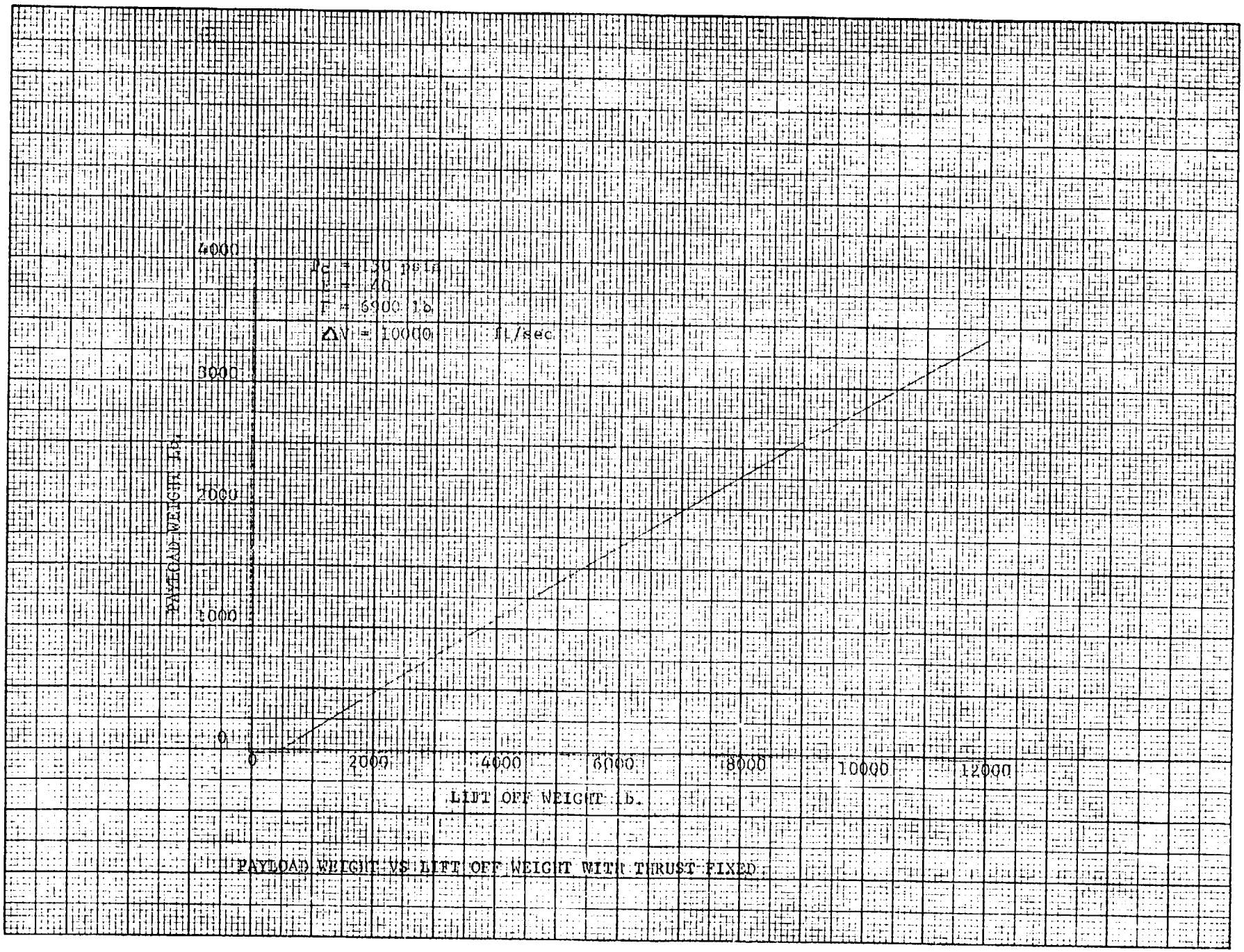

PAYLOAD WEIGHT VS LIFT OFF WEIGHT WITH THRUST FIXED

Figure 2-

K+E 10 TO ½ INCH 46 1473
X 10 INCHES MADE IN U.S.A.
KEUFFEL & ESSER CO.

Reproduced from best available copy.

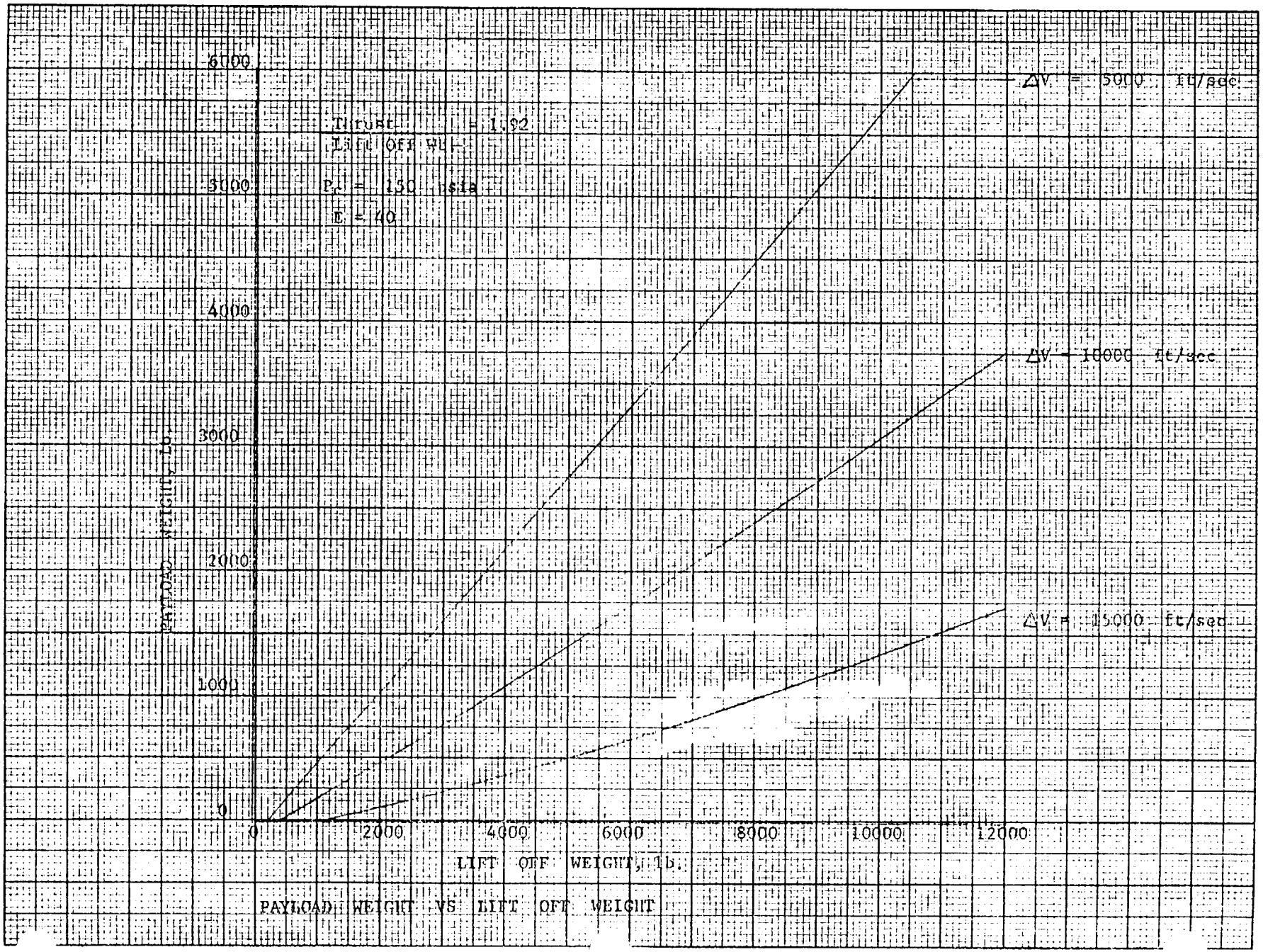

PAYLOAD WEIGHT VS LIFT OFF WEIGHT

Figure 2-16

2.5 HYBRID SYSTEM ANALYSIS

The hybrid propulsion system consists of five (5) major assemblies: the pressurization system, oxidizer and tank system, oxidizer control system, case, fuel grain and the nozzle assembly.

Although hybrid systems are new and some development is necessary, there is no reason that the ultimate predicted reliability cannot be reached in the immediate future given adequate reliability and quality controls.

2.5.1 System Success Diagram and Reliability Summation

The functional success diagram is shown in figure 2-17. This diagram depicts the major assemblies and their interaction chain which is necessary for success. The subsystem assemblies have a series relationship with each other such as that shown in the math model below.

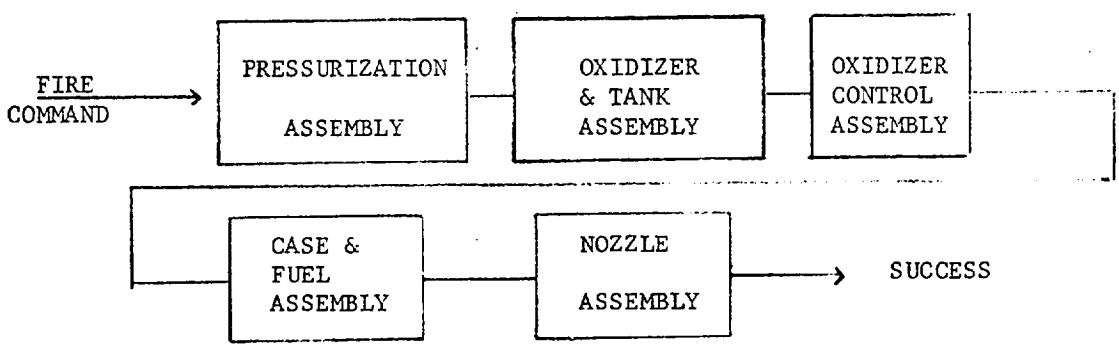

$R_{system} = R_{pressurization} \times R_{oxidizer} \times R_{ox.\ control} \times R_{case\ \&\ fuel} \times R_{nozzle}$

$R_{system} = (.999445)(.998915)(.998451)(.999432)(.998318)$

$R_{system} = .9944$ max.

Figure 2-17. Hybrid Propulsion System Functional Success Diagram

2.5.2 Pressurization Assembly

The pressurization assembly consists of high pressure helium tankage, controls for pressurizing them and additional controls for the initiation and regulation of the pressurization gas as it is needed in the oxidizer tank. The failure mode analysis of the pressurization system indicates that most failures will result in either no ignition or low thrust as a result of loss of helium due to leakage.

The functional success diagram is shown in figure 2-18 below:

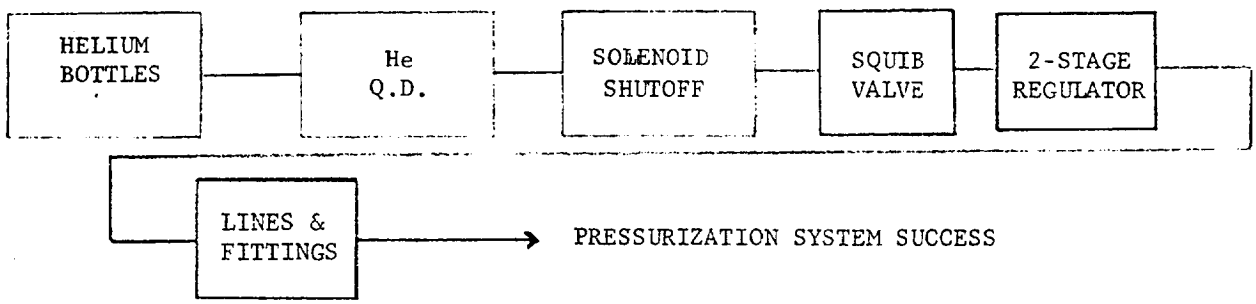

Figure 2-18. Pressurization System Functional Success Diagram

2.5.3 Oxidizer Tank Assembly

The oxidizer tank assembly consists of the tank itself and controls for filling, draining and venting the tank as required. The system for filling and draining the tank offers a degree of redundancy in the failed-open mode, which eliminates approximately 1,000 failures per 10^6 missions. The analysis shows that the highest number of failures will result in low thrust because the vent valve failed.

The functional success diagram is shown in figure 2-19 below:

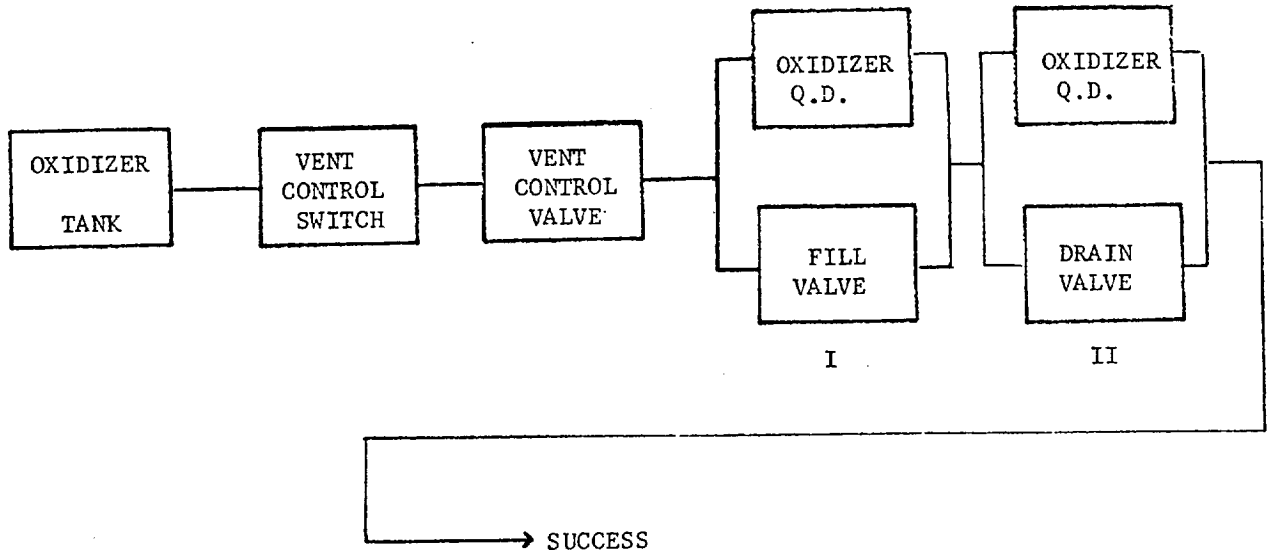

$$R_{assembly} = R_{tank} \times R_{sw} \times R_{vent} \times R_I \times R_{II}$$

$$R_I = R_{II} = R_{Q.D.}R_{valve} + R_{Q.D.}Q_{valve} + Q_{Q.D.}R_{valve}$$

$$= R_{Q.D.}R_{valve} + R_{Q.D.} - R_{Q.D.}R_{valve} + R_{valve} - R_{Q.D.}R_{valve}$$

$$= R_{Q.D.} + R_{valve} - R_{Q.D.}R_{valve}$$

$$\therefore R_{assembly} = R_{tank} \times R_{sw} \times R_{vent} \times 2 \left[R_{Q.D.} + R_{valve} - R_{Q.D.}R_{valve} \right]$$

Figure 2-19. Oxidizer Tankage Functional Success Diagram

2.5.4 Oxidizer Control Assembly

The oxidizer control assembly consists of the oxidizer valve, an electronic control unit and motors to open and close the valve and the injectors which provide the means to spray the oxidizer in the combustion chamber. The three (3) motors offer a degree of redundancy in that any two will override a failed third and still meet mission requirements.

The system was analyzed on the basis that no modulation of thrust would be required and that response time was not a critical factor. However, the system design is such that even if modulation is required and response (within normal limits) becomes critical, only a small increase in failure rate will be incurred.

Failure to ignite, terminate and low/zero thrust all contribute more or less equally to system failures as a result of failures of the electronic control unit. It is not expected that the injector will be as significant a contributor to failures in a hybrid system as it would be in a liquid engine because the criticality of dimensional tolerances, fuel to oxidizer lead or lag considerations and interpropellant weld considerations are not required.

The functional success diagram for the oxidizer control assembly and its associated electronic control unit are shown below in figures 2-20 and 2-21, respectively.

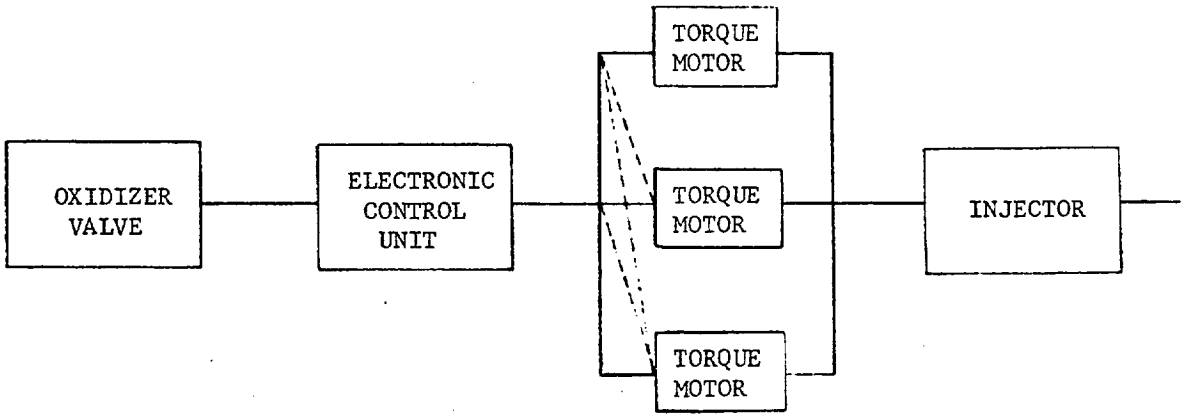

Figure 2-20. Oxidizer Control Valve Functional Success Diagram

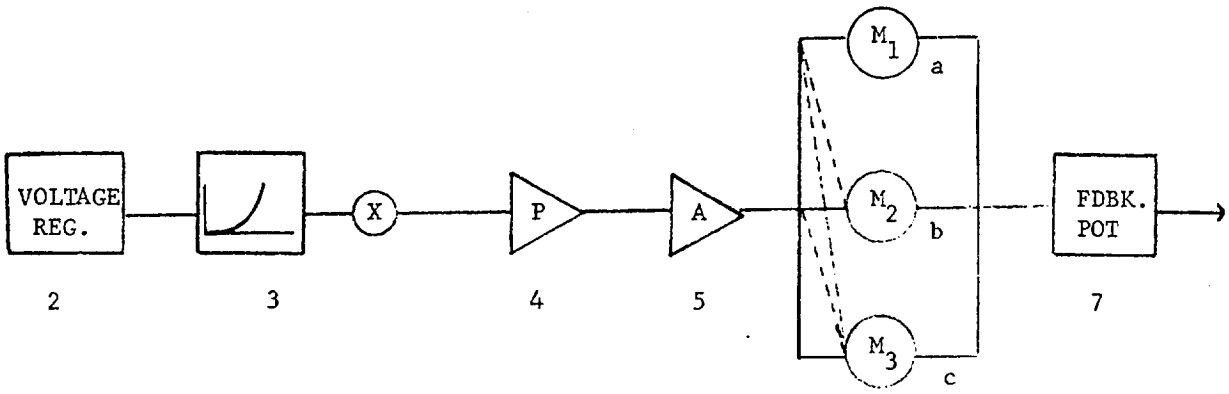

$$R_{system} = R_2 R_3 R_4 R_5 R_6 R_7$$

$$R_6 = R_a R_b R_c + Q_a R_b R_c + R_a Q_b R_c + R_a R_b Q_c = 1$$

$$R_a = R_b = R_c$$

$$Q_a = 1 - R_a$$

$$\therefore \; Q_a = Q_b = Q_c$$

Figure 2-21. Electronic Control Unit Functional Schematic

2.5.5 Case and Fuel Assembly

The case and fuel assembly is made up of a double wound filament case, insulation/lines and the fuel grain. Since the oxidizer and fuel are normally hypergolic, an ignition system is not required.

The safety factors for both the case and insulation are sufficiently high so as not to be a significant contributor to the system unreliability. The major failure contributions will be the result of fuel-binder variations which result in too fast or too slow a burning rate. The failure rates

given may be conservative since they are based upon solid motor experience which must control fuel binder, oxidizer and other additives very closely to get the correct combustion rate. In a hybrid system this is not expected to be as critical as in a solid motor. In addition all failures due to grain cracking, slumping or spalling have been entirely eliminated.

The functional success diagram for the case and fuel assembly is shown below in figure 2-22.

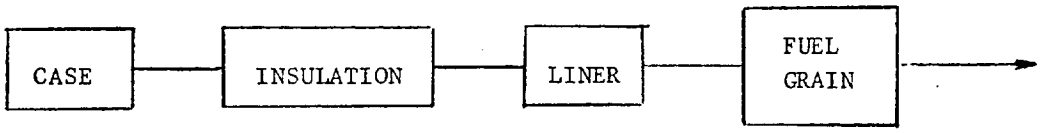

Figure 2-22. Case and Insulation Functional Success Diagram

2.5.6 Nozzle Assembly

The nozzle assembly consists of a buried graphite nozzle with an annealed pyrolytic graphite throat and a filament wound case. The great majority of the failures are expected to be the result of structural failure of the nozzle or throat resulting mainly in loss of thrust or in some cases loss of vector control.

The functional success diagram for the nozzle assembly is shown below in figure 2-23.

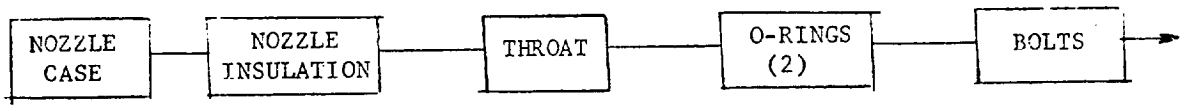

Figure 2-23. Nozzle Assembly Functional Success Diagram

2.5.6. Failure Mode Analysis

The failure mode analysis worksheets for the hybrid propulsion system appear in figure 2-24. These sheets summarize the modes of failure and the number of failures per million missions for each component. The effect of a given failure mode on the system is also given.

2.5.7 Reliability Growth of Hybrid Propulsion Systems

The expected reliability growth of the high energy hybrid propulsion system at the 90% confidence level is plotted in figure 2-25. This expected growth is based on the current hybrid target vehicle propulsion system development program at UTC under Air Force Contract No. AF 04(511)-11632. Although the hybrid target vehicle has multimission capability and is a pre-packaged system, the problem areas and failure modes are similar to those expected for a high energy upper stage propulsion system. The method of prediction is related to the technique used in calculating the reliability of the UTC FW-4S solid motor.

I Item	Subscript	Code Number	Part/Component or Subsystem / Part Type	Failure Mode	% Stress	Generic Failure Rate	Q Quantity	K_a Application Factor	K_u Use Factor	Adjusted Failure Rate / Probabilit of Failure
1			Helium Bottles	Structural Failure		.01	4			.04
				Leakage		.01	4			.04
				Low Pressure		.01	4			.04
2			Helium Q. D.	Leakage		.112	1			.112
3			Solenoid Shutoff	Valve Leaks		11.0	1			11.0
			Valve	Valve Fails to Open		11.0	1			11.0
				Valve Fails to Close		11.0	1			11.0
4			Solenoid Activ-	Fails to Open		11.0	1			11.0
			ation Valve	Leaks		11.0	1			11.0
5			2-Stage	Regulates above		6.7	1			6.7
			Regulator	tol.						
				Regulates below tol.		6.7	1			6.7
6			Lines & Fittings	Rupture		neg.	-			-

C = Coast Period
M = Maneuver Period

ANALYSIS

"A"

System

Next higher assy: Hybrid Motor

Code number:

By:

Date:

Figure 2-

Time Period	Time (Secs)	K_{op}	K_{op}^{t} x 110^3	HIGH THRUST		LOW THRUST/ NO THRUST		FAILURE TO IGNITE		FAILURE TO TERMINATE THRUST		COMBUSTION INSTABILITY		LOSS OF VECTOR CONTRO
				Modes										
C & M	86,300 100	1 900	176.3					.1	.0020					
C & M	86,300 100	1 900	176.3			1	.0196	1	.0196					
C & M	86,300 100	1 900	176.3			1	.0196							
C & M	86,300 100	1 900	176.3			70	3.8395	10	.5485					
C & M	86,300 100	1 900	176.3			10	53.8694							
C & M	86,300 100	1 900	176.3											
C & M	86,300 100	1 900	176.3			20	107.7388							
C & M	86,300 100	1 900	176.3					50	269.3471					
C & M	86,300 100	1 900	176.3			10	53.8694							
C & M	100	900	176.3	10	32.8114									
C & M	86,300 100	1 900	176.3			10	32.8114							
C & M	86,300 100	1 900	176.3											
Time Period:														
TOTALS					32.8114		252.1677		269.9172					

I Item	Subscript	Code Number	Part/Component or Subsystem / Part Type	Failure Mode	% Stress	Generic Failure Rate	Quantity	K_s Application Factor	K_u Use Factor	Adjusted Failure Rate / Probability of Failure
6			Oxidizer Tank	Structural Failure			1			.01
				Leakage			1			.01
			Vent Control Sw.	Actuates above Tol.		.14	1			.14
				Actuates above Tol.		.14	1			.14
				Fails to Actuate		.14	1			.14
			Vent Control Vlv.	Fails to Open		11.0	1			11.0
				Fails to Close		11.0	1			11.0
		*	Fill & Drain Vlv.	Fails Open		11.0	2			22.0
				Fails Closed		11.0	2			22.0
				Leaks		11.0	2			22.0
		*	Quick Disconnect	Leaks		.112	2			.224

C = Coast Period
M = Maneuver Period

* Redundant in Open Modes

N-1141 (4/67) Test

ADE ANALYSIS

XSHEET "A"

DIZER TANK

Next higher assy: Hybrid Motor

Code number:

By:

Date:

Figure 2-2

d ity e	Time Period	Time (Secs)	K_{op}	K_{op} x 10^3	Hybrid Engine System Modes: HIGH THRUST		LOW THRUST/ NO THRUST		FAILURE TO IGNITE		FAILURE TO TERMINATE THRUST		COMBUSTION INST-ABILITY		LOSS VECTO CONTR
	C & M	86,300 100	1 900	176.3			100	.4897							
							5	.0245	1	.0049					
	& M	86,300 100	1 900	176.3	1	.0686	1	.0686							
	C & M	86,300 100	1 900	176.3			5	.3428							
	C & M	86,300 100	1 900	176.3			100	6.8561							
	C & M	86,300 100	1 900	176.3	10	53.8694	90	484.8248							
	C & M	86,300 100	1 900	176.3			100	538.6942							
	C & M	86,300 100	1 900	176.3											
	C & M	86,300 100	1 900	176.3											
	C & M	86,300 100	1 900	176.3											
	C & M	86,300 100	1 900	176.3											
Time Period:															
TOTALS						53.9380		1031.3017		.0049					

FAILURE MO
BASIC WORK
OXIDIZE

I Item	Subscript	Code Number	Part/Component or Subsystem / Part Type	Failure Mode	% Stress	Generic Failure Rate	Quantity	K_a Application Factor	K_u Use Factor	Adjusted Failure Rate / Probability of Failure
1			Oxidizer Valve	Leaks		6.5	1			6.5
				Fails to Open		6.5				6.5
2			Voltage Regulator	Fails to Regulate		2.34	1			2.34
				in Spec.						
3			Function Gen.	No Output		3.89	1			3.89
4			Preamplifier	Short or Open		24.2	1			24.2
5			Driving Amplifier	Short or Open		3.02	1			3.02
6			Motor	Failure to Respons		14.48	3			
7			Feedback Pot.	No Output		21.50	1			21.50
8			Wiring Harness	Allows shorts		--	1			--
9			Injector	Leaks		3.41	3			10.23
				Fails to Open		3.41	3			10.23

C = Coast Period
M = Maneuver Period

-1141 (4/67) Test

DE ANALYSIS
SHEET "A"
ONTROL

Next higher assy: Hybrid Motor
Code number:
By:
Date:

Figure 2-24

ty	Time Period	Time (Secs)	K_{op}	$K_{op}t$ x 10^3	DSV-3E Modes: HIGH THRUST		LOW THRUST/ NO THRUST		FAILURE TO IGNITE		FAILURE TO TERMINATE THRUST		COMBUSTION INSTABILITY	LOSS OF VECTOR CONTROL
	C	86,400	1	86.4			2.0	3.1200			2	3.1200		
	M	100	1250	125			10	2.2569						
	& M	86,300 100	1 900	176.3	10	11.4595	10	11.4595						
	C & M	86,300 100	1 900	176.3										
	C & M	86,300 100	1 900	176.3	5	9.5251			90	171.4517				
	M	100	900	90	10	60.5	60	363.0			20	121.0		
	M	100	900	90	10	7.55	60	45.30			20	15.10		
	M	100	1250	125					50	.3799	50	.3799		
	M	100	1250	125	20	149.3055			50	373.2636	25	186.6318		
	C & M	--	1250	--										
	C	86,400	1	86.4	10	8.1840					10	8.1840		
	C	100	1500	150					1	1.4208				
Time Period:														
TOTALS					246.5241		426.1364		545.5160		331.2957			

I Item	Subscript	Code Number	Part/Component or Subsystem / Part Type	Failure Mode	% Stress	Generic Failure Rate	Q Quantity	K_s Application Factor	K_u Use Factor	Adjusted Failure Rate / Probability of Failure
			Case	Case Ruptures			1			Neg.
				Leak at Metallic						
				Interfaces						Neg.
			Insulation	Erodes too Rapidly			1			Neg.
				Insul/Case Bond Fails						30
				Insul/Liner Bond Fails						50
			Fuel	Pc too high						15
				Pc too low						30

ODE ANALYSIS
KSHEET "A"
SYSTEM

Next higher assy: Hybrid Motor
Code Number:
By:
Date:

Figure 2-

d ity	Time Period	Time (Secs)	K_{op}	K_{op} x 10^3	Modes: THRUST TOO HIGH		THRUST TOO LOW/ NO THRUST		FAILURE TO IGNITE		FAILURE TO TERMINATE THRUST		COMBUSTION INSTABILITY		LOSS C VECTOR CONTRC
	100 sec	100	1500	150			100								
	100 "	100	1500	150			100								
	100 "	100	1500	150			5								
	100 "	100	1500	150			1	.30							
	100 "	100	1500	150			10	5.0							
	100 "	100	1500	150	20	125.0000									
	100 "	100	1500	150			25	312.5000	10	125.0000					
Time Period:															
TOTALS					125.0000		312.80000		125.0000						

I Item	Subscript	Code Number	Part/Component or Subsystem / Part Type	Failure Mode	% Stress	Generic Failure Rate	Q Quantity	K_s Application Factor	K_u Use Factor	Adjusted Failure Rate / Probability of Failure
			Nozzle Case	Structural Failure			1			Neg.
			Nozzle Insulation	Insulation Structural Failure			1			Neg.
				Failure of the Insulation Bonds						45
			Throat	Structural Failure			1			30
				Excessive Erosion						5
			O-Rings	O-Ring Leaks Hot Gas		.02	2			.04
			Bolts	Bolt Fails Structurally			24			Neg.

DE ANALYSIS
HEET "A"
CHAMBER ASSEMBLY

Next higher assy: Hybrid Motor
Code number:
By:
Date:

ty	Time Period	Time (Secs)	K_{op}	$K_{op}t$ x 10^3	DSV - 3E Modes: THRUST TOO HIGH	THRUST TOO LOW/ NO THRUST	FAILURE TO IGNITE	FAILURE TO TERMINATE	COMBUS-TION INSTABILITY	LOSS OF VECTOR CONTROL
	M	100	1500	150		100				
	M	100	1500	150		100				
	M	100	1500	150		25 468.7504				25 468.750
	M	100	1500	150		50 625.0005				1 12.
	M	100	1500	150		50 104.1668				1 2.08
	M	61	1500	150		10 .1667				10 .166
	M		1500	150		100				
	Time Period:									
	TOTALS					1198.0844				483.50

K+E 10 TO ½ INCH 46 1473
7 x 10 INCHES MADE IN U.S.A.
KEUFFEL & ESSER CO.

Reproduced from best available copy.

Figure 2-25. Hybrid Propulsion System Reliability Growth Potential

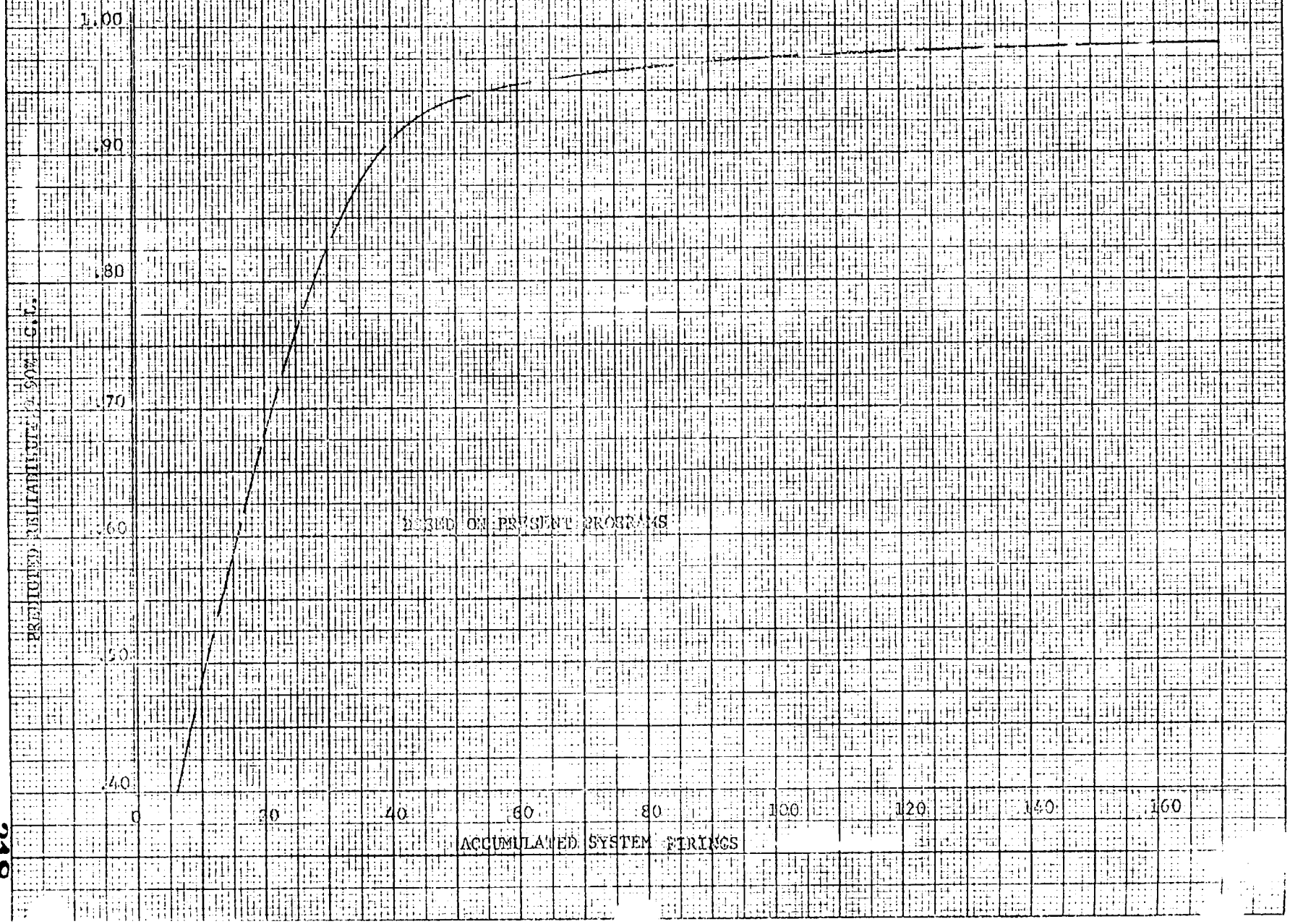

2.6 System Development and Production Costs

The development and production costs for the hybrid propulsion system are calculated with a computer program subroutine developed during this contract period. The Value Effectiveness Procedure (VEP) provides a rapid means of generating parametric costing data. The program model is primarily based on costing information in reference 2-3. The expected accuracy of the engineering cost data generated by this program is ±25%.

The first unit production costs are based on the component weight in the manner shown in Table 2-VII. At present there are no hybrid upper stages in production, hence the costing data were based on combined liquid and solid propulsion experience. All costing was done directly proportional to the component weight since only limited data were available.

The research and development costs of rocket propulsion systems have been correlated with various techniques. However, for the hybrid system the following expression should give satisfactory engineering costs for systems simular to the subject base system.

$$\text{R\&D Costs (Millions of Dollars)} = 3.3\ (F/1000)^{.4}\ (.90 + .01\,\text{Nehu}) + C\,\text{Nehu}$$

where

F = Thrust in pounds

C = First unit projection costs in millions of dollars

Nehu = Number of equivalent hardware units required in the development program

λ = Learning rate factor

Parametric data on hybrid costs are summarized in Table 2-VIII for a range of pressures and thrust levels. The R&D costs are for fifteen

TABLE VII

FIRST UNIT PRODUCTION COSTS

Fabrication and Assembly Cost

$$FAAC = \left[\sum_{\substack{\text{All components} \\ \text{plus final ass'y}}} \left(\frac{\text{Labor Hours}}{\text{Pound Component}} \right) \times \left(\text{Component Weight, lbs} \right) \right]$$

$$\left[\begin{array}{l} \text{Cost per hour} \\ \text{for labor +} \\ \text{burden + G\&A} \end{array} \right] \left[\begin{array}{l} \text{Multiplying fac-} \\ \text{tor to include final} \\ \text{test costs} = C_1 \end{array} \right] \left[\begin{array}{l} \text{Multiplying factor} \\ \text{to include engin-} \\ \text{eering planning} \\ = C_2 \end{array} \right]$$

Materials Cost

$$MC = \left[\sum_{\substack{\text{All Com-} \\ \text{ponents}}} \left(\frac{\text{Material Cost}}{\text{Pound Component}} \right) \left(\text{Component Weight, lbs.} \right) \right]$$

Engineering and Tooling Cost

$$EATC = \left[\text{Multiplying Factor} = C_3 \right] \left[FAAC + MC \right]$$

Total Manufacturing Cost

$$TMC = FAAC + MC + EATC$$

Engineering Changes

$$EC = \left[\text{Multiplying Factor} = C_4 \right] \left[FAAC + MC \right]$$

Total Production Cost Including Fee

$$TPC = \left[1 + C_3 + C_4 \right] \left[FAAC + MC \right] \left[1 + \frac{\text{Percent Fee}}{100} \right]$$

The first unit production cost is predicted; learning rates can then be applied to compute the average cost of a specific number of total units to be produced.

TABLE 2-VIII

HIGH ENERGY HYBRID PROPULSION SYSTEM COSTS
(ϵ = 40, F/W_o = 1.92, 15 Units for R&D)
Costs in Millions of Dollars

THRUST LEVEL lbf	CHAMBER PRESSURE psia	TOTAL 1st UNIT COST M$	R&D COSTS M$
2,000	75	.055	5.298
	150	.056	5.312
	300	.064	5.411
	500	.077	5.576
6,900	75	.141	9.353
	150	.146	9.419
	300	.170	9.738
	500	.211	10.265
10,000	75	.193	11.231
	150	.200	11.323
	300	.236	11.792
	500	.294	12.556
20,000	75	.344	15.987
	150	.358	16.173
	300	.428	17.090
	500	.542	18.587

-56-

equivalent hardware units. In Figure 2-26 the first unit and R&D cost are plotted as functions of propellant weight for the hybrid system. The R&D cost is plotted in Figure 2-27 as a function of the number of equivalent propulsion units used for testing.

The first unit propulsion cost per pound of payload appears in Figures 2-28 as a function of thrust level for a stage velocity increment of 10,000 ft/sec.

HYBRID 1st UNIT AND R&D COST VS. PROPELLANT WEIGHT

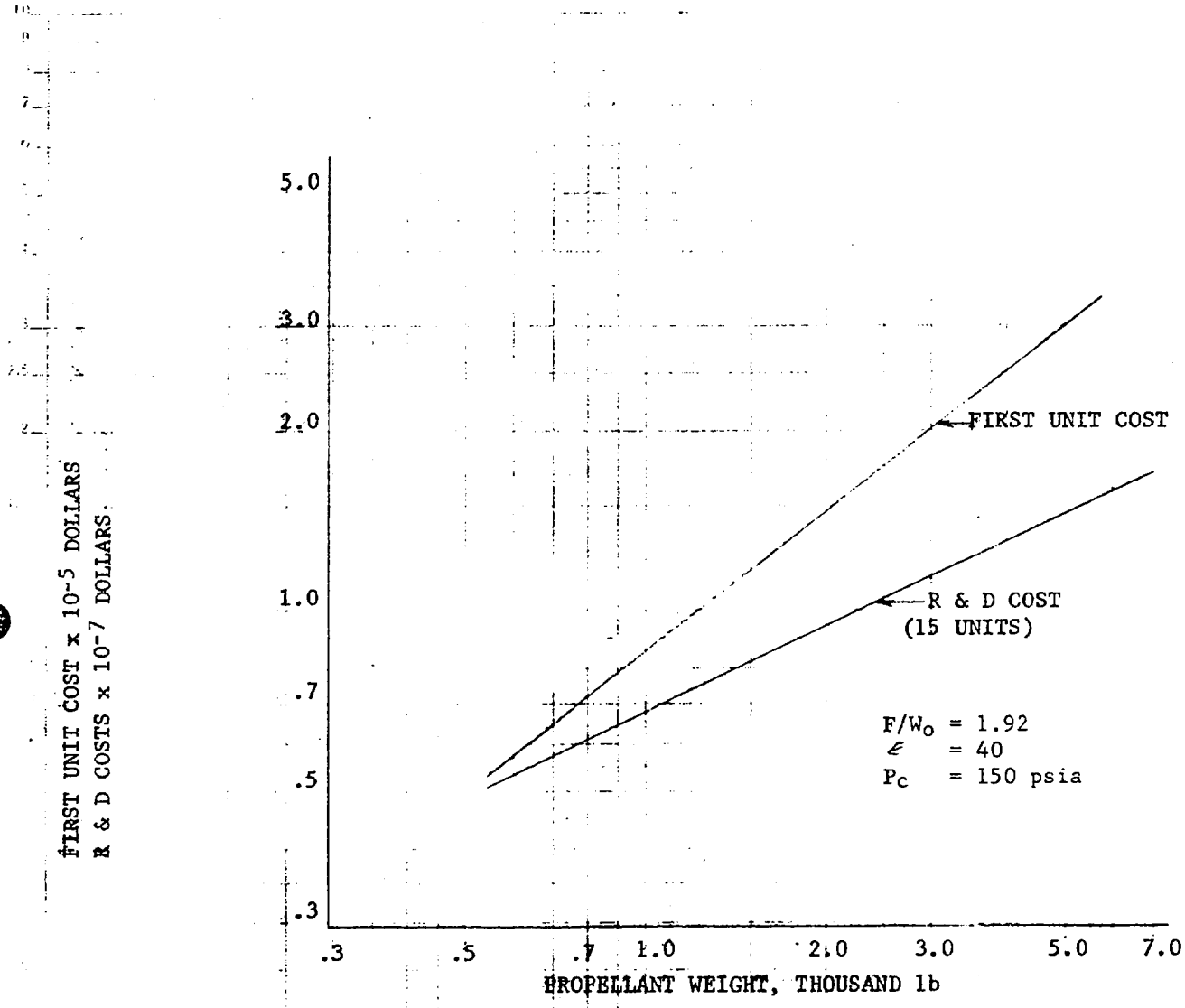

Reproduced from best available copy.

Figure 2-26

HYBRID R&D COST VS. NUMBER OF EQUIVALENT HARDWARE UNITS

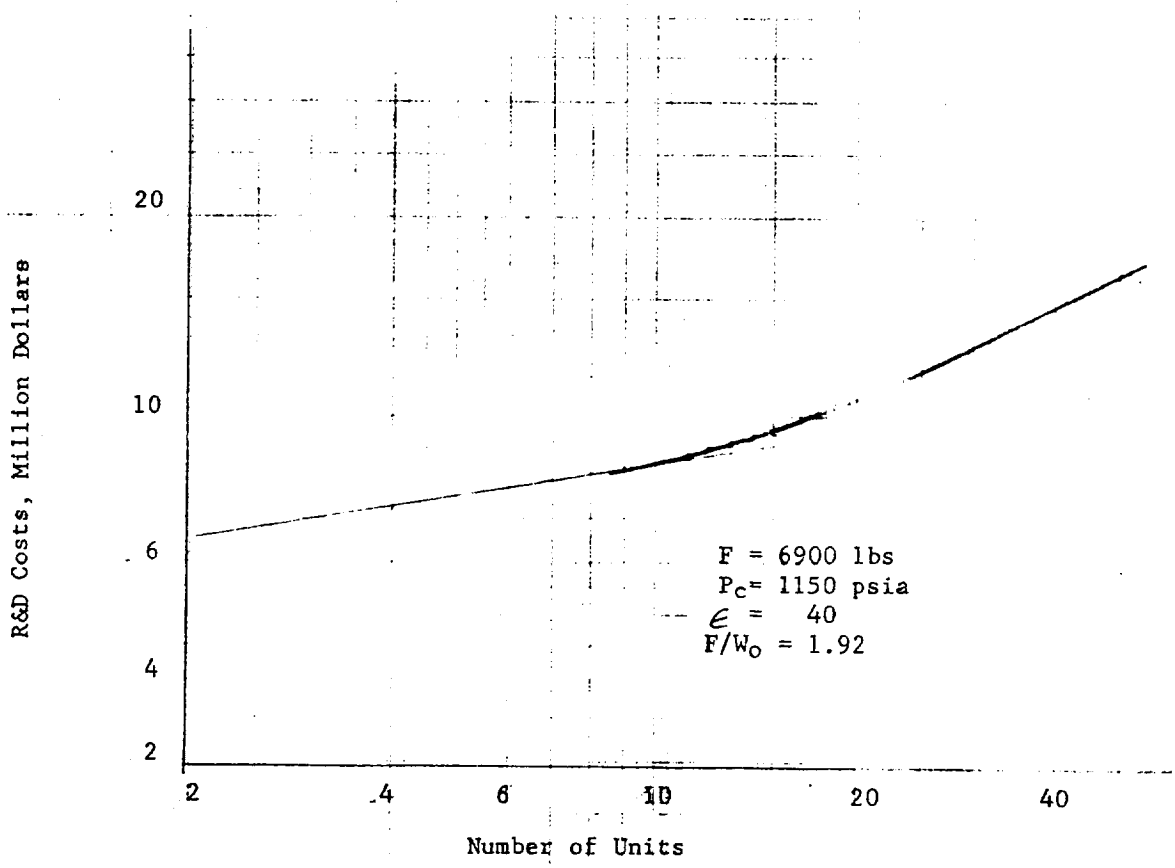

Reproduced from best available copy.

Eigure 2-27

HYBRID 1st UNIT PRODUCTION COST PER POUND OF PAYLOAD

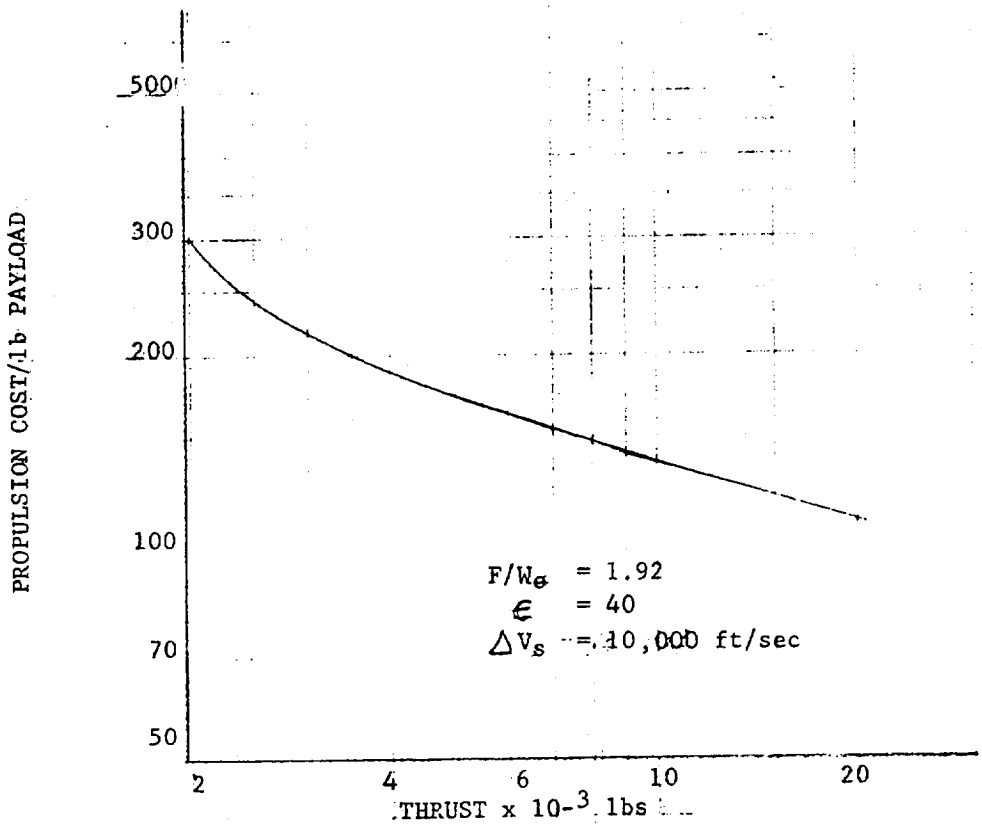

Reproduced from best available copy.

Figure 2-28

3.0 FW-4S SOLID PROPULSION SYSTEM

3.1 SOLID PROPELLANT BASE SYSTEM DESCRIPTION

The FW-4S Solid Propulsion System was developed as a fourth stage for the Scout Launch Vehicle. This system is now also used with other booster vehicles. The motor uses a single start non-sterilizable propellant and is described in the following pages taken from UTC Brochure 65-8.

- HIGH PERFORMANCE UPPER STAGE MOTOR
- FILAMENT-WOUND FIBERGLASS CASE CONSTRUCTION
- ADVANCED, LIGHTWEIGHT COMPOSITE NOZZLE
- ADAPTABLE TO A VARIETY OF MISSION APPLICATIONS

INTRODUCTION

In early 1964 as a result of an evaluation conducted jointly by Air Force, Navy and NASA, United Technology Center was selected to undertake development and qualification of an improved solid propellant rocket motor for the fourth stage of the Scout vehicle. The motor developed under this program, the FW-4S (Air Force designation SR57-UT-1), was designed and fabricated to be interchangeable with existing upper-stage motors of such vehicles as Scout and Thor and to provide increased payload capability for these vehicles. Eighteen FW-4S motor firings, both at sea-level and simulated altitude conditions, were conducted in the course of motor development and qualification. Flights were made in mid-1965 on Thor and Scout vehicles.

This brochure presents data on the design, performance, and environmental capabilities of the FW-4S solid propellant rocket motor. General cost and delivery information are also provided.

MOTOR DESCRIPTION

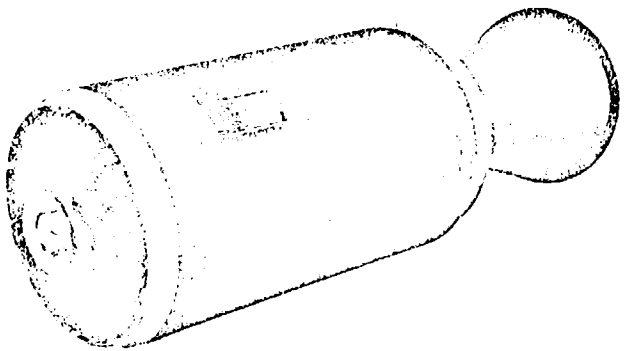

The FW-4S rocket motor is 19.6 inches in diameter with 18-inch diameter interstage flange, is 58.43 inches in length and weighs 660.5 pounds. The motor inert weight is 55.5 pounds and the propellant weight is 605 pounds, resulting in a motor mass fraction of 0.92. The thrust axis is aligned with the motor centerline within 0.00035 radians, and the displacement of the thrust axis from the motor centerline at any point between the nozzle throat and the nozzle exit plane does not exceed 0.007 inch. A cut-away view of the motor is presented in figure 3-1and the pertinent motor interface dimensions are given in figure 3-2.

The motor case (shown in figure3-3) is fabricated from S-994 fiberglass and epoxy resin. The cylindrical wall thickness of 0.08 inch, and the domes have geodesic contours with a nominal wall thickness of 0.03 inch. The case polar bosses are fabricated from aluminum. The

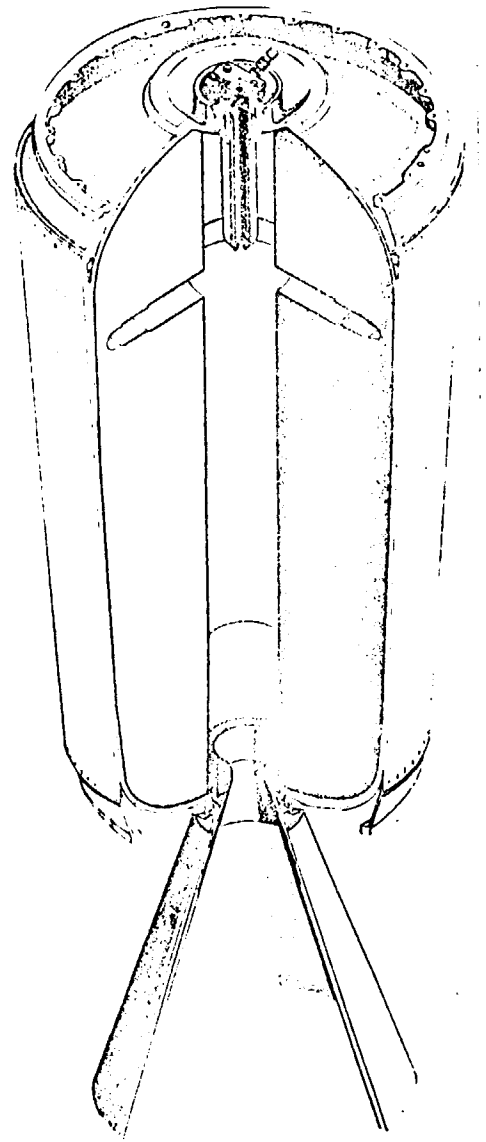

Reproduced from best available copy.

Figure 3-1 Cutaway View of the UTC FW-4S Solid Motor

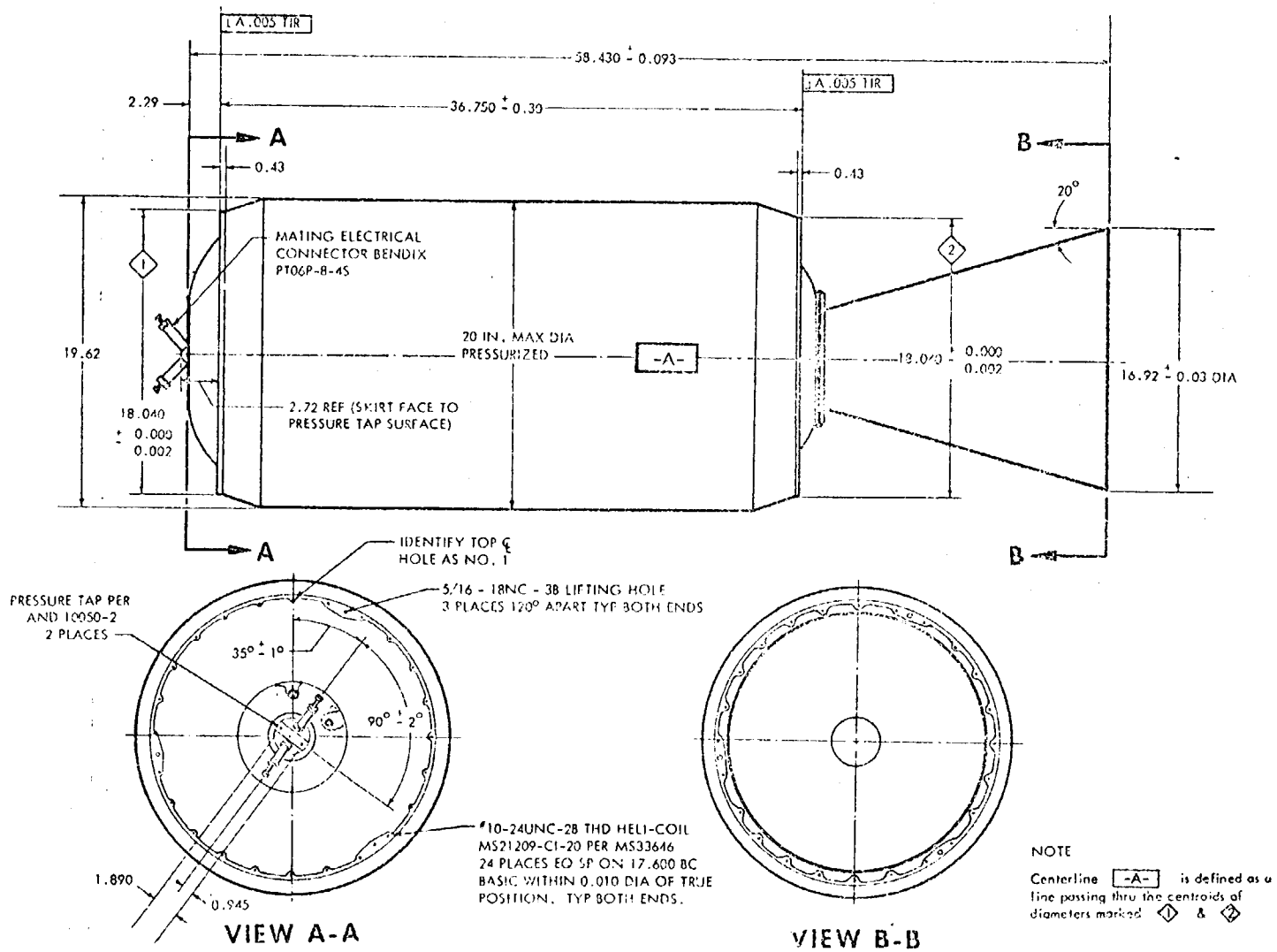

Fig. 3-2 FW-4S Pertinent Motor Dimensions

Reproduced from best available copy.

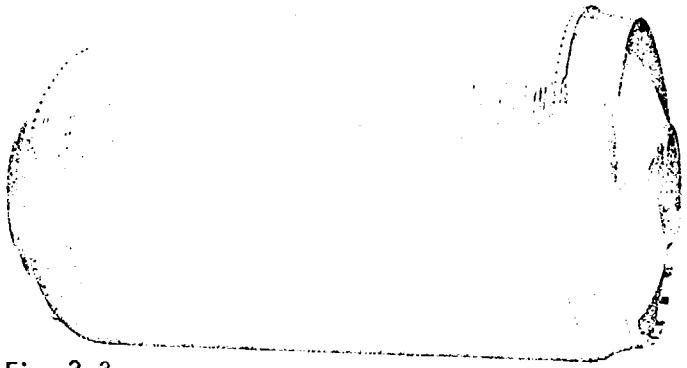

Fig. 3-3 FW-4S Motor Case

aluminum interstage flanges are bonded and riveted to the integrally wound fiberglass skirts of the motor case. At the proof pressure of 900 psi, the case wall stress is 110,000 psi. The case burst stress is in excess of 160,000 psi, which is 50 percent above the motor operating stress. The interior of the case is insulated with silica-filled buna-N rubber. The grain is a case bonded cylindrical charge with a transverse slot. The propellant is a composite system of polybutadiene acrylic acid/acrylonitrile (PBAA/AN) binder, ammonium perchlorate oxidizer, and aluminum fuel. The liner is a PBAN system compatible with the propellant.

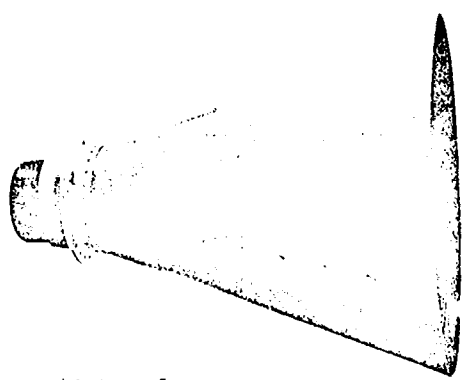

Fig. 3-4 FW-4S Nozzle

The nozzle (Fig. 3-4) is a composite structure consisting of an aluminum nozzle attach flange, exit-cone subassembly, and throat subassembly. Exit cone construction utilizes ablation-resistant graphite-phenolic backed up with light-weight silica-phenolic material which extends to the exit plane. The exit cone liner is reinforced by a stainless steel shell for structural rigidity. The steel shell is bonded and riveted to the aluminum nozzle attach flange. The nozzle throat consists of graphite supported by a ring of silica-phenolic material which is bonded to the aluminum nozzle attach flange. The nozzle half angle is 20°, the nozzle throat diameter is 2.28 inches, and the initial expansion ratio is 52.8.

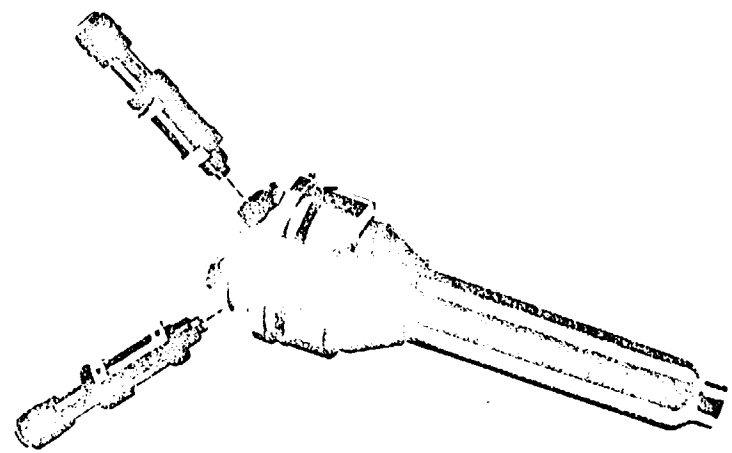

Fig. 3-5 FW-4S Igniter

The igniter (Fig. 3-5) is a rocket-type device utilizing a propellant charge similar to that used in the main motor. The igniter case and igniter cap are fabricated from aluminum and are insulated with silica-filled buna-N rubber. Two delay initiators are used to ignite a 4.8 gram boron potassium nitrate pellet charge, which in turn initiates the igniter propellant charge.

331

Reproduced from best available copy.

MOTOR PERFORMANCE

At 0 rpm the average motor thrust is 5350 pounds, the maximum thrust is 6000 pounds, and the action time is 32.1 seconds. At 200 rpm the average motor thrust is 6250 pounds, and the action time is 30.5 seconds.

An FW-4S motor ballistic performance summary at spin rates of 0 and 200 rpm is presented in figure 3-6.

The FW-4S motor ignition transient is presented in figure 37. Thrust vs time and pressure vs time curves for spin rates of 0 and 200 rpm are shown in figures 38 and 39. Maximum motor case temperature during firing and after motor shutdown is 500° F, occurring in the aft cylindrical section of the motor case.

Figure 10 presents the average temperature vs time history for the motor case exterior. Accelerations imposed on various payloads at spin rates of 0 and 200 rpm are presented in figures 31 and 32.

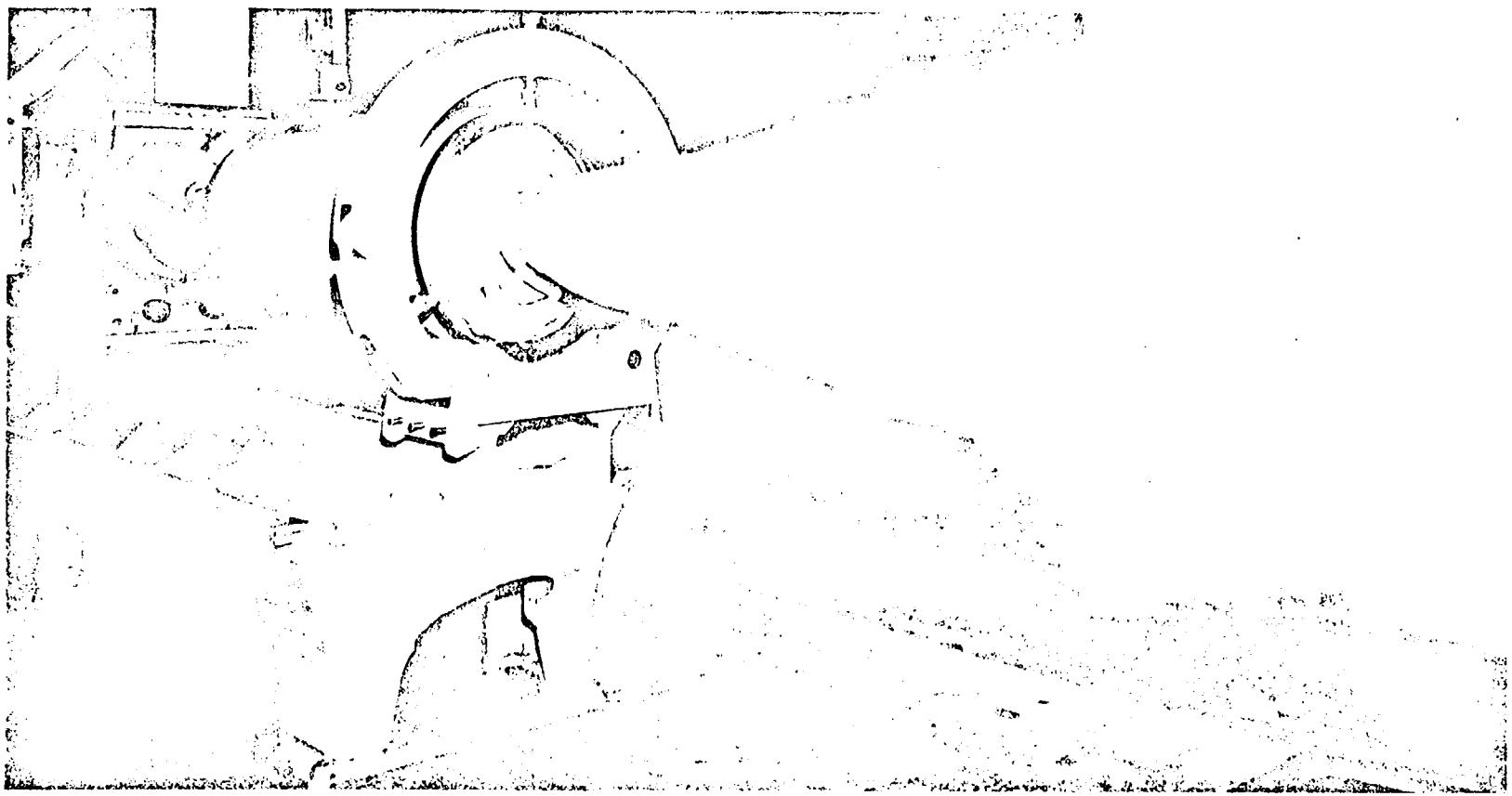

Test firing of FW-4S motor at 200 rpm

Reproduced from best available copy.

BALLISTIC PERFORMANCE SUMMARY AT VACUUM CONDITIONS			
PARAMETER	CONDITIONING TEMP., °F	NOMINAL RATING AT ZERO rpm	NOMINAL RATING AT 200 rpm
Average action time chamber pressure, psia	40	620	670
	70	640	690
	100	670	710
Average action time thrust, lb_f	40	5,100	5,390
	70	5,350	5,620
	100	5,600	5,880
Action time total impulse lb_f-sec	40	171,600	171,600
	70	171,600	171,600
	100	171,600	171,600
Action time, sec	40	33.7	31.8
	70	32.1	30.5
	100	30.7	29.2
Ignition delay time, sec	40	0.140	0.140
	70	0.120	0.120
	100	0.090	0.090
Maximum thrust, lb_f	40	5,850	6,000
	70	6,000	6,250
	100	6,280	6,500
Maximum chamber pressure, psia	40	740	740
	70	760	770
	100	795	800

Fig. 3-6 FW-4S Ballistic Performance Summary at Vacuum Conditions

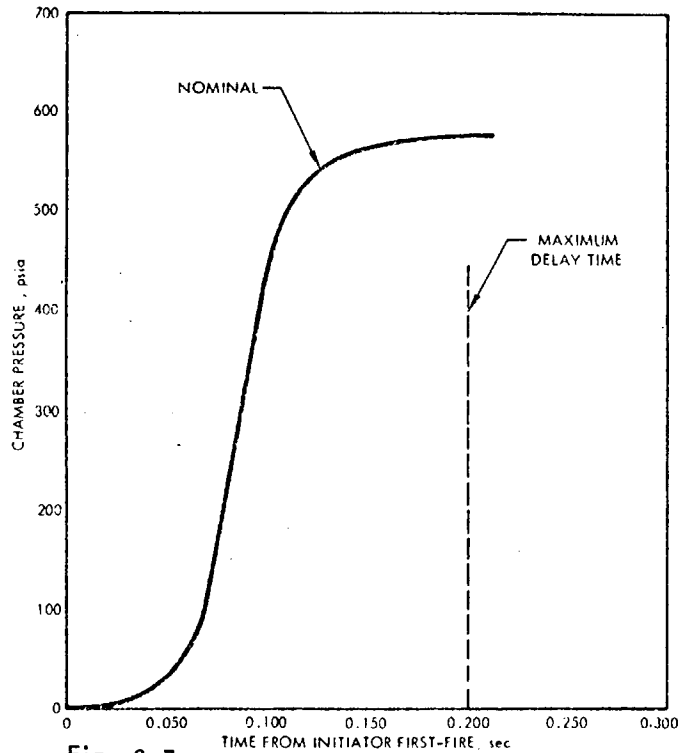

Fig. 3-7 FW-4S Motor Ignition Transient

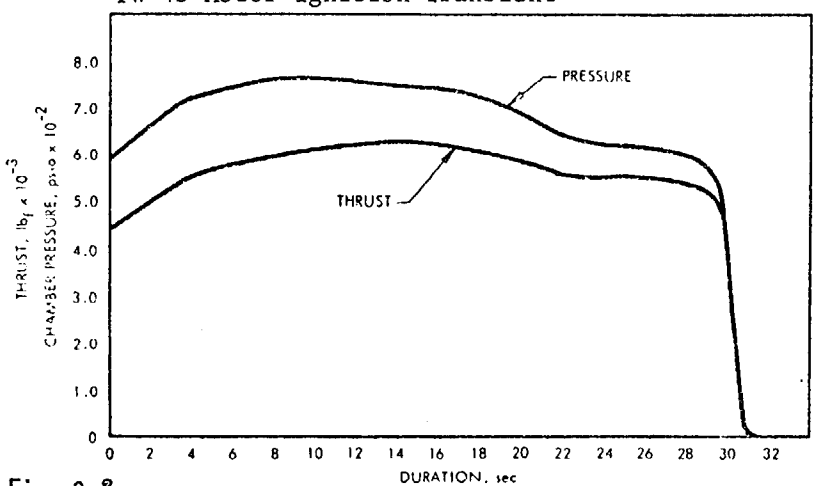

Fig. 3-8 CHAMBER PRESSURE AND THRUST VS TIME-VACUUM CONDITIONS - 200 RPM (70° F)

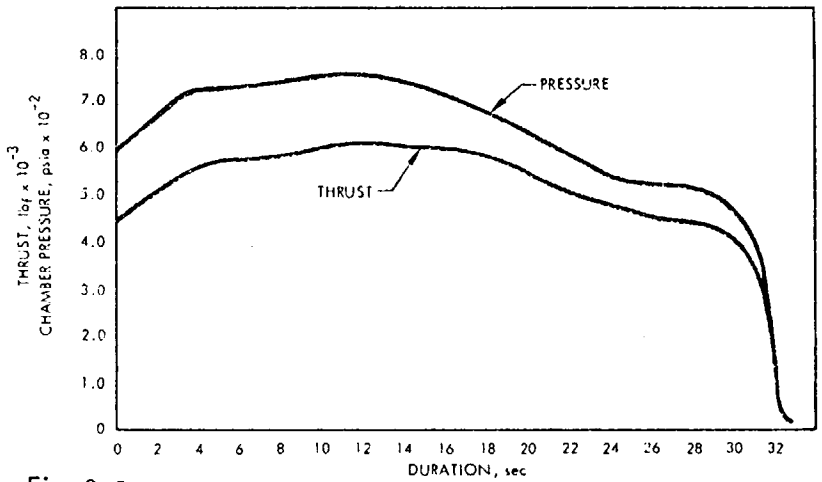

Fig. 3-9 CHAMBER PRESSURE AND THRUST VS TIME-VACUUM CONDITIONS - 0 RPM (70° F)

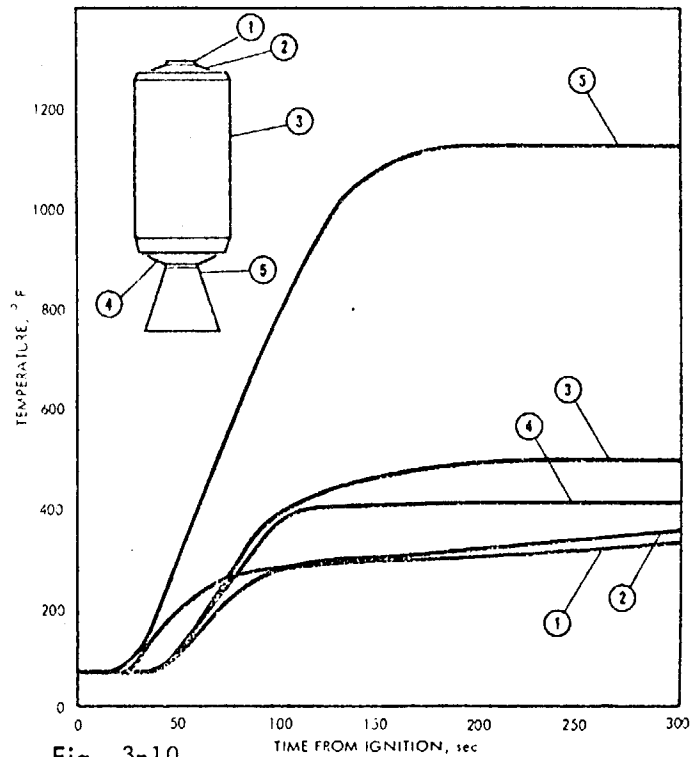

Fig. 3-10 MOTOR TEMPERATURE VS TIME

Reproduced from best available copy.

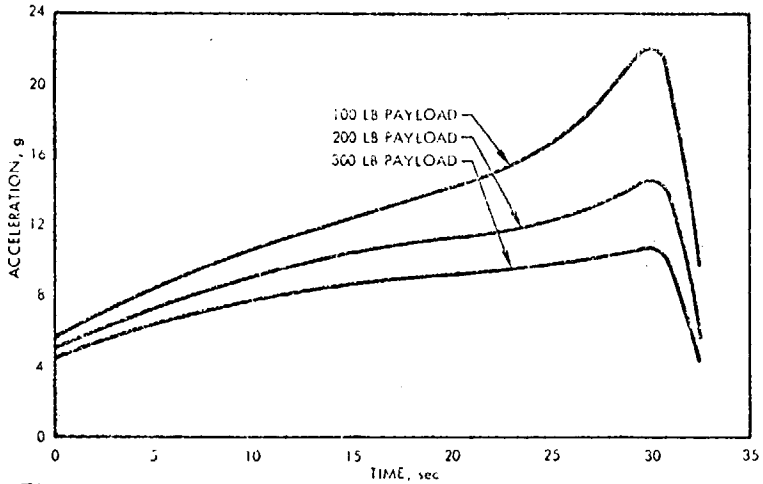

Fig. 3-11 PAYLOAD ACCELERATION VS TIME (0 RPM AT 70° F)

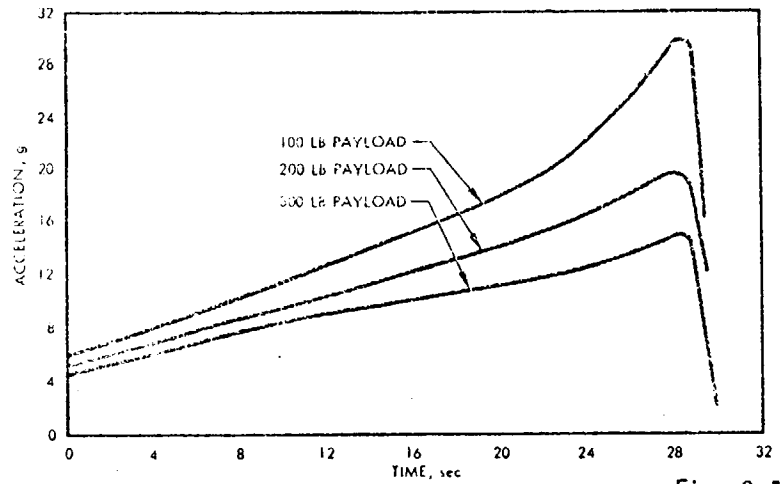

PAYLOAD ACCELERATION VS TIME (200 RPM AT 70°F) Fig. 3-12

Reproduced from best available copy.

MOTOR WEIGHT SUMMARY

FW-4S motor weight in prefire condition is 660.5 pounds. Postfire weight is 52 pounds. The longitudinal center of gravity is initially 20.8 inches aft of plane A-A of figure 32, shifting to 25.0 inches aft at web burnout. FW-4S motor weight breakdown is presented in figure 3-13, the motor weight vs time history is shown in figure 3-14, and the motor mass properties sequential breakdown is shown in figure 3-15. Longitudinal center of gravity vs time history and the motor moment of inertia vs time history are shown in figures 3-16 and 3-17.

MOTOR WEIGHT BREAKDOWN	
Case	24.1 lb
Insulation	15.8 lb
Liner	1.6 lb
Nozzle	11.4 lb
Igniter	2.2 lb
Inert	1.8 lb
Charge	0.4 lb
Miscellaneous Hardware	0.4 lb
Propellant	605.0 lb
Total Motor	660.5 lb
Burnout Motor	52.0 lb

FW-4S Motor Weight Breakdown Fig. 3-13

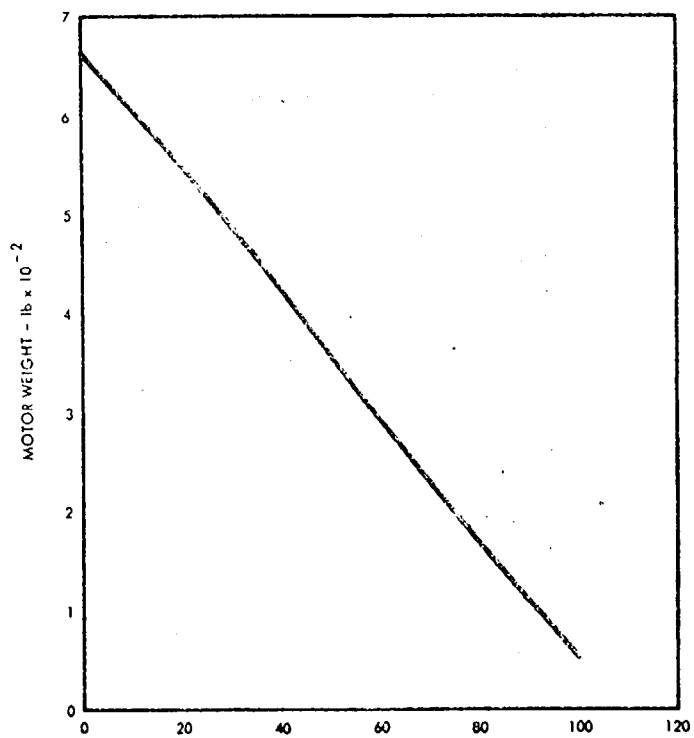

Fig. 3-14 MOTOR WEIGHT VS TIME

FW-4S ROCKET MOTOR MASS PROPERTIES SEQUENTIAL BREAKDOWN			
	PRELAUNCH	MIDBURN	BURNOUT
Weight - lb	660.5	357.0	52.0
Center of Gravity - in.*			
Longitudinal	20.8	23.7	25.0
Lateral	0.0	0.0	0.0
Vertical	0.0	0.0	0.0
Moment of Inertia - Slug ft^2			
Roll	7.1	5.3	0.6
Pitch	22.2	12.0	3.6
Yaw	22.2	12.0	3.6

* From forward face of forward polar fitting.

Fig. 3-15

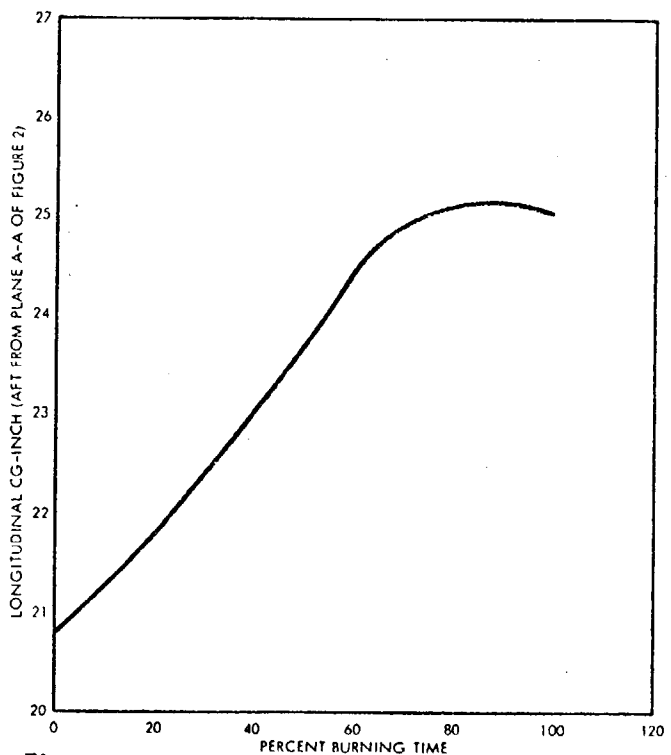

Fig. 3-16 LONGITUDINAL CENTER OF GRAVITY VS TIME

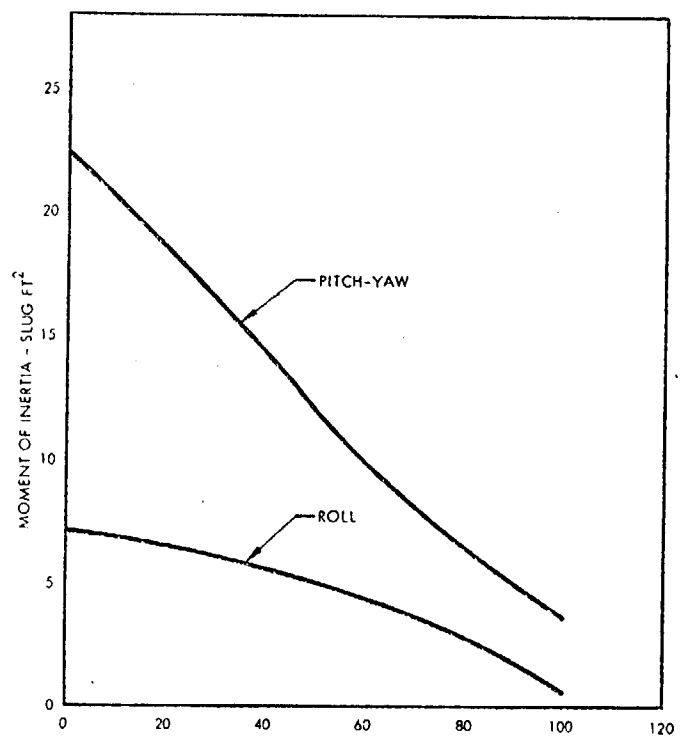

Fig. 3-17 MOMENT OF INERTIA VS TIME

Reproduced from best available copy.

ENVIRONMENTAL CONSIDERATIONS

The FW-4S motor will perform within specified limits when fired between 40° F and 100° F at spin rates from 0 to 200 rpm. The acceptable storage range for this motor is 30° F to 110° F for a period of 3 years. The FW-4S motor, further, is qualified to withstand the loads shown in figure 18. The motor has been tested under simultaneous application of these loads. Failure occurred at a bending moment 290 percent above limit loads when combined with an axial load 130 percent above the limit load.

The FW-4S shipping container has been qualified and provides adequate motor protection in normal handling and shipping by common carrier. The shipping container is ICC-approved for use with this Class II motor.

FW-4S ROCKET MOTOR LIMIT* LOAD DIAGRAM

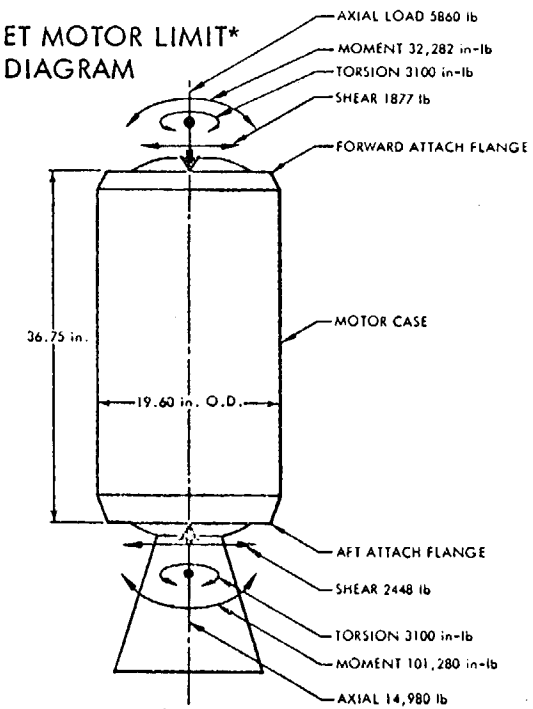

*Ultimate load conditions are 1.3 times limit load.

Fig. 3-18
FW-4S Motor Limit Load Diagram

APPLICATIONS

The FW-4S motor is designed for use as an upper stage for boost vehicles with orbital, probe and/or re-entry missions. The FW-4S motor is also adaptable for use as a retro-rocket for space vehicles, as a sounding rocket, and other applications.

UTC Brochure 65-20 provides information regarding such possible variations to the basic FW-4S motor as propellant weight, motor length, ignition delay, nozzle length, interstage attachments, etc.

Additional information regarding your specific mission requirements may be readily obtained by contacting our nearest field office (see inside back cover).

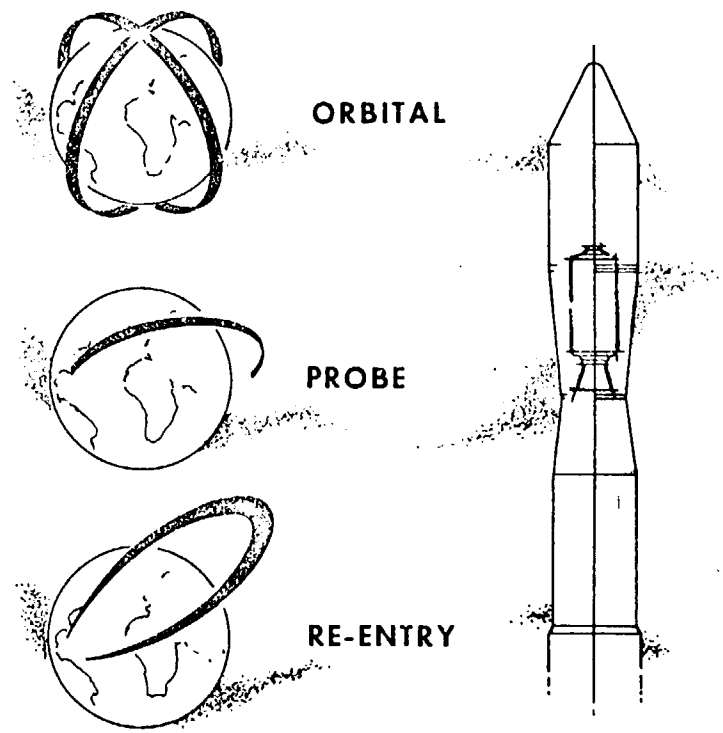

3.2 PARAMETRIC SOLID MOTOR PERFORMANCE

The FW-4S motor is characterized for only one grain design at a single nominal pressure of 650 psia. Therefore, all of the design variations are based on increasing the grain length and the throat diameter while maintaining the grain diameter and the chamber pressure. Pertinent solid propellant motor peformance and weight data for the base design and its variations are summarized in Tables 3-I and 3-II. The primary design variations available on the FW-4S motor are described in UTC Brochure 65-20 which follows.

TABLE 31-
UTC SOLID PROPELLANT PERFORMANCE EVALUATION

Parameter	Measured Value (for "base" system)	Predicted Value (for "base" system)	Prediction Methods (Equations, Tables, Graphs, etc.) For New Systems	Limitations of Prediction Method (Thrust range, P_c range, throttle range, etc.)	Expected Accuracy of Predicted Performance
Steady State Isp Pulse mode Isp if applicable	286 sec N/A		Section 2.3	F = 3000-11000# P_c = 650 Only ϵ = 25-100	1%
Minimum Impulse Bit	N/A				
Reproducibility of Impulse Bit	N/A				
Total Impulse Cutoff Accuracy	± 2%			See Section 3.3.6.3 For Added Information	
Throttled Performance	N/A				
Thrust Vector Alignment	.3 mrad				
Thrust Centerline Offset	7 mils				

TABLE 3-II- SUBSYSTEM AND COMPONENT WEIGHT DATA
SOLID PROPELLANT

"BASE" SUBSYSTEM OR COMPONENT DESCRIPTION:	Dry Weight (for "base" subsystem)	Burnout Weight (for "base" subsystem)	Predicted Weight for the "base" system	Prediction Methods (Tables, Graphs, Equations, etc.) For New Subsystems	Limitations of Prediction Techniques (Thrust range, P_c range, etc.)	Expected Accuracy of Predicted Weight
Fuel System				Directly Proportional to Length	F = 3000-11000# Pc = 650 only ϵ = 25 - 100	1%
Case	24.1	24.1				
Insulation	15.8	12.7				
Liner	1.6	1.6				
Propellant	605.0	0.0				
Nozzle & MISC.						
Nozzle	11.4	11.4				
Miscellaneous	0.4	0.4				
Ignitor						
Inert	1.8	1.8				
Charge	.4	.0				

- High Performance
- High Mass Fraction
- High-Strength Fiberglass Case
- Advanced Composite Nozzle
- Multiple Applications

INTRODUCTION

This brochure describes some of the potential variations of the FW-4S motor and their effect on other parameters. The companion brochure, UTC 65-8, provides detailed data on the FW-4S motor. Sufficient technical details are presented to enable the selection of the optimum design for a range of mission requirements. The basic FW-4S motor design features are maintained, while the case length, propellant weight, interstage flanges, and nozzle lengths are permitted to vary. The casing diameter, dome contours, wall thicknesses, maximum operating pressure, propellant formulation, nozzle and igniter construction, and basic motor materials are maintained the same as in the FW-4S motor. The parametric data provided include motors having gross weights in the range of 250 to 1400 pounds.

Some of the motor variations included are minor, such as modified attach flanges for weight savings or interfacing with other missile structures. Other variations may require verification firings, and those involving large excursions from the basic FW-4S motor may require more extensive testing.

Reproduced from best available copy.

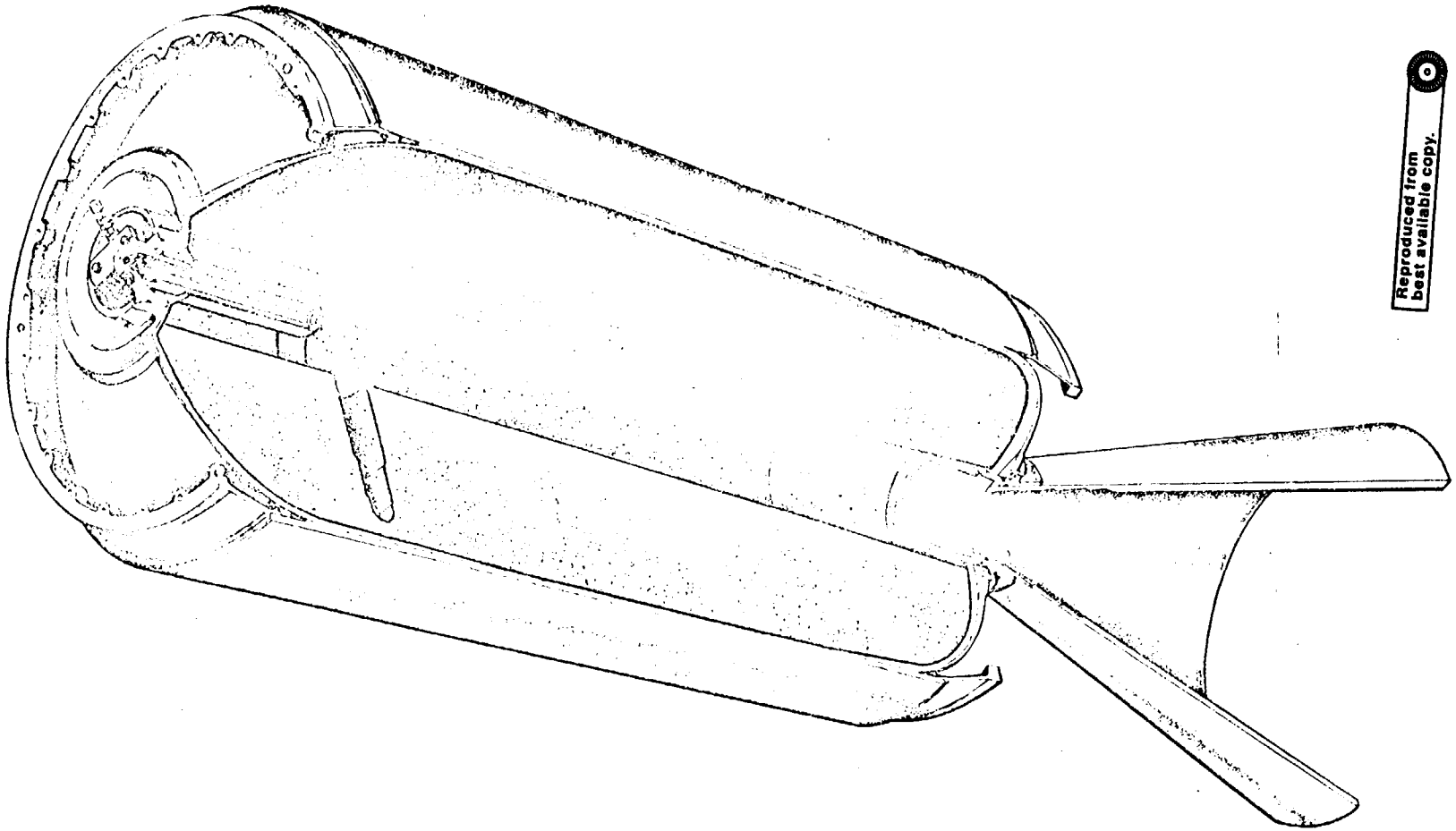

FW-4S Motor Cutaway, Showing Internal Components

Figure 3-19

TECHNICAL DISCUSSION

Motor Description

The FW-4S rocket motor is shown in figure 3-19 The motor is 19.6 inches in diameter and has an overall length of 58.5 inches. The motor has a fiberglass-epoxy case containing 606 pounds of class II propellant, a high expansion ratio nozzle, and a rocket-type igniter containing delay initiatiors. Sufficient internal insulation is provided to maintain the case temperature below 500° F after burnout when spun at 200 rpm or less.

The interface dimensions for the FW-4S motor are presented in figure 3-20

Motor Variations

NOZZLE LENGTH, BURNING TIME, AND INTERSTAGE FITTING VARIATIONS

Several minor variations can be made to the basic FW-4S motor. For example, it may be desirable to reduce the nozzle length permitting a shorter interstage. As the projected nozzle length "n" is changed, the nozzle weight and expansion ratio vary. The resulting effects on the nominal 286-second specific impulse and the 11.5-pound nozzle weight as a function of the nozzle length are presented in figure 3-21

The motor burning time may be increased by increasing the throat area thereby reducing the motor chamber pressure and the propellant burning rate. This increased burning time can be used to reduce the acceleration imparted to the payload. If all nozzle dimensions are maintained other than the throat, the effects on specific impulse and payload acceleration presented in figure 3-22 are obtained.

The FW-4S can be adapted to various existing missile attach structures as shown in fig. 3-23. Attachment flanges (1) and (2) are presently being used on the FW-4S motor. Attachment flanges (3) and (6) would offer some weight savings and attachment flange (4) is compatible with both Scout and Thor-Delta.

Ballistic Variations

GENERAL

The FW-4 designation defines a motor with a maximum diameter of 20 inches and a length of "L" inches from forward to aft attach planes. The FW-4S designation is a special case of the FW-4 motor with an "L" dimension of 36.75 inches. The motor length, propellant weight, and nozzle configuration have been allowed to vary in these parametric studies. The major design parameters such as propellant formulation, nozzle design, and igniter and case hardware have been maintained. The throat dimension has been sized in all motors of case length "L" to maintain the maximum operating pressure the same as the FW-4S motor. This ensures similarity with propellant ballistics and operating stress levels for all components. All FW-4 motors would have the same minimum burning time, maximum chamber pressure, case wall thickness, and materials of construction. The motor case wall temperature will not exceed 500° F during firing or after burnout when spun at speeds up to 200 rpm.

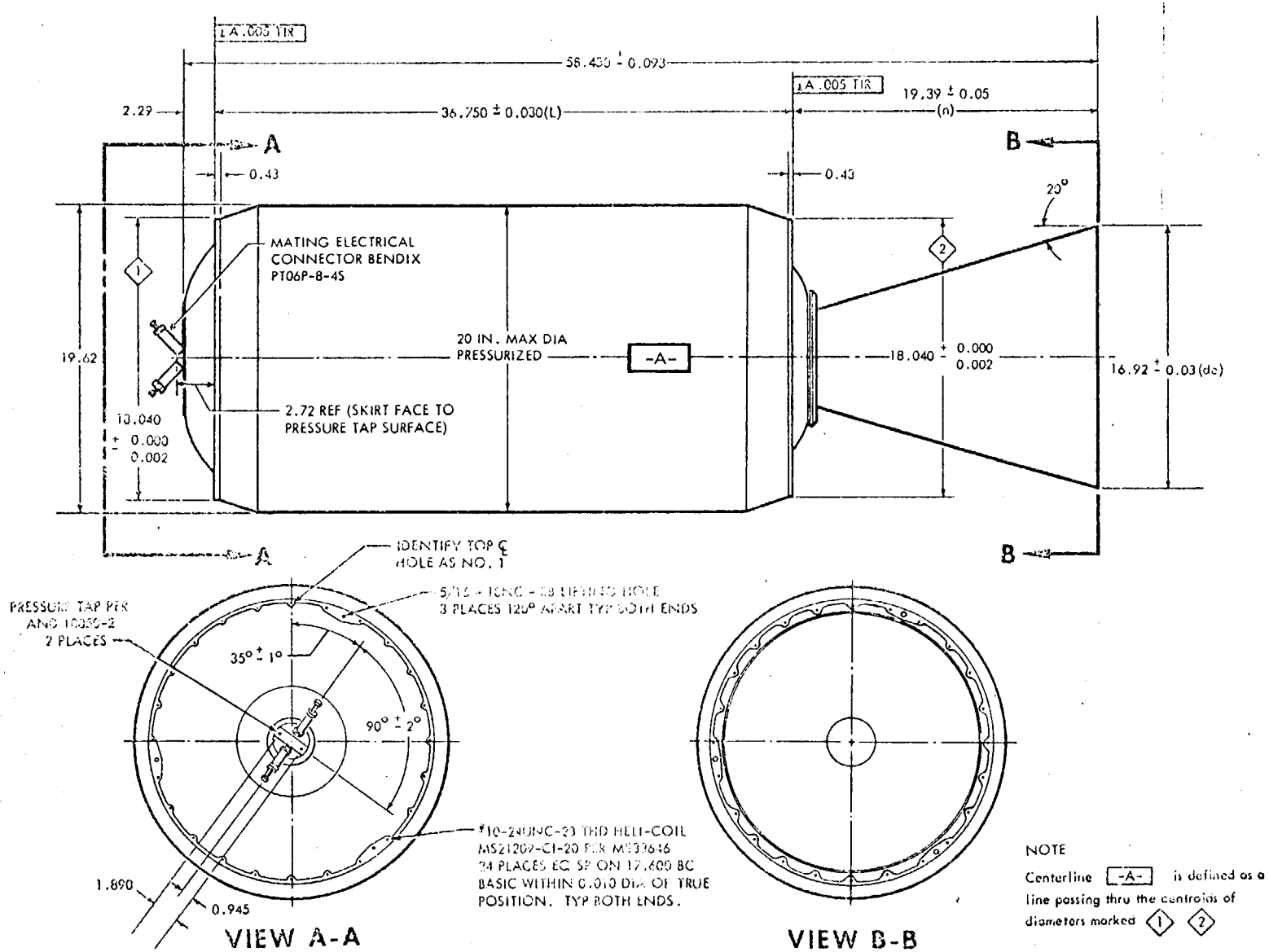

Figure 3-20 FW-4S Pertient Internal Dimensions

SUGGESTED WORK SHEET

WORK SHEET

ENVELOPE

Case Length (L)

Basic FW-4S case length (36.75 inches)

(See figure 6.) New case length for different propellant weight _____ ( )

(See figure 5.) Effect of different attach fittings (+ or -) _____ ( ) (1)

Resulting case length _____

Nozzle Projection (n)

Basic FW-4S Nozzle Projection (19.39 inches)

(See figure 7.) Nozzle throat diameter _____ (2)

(See figure 14.) Resulting nozzle projection _____

Overall motor length = (1) + (2) _____

(See figure 15.) Nozzle exit diameter _____

WEIGHTS

(See figure 10.) Inert weight using new case length _____ ( )

(See figure 16.) Effect of different nozzle length (+ or -) _____ ( )

(See figure 5.) Effect of different attach fittings (+ or -) _____ ( ) (3)

Resulting prefire inert weight _____ (4)

Postfire weight = (3) - 5 pounds _____

IMPULSE

Basic FW-4S propellant weight (606.0 pounds) _____ (5)

(See figure 6.) New propellant weight _____ (6)

Motor weight at launch = (3) + (5) = _____

Basic FW-4S propellant specific impulse = 286 sec

(See figure 7.) Effect of case length on throat _____ (7)

(See figure 14.) Effect of nozzle length on expansion ratio _____ (8)

(See figure 13.) Resulting specific impulse _____

Motor total impulse = (5) x (7) = _____

$$\Delta V^{*} = 0.993\,(7)\,g\,\ln\frac{(6)+P}{(4)+P}$$

where P is the gross payload boosted.

*Vacuum conditions and "g" free.

Note: If a spin rate below 150 rpm is to be used, the casing insulation weight may be reduced 6 lb.

Motors over 43 inches in length require a grain design utilizing an additional slot located to obtain the desired pressure-time history. The additional propellant slot requires additional insulation in the motor aft end, resulting in a step increase in inert weight.

In the following discussion, two variations of the FW-4 motor will be investigated. The first will utilize the FW-4S nozzle configuration, and then the nozzle configuration will be allowed to change to the desired projected length or expansion ratio.

VARIATIONS BY CHANGING CASE LENGTH (NOZZLE ENVELOPE FIXED)

For FW-4 motors that have the same external nozzle configuration as the FW-4S motor (figures 3-24, 25, 26, 27, 28, 29 and 30) apply directly in determining all performance parameters. On all curves the symbol ⊕ designates the position of the FW-4S and the effect of any changes in motor length can be read directly from these figures. The first curve presented is fig 3-24 which gives the relationship between motor case length and propellant weight. Length "L" is defined as the distance between mounting flanges and is 36.75 inches for the FW-4S motor which contains 606 pounds of propellant. For a motor of the desired propellant weight and case length "L" determined from fig 3-24 all other figures can be entered for determination of performance variations. For a motor of length "L", the throat diameter can be obtained from fig 3-25. Also shown on this figure is the nozzle expansion ratio for a motor with an external nozzle configuration identical to the FW-4S motor. Fig 3-26 presents the specific impulse knowing the motor case length, again using the fixed external nozzle shape. Finally, the total impulse can be obtained using the propellant weight and the obtained specific impulse above. This is presented versus motor length in fig. 3-27. To obtain the hardware weights and resulting mass ratio, figures 3-28, 29 and 30 have been plotted versus motor case length, and from figure 24 the desired parameters can be obtained. The weights include a complete motor ready to fire with igniter. The included nozzle weight has an external configuration shown in fig-3-28 (i.e., the FW-4S configuration), and the weight has been adjusted for throat size as determined in fig 3-25. The motor burnout weights are presented in figure 3-30

VARIATIONS BY CHANGING NOZZLE ENVELOPE

Further parametric studies can be made on the FW-4 motor if the nozzle envelope is allowed to vary. It may be desirable to shorten the nozzle projected length to allow a shorter interstage structure or increase the nozzle length raising the exit plane diameter to improve the overall expansion ratio resulting in higher performance. For this study the nozzle half-angle has been maintained at 20°, and the performance has been scaled up or down from the specific impulse obtained on the FW-4S vacuum motor firings.

Figures 3-31, 32, 33, and 34 have been plotted so that fig 3-32 gives the nozzle length for a desired expansion ratio based on the desired specific impulse from figure 3-31 and the required throat area from fig 3-25. Knowing the nozzle expansion ratio, fig 3-33 allows the determination of the exit diameter for determining the complete nozzle envelope. Finally, fig 3-34 shows the amount of weight that must be added or subtracted to the total motor inert weight from fig. 3-28 as a result of the nozzle envelope change.

SUGGESTED WORK SHEET

Included on the following page is a suggested work sheet for determining the overall performance parameters of any FW-4 motor with any nozzle configuration, attach flange, and desired propellant weight.

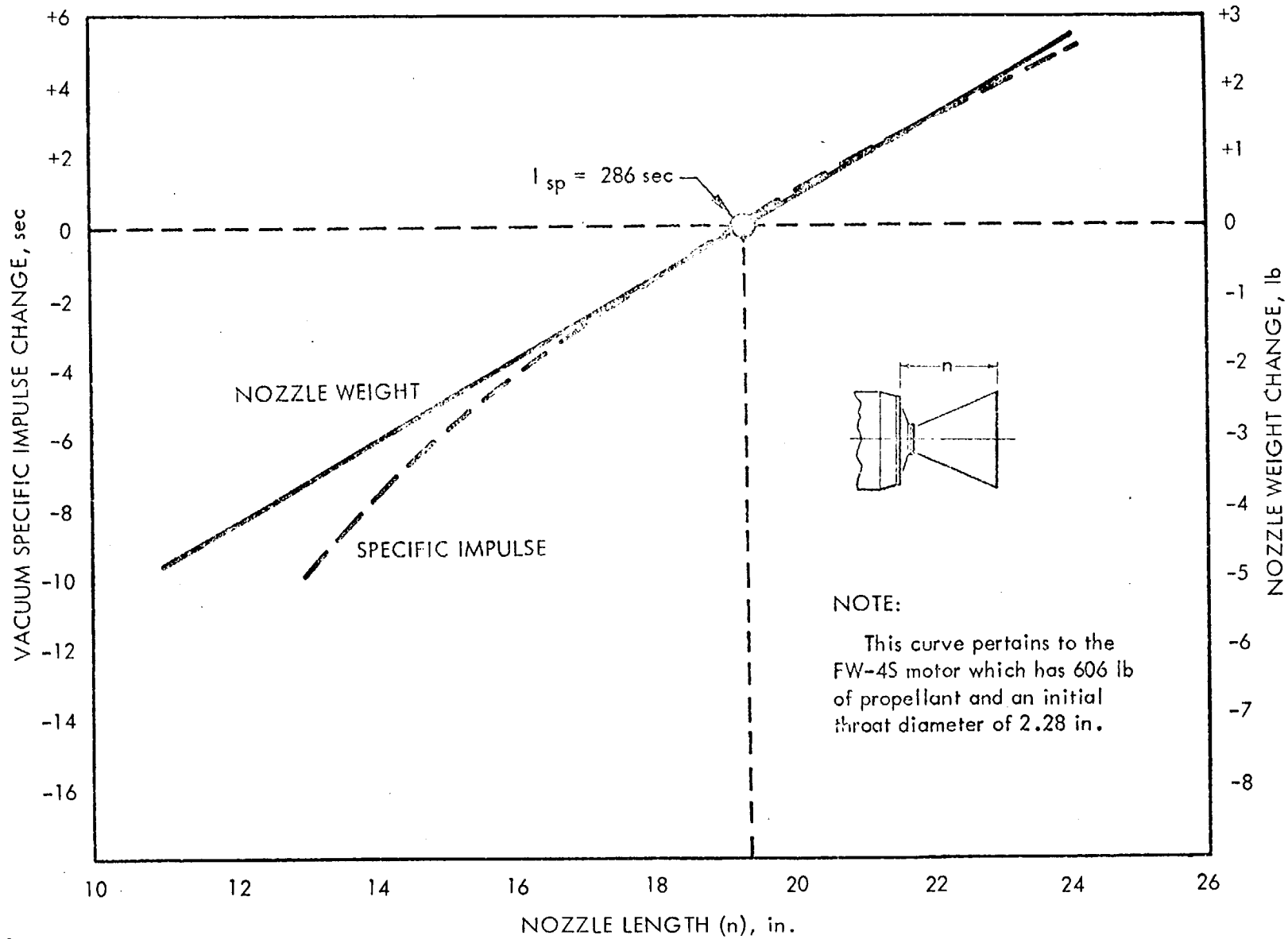

FW-4S Vacuum Specific Impulse and Nozzle Weight Vs. Nozzle Length

Figure 3.-21

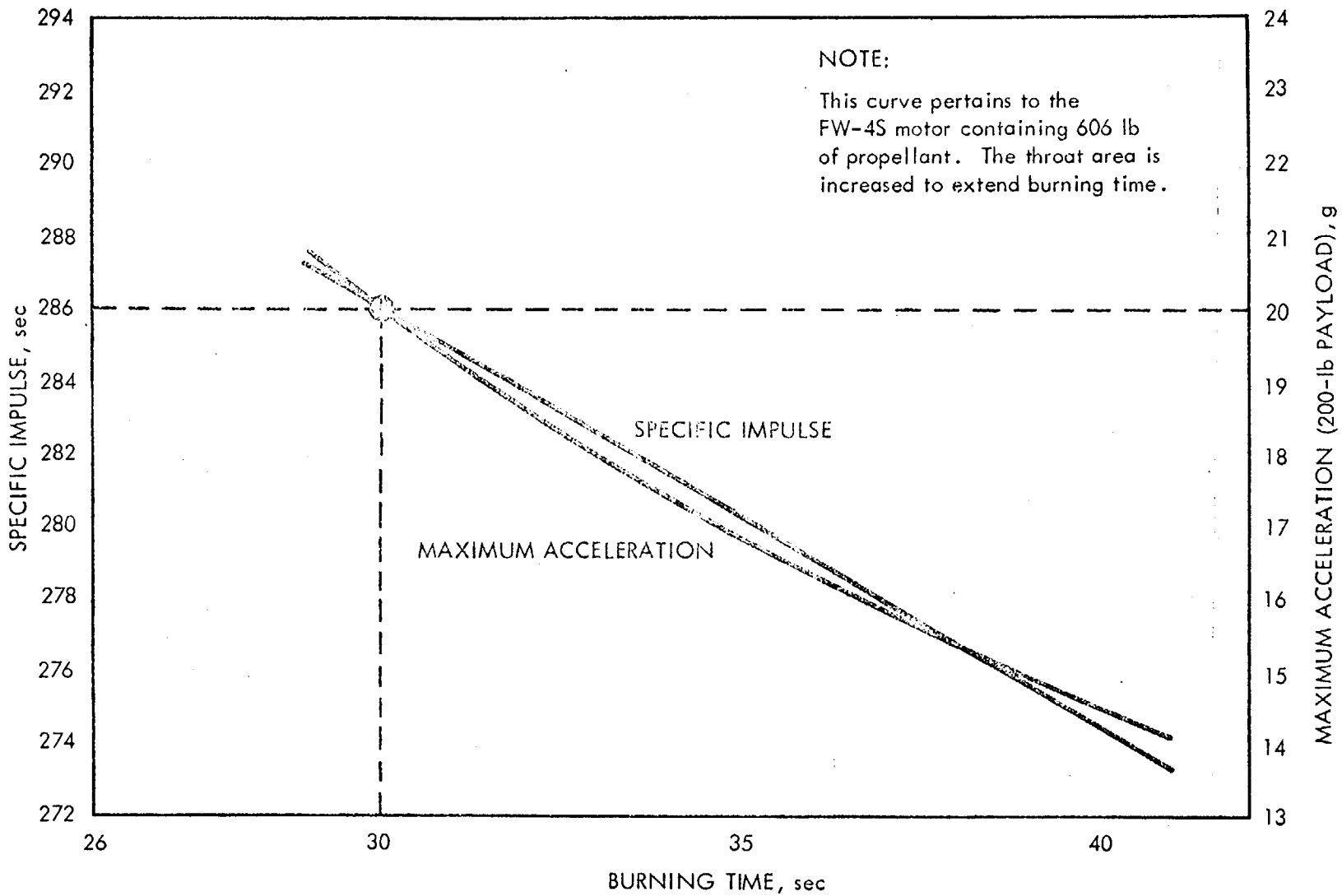

Figure 3-22 FW-4S Vacuum Specific Impulse vs. Burning Time

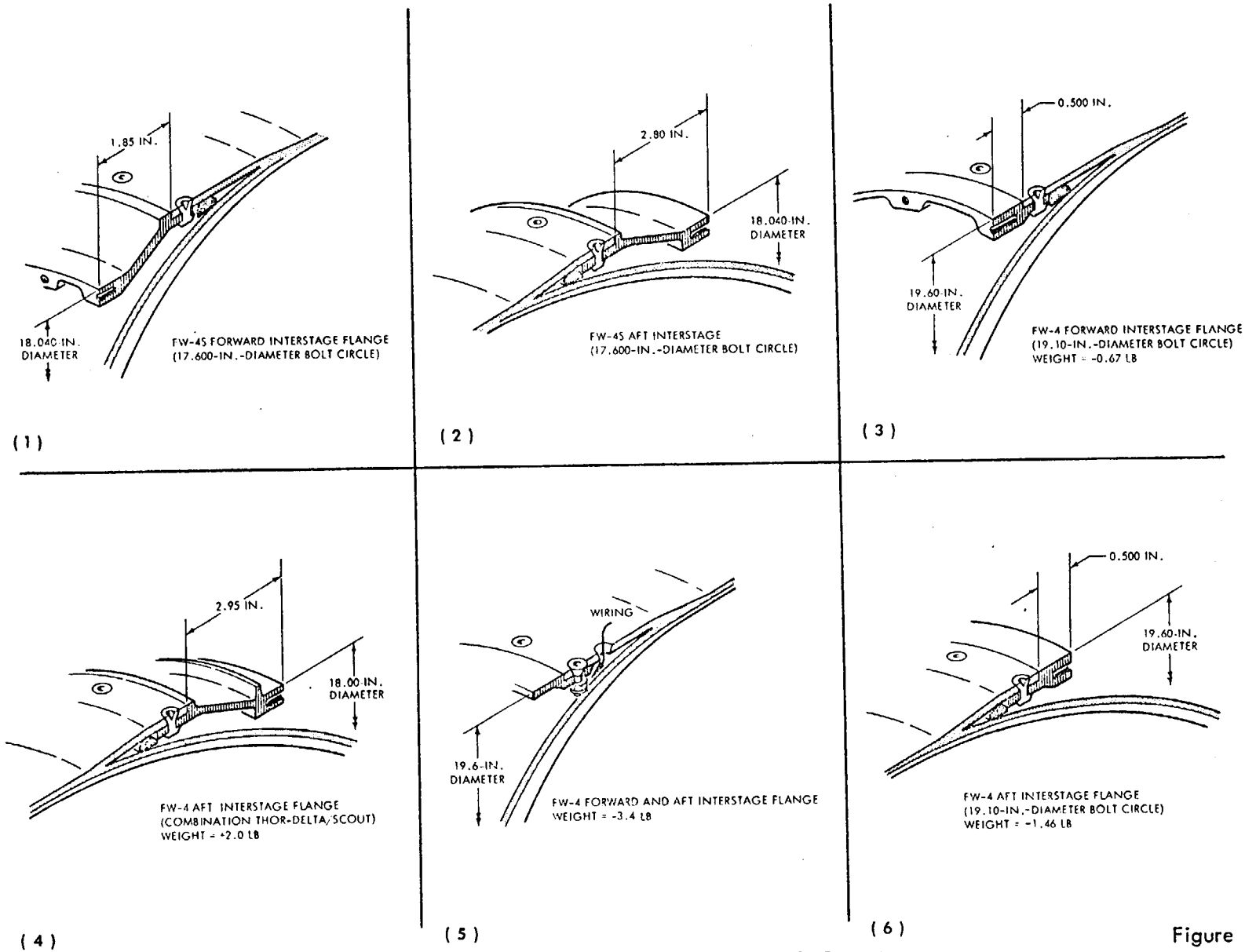

Figure 3-23

FW-4S Missile Attach Structures

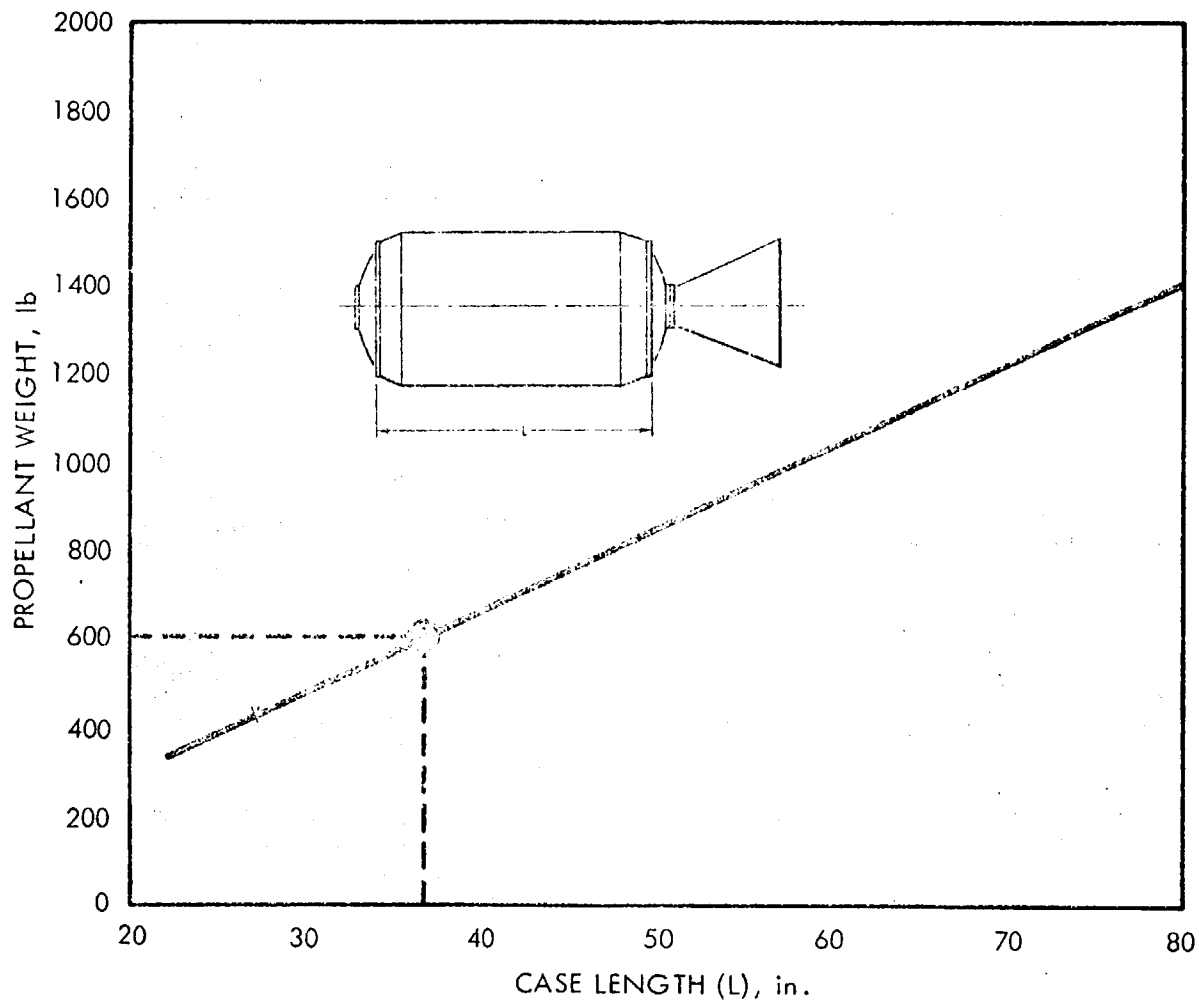

Figure 3-24 FW-4S Propellant Weight vs. Case Length

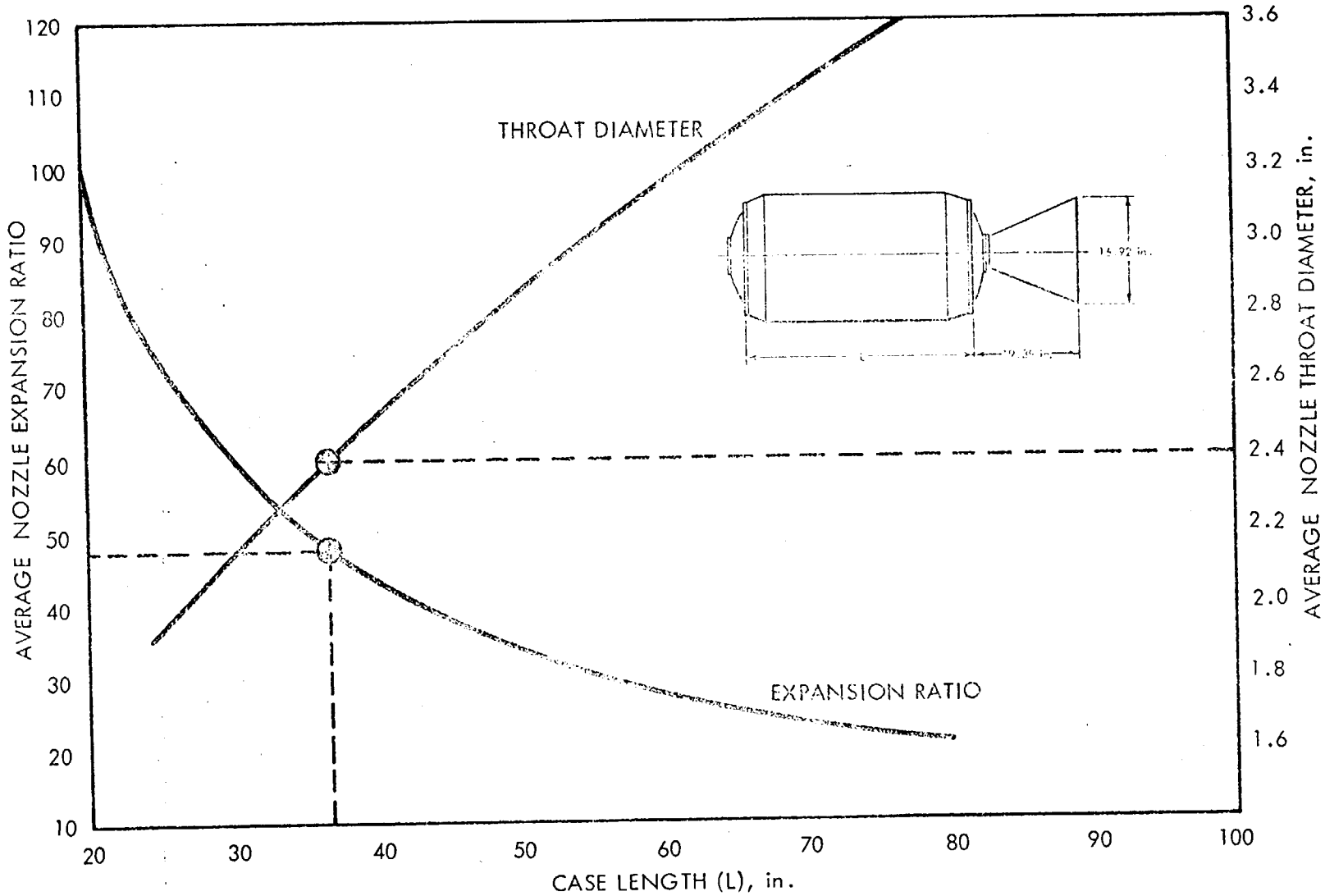

FW-4S Average Nozzle Expansion Ratio and Throat Diameter vs. Case Length

Figure 3-25

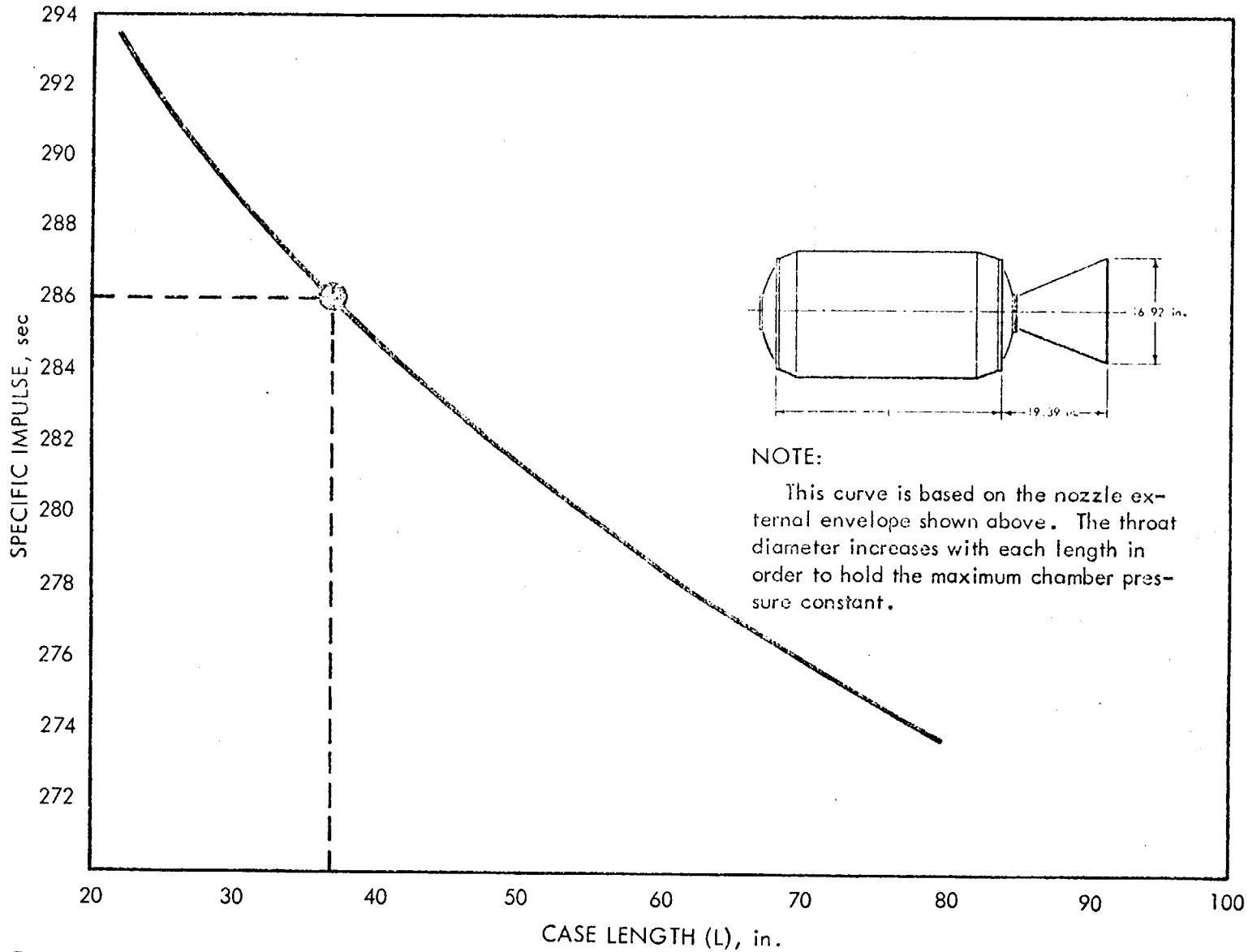

Figure 3-26 FW-4S Specific Impulse vs. Case Length

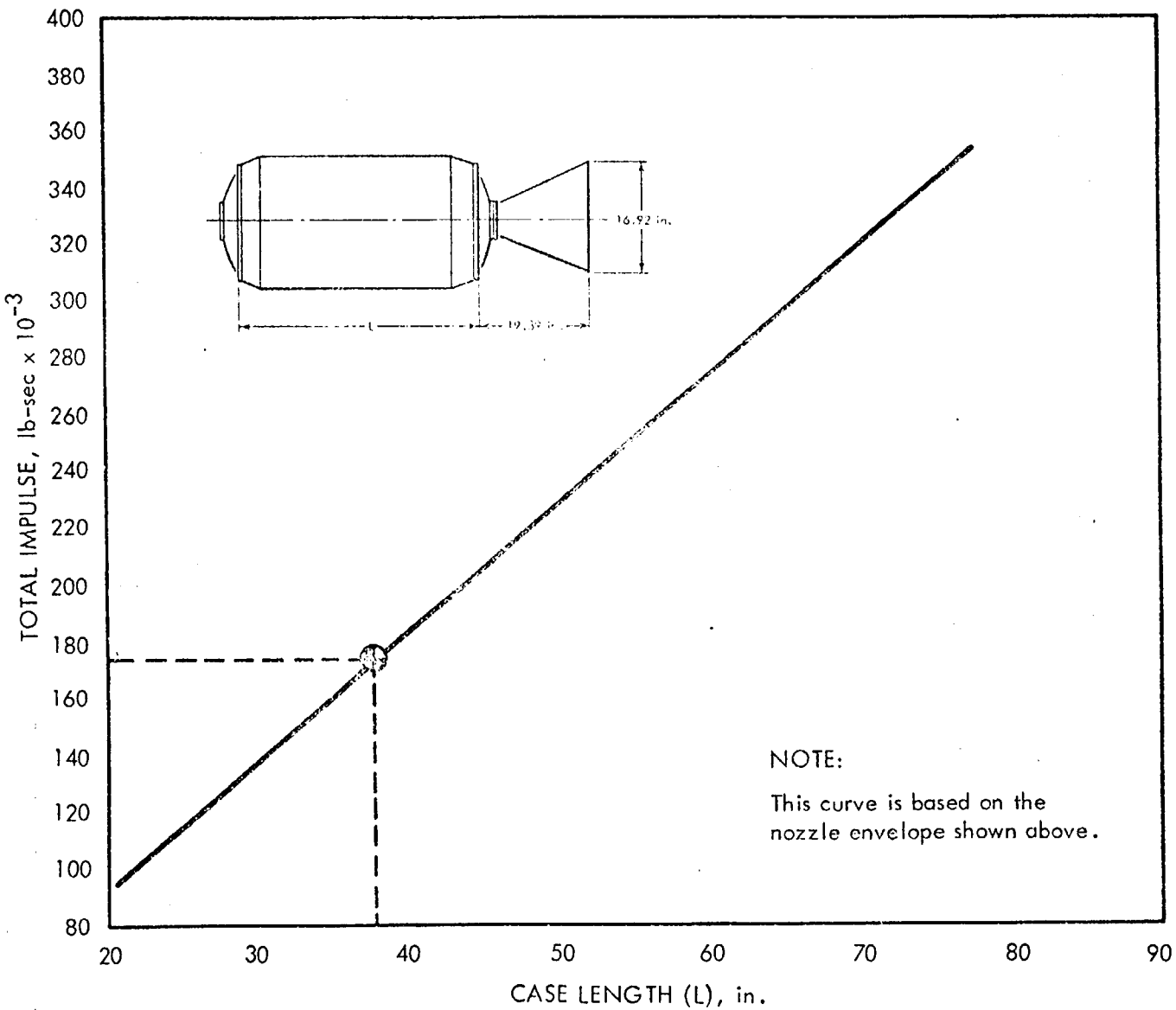

FW-4S Total Impulse vs. Case Length

Figure 3-27

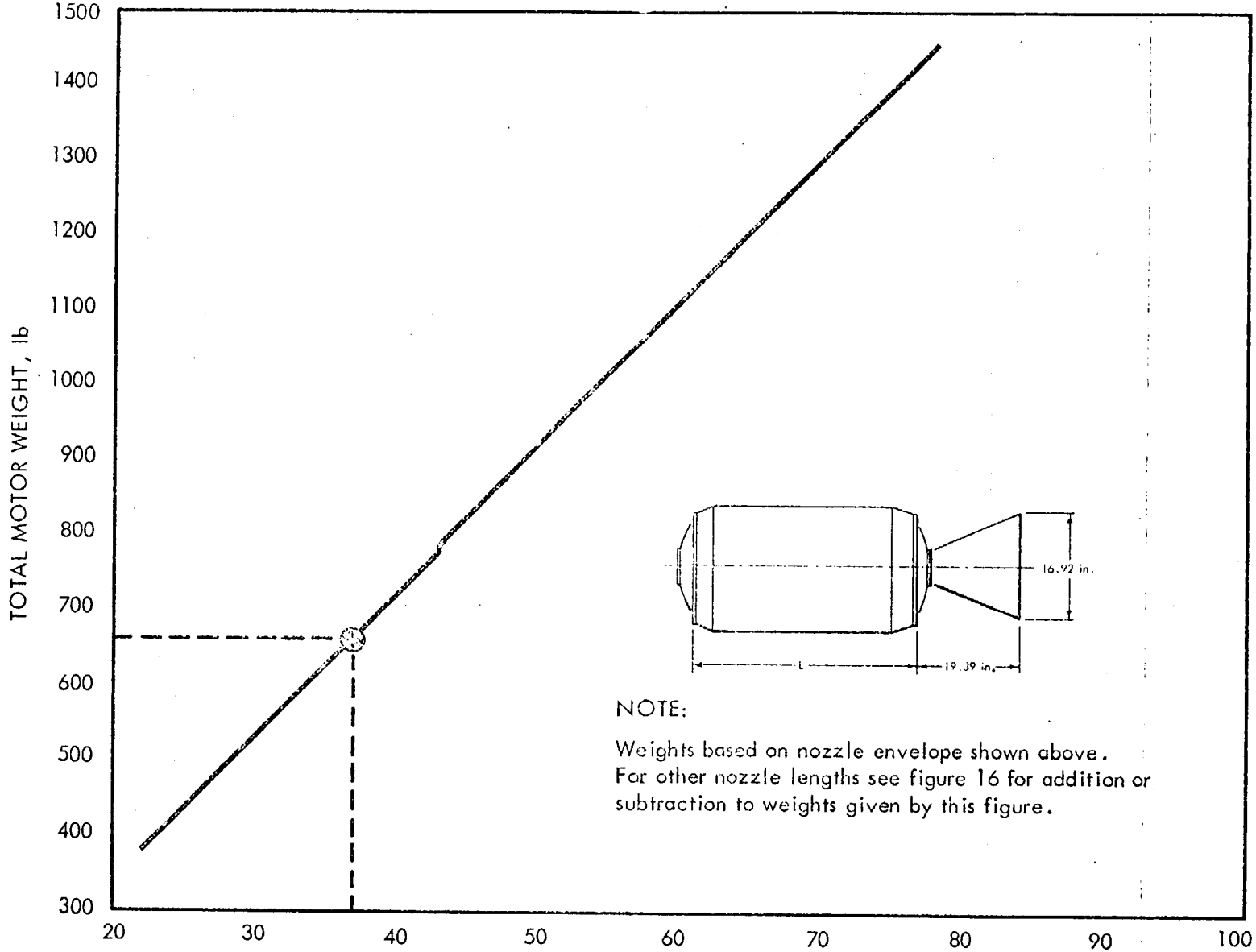

Figure 3-28

FW-4S Total Motor Weight vs. Case Length

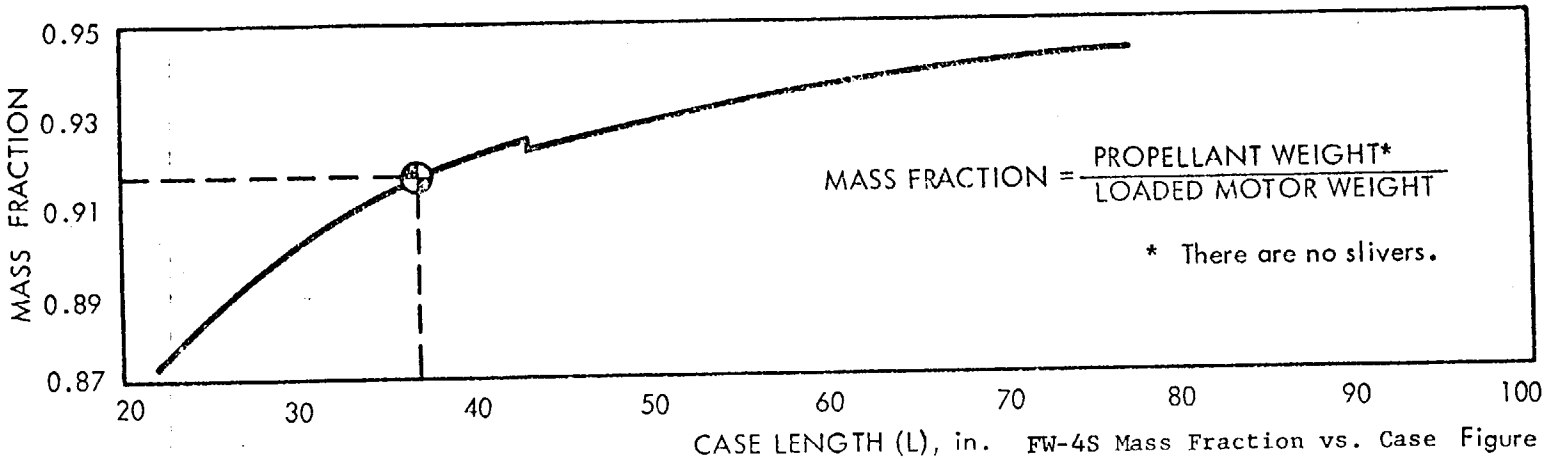

FW-4S Mass Fraction vs. Case Length Figure 3-29

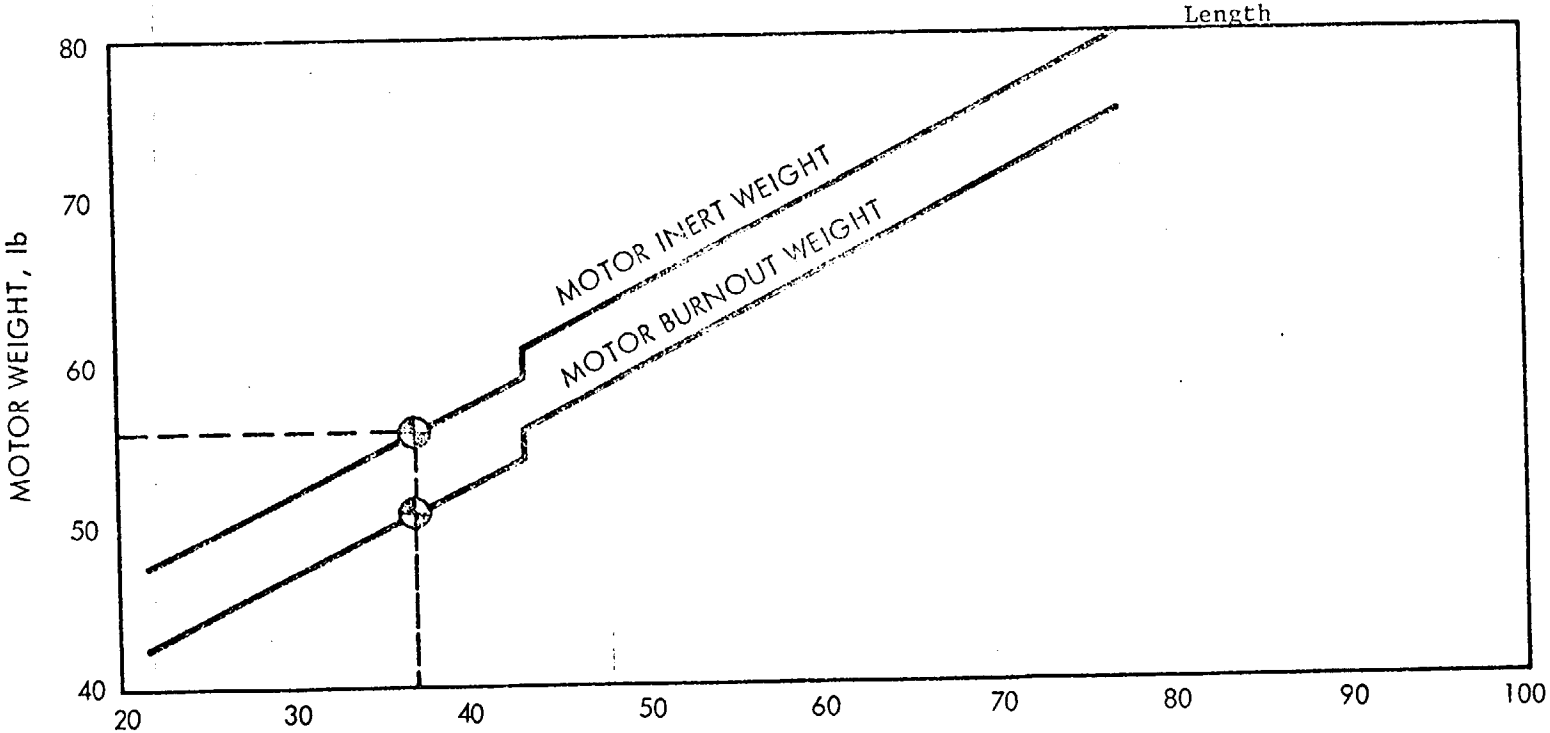

FW-4S Motor Weight vs. Case Length Figure 3-30

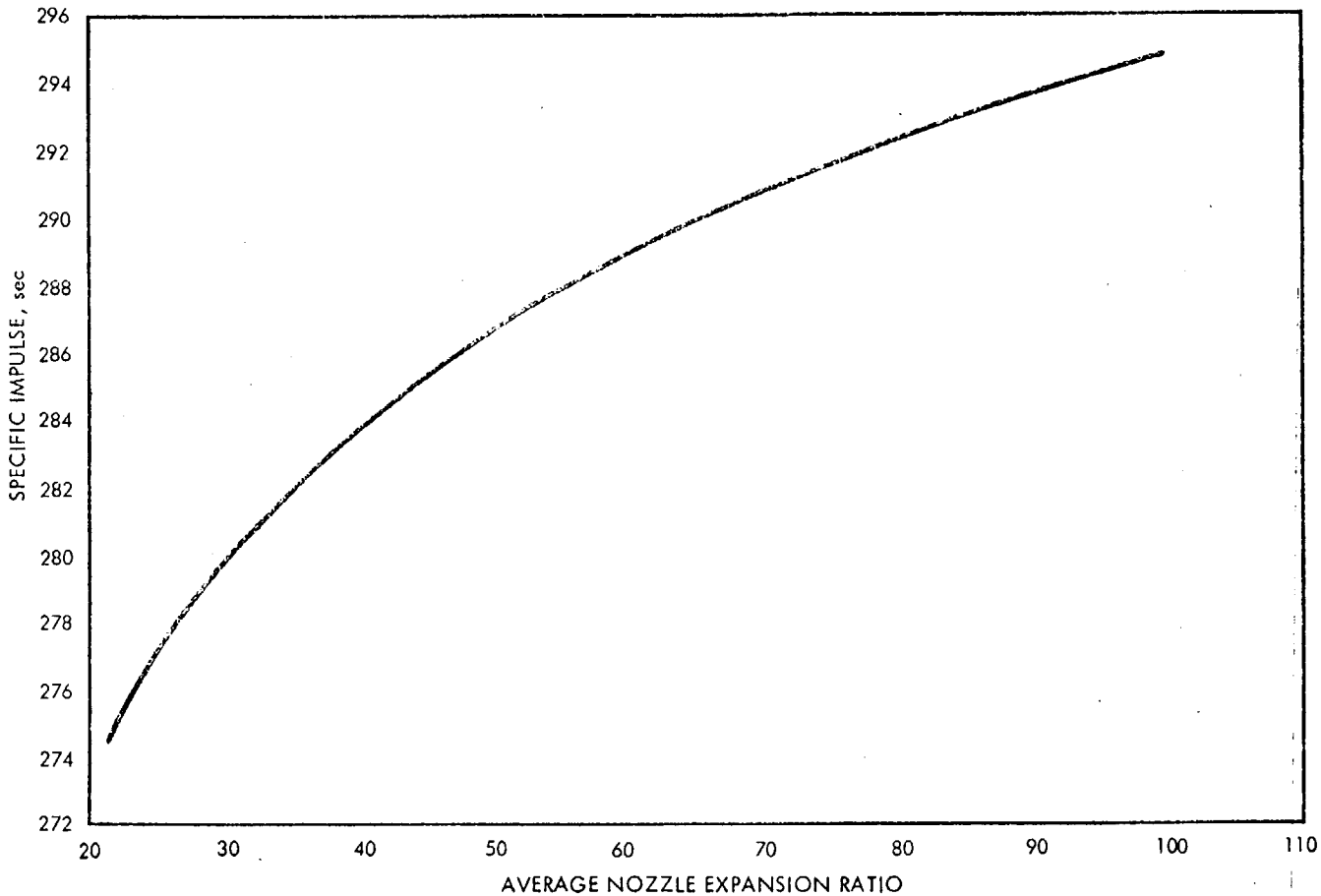

Figure 3-31 FW-4S Specific Impulse vs. Nozzle Expansion Ratio

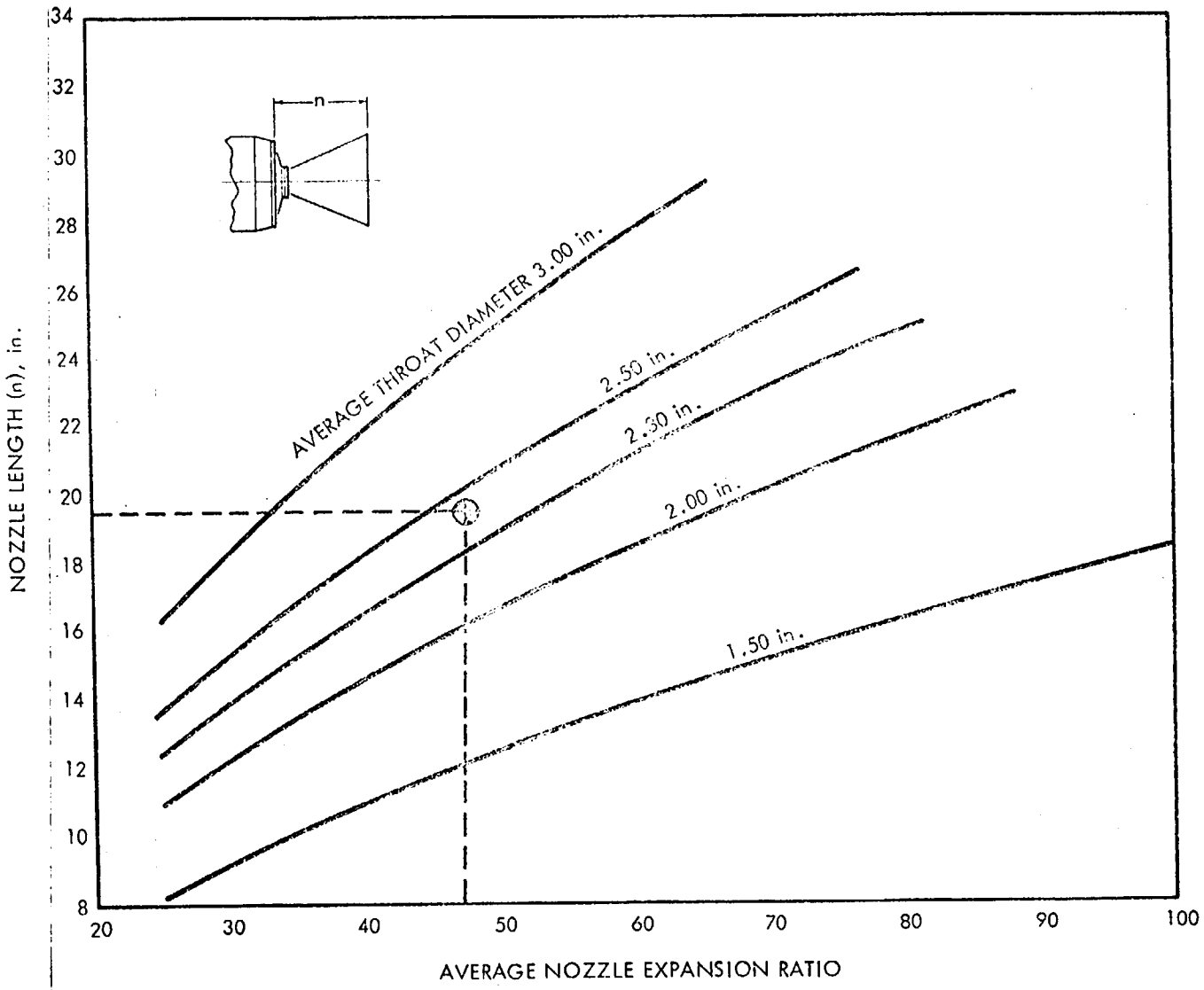

FW-4S Nozzle Length vs. Nozzle Expansion Ratio

Figure 3-32

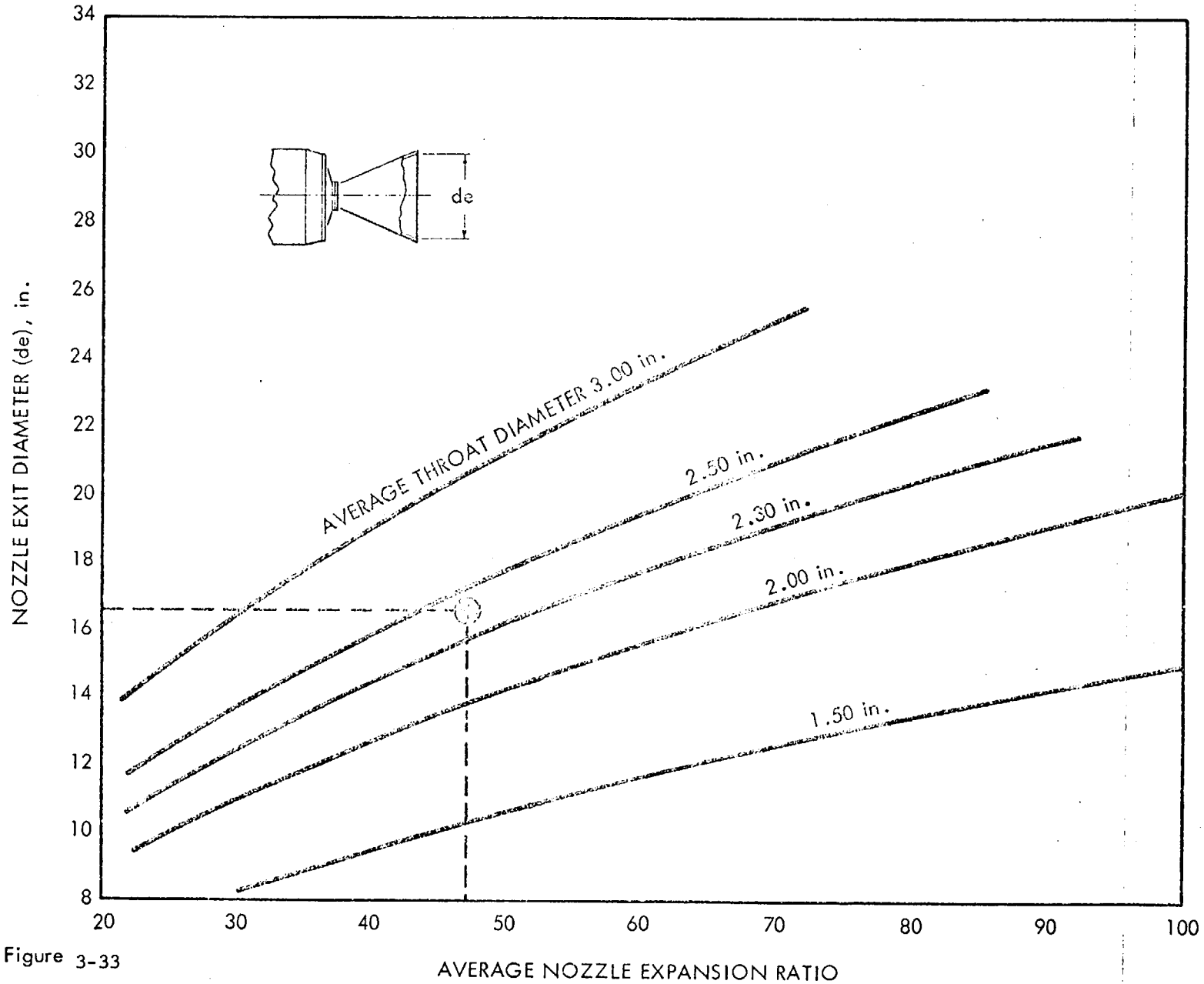

Figure 3-33

FW-4S Nozzle Diameter vs. Nozzle Expansion Ratio

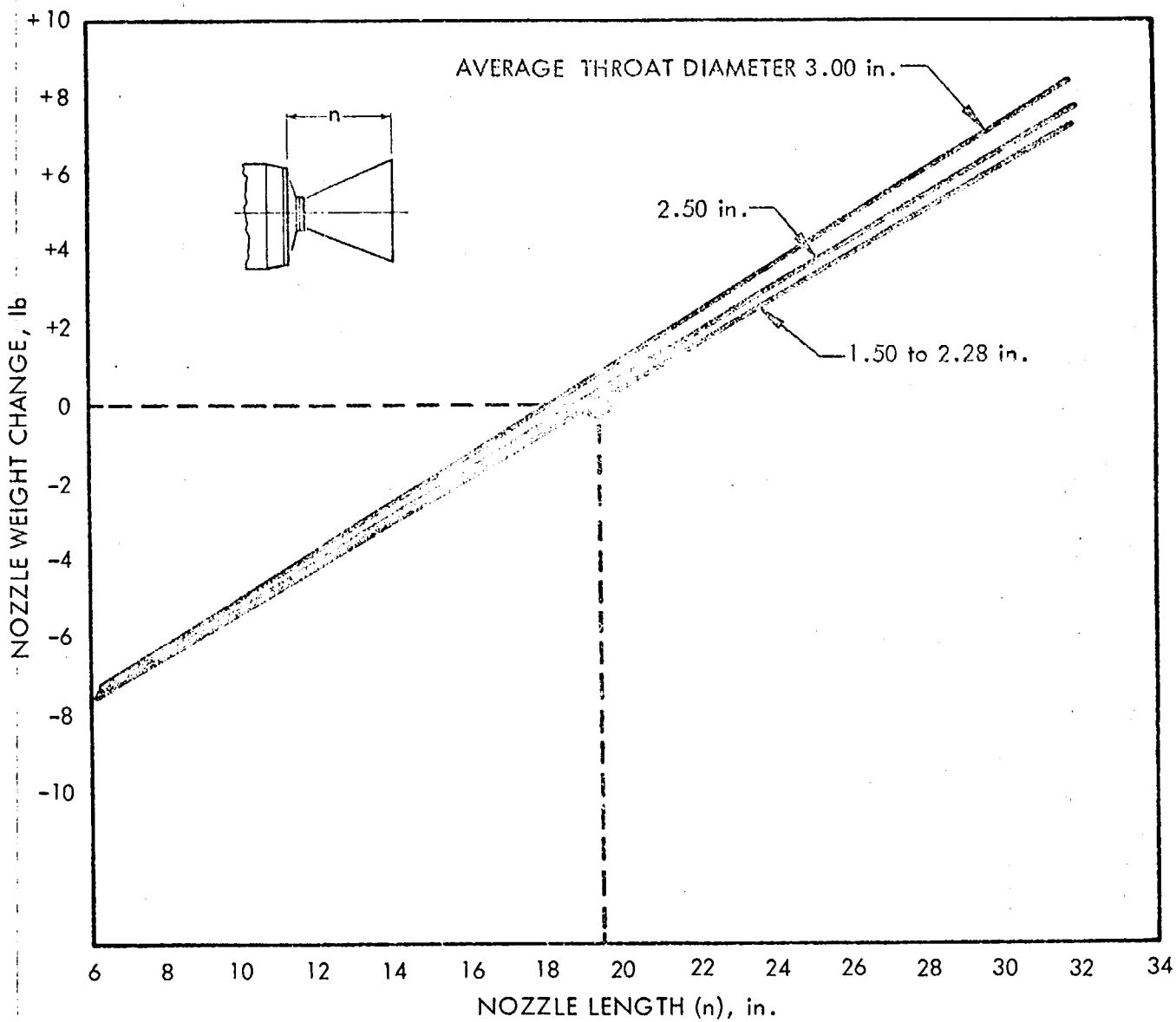

FW-4S Nozzle Weight Change vs. Nozzle Length

Figure 3-34

3.3 SOLID MOTOR RELIABILITY ANALYSIS (RELIABILITY PREDICTION)

The motor consists of four major assemblies: the igniter, the case and propellant, the attachment, and the nozzle. Manufacturing of the igniter assembly and propellant is performed by UTC, while the case and nozzle are obtained by subcontract from vendors having reliability program requirements as contractual obligations.

The general integrity of the motor, essentially as designed for flight prototype, has been demonstrated by the firing of thirty-two Scout motors. No significant reliability problems are anticipated which will preclude the fulfillment of the reliability objective of .98.

3.3.1 Motor Success Diagram and Reliability Model Summation

The functional success diagram for the motor subsystem is shown in figure3-35 This diagram presents the major subsystems, each of which must operate successfully for propulsion performance, in serial form. The mission reliability mathematical model for the motor system is:

$$R_{Motor} = R_{Ignition} \times R_{Case} \times R_{Nozzle} \times R_{Attach} \times R_{Propellant}$$

$$R_{Motor} = (.99964)\ (.99991)\ (.99986)(.99999^{+})\ (.99934)$$

$$R_{Motor} = (.99875)$$

3.3.2 Ignition Subsystem

The ignition subsystem for the motor is a UTC-developed assembly. The assembly consists of a forward-mounted rocket-type motor composed of three major pyrotechnic components; two electrically actuated delay initiators, a pelletized booster charge, and the igniter motor. The igniter motor is loaded with an internal-burning propellant grain of an ammonium perchlorate formulation developed by UTC. An allocation of .99964 reliability was apportioned to the ignition subsystem. This can be exceeded.

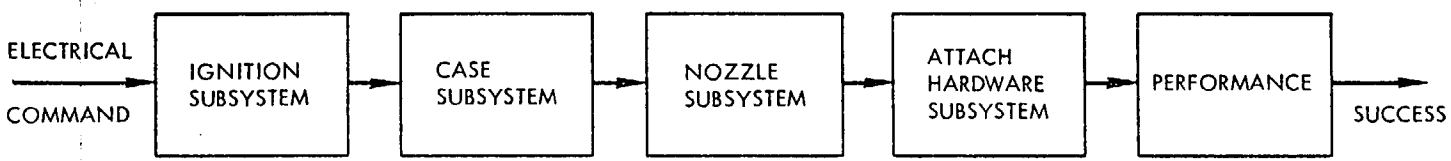

$(R_{Ignition})$

1. Igniter delay of 6.0 ± 0.5 sec at 5.0 amp
2. Ignition delay from initiator discharge until 90% initial equilibrium pressure, ≤ 200 ms at 77° F
3. Shall provide chemical energy necessary for main propellant ignition

(R_{Case})

1. Propellant shall provide chemical energy necessary for conversion to kinetic energy
2. No debonding of insulation and liner
3. No loss of structural integrity

(R_{Nozzle})

1. Shall provide expansion of combustion gases
2. No loss of structural integrity
3. Shall provide containment of combustion gases for max thrust generation

(R_{Attach})

No loss of structural integrity

$(R_{Performance})$

Shall meet performance requirements stated in model specification

a. Impulse
b. Ignition delay
c. Ignition

Figure 3-35 Solid Motor Reliability Success Diagram

A diagram of the electromechanical and pyrotechnic components of the ignition subsystem is shown in figure 3-36.

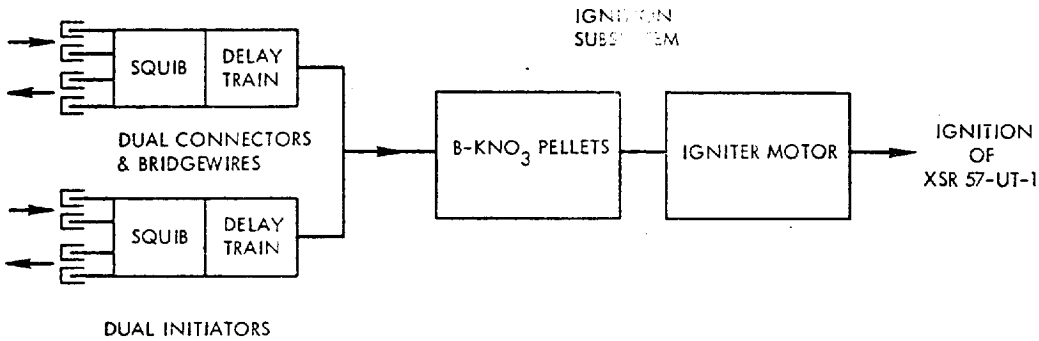

Figure 3-36. Ignition Subsystem Reliability Diagram

3.3.2.1 Failure Mode and Effect Analysis

The ignition subsystem reliability during the countdown and launch phase is based upon an analysis of possible failure modes, their probability of occurrence, and their consequence on mission performance. Results of the analysis are shown in table 3-III.

3.3.2.2 Mathematical Model and Estimation

The ignition subsystem for the Scout contains the following interconnected, but independent, components:

A. Dual-delay initiators

B. B-KNO_3 pellets

C. Igniter motor.

The assemblies, except for the dual-delay initiators, (which contain redundant units,) consist of nonredundant, serially operated components. There are redundant bridge wires in each initiator.

The specified design limit for operation of the delay train is 6.0 ± 0.5 sec. This is the time from electrical activation to pellet ignition. The delay train may fail in the following three modes:

A. Delay train inoperative

TABLE 3-III

INHERENT DESIGN RELIABILITY FOR SCOUT MOTOR

$\overline{X}i$	Item	Primary Mode of Failure	SF	Margin of Safety MS	b %	a %	Probability of Success
1.	Igniter case	Rupture during ignition	1.3	1.25	±3	±2	Φ [65.97] = .999999+
2.	Igniter closure	Rupture	1.3	0.62	±3	±2	Φ [52.53] = .999999+
3.	Motor case	Rupture	1.3	0.35	±2	±5	Φ [42.20] = .999999+
4.	Propellant	Grain failure during firing and spin	1.3	0.20	±5	±1	Φ [23.64] = .999999+
5.	Nozzle flange	Flange bolt tension failure	1.3	0.28	±5	±2	Φ [25.76] = .999999+
6.	Forward polar fitting	Bending stress failure	1.3	0.09	±3	±2	Φ [29.62] = .999999+
7.	Aft polar fitting	Bending stress failure	1.3	0.25	±3	±2	Φ [38.61] = .999999+
8.	Throat insert	Shear failure	1.3	0.20	±2	±5	Φ [33.49] = .999999+
9.	Nozzle exit cone	Bending stress failure in phenolic liner	1.3	0.63	±7	±7	Φ [23.40] = .999999+
10.	Attach structure	Bending failure in stub skirt	1.3	0.20	±7	±2	Φ [17.57] = .999999+
11.	Motor case attachments	Fastener screw shear failure	1.3	0.18	±5	±2	Φ [19.44] = .999999+

Where:

a = 3 coefficients of variation of failure stress = $3\sigma_1/\overline{X}_1$

b = 3 coefficients of variation of failure strength = $3\sigma_2/\overline{X}_2$

MS = Margin of safety

SF = Safety factor

$\overline{X}_1$ = Mean stress

$\overline{X}_2$ = Mean strength

σ_1 = Standard deviation of stress

σ_2 = Standard deviation of strength

$$K = SF\ (MS + 1)$$

$$Z = \frac{3\left[K\left(\frac{1+a}{1-b}\right) - 1\right]}{\sqrt{a^2 + b^2K^2\left(\frac{1+a}{1-b}\right)^2}}$$

ΦZ = Area under the normal probability curve

B. Delay train burns less than 5.5 sec

C. Delay train burns longer than 6.5 sec.

The probability of the delay train failing is equal to the probability summation of modes B and C above. In addition, modes A and B are equally probable. With the above assumption, the reliability of the igniter system may be expressed as:

$$R_{Ignition} = \left\{ \left(2R_c - R_c^2\right) R_S R_{dt} R_{ds} \left[2 - \left(2R_c - R_c^2\right) R_S R_{DT} R_{ds}\right] \right\} R_P R_M$$

Where:

R_c = Reliability of the connector and bridgewire

R_S = Reliability of the squib

R_{dt} = Reliability of the delay train

R_{ds} = Reliability of the delay train not failing short

R_P = Reliability of the B-KNO_3 pellets

R_M = Structural reliability of the igniter motor.

From past UTC experience, IDEP data and generic failure rates the following reliabilities are estimated for the environment expected.

R_c = .99999

R_S = .99750

R_{dt} = .99750

R_{ds} = .99875

R_p = .99969

From table 3IV, which is the structural reliability of all the Scout motor components, the structural reliability (R_M) of the igniter is .99999. Substituting these reliability values into the ignition reliability mathematical model, equation

$$R_{Ignition} = (.99996)\ (99969)(.99999+)$$

$$= (.99964)$$

TABLE 3-IV

IGNITION SUBASSEMBLY FAILURE MODES

Item	Function	Failure Mode	Failure Effect	Design Features and Control Measures
Ignition Assembly				
Initiator squibs (integral part of delay initiator)	Provide pyrotechnic energy to ignite delay train powder	(a) No ignition	(a) Failure to ignite ignition assembly on command resulting in mission abort	(a) Squibs selected have proven reliability and are of dual-bridgewire type. Design verification tests were conducted on 141 initiator squibs which included the delay train and the booster charge. Bruceton sensitivity tests were performed as a sample of 30 units. The 50% firing point was 3.95 amp. The 99.99% firing point with 95% confidence is 4.54 amp, and the 0.01% firing point with 95% confidence is 3.33 amp. Rigid quality control is exercised to ensure adherence to workmanship and performance. Initiator is accepted per UTC drawing 5M0034.
		(b) Delayed ignition	(b) Failure effect is covered in (a)	(b) Design features are covered in (a).
Delay train (integral part of delay initiator)	Provide discrete time delay between squib initiation and ignition of motor by means of burning rate and length of powder train and to provide pyrotechnic energy to ignite booster	(a) No ignition	(a) Failure to propagate	(a) Initiator is per UTC 5M0034 drawing. Pyrotechnic powder train has known and proven reliability, known burning characteristics, and is sized to provide 6.0 ± 0.5 sec igniter delay at 5.0 amp. Dual initiator assemblies are utilized to minimize malfunction effect on mission success. Design and performance tests have been conducted. Rigid quality control is being maintained.
		(b) Hangfire	(b) Reduced vehicle trajectory and performance	(b) Design features are covered in (a).
		(c) Delay time out of tolerance	(c) Failure effect is covered in (b)	(c) Design features are covered in (a).
Booster	Provide amplification of pyrotechnic energy supplied by delay train powder to assure ignition of pellets	(a) No ignition	(a) Failure to propagate pyrotechnic energy	(a) Booster material and sizing are of known physical properties and proven reliability. Design and performance have been verified with the firing of 141 squibs as the squibs, delay train, and booster are all contained in one unit and tested as such. Rigid quality control will be maintained in processing, manufacturing, and inspection.

TABLE 3-IV

IGNITION SUBASSEMBLY FAILURE MODES (Cont'd)

Item	Function	Failure Mode	Failure Effect	Design Features and Control Measures
Booster (continued)		(b) Hangfire	(b) Failure to perform within allowable ignition delay tolerances	(b) Design features are covered in (a).
		(c) Delayed ignition	(c) Failure effect is covered in (b).	(c) Design features are covered in (a).
Pellets	Provide pyrotechnic chemical energy to initiate burning of propellant in igniter motor	(a) No ignition	(a) Failure to ignite propellant in igniter motor	(a) Initiator pellets and sizing per UTC 4MDS-41801 and are of known physical properties. Reliability of similar pellets has been proven on the Titan III-C 120 in. solid-propellant rocket booster program. The retainer was changed from aluminum to stainless steel to retard the erosion rate of the retainer, maintain pressure, and prevent snuffing out of pellets under vacuum. Design incorporates integral bonding, environmental seals, and potting to ensure performance at high altitudes. Sizing will be in accordance with development and qualification testing. Rigid quality control and reliability surveillance is being maintained.
		(b) Delayed ignition	(b) Failure to perform within allowable ignition delay tolerances	(b) Design features are covered in (a).
		(c) Overpressurization	(c) Possible damage to rocket motor grain affecting ballistic performance	(c) Design features are covered in (a).
		(d) Pellet basket and igniter case rupture	(d) Failure effect is covered in (c).	(d) Design features are covered in (a).
Igniter motor	Upon ignition provides chemical heat energy directed through nozzle to ignite main propellant in rocket motor case	(a) No ignition	(a) Failure to ignite rocket motor propellant	(a) Propellant being used is a standard igniter formulation, UTP 1095, of known physical and ballistic behavior. Reliability of the pellets has been demonstrated in test firings of similar rocket motors. Six igniter motors will be test fired to verify design integrity, performance capabilities and reliability. Igniter case is of aluminum and sized for a margin of safety of 1.25 and with tapered wall to ensure controlled consumption after igniter operation. Rigid quality control during fabrication and assembly is being maintained.

TABLE 3-IV

IGNITION SUBASSEMBLY FAILURE MODES (Cont'd)

Item	Function	Failure Mode	Failure Effect	Design Features and Control Measures
Igniter Motor (continued)		(b) Delayed ignition	(b) Failure to operate within allowable tolerances	(b) Design features are covered in (a).
		(c) Overpressurization	(c) Possible damage to rocket motor grain and case affecting ballistic performance and structural integrity resulting from case rupture due to grain malfunction or due to noncontrolled burn-away of case causing large fragment to be ejected	(c) Design features are covered in (a).
		(d) Cracking of propellant and ballistic degradation, plugging of nozzle throat	(d) Failure effect is covered in (c).	(d) Design features are covered in (a).

3.3.3 Case Subsystem

The case subsystem shown in figure 3-37 consists of three statistically independent, serially related assemblies; the case assembly, the insulation the liner.

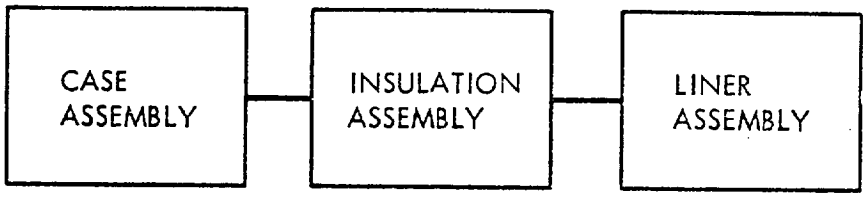

Figure 3-37 Case Subsystem Reliability Model

3.3.3.1 Failure Mode and Effect Analysis

A summary of possible failure modes, their probability of occurrence during the case subsystem flight action time T-0 to T+37 sec and their resultant failure effect and consequence on the mission are presented in table

3.3.3.2 Mathematical Model and Estimation

The case subsystem reliability is defined as the probability of the concurrent performances of the assemblies within their respective limits. From the above assumption, the case subsystem reliability is:

$$R_{Case} = R_C \times R_I \times R_L$$

where:

R_C = The probability that the case will successfully retain the products or propellant combustion for the duration of the mission

R_I = The probability that the insulation will successfully withstand the heat of combustion

TABLE 3-V

MOTOR CASE SUBASSEMBLY Failure Modes

Item	Function	Failure Mode	Failure Effect	Design Features and Control Measures
Case Assembly				
Case	Pressure container for propellant and combustion products. Integral structural member of launch vehicle	(a) Rupture due to overpressurization, or excessive structural loads	(a) Loss of thrust, catastrophic failure, and mission abort	(a) Motor case is fabricated per UTC drawing 5M0019 with filament-wound glass-epoxy combination with integral end fittings. The glass hoop and helical windings are per UTC Specification 5ZCS0008. The resin system is ERL 2256/MPDA or EPON 828/NMA. Skirts are integrally wound, using unidirectional glass cloth and hoop windings and EC 2216/BA resin system. Design requires proof-pressure test of 850 psi and a required burst pressure of 1000 psi min. Two cases have been hydroburst tested to 1485 psi and 1500 psi. Fabrication is on winding machines capable of producing cases to close tolerance, under automatic control. Rigid quality control includes proof-pressure test of 850 psi and inspection. Conservative design factors and established fabrication techniques are employed.
End Fittings (Fwd and Aft)	Provides mechanical and structural means to attach nozzle and igniter assemblies to the rocket motor case	(a) Separation due to vibration, spinning, yielding, fatigue, shock, and fracture shear	(a) Leakage of hot gases and ejection of nozzle and igniter assemblies leading to catastrophic failure and mission abort	(a) Material being used is aluminum 7079-T6 per QQ-A-367 to assure structural soundness, light weight, and sized with a safety margin of 0.18. End fittings will be machined from forgings and heat treated to develop maximum strength. Quality control measures include coupon tests and dye-penetrant inspection per MIL-I-6866.
		(b) Loosening due to vibration, spinning, yielding, fatigue, shock, and fracture shear	(b) Loss of structural integrity with motor case	(b) Loosening is controlled by integral winding with the motor case.
Insulation	Provides thermal protection to case during burning	(a) Debonding	(a) Loss of performance and possible catastrophic rupture of case	(a) Insulation used is silica-asbestos loaded buna-N rubber, per UTC 4MDS-40717 and fabricated in accordance with UTC 40DS-90201, having known and proven thermal insulation and ablation characteristics. Insulation design and reliability of the insulation has been proven with the

TABLE 3-V

MOTOR CASE SUBASSEMBLY FAILURE MODES (Cont'd)

Item	Function	Failure Mode	Failure Effect	Design Features and Control Measures
Insulation (continued)				successful firing of four TM-3A static firing spin tests. This material and process is used on numerous rocket motors including Titan III booster, Titan II translation rocket, and other motors which have been successfully test fired without insulation degradation. Rigid quality control surveillance is being maintained of vendor fabrication and inspection of insulation.
		(b) Char	(b) Failure effect is covered in (a).	(b) Design features are covered in (a).
		(c) Burnthrough	(c) Failure effect is covered in (a).	(c) Design features are covered in (a).
Liner.	Bonding agent for propellant grain to insulation and case	(a) Debonding	(a) Degradation in ballistic performance	(a) Liner being used is UTC AL-122-2C material which has extensive use history and demonstrated reliability based on no failures. Four TM-3A motors static firing spin tests verified the reliability and integrity of the liner with no failure. Material is centrifugally cast to ensure adherence and uniform dispersion. Rigid process controls in material formulation is being maintained.
		(b) Char	(b) Failure effect is covered in (a).	(b) Design features are covered in (a).
		(c) Burnthrough	(c) Failure effect is covered in (a).	(c) Design features are covered in (a).

R_L = The probability that the liner will successfully hold the bond between the case and the propellant or the bond between the insulation and the propellant

3.3.3.3 Reliability Prediction

The design reliability R_C considers the motor case and the polar adapters requirements from table IV.

$$R_C = (.999999)^3$$

$$R_C = .999997$$

United Technology Center's past experience with this insulation assembly and the liner assembly indicates that the reliability demonstrated for both assemblies is .999999. Substituting these values into the mathematical model, the case subsystem reliability is:

$$R_{Case} = (.999997)\ (.999999)\ (.999999)$$

$$= .99999^{+}.$$

3.3.4 Nozzle Subsystem

The nozzle chokes flow and provides for expansion of the gases at subsonic and supersonic velocities. The reliability diagram of the nozzle is shown in figure 3-38

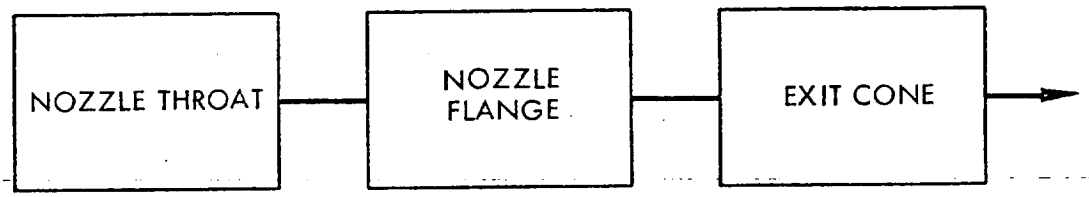

Figure 3-38 Nozzle Subsystem Reliability Diagram

The nozzle subsystem consists of three statistically independent assemblies; the nozzle throat assembly, the nozzle flange assembly, and the exit cone assembly.

3.3.4.1 Failure Mode and Effect Analysis

A summary of possible failure modes, failure effects, and mission consequences is presented in table 3-VI

3.3.4.2 Mathematical Model and Estimation

The nozzle subsystem reliability mathematical model is:

$$R_N = R_T \times R_F \times R_{EC}$$

Where:

R_T = The probability that the nozzle throat assembly will successfully provide for expansion of the combustion gases for the duration of the mission without structural failure

R_F = The probability that the nozzle flange assembly will successfully retain its structural integrity while under mission environments for the required duration of the mission

R_{EC} = The probability that the exit cone assembly will successfully provide containment of combustion gas expansion for maximum thrust generation.

Substituting the structural reliabilities into the mathematical model, the reliability for the nozzle subsystem is:

$$R_{Nozzle} = (.999999^+)^3$$
$$= .99999^+.$$

3.3.5 Attach Hardware Subsystem

The attach hardware subsystem consists of a forward attach to the payload and an aft attach to the lower stage. The attach hardware diagram is shown in figure 3-39.

TABLE 3-VI

NOZZLE SUBASSEMBLY FAILURE MODES

Item	Function	Failure Mode	Failure Effect	Design Features and Control Measures
Nozzle throat assembly	Chokes flow and conditions gases for expansion	(a) Excessive erosion	(a) Loss of throat efficiency	(a) Throat insert material is ATJ Graphite per UTC 5MCS0005, Class I. Material and fabrication process selected are of known properties and behavior under propellant burning conditions. Design has been verified by the successful firing of four TM-3A spin tests. Unit machined as part of exit cone assembly to ensure axial alignment. Rigid quality control includes alcohol wipe for inspection of cracking in final part, controls on materials, processes, and workmanship.
		(b) Thermal stress cracking	(b) Ejection of pieces with resulting axial displacement of thrust vector	(b) Design features are covered in (a).
		(c) Movement of throat affecting axial alignment and possible ejection	(c) Failure effect is covered in (a) and (b).	(c) Design features are covered in (a).
Nozzle flange	Provides mechanical and structural means to attach nozzle assembly to rocket motor case	(a) Separation due to vibration, yielding, fatigue, and fracture	(a) Leakage of hot gases and ejection of nozzle assembly leading to catastrophic failure and mission abort	(a) Material selected is aluminum 7075-T6 per QQ-A-367 to assure structural soundness, light weight, and sized with a safety margin of 0.28. Flange will be machined from forging. Product assurance control measures include penetrant inspection per MIL-I-6866, process controls, and workmanship.
		(b) Loosening due to vibration, yielding, fatigue, and fracture	(b) Loss of structural integrity with case	(b) Exit cone is bonded to the nozzle flange with Adhesive, HT-424 per MIL-H-5090, Type III. Bond is ultrasonically inspected per UTC 4MDS-90410, Bond quality levels to be Type I, Class I. Nozzle flange is bolted to the motor case with 24 MS24678-12 socket head cap screws, WC-3 Washers, and MS20495-C32 lockwire to ensure against loosening or separation of nozzle assembly from the motor case.

TABLE 3-VI

NOZZLE SUBASSEMBLY FAILURE MODES (Con'd)

Item	Function	Failure Mode	Failure Effect	Design Features and Control Measures
Exit cone	Provides for containment of expansion of combustion gases for maximum thrust generation at operational altitude	(a) Structural failure due to shock, spin vibration, loading, ablation, and burn-through	(a) Loss of efficiency. Possible impingement of rocket exhaust gases on vehicle components	(a) Design provides basic structural material of PH 15-7 MO STEEL per AMS-5520, Cond. A. Material ensures structural soundness, lightweight and sized with a safety margin of 0.63. Structural member is fabricated as a weldment and welded per MIL-W-8611, radiographic inspected per UTC 40DS-90401 and accepted per NAVSHIPS-250-1500, Section 10, Appendix II, Note 5. Exit cone liner is tape-wrapped, low-density silica paper, phenolic resin impregnated per UTC 5MCS0001 and mechanically interlocked with tape, graphite cloth, phenolic resin impregnated per UTC 5MCS0003. Exit cone is fabricated per UTC 5MPS0006. The materials used were chosen for erosion and temperature protection during rocket motor web action time. Four successfully fired TM-3A firing spin tests have proven design integrity and erosive and thermal properties of the materials. Structural material is bonded to the exit cone liner with adhesive, HT-424, per MIL-A-5090, Type III, per UTC 4MPC0004 and ultrasonically inspected per UTC 4MDS-90410 with bond quality level to be Type I, Class I. Quality Assurance includes rigid process control during fabrication, assembly, and quality control surveillance and inspection.

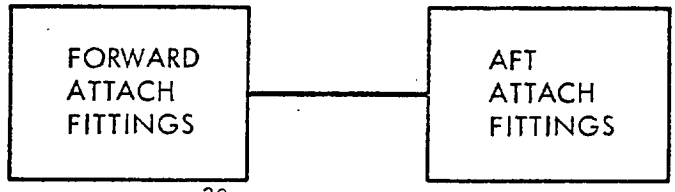

Figure 3-39 Attach Hardware Subsystem Reliability Moded

3.3.5.1 Failure Mode and Effect Analysis

A summary of the possible failure modes, failure effects, and mission consequences is presented in table 3-VII.

3.3.5.2 Mathematical Reliability and Estimation

The reliability of the attach hardware subsystem is the probability of successful maintenance of structural integrity such that the mission is a success. The attach hardware reliability can be described in the following manner:

$$R_{Attach} = R_{FP} \times R_{AP}$$

Where:

R_{FP} = The probability that the forward polar fittings will maintain their structural integrity

R_{AP} = The probability that the aft polar fittings will maintain their structural integrity.

From table the reliability for the attach subsystem is:

$$R_{Attach} = .99999.$$

3.3.6 PROPELLANT RELIABILITY

The two critical parameters which determine performance and their three-sigma limits are listed in table 3VIII These factors are very much interdependent so that the usual assumption of independence made in reliability calculations is invalid. The failure of the motor to meet one parameter while meeting the other is very unlikely. The degree of dependence is assumed to be equally distributed between the two parameters and is the result of propellant mix variations. The variations in turn would be the cause of failure modes presented in Paragraph 4.1.7.2.

TABLE 3-VII

ATTACH HARDWARE SUBASSEMBLY FAILURE MODES

Item	Function	Failure Mode	Failure Effect	Design Features and Control Measures
Attach Hardware				
Forward and aft attach fittings	Provides for structural mounting of fourth-stage rocket motor to vehicle and payload	(a) Fracture due to vibration, shock, spin yielding, and fatigue during flight	(a) Loss of structural integrity with vehicle resulting in mission abort	(a) Material selected is Aluminum 7075-T6 per QQ-A-367 and ensures structural soundness, lightweight and sized with a safety margin of 0.25 fitting and safety margin of 0.09 for the forward and fitting. Fittings will be machined from forging and heat treated to develop maximum strength. Product assurance control measures include penetrant inspection per MIL-I-6866, coupon tests, and rigid process control during fabrication and assembly.
		(b) Loosening due to vibration, shock, spin yielding, and fatigue during flight	(b) Failure effect is covered in (a)	(b) Fittings are attached to the motor case by the use of 100 PT100-R5-3 Pull Thru blind fasteners, to ensure against loosening during operation.

TABLE 3-VIII

PROPELLANT PERFORMANCE RELIABILITY

Parameter	Specification Mean	Specification Three-Sigma Limits	P Not Failing
Impulse	175,000 lb-sec	±3500 lb-sec	.99987
Action time	37.48 sec	±5.25 sec	.99987

3.3.6.1 Failure Mode and Effect Analysis

A summary of the possible failure modes, failure effects and mission consequence is presented in Table 3-IX.

3.3.6.2 Mathematical Reliability and Estimation

The reliability of the propellant is the probability that the impulse and action time will meet the nominal 3 σ specification limits and the propellant strength will not be exceeded. This can be described in the manner below:

$$R_{Propellant} = P_{Action\ Time} \times P_{Impulse} \times R_{Strength}$$

$$R_{Propellant} = .99934$$

TABLE 3-IX

PROPELLANT SUBASSEMBLY FAILURE MODES

Item	Function	Failure Mode	Failure Effect	Design Features and Control Measures
Propellant	Upon ignition provides the chemical energy in combustion products for conversion to kinetic energy through nozzle	(a) Cracking	(a) Loss of axial thrust, degradation in ballistic performance, and possible catastrophic failure due to overpressurization and subsequent case rupture	(a) Propellant selected is UTC 30964 formulation of known physical and ballistic behavior. Rigorous process and quality control is maintained during formulation, mixing, casting, and cure. Propellant samples taken and verification firings made for ballistic index and batch to batch acceptance. Design verification included four TM-3A static firing spin tests based on successful firings. Development and qualification tests will be conducted to ensure ballistic performance under maximum spin rate and operating altitude. Rigorous process and quality control are maintained during formulation, mixing, casting, and cure.
Propellant		(b) Slumping	(b) Failure effect is covered in (a).	(b) Design features are covered in (a).
		(c) Mechanical integrity	(c) Failure effect is covered in (a).	(c) Design features are covered in (a).
		(d) Out-of-tolerance ballistic performance under varying spin rates	(d) Failure effect is covered in (a).	(d) Design features are covered in (a).

see Table 3-VIII

3.3.6.3 Reliability versus Total Impulse Cutoff Accuracy

The reliability of the propellant is dependent upon the specification limits. As the specified cutoff impulse accuracy is increased, the probability of meeting the requirement decreases unless quality control measures are increased at additional cost. In figure 3-40 the probability of meeting impulse specifications is plotted as a function of percent total impulse cutoff accuracy. This curve is for the present UTC Scout Motor. Both cutoff accuracy and propellant reliability of the motor can be increased at additional cost.

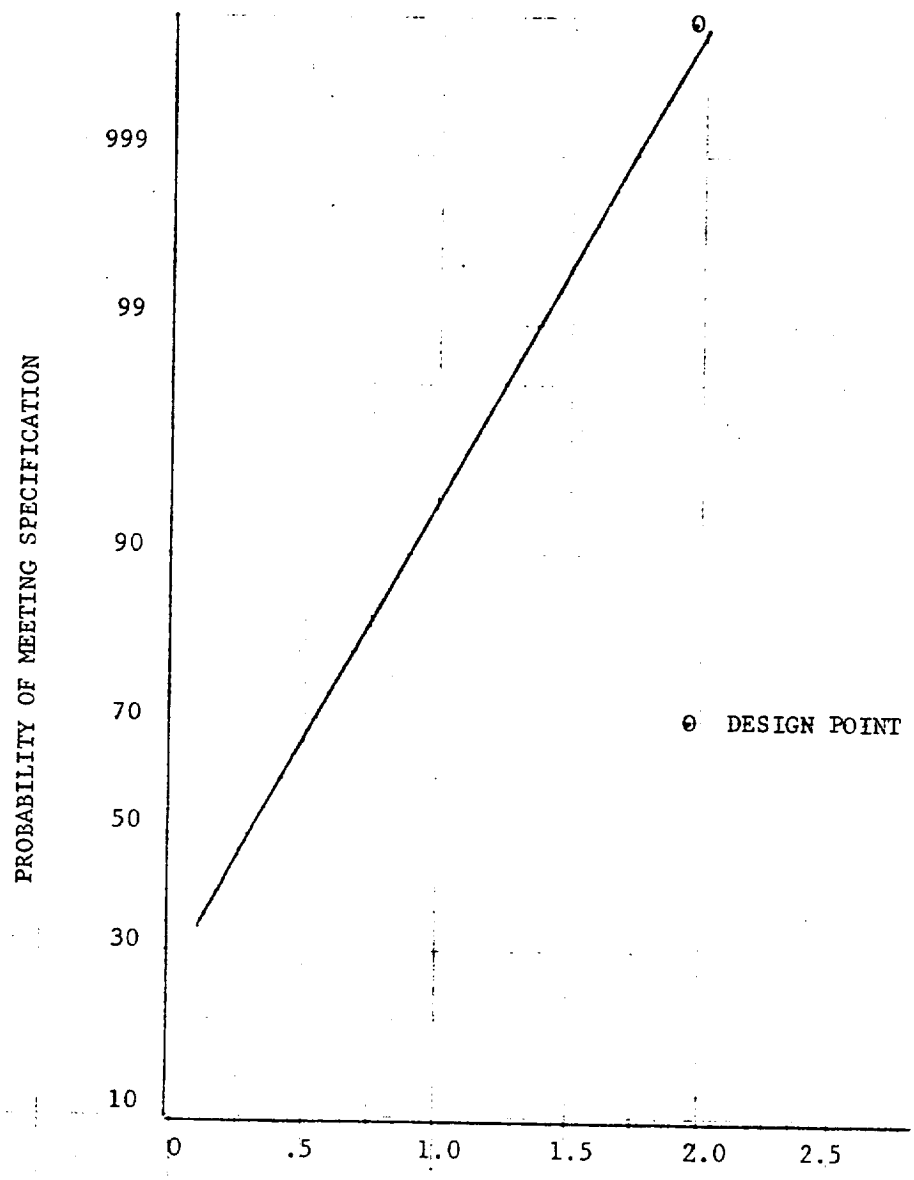

CUTOFF SPECIFICATION

Figure 3-40

3.3.7 Reliability Growth Of The FW-4S Solid Motor

The reliability growth curve shown in figure3-41 is the result of plotting accumulated firings against the lower 90% confidence limit of a Poisson success distribution. Failures shown by the dips in the curve were excluded from the fired population if corrective action was taken and that corrective action resulted in three (3) consecutive successes. This results in a conservative estimate of the lower limits of the reliability. It does not consider the reliability growth resulting from the removal of an obvious failure mode. On the other hand it removes from the population a failure mode which no longer exists.

The solid motor reliability growth is based on the UTC Scout 4th Stage which shows a steady upward reliability growth based upon well developed solid motor technology. During this program two failures have occurred, the first was the last motor of the development series and was of such a nature that only a slight redesign of the case was required. The second failure occurred during a recent flight and necessitated an extensive nozzle redesign. This failure mode will be excluded in the future. If successful, the growth curve will follow the upper dashed line as the maximum reliability growth, assuming no failures. The lower dashed line represents the lowest expected reliability growth after two successive failures.

3.4 SOLID MOTOR SYSTEM DEVELOPMENT AND PRODUCTION COSTS

The system development and production costs of the FW-4S are summarized in Table 3-X. The percentage distributions of the total cost into pertinent catagories are presented in Table 3-XI. Any variation of the basic FW-4S motor length would require a short development program which would cost approximately 25% of the FW-4S development program. The variation in production cost is plotted in figure 3-42 as a function of propellant weight.

K+E X 10 TO ½ INCH 46 1473
X 10 INCHES MADE IN U.S.A.
KEUFFEL & ESSER CO.

SOLID MOTOR RELIABILITY GROWTH VS. SYSTEM FIRINGS

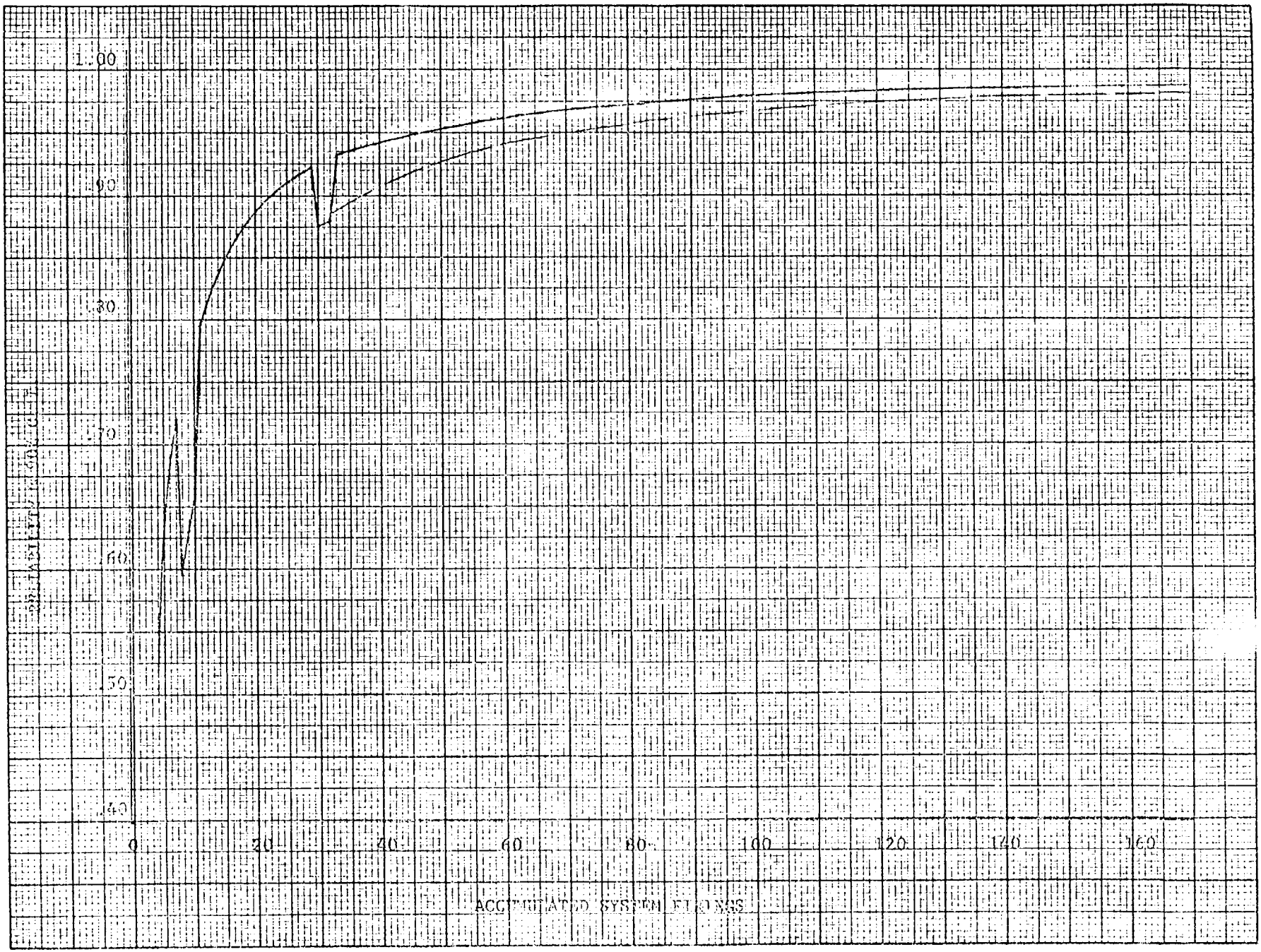

Figure 3-40

PROPRIETARY INFORMATION

TABLE 3-X

FW-4S SYSTEM DEVELOPMENT AND PRODUCTION COST SUMMARY

Development Cost	Millions of Dollars

Production Cost

TABLE 3-XI

FW-4S COST BREAKDOWN

DEVELOPMENT COSTS

System Requirements: _____ Total Seconds Testing: 250

Propulsion System	Percent of Total Cost of Development					
	Eng'g.	Manufac-turing	Hardware	Testing (pre-qual.)	Qual. Assur. Testing	Prog. Managmt.
Bipropellant						
Solid FW-4S	28	37	20	3	N/A	2
Hybrid						
Hi P_c Pumped						
ACS Monoprop.						

PRODUCTION COSTS

System Requirements: _____ No. Units: 7

Propulsion System	Percent of Unit Production Costs					
	Fabri-cation	Material	Eng'g. & Tooling	Final Test	Facilities	Eng'g. Changes
Bipropellant						
Solid	26	14	14	26	13	7
Hybrid						
Hi P_c Liquid						
ACS Application: Monoprop.						
ACS Application: Bipropel.						

-120-

Normalized Production Cost of FW-48
As a Function of Propellant Weight

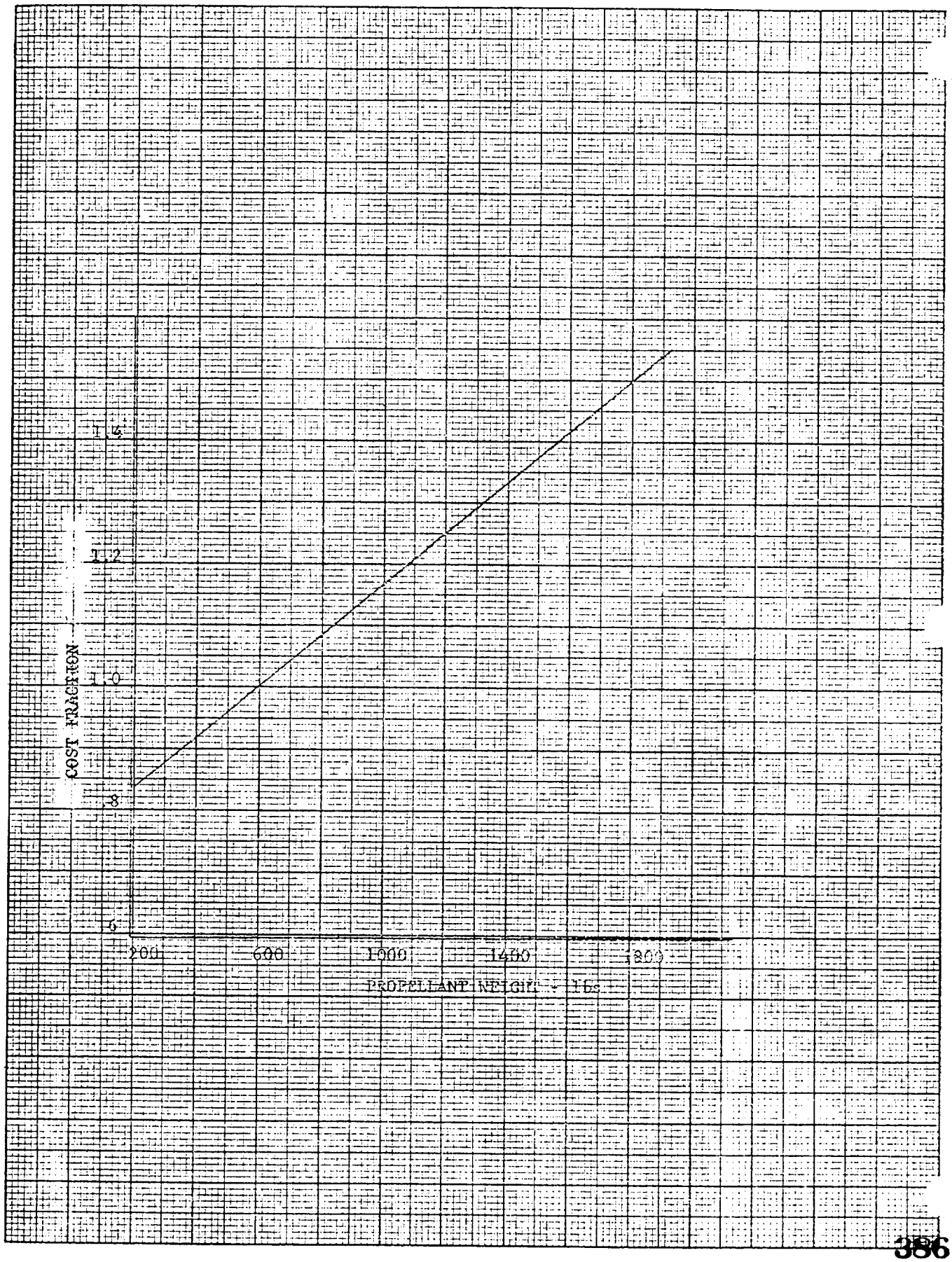

Figure 3-42

4.0 VOYAGER MISSION ANALYSIS

4.0 VOYAGER MISSION ANALYSIS

A preliminary design study on a Voyager de-orbit solid motor is in progress at UTC. The study has not been completed, however, some probable design parameters of the de-orbit motor are listed in Table 4-I. This motor design uses a sterilizable solid propellant, which consists primarily of AP and UTREZ binder with no metal additive.

The motor design parameters resulting from the FW-4S parametric data are listed in Table 4-I. The ratios of the parametric data to the preliminary design data are also tabulated for comparison. The relatively large differences between the two motor designs are due primarily to the slower burn rate and lower specific impulse of the sterilizable propellant.

THIS PAGE LEFT BLANK

5.0 CONCLUSIONS AND RECOMMENDATIONS

5.1 HYBRID MOTOR DESIGN CRITERIA

1. Development status of hybrid propulsion systems required extrapolations of vacuum performance data from sea-level demonstration firings. High altitude tests are required to confirm the kinetic loss, nozzle flow loss, and the predicted motor performance. As high altitude performance data becomes available in future programs the performance analysis should be upgraded.

2. Reliability predictions for the hybrid propulsion system was based upon analytical evaluation of the hybrid base system used in this report. The inherent reliability of .9944 is a probable upper limit for non-redundant hybrid upper stage propulsion systems. As flight data, becomes available in future programs the hybrid reliability analysis should be upgraded.

3. Cost predictions for the hybrid system were based upon data for liquid propellant feed systems, solid propellant motor production data and hybrid motor demonstration programs. As cost data becomes available from future hybrid development and production programs, the hybrid cost analysis should be upgraded.

4. Application of hybrid propulsion systems to missions requiring pulse mode operations was not considered to be practical with state of the art technology.

5. The effect of sterilization on hybrid design criteria was not evaluated in this study due to lack of readily available data. Sterilization data should be prepared for hybrid propulsion systems due to the probable requirement for sterile propulsion systems in many future missions.

6. This study was limited to presenting parametric hybrid data on the FLOX-Lithium fuel system demonstrated under NASA Contract No. NAS7-311 which was readily available. The reliability data presented in this report would be similar for earth-storable hybrid systems. However, both the cost and performance for non-sterilizable earth-storable propellants would be between 10 to 20% lower depending on the propellant system and mission requirements.

5.2 SOLID MOTOR DESIGN CRITERIA

1. The solid propellant motor design criteria was limited exclusively to the UTC FW-4S upper stage motor in accordance with the scope of UTC's participation in this NASA study. The parametric solid motor design criteria is this report was therefore limited in range to the practical extension of the nominal FW-4S design specifications.

2. The relatively large difference between the Voyager deorbit propulsion system evaluation using the parametric design curves in this report and a recently completed UTC preliminary design study independent of this contract resulted primarily from the sterilization requirement.

3. This report was limited to presenting parametric solid motor data on the FW-4S system. The performance, grain ballistics, cost, and reliability of solid motors vary with the amount and type of metal loading in the propellant. These effects could be evaluated, but would require additional data compiling and analysis beyond the scope of this study.

REFERENCES

2-1. D. E. Wilcox, and Q. W. Mason, "Computer Study of One Dimensional Nonequilibrium Nozzle Flow Assuming Instantaneous Freezing of Recombination Reactions," UTC TM-13-63-U12, January 1964.

2-2. J. H. Ahlberg, S. Hamilton, D. Migdal, and E. N. Nilson, "Truncated Perfect Nozzles in Optimum Nozzle Design," ARS Journal, May 1961.

2-3 C. N. Jennings, "Procedure for the Design and Optimization of Liquid Rocket Propulsion Systems," Space General Corp., SGC 837FR, April 1966.